MODELING AND CONTROL ARCHITECTURE DESIGN OF MULTI-EVAPORATOR PUMPED TWO-PHASE SYSTEM

A Dissertation

by

KAIMI GAO

Submitted to the Office of Graduate and Professional Studies of
Texas A&M University
in partial fulfillment of the requirements for the degree of

DOCTOR OF PHILOSOPHY

Chair of Committee,	Bryan P. Rasmussen
Committee Members,	Garng M. Huang
	Pilwon Hur
	Shima Hajimirza
Head of Department,	Andreas Polycarpou

Auguest 2019

Major Subject: Mechanical Engineering

ABSTRACT

Two-phase cooling systems are being explored actively as a promising technology for energy-intensive electronics systems. The latent heat of vaporization results in a high heat-transfer coefficient. However, the system may suffer a sudden increase in temperature when the heat flux exceeds the critical heat flux, causing a dramatic rise in surface temperature and a sudden reduction in heat-transfer coefficient. This can lead to burnout or system failure. This research focuses on control-oriented dynamic modeling of a pumped two-phase system with multiple evaporators. Further, the multi-evaporator pumped two-phase system is integrated with a vapor compression system. To avoid the appearance of critical heat flux, the exit quality of the evaporator must to be constrained to less than one, which means that only two-phase fluid is allowed at the outlet of the evaporator. This research uses the dynamic model to explore control architectures that provide avoidance of critical heat flux in two-phase cooling for multiple evaporators under dynamic heat loads.

DEDICATION

To my family and friends.

ACKNOWLEDGEMENTS

I would like to thank my committee chair, Dr. Bryan Rasmussen for his continuous assistance and guidance throughout my study and research. I would also like to thank my committee members Dr. Shima Hajimirza, Dr. Pilwon Hur, and Dr. Garng Huang for serving on my thesis committee.

Thanks also go to my friends and colleagues and the department faculty and staff for making my time at Texas A&M University a great experience. Finally, thanks to my mother and father for their encouragement and to my husband for his patience and love.

CONTRIBUTORS AND FUNDING SOURCES

This work was supervised by a dissertation committee consisting of Dr. Bryan Rasmussen (advisor), Dr. Shima Hajimirza and Dr. Pilwon Hur of the Department of Mechanical Engineering and Dr. Garng Huang of the Department of Electrical Engineering. All work for the dissertation was completed independently by the student.

Graduate study was funded through several sources listed below. The views expressed in this thesis are those of the author and are not representative of the supporting organizations.

Sep .2015 – Dec. 2016: Work was performed under the sponsorship of Advanced Cooling Technologies, Inc (ACT). Topic: N152-115, Active thermal control system optimization. Contract No.: N00014-16-P-2005. Any opinions, findings, and conclusions or recommendations expressed in this material are those of the authors and do not necessarily reflect the views of the sponsor.

Jan. 2017 – Dec. 2018: Research was indirectly supported by the US Department of Energy, Office of Energy Efficiency and Renewable Energy, Advanced Manufacturing Office, Industrial Assessment Center (IAC) Program Award Number: DE-EE007700. Any opinions, findings, and conclusions or recommendations expressed in this material are those of the authors and do not necessarily reflect the views of the US Department of Energy.

NOMENCLATURE

List of Abbreviations

PTP	Pumped Two-phase
VCC	Vapor Compression Cycle
CHF	Critical Heat Flux
T	Temperature [°C]
SH	Superheat [°C]
V	Vapor
TP	Two-phase
L	Liquid
FCV	Finite Control Volume
MB	Moving Boundary
SMB	Switch Moving Boundary

List of Symbols

Variable	Explanation
P	Pressure [kPa]
$\dot{m}$	Mass flow [kg s^{-1}]
P_{ratio}	Pump pressure ratio
$h_{po,isentropic}$	Pump outlet refrigerant isentropic enthalpy [kJ kg^{-1}]
h_{po}	Pump outlet refrigerant enthalpy [kJ kg^{-1}]
h_{pi}	Pump inlet refrigerant enthalpy [kJ kg^{-1}]

ω_P	Pump speed [rpm]
η_{vol}	Pump volumetric efficiency
η_p	Pump isentropic efficiency
ρ_p	Pump refrigerant density [kg m^{-3}]
V_p	Pump volume [m^3]
A_v	Valve opening Area [m^2]
C_d	Valve discharge coefficient
P_{vi}	Valve inlet pressure [kPa]
P_{vo}	Valve outlet pressure [kPa]
ρ_f	Density of refrigerant at liquid phase[kg m^{-3}]
ρ_g	Density of refrigerant at vapor phase[kg m^{-3}]
T_r	Temperature of refrigerant[°C]
T_w	Heat exchanger wall temperature[°C]
T_a	External air/fluid temperature[°C]
α_i	Heat-transfer coefficient between tube wall and internal fluid[W $m^{-2}K^{-1}$]
α_o	Heat-transfer coefficient between tube wall and external fluid[W $m^{-2}K^{-1}$]
A_{cs}	Cross-sectional area of the inside of the tube[m^2]
A_i	Internal surface area of the heat exchanger[m^2]
A_o	External surface area of the heat exchanger[m^2]
$(C_p\rho V)_w$	Thermal capacity of the tube wall per unit length[J $K^{-1}m^{-1}$]
$\bar{\gamma}$	Mean void fraction
μ	Weight factor for external air temperature

S	Heat exchanger slip ratio
t	Time[s]
Z	Matrix
x	State vector, Vapor quality
$\dot{x}$	Time derivative of state vector
u	System input
C_d	Discharge coefficient
$Mass$	Heat exchanger material mass[kg]
d	Heat exchanger tube diameter[m]
G	Matrix
$U\Sigma V^H$	Matrix singular value decomposition
$\gamma(G)$	Condition number of a matrix
$\bar{\sigma}(G)$	Maximum singular value
$\underline{\sigma}(G)$	Minimum singular value
c	Specific heat [J $kg^{-1}K^{-1}$]

Subscripts	Explanation
1,2,3	1st, 2nd, 3rd Region in the heat exchanger; 1st evaporator in parallel, 2nd evaporator in parallel, 3rd evaporator in parallel
e	Evaporator
c	Condenser
r	Refrigerant

w	Wall
v	Valve
p	Pump
i	Inlet
o	Outlet
vol	Volumetric
cs	Cross-sectional
f	Saturated liquid
g	Saturated vapor
j	j^{th} evaporator in parallel
n	Number of evaporators in parallel

TABLE OF CONTENTS

Page

LIST OF FIGURES

Page

LIST OF TABLES

Page

1. INTRODUCTION

In recent years, with the increased usage of high-power electronics in data centers, buildings, and all-electric vehicles, cooling technologies are becoming more important for these types of applications [1]. In 2014, data centers in the United States (US) consumed an estimated 70 billion kWh, representing 1.8% of total US electricity consumption [2]. Energy use is expected to continue increasing in the near future, so energy-efficient cooling systems are in high demand.

Data centers usually are cooled by natural and forced convention using ambient air. Military and defense-related systems also use air cooling, but in many cases single-phase liquid cooling has been required for high-energy laser arrays and high-power radars [3]. Forced-air and single-phase liquid cooling systems are insufficient to meet the increased cooling demand in electronics systems because of their low thermal conductivity, low thermal capacity, and high pressure drop [4, 5]. Refrigerant two-phase cooling is drawing attention as a more efficient way to cool high-power electronics.

Refrigeration two-phase cooling can be implemented in various configurations. The most common configuration utilizes a vapor compression cycle (VCC). VCC uses a circulating fluid as the medium which absorbs and removes heat from the space to be cooled and subsequently rejects that heat elsewhere. VCC uses a compressor to compress low-temperature vapor to higher-temperature vapor and establish a pressure differential to move the fluid in the cycle. Evaporator and condenser operate at two different pressures. An alternative configuration, pumped two-phase (PTP), involves a liquid pump to provide head pressure to circulate the fluid in the cycle. In contrast with VCC, both evaporator and condenser operate at the similar pressure.

Comparing with single-phase liquid cooling, the required mass flow rate for two-phase cooling system is much smaller than for a single-phase liquid cooling system, because the latent heat of evaporation h_{fg} of a fluid is larger than the specific heat capacity of a fluid times the allowed temperature gradient $c_p \Delta T$. This results in a smaller diameter for a two-phase system than for a single-phase system. With the benefits as reduce size, lower flow rate and higher efficiency, two-phase refrigerant cooling can be more suitable for high power electronics.

In the last two decades, much research has been performed around modeling and control design for VCC cooling. Only a few recent published studies have focused on control-oriented PTP cooling modeling and control design. This work mainly fills the gap of multi-evaporator PTP system dynamics modeling and the development of control architectures that have the ability to achieve high performance over different heat load conditions.

This dissertation is divided into two parts. The first portion presents the development, simulation, and control architecture design of a multi-evaporator PTP system. The second portion presents integration of a multi-evaporator PTP system with a VCC to extend to applications such as integrating data center chip level cooling with building centralized chiller, navy ship radar array cooling with vapor compression refrigeration cooling. Model development, simulation, and control architectures are discussed in detail.

In summary, this dissertation proposes a control-oriented modeling method of a multi-evaporator PTP system and its integration with a VCC for cooling electronics. The model has the ability to handle a large number of evaporators in parallel, providing important insight to real system design and application. With the model, new control architectures were developed and evaluated under different heat load conditions. When the control architectures were applied on the system, improvement was observed in the performance of PTP cooling.

The remainder of the dissertation is organized as follows. A background and literature review are presented in Chapter 1. A dynamic modeling method of the proposed system is discussed in Chapter 2 with its challenges and solutions of including large numbers of evaporators in parallel. Further presented in Chapter 2 is a system schematic of a multi-evaporator PTP system, along with detailed information and system parameters. Chapter 3 then presents two control architectures to compensate for nonlinearities and coupling in multi-evaporator systems and to ensure avoidance of critical heat flux (CHF). Simulation cases with the proposed control architectures are presented for the proposed PTP multi-evaporator model with different load conditions and heat flux impulses. The results are discussed and compared. In Chapter 4, modeling methods for the integrated PTP-VCC are discussed. In Chapter 5, a time-scale analysis of the dynamics of the PTP-VCC is presented to study the dynamics behavior of the two cycles together with the control architecture design. A conclusion and future work recommendations are summarized in Chapter 6.

1.1. Background and Literature Review

1.1.1. Air, Liquid, and Two-Phase Cooling

Three major cooling techniques typically are used in high-energy consumption electronics systems such as data centers: air cooling, liquid cooling, and two-phase cooling.

Air Cooling

In an air-cooling system in a data center application, cold air blows into the server and removes the heat generated by chips. After passing through the server, the temperature of the air

increases. In order to reuse the air, building chilled water is used to bring down the temperature of the air. The facility needs a chiller to cool the chilled water to a temperature lower than the ambient temperature so that there will be sufficient heat transfer between the air and the building chilled water. Then heat usually is rejected to ambient air through a cooling tower. Regardless of the relatively low heat-transfer coefficient of air cooling and the increasing heat load on the chip, research and development have focused on the thermal resistance of the chip and heat sink [6].

Liquid Cooling

Liquid cooling, as compared with air cooling, is a more efficient method of transferring heat because of its higher volumetric specific heat and higher heat-transfer confidence. It also reduces the overall thermal resistance of the heat-transfer circuit for data center applications. An IBM study in 2009 [7] found that liquid cooling uses 40% less total energy compared with air cooling in data center applications. Liquid cooling also reduces the size and cost of equipment. However, tremendous pumping power is required to keep the temperature gradient in the fluid within acceptable limits. When comes to the choice to cooling liquid, fluids with good thermal properties like water, has reliability concerns due to potential damage to electronics in the case of leaks. Electronic-friendly dielectric liquids, such as certain refrigerants, have poor thermal properties in the single phase and come with a high equipment cost.

Two-Phase Cooling

Nucleate boiling is one of the most efficient ways to remove heat from a component [8-11]. Two-phase cooling is of particular interest for electronics-cooling applications. Agostini et al. [12] outlined several desirable features of two-phase cooling that make it a promising medium

to long-term solution because of its high heat transfer efficiency and high heat-dissipation rate. Substantially reduced thermal resistance can be provided by two-phase cooling in an order of magnitude less than that of air and significantly below that of liquid cooling [6].

1.1.2. Refrigerant Two-Phase Cooling Systems

Refrigerant two-phase cooling has proved its effectiveness in various fields. The most common application is heating, ventilation, and air conditioning and refrigeration (HVAC&R), where the general thermodynamics cycle behind the application is VCC. An alternative configuration is PTP refrigerant cooling, which involves a liquid pump to provide head pressure to circulate the fluid in the cycle. A detailed discussion on the two cycles is presented below.

Figure 1 shows a system diagram of a VCC. The VCC has four major components: compressor, condenser, expansion valve, and evaporator. Figure 2 shows a system diagram of PTP cycle. The PTP cycle has three major components: pump, condenser and evaporator. Valve is an optional component before the evaporator to control the mass flow rate of the refrigerant entering evaporator.

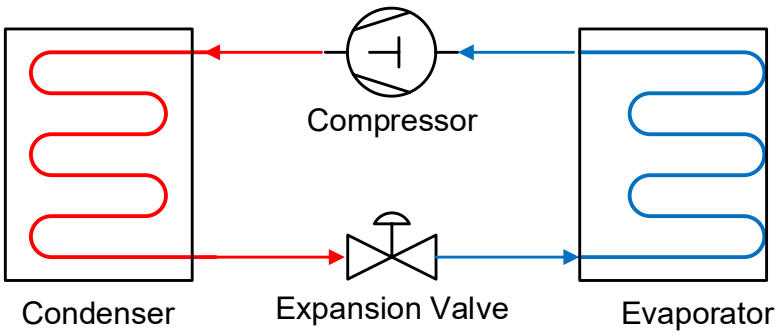

Figure 1: System diagram of a VCC cooling system

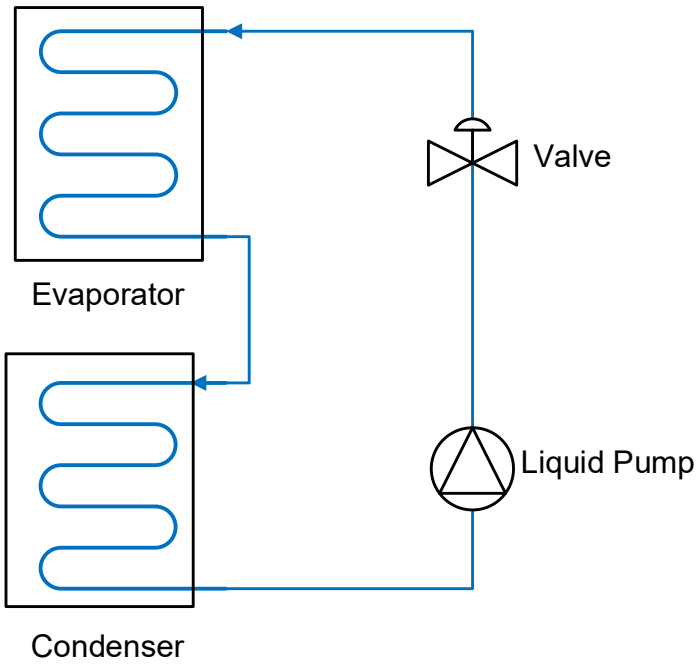

Figure 2: System diagram of a PTP cooling system

Figure 3 shows the pressure enthalpy diagram of a PTP cycle and a VCC. The red dotted line is a typical VCC. Heat is removed from a low-pressure evaporator and is rejected to external fluid in a high-pressure condenser. Superheat is needed at the outlet of the evaporator to prevent flooding in the compressor. The blue solid line is a PTP cycle. In the cycle, heat is transferred by evaporating and condensing the working fluid. Both evaporation and condensation occur at approximately the same pressure assuming pressure drop is negligible. A pump is needed to provide the head pressure to circulate the fluid in the cycle. From the pressure enthalpy diagram, we can see that the PTP evaporator operating pressure is higher than that in the VCC. This difference is caused by to the fact that the PTP cycle tends to work in ambient temperature and has a saturated evaporating temperature close to ambient temperature. Using VCC for cooling electronics sometimes can cause problems like condensation due to operating temperature being lower than ambient temperature. When choosing the proper refrigerant, the saturated boiling

temperature in the evaporator in the PTP cycle can be higher than ambient temperature to avoid condensation on the electronics. Also, less energy is needed by the pump in a PTP system comparing with using a compressor in a VCC system.

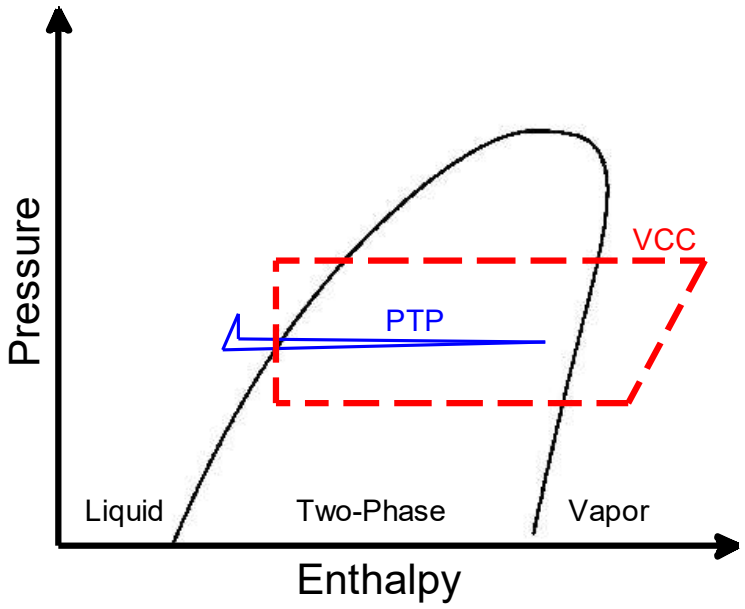

Figure 3: Pressure-enthalpy diagram of VCC and PTP

However, both configurations present the risk of CHF when a system experiences large transient heat load [13, 14]. CHF describes the thermal limit of the phenomenon where a phase change occurs during heating. Large bubbles start to form on the heating surface and cause a sudden reduction in heat-transfer coefficient, causing a localized overheating problem. In Figure 4 CHF is marked where fluid starts to cross the boundary from nucleate boiling to film boiling. The system must operate away from the CHF point to prevent localized overheating. This localized overheating can lead to burnout or system failure. To avoid CHF, the exit quality of the evaporator needs to be controlled.

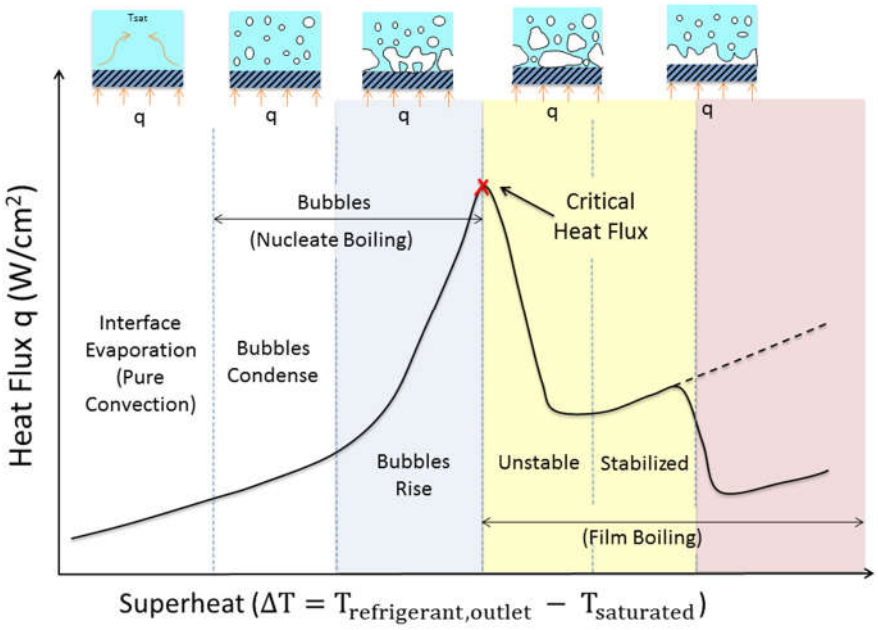

Figure 4: Boiling curve of two-phase fluid

Researchers have explored both VCCs and PTP cycles experimentally for cooling electronics. A pumped liquid multiphase cooling system (PLMC) was proposed by Hannemann et al. [15] for high energy consumption devices such as microprocessors and large radar systems. The proposed PLMC includes a high-performance cold plate (evaporator), an air-cooled condenser and a liquid pump. The proposed system was tested with refrigerant HFC134a and compared between a single-phase water loop. Their results demonstrated the significant benefits such as efficiency, reduced size and weight when using pumped two-phase cooling. However, the research did further state the CHF avoidance strategy when the system was exposed to load changes. Trutassanawin et al. [16] designed and built a small scale refrigeration system for notebook computer including a microchannel condenser, a microchannel evaporator, a capillary tube as the expansion device and a mini-compressor,. Their system showed 25%-30% of the Carnot efficiency which was similar to the efficiency of today's household refrigerators. Mongia

et al. [17] experimentally studied a miniature-scale refrigeration system for cooling electronics. Their system included a microchannel condenser, a microchannel evaporator, a manual needle value as throttling device, a heat spreader, a small-scale compressor and two compressor cooling fans. From their research, the conclusion was made that a suitable control strategy was required to improve its performance as well as a new compressor design. Marcinichen et al. [18] compared multi- evaporator VCCs and PTP cycles for cooling a computer blade server. The experimental data showed less pumping power needed for the liquid pumping cycle and the VCC having the potential for energy recovery because of higher condenser temperature.

1.1.3. Control of Refrigerant Cooling Systems

Given the proven effectiveness of refrigerant cooling, active control schemes are needed to improve performance and ensure operational safety of electronics systems. Marcinichen et al. [19] proved the effectiveness using single-input-single-output (SISO) strategies for VCCs and pumped liquid cycles for CHF avoidance with heat load input to be a known parameter in the field of electronics cooling. Marcinichen et al. [18] and Wu et al. [20] published a control strategy design and testing on a hybrid cycle. The hybrid cycle involves a PTP cooling loop to remove the heat from chips, a liquid separator to direct the refrigerant to a VCC loop to remove the heat from the PTP loop, and an external water loop to reject the heat from the condenser in the VCC loop. In such an application, the CHF constraint and secondary components can alter cycle behavior significantly. Therefore, it must be designed and controlled carefully to maintain safe and efficient operating conditions.

1.1.4. Control-Oriented Modeling of Refrigerant Cooling Systems

With the increasing interest in using two-phase fluids for high-heat flux cooling, a system model that can be used for control scheme design for cooling electronics is drawing attention. Heydari [21] developed a simulation program including a miniature compressor, capillary tube, compact condenser, and cold plate evaporator to evaluate performance of miniature refrigeration systems for high performance computers. Higher COPs were observed with lower condensing temperatures. A steady state multi-evaporator VCC model was proposed by Zhou et al. [22, 23] for high heat flux removal. The research was mainly for system characteristic validation and operating condition optimization, not for control design. Juan et al. [24, 25] developed a lumped-parameter first-principle dynamic model of a VCC cooling for electronics systems. The model was compared with experiment data and showed the ability to capture the essential behavior of the system. Then gain-scheduling control was used for CHF avoidance. Zhang et al. [26] used a finite different method to cover the comprehensive mass, energy and momentum balance of two-phase exchanger in VCC dynamic modeling for electronics cooling. Yang et al. [27] proposed a systematic approach to synthesize robust and gain-scheduled controllers for a single-evaporator VCC for cooling of large transient heat load.

Compared to a conventional VCC, less research can be found in modeling PTP systems. Kelkar and Patankar [28] published a steady state computation modeling method for a multi-evaporator PTP cycle and proved its effectiveness for data center cooling applications. Chen et al. [29] proposed a steady state single-evaporator PTP model that demonstrated the ability to predict the characteristics and performance of pumped two-phase cooling systems. The micro-evaporator used the correlation between pressure drop, flow rate and heat generation with experiments.

Control-oriented modeling of VCCs for cooling electronics have been studied by multiple researchers, while the majority of modeling studies on PTP systems have focused on system fluid properties. A control-oriented PTP model that balances simplicity and accuracy and that captures the complex heat and mass flow dynamics can be highly valuable for refrigerant-cooling applications. With a control-oriented PTP model, control schemes can be studies for CHF avoidance in PTP cycles.

In a refrigerant cooling system, components like pumps, compressors, expansion valves, and receivers have dynamics on different time scale compared with the heat exchangers. Modeling the heat exchangers properly is the main challenge. In the literature, two heat exchanger modeling approaches are used commonly: finite-control volume (FCV) models and moving-boundary (MB) models. In the FCV approach, the heat exchanger is separated into fixed-volume zones or cells by discretizing the governing partial differential equations (PDEs) that describe the heat exchanger with time and spatial variations. FCV has the advantage of including detailed fluid behavior, thermophysical gradients, and distributed parameters [30]. The advantages of complex spatial characteristics and increased accuracy through greater details also results in higher dynamic order and greater computational time [31-33]. In contrast with the FCV approach, the MB approach divides the heat exchanger into several regions based on fluid phase, such as subcooled liquid, two-phase mixture, and superheated vapor [34]. The boundaries between regions are modeled as dynamic variables. The MB approach preserves the simplicity of lumped-parameter models while still having the ability to capture the salient dynamics of multiple-fluid-phase heat exchangers [24, 25]. Bendapudi et al. [35], Rasmussen [30], and Rodriguez [36] provided a comparison between FCV and MB approaches. Their results showed both approaches can provide similar simulation results, but the FCV approach showed slower

computational ability due to the requirement of including more control volumes during the calculation. Switching-moving-boundary (SMB) models are extensions of the MB model. Based on different profile assumption, the SMB model has the ability to handle the disappearance and appearance of phase regions by switching between different MB models during simulation. Willatzen et al. [37] used the SMB method to handle the disappearance and appearance of a superheated region based on outlet enthalpy conditions. Zhang and Zhang [38] presented a void fraction switching mechanism for a two-phase region that improved the model's numerical stability. McKinley and Alleyne [39] proposed a combination of void fraction and region length. Li and Alleyne [40] later expanded this method to describe the severe transient behaviors in heat exchangers. Cecchinato and Mancini [41] proposed an intrinsically mass conservative switching method involving two-phase region length and density for the evaporator. Qiao et al. [42] utilized exit enthalpy and void fraction as a switching mechanism for a flash tank vapor injection heat pump system. Bonilla et al. [43] proposed varying threshold enthalpy and switching length to avoid numerical singularity in calculation. Rodriguez and Rasmussen [36] provided a comparison of different switching approaches and made recommendations for commonly used minimum thresholds. All models showed satisfactory performance in their specific applications. However, the models mentioned in the literature review are single heat exchanger. They cannot be taken directly to multi-evaporator PTP system modeling. A multi-evaporator PTP system requires integrating multiple evaporator models with a condenser model.

In this research, a dynamic multi-evaporator PTP system model was proposed and tested. Up to hundreds of evaporators can be simulated within a reasonable computational time. The model provides the possibility to test a potential system without investing a lot of time and money associated with building a physical prototype system. Different active control strategies

were developed to maintain constant operating conditions and avoid CHF conditions despite changing heat loads. In the application such data center cooling, a chip-level pumped two-phase system can be integrated with the building centralized chiller. A multi-evaporator PTP system was integrated with a VCC system by a refrigerant to refrigerant heat exchanger. Control architectures were explored further on the integrated system.

2. MULTI-EVAPORATOR PUMPED TWO-PHASE SYSTEM MODEL

In most electronics cooling applications, numerous components need to be cooled for normal operation. In data center applications, multiple chip processors on different levels of server racks generate heat. A two-phase refrigerant cooling system with the ability to dissipate different levels of heat from multiple target components is valuable. The PTP refrigerant cooling system proposed in this research was set up with multiple evaporators in parallel to remove heat generated from different chip processors and to maintain constant operating conditions.

A PTP cooling system does not have a specific configuration. There are three key components: a pump to provide enough head pressure to circulate the refrigerant, an evaporator to cool the target components, and a condenser to reject the heat to external fluid. Optional components include: preheater to control coolant temperature at the evaporator inlet, surge tank with temperature control to control system pressure, accumulator to prevent cavitation in the pump, valves for flow control, etc. Figure 5 shows a PTP cooling system configuration with key components and optional components.

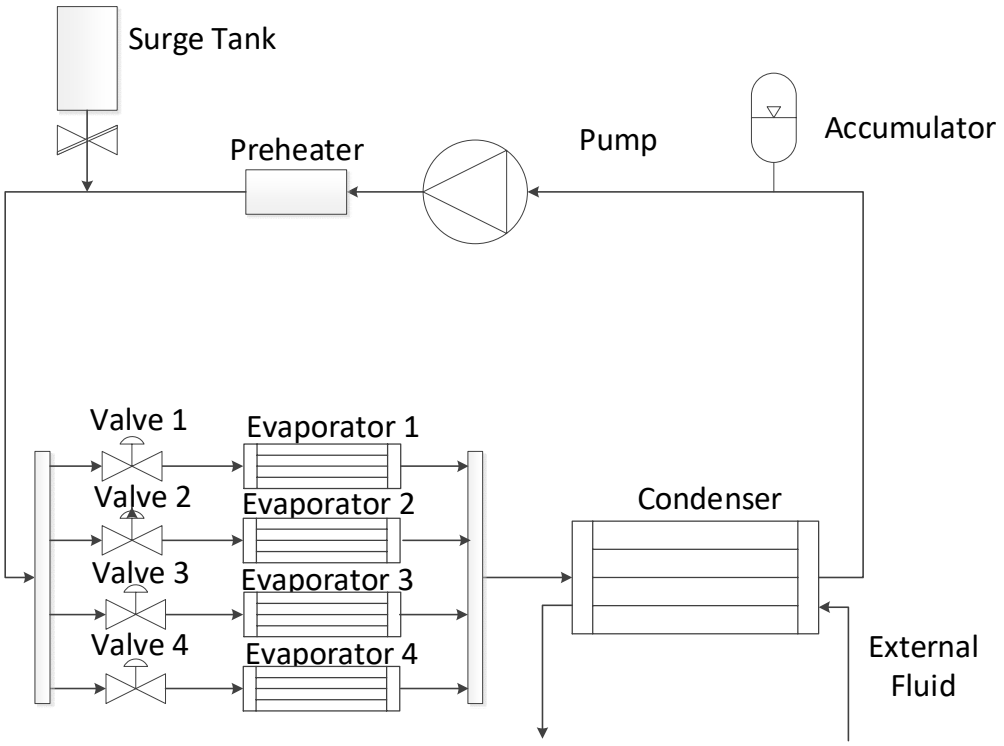

Figure 5: Multi-evaporator PTP system with key components and optional components

2.1. System Configuration Analysis

As stated above, a pump, evaporators, and a condenser must be included in the system to provide the basic cooling function of the system. In order to preserve the model's simplicity while still having the advantage of operating at different load conditions, a variable-speed pump and mass-flow-controlling valves were deployed in the configuration. The valves are placed before each evaporator to control the flow rate and to control evaporator exit vapor quality. A constant reservoir is placed between the pump and valves to provide constant pressure and enthalpy to the valves.

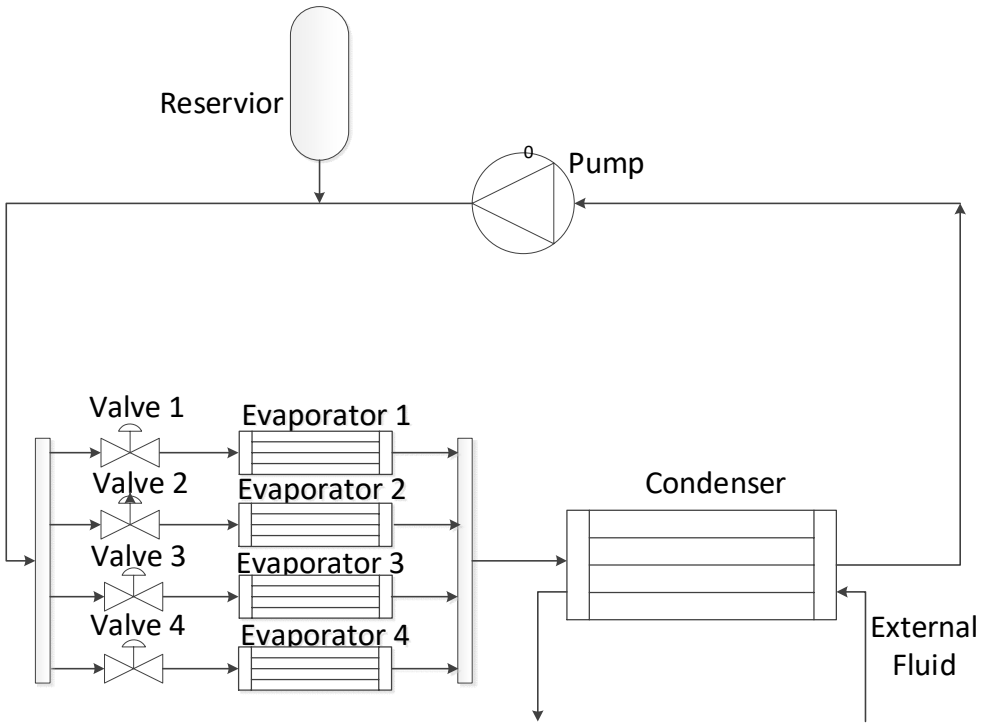

Figure 6: System configuration

Figure 6 shows a four-evaporator PTP cooling system configuration. In general, the system can have any number of evaporators in parallel to handle multiple distributed heat loads. A pump is needed to provide enough head flow to circulate the refrigerant. Valves are installed before the evaporators for flow control. The evaporators (heat sinks) provide saturated boiling, utilizing the latent heat of vaporization to remove heat generated by chips. A constant reservoir is placed between the pump and valves. Water is used as the external fluid for heat removal in the condenser.

The pump model and valve model were chosen as physics-based models to correlate relationship between pressures across the components with mass flow rate, as shown in Equation (1). In order to calculate the mass flow rate, inlet and outlet pressure of the pump or valve need to be known. These components can be referred to as mass-flow-rate components. Heat

exchanger models such as evaporators and condensers correlate the inlet and outlet mass flow rates to the pressure gradient. Inlet and outlet mass flow rates of a heat exchanger are known variables for calculating pressure and other fluid properties. A heat exchanger model can be referred to as a pressure component.

$$\dot{m} = f(\Delta P) \quad \textbf{(1)}$$

$$\dot{P} = f(\Delta \dot{m}) \quad \textbf{(2)}$$

With the system schematic setup shown in Figure 6, the system components cannot be modeled separately and then connected together to form a closed loop system. The relationship between pressure and mass flow rate is presented in Figure 7. For figure simplicity, only one evaporator and one valve are shown in the loop. With the lack of mass flow rate components between the evaporators and condenser, the evaporators and condenser are modeled together as a combined heat exchanger.

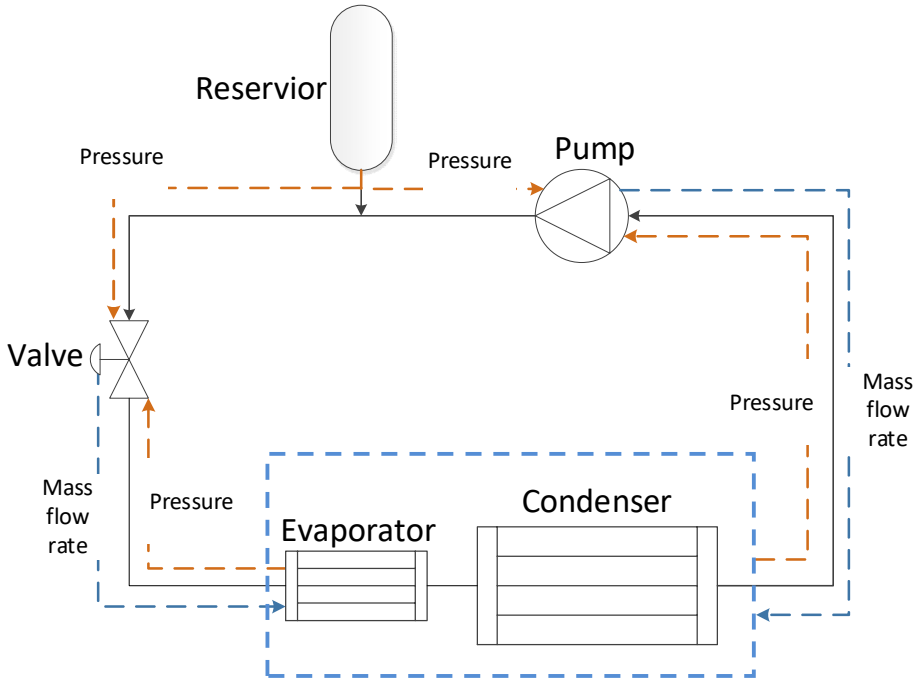

Figure 7: System configuration - Pressure/mass-flow-rate relationship

2.2. Pump

The variable-speed pump governing equation is shown in Equation (3). It used as a semi-empirical map with varying pump efficiency. The volumetric and isentropic efficiencies were interpolated as functions of the pressure ratio and pump speed from semi-empirical maps, as shown in Equations (4), (5), and (6). The pump speed was rate-limited in order to capture the limitations of a real pump.

$$\dot{m}_p = \omega_p V_p \rho_p \eta_{vol} \tag{3}$$

$$\frac{h_{po,isentropic} - h_{pi}}{h_{po} - h_{pi}} = \eta_p \tag{4}$$

$$\eta_{vol} = f(P_{ratio}, \omega_p) \tag{5}$$

$$\eta_p = f(P_{ratio}, \omega_p) \tag{6}$$

2.3. Valve

The governing equation for the valve model was modified from the standard orifice flow equation, as shown in Equation (7), where $\dot{m}_v$ is the mass flow rate through the valve, A_v is the area of valve opening, and C_d is the coefficient of discharge. A semi-empirical map was used to calculate the product of the coefficient of discharge and area of valve opening as a function of the pressure difference, $\Delta P = P_{vi} - P_{vo}$ and the percentage of valve-opening input.

$$\dot{m}_v = A_v C_d \sqrt{\rho(P_{vi} - P_{vo})} \tag{7}$$

2.4. Combined Heat Exchanger

The dynamics of a PTP system are dominated by the heat exchangers. The reason is that the valve model and pump model are physics-based static relationships. The dynamics of the heat exchangers evolve on slower time scales than valve and pump model.

As mentioned in the literature review, the most commonly used dynamic heat exchanger modeling methods are the moving boundary (MB) and finite control volume (FCV) approaches. The switch moving boundary (SMB) approach is an extension of MB where the model is switched between different MB modes. Each approach has its own unique advantages. MB, sometimes known as the lumped-parameter approach, with parameters lumped in regions defined by fluid phase and the fluid-phase transition point being a dynamic variable, can catch the complex spatial characteristics of fluid properties with less computational time. The FCV approach can provide more detailed spatial variables with greater computational time.

Both modeling methods are valuable in PTP heat exchanger modeling. MB has the ability to greatly improve computational time, while FCV can provide detailed temperature profile along the tube length.

Figure 8 shows the real time factor comparison of FCV method versus MB method running on a standard desktop computer. To simplify the process, one FCV evaporator model and one MB evaporator model were used. The real-time factor is defined as computational time over length of simulated time. The real time factor of FCV method was tested from including three control volumes up to including thirty control volumes in the evaporator. Results showed the increasing real time factor when including more control volumes in the evaporator, regardless of the exponentially increasing real time factor with multiple evaporators in parallel in the FCV

approach. To handle a larger number of parallel evaporators simulated in a reasonable computational time, the MB modeling approach was found to be more suitable. SMB method was chosen as the modeling approach to handle the appearance and disappearance of fluid phase regions while still have reasonable computational time.

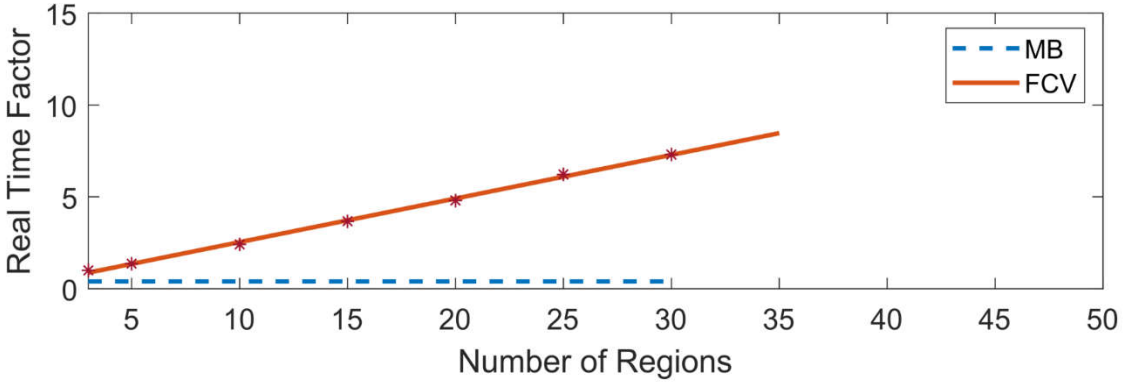

Figure 8: Real time factor comparison between MB model and FCV model

The heat exchanger models in the literature have been developed as a single component like an evaporator or condenser. Research has not been performed on combined modeling of parallel evaporators and condensers. Aiming to fill this gap, a combined heat exchanger was developed for two-phase cooling.

The derivation approach used several modeling assumptions associated with the refrigerant flow in the heat exchanger. The following assumptions have been used commonly in past modeling efforts [34] and also summarized in [44]:

- The heat exchanger is assumed to be a thin, long, horizontal tube.
- The heat exchanger refrigerant flow is treated as one-dimensional fluid flow
- The refrigerant axial conduction is negligible.

- The heat exchanger refrigerant pressure is assumed to be uniform.

The model's governing equations are obtained by integrating the PDEs along the length of the heat exchanger tube to remove spatial dependence. Equations (8) and (9) replicate the conservation of refrigerant mass and energy, where $\vec{u}$ is defined as the fluid velocity vector, $\vec{f}$ as the body force vector, and σ as the stress tensor. Given the assumptions outlined previously, Equations (8) and (9) can be simplified to one-dimensional PDEs as Equations (10) and (11). An explanation of PDEs and detailed calculation steps can be found in previous work [45]. The dynamics associated with conservation of momentum is neglected because they are on a time scale much faster than the thermal dynamics. With an additional refrigerant wall energy conservation Equation (12), Equations (10), (11), and (12) form the governing PDEs for a heat exchanger.

$$\frac{\partial \rho}{\partial t} + \nabla \cdot (\rho \vec{u}) = 0 \tag{8}$$

$$\frac{\partial (\rho \vec{u})}{\partial t} + \nabla \cdot (\rho \vec{u} \vec{u}) = \rho \vec{f} + \nabla \cdot \sigma \tag{9}$$

$$\frac{\partial (\rho A_{CS})}{\partial t} + \frac{\partial (\dot{m})}{\partial z} = 0 \tag{10}$$

$$\frac{\partial (\rho A_{CS} h - A_{CS} P)}{\partial t} + \frac{\partial (\dot{m} h)}{\partial z} = p_i \alpha_i (T_w - T_r) \tag{11}$$

$$(C_P \rho A)_w \frac{\partial (\rho T_w)}{\partial t} = p_i \alpha_i (T_r - T_w) + p_{ex} \alpha_{ex} (T_{ex} - T_w) \tag{12}$$

In order to model the combined heat exchanger properly, all potential flow conditions were identified in each evaporator and condenser. Two conditions occurred in the evaporator, as shown in Figure 9. Condition 1 is the evaporator having one control volume with a two-phase region only. Condition 2 is the evaporator having two control volumes, which are two-phase and

superheated regions. Similar to an SMB condenser model, two conditions occurred: a two-phase and subcooled region in one condition and a superheated, two-phase, subcooled region in another. Figure 10 demonstrates the conditions.

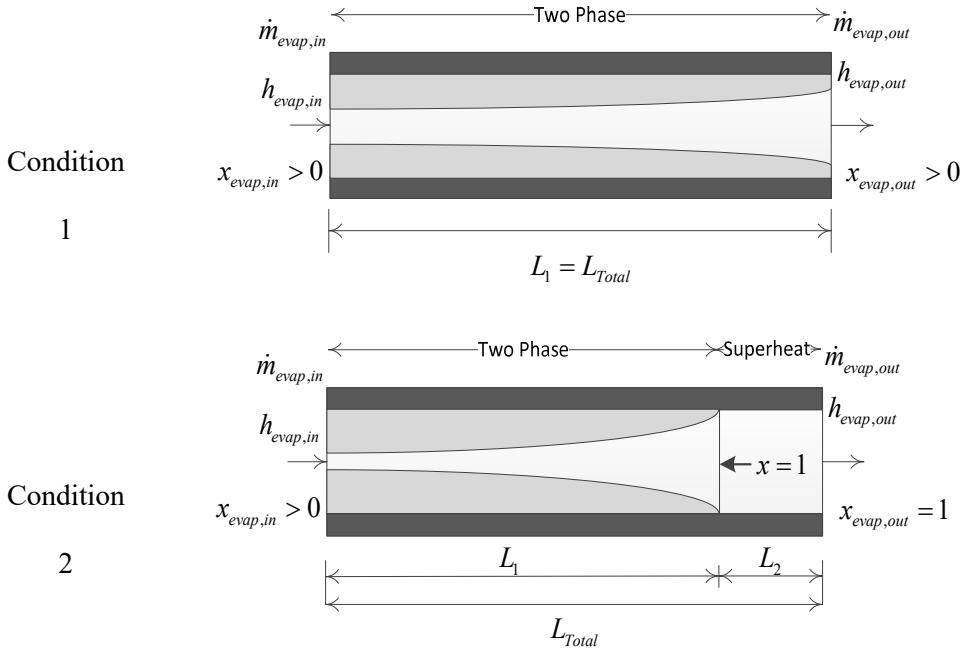

Figure 9: Evaporator conditions

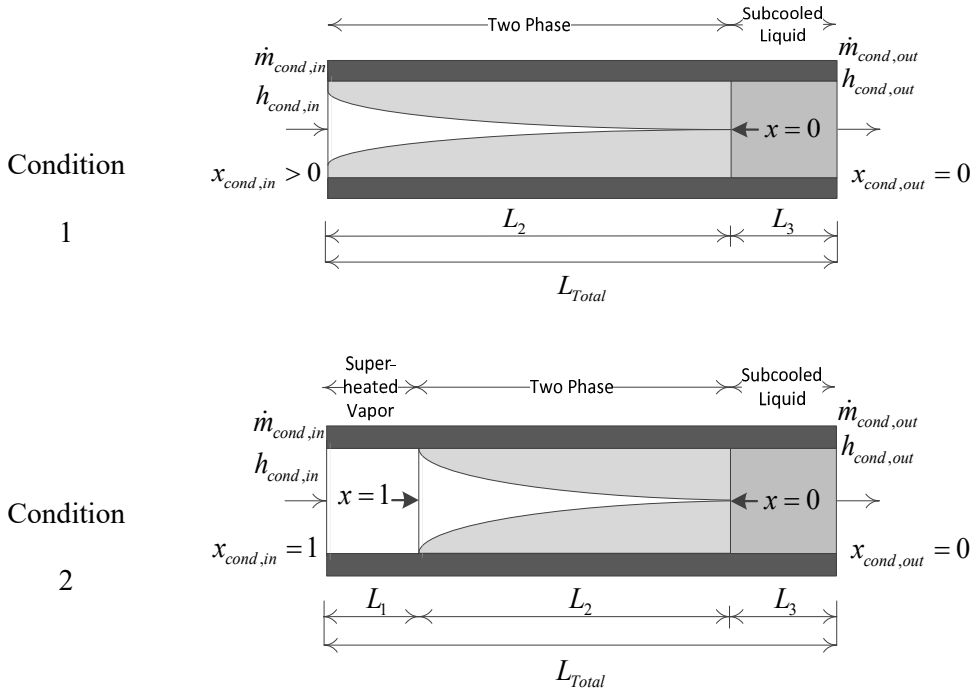

Figure 10: Condenser conditions

The integration along the length was based on Leibniz's equation, with z representing spatial coordinate. For each heat exchanger, the limits of integration depended on how the regions were defined. Table 1 lists the symbols used in equation derivation.

Table 1: Parameters used in the expression of conservation equations

Symbol	Description
P	Pressure of refrigerant
ρ_f	Density of refrigerant at liquid phase
ρ_g	Density of refrigerant at vapor phase
h_f	Enthalpy of refrigerant at liquid phase
h_g	Enthalpy of refrigerant at vapor phases
T_r	Temperature of refrigerant
T_w	Tube wall temperature

Table 1: Continued

Symbol	Description
T_a	External air/fluid temperature
α_i	Heat-transfer coefficient between tube wall and internal fluid
α_o	Heat-transfer coefficient between tube wall and external fluid
A_{cs}	Cross-sectional area of the inside of the tube
A_i	Internal surface area of the heat exchanger
A_o	External surface area of the heat exchanger
$\dot{m}$	Mass flow rate of refrigerant flowing along the tube
$\left(C_p \rho V\right)_w$	Thermal capacity of the tube wall per unit length
$\bar{\gamma}$	Mean void fraction
μ	Weight factor for external air temperature

$$\int_{z_1(t)}^{z_1(t)} \frac{\partial f(z,t)}{\partial t} dz = \frac{d}{dt}\left[\int_{z_1(t)}^{z_1(t)} f(z,t)dz\right] - f(z_2(t),t)\frac{d\left(z_2(t)\right)}{dt} + f(z_1(t),t)\frac{d\left(z_1(t)\right)}{dt} \quad \textbf{(13)}$$

After integrating along the length for each fluid region, the calculated ordinary differential equations were combined and organized into matrix form for each heat exchanger. The detailed steps for solving the PDEs are listed in the Appendix. The final results of the integrated heat exchanger governing PDEs into a matrix form can be presented in the form of Equation (14), where x is the state vector and u is the input vector.

$$Z(x,u)\,\dot{x} = f(x,u) \quad \textbf{(14)}$$

For an evaporator, the explicit time derivatives presented in the equations for conservations of refrigerant mass, refrigerant energy, and wall energy are L_1 , the length of the two-phase region defined by the MB; P_e , the refrigerant pressure in the evaporator; h_{ero} , the

outlet refrigerant enthalpy; and the wall temperatures in the two-phase and superheated regions of the evaporator, $T_{w_1,e}$ and $T_{w_2,e}$. In addition, $\overline{\gamma}_{\mathrm{e}}$, the mean void fraction is included in the state.

Void fraction has been used as a key parameter to describe certain characteristics of two-phase flow, which is defined as the ratio of vapor volume to total volume. In the PTP system, evaporator exit vapor quality is of particular interest as a dynamic variable due to the explicit information it contains for a two-phase fluid. Therefore, mean void fraction must be a time-varying parameter. Several mean void faction prediction methods were proposed based by experimental correlations for different fluids and conditions. Mass Flux Dependent, Lockhart-Martinelli, Homogeneous, Slip Ratio are the four main types. Among the four types, Homogeneous, Slip Ratio are remarkably simple, where the other two are complex. Here, the void faction is defined by the slip ratio as Equation (15), where x is the fluid vapor quality. Equation (16) and (17) are calculated based on the integration of Equation (15) with the assumption that the slip ratio, S, does not dependent on fluid vapor quality, where $\beta = 1 - \alpha$ and $\alpha = \left(\frac{\rho_f}{\rho_f}\right) S$.

$$\gamma = \frac{1}{1 + \left(\frac{1-x}{x}\right)\left(\frac{\rho_g}{\rho_f}\right) S} \tag{15}$$

$$\overline{\gamma} = \frac{1}{x_2 - x_1} \int_{x_1}^{x_2} \gamma(x)\, dx \tag{16}$$

$$\overline{\gamma} = \frac{1}{\beta} + \frac{1}{x_2 - x_1}\left[\frac{\alpha}{\beta} \ln\left(\frac{\beta x_1 + \alpha}{\beta x_2 + \alpha}\right)\right] \tag{17}$$

The vector x for evaporator can be expressed in the form of $x = [L_{1,e} \quad P_e \quad h_{r2,e} \quad T_{w_1,e} \quad T_{w_2,e} \quad \overline{\gamma}_e]^T$, where $h_{2,e} = \frac{1}{2}(h_{ero} + h_g)$. Equation (20) shows the

state space representation of the evaporator model. Q_1 and Q_2 represent the heat load on each fluid region as in Equation (18) and (19).

$$Q_1 = \frac{L_1}{L_{total}} Q \tag{18}$$

$$Q_2 = \frac{L_{total} - L_1}{L_{total}} Q \tag{19}$$

As illustrated in Figure 9, a two-phase-only evaporator system matrix is presented in Equation (20). The system matrix of an evaporator with a two-phase region and superheated vapor region is presented in Equation (21). Z matrix elements are listed in Table 2.

In the evaporator two-phase-only condition, refrigerant energy conservation, mass conservation, and wall conservation were performed only in the two-phase region. Thus, $\dot{h}_{2,e} = k_{eh}(h_g - h_{r2,e})$ and $\dot{T}_{w,2} = k_{ew}(T_{w_1,e} - T_{w_2,e})$ were added to the governing equations for smooth transient behavior when switching between Equation (20) and Equation (21). To be noted, $\overline{\gamma}_{e,total}$ in the system matrix was calculated based on Equation (17), while $\overline{\gamma}_e$ is the integration of $\dot{\overline{\gamma}}_e$ at each time step. $\dot{m}_{int,e}$ is included in the calculation as the interface mass flow rate between the two-phase region and superheated vapor region.

$$\begin{bmatrix} z_{11} & z_{12} & 0 & 0 & 0 & z_{16} & z_{17} \\ z_{21} & z_{22} & z_{23} & 0 & 0 & 0 & z_{27} \\ z_{31} & z_{32} & 0 & 0 & 0 & z_{36} & z_{37} \\ z_{41} & z_{42} & z_{43} & 0 & 0 & 0 & z_{47} \\ z_{51} & 0 & z_{54} & 0 & 0 & 0 & 0 \\ z_{61} & 0 & z_{65} & 0 & 0 & 0 & 0 \\ 0 & z_{72} & 0 & 0 & 0 & z_{76} & z_{77} \end{bmatrix} \begin{bmatrix} \dot{L_{1,e}} \\ \dot{P}_e \\ \dot{h}_{2,e} \\ \dot{T}_{w1} \\ \dot{T}_{e,w2} \\ \dot{\overline{\gamma}}_e \\ \dot{m}_{int,e} \end{bmatrix}$$

$$= \begin{bmatrix} \dot{m}_{eri}\,(h_{eri} - h_{1,e}) - \dot{m}_{ero}\,(h_{ero} - h_{1,e}) + \alpha_{i1,e} A_{i,e} L_{1,e} \left(T_{w_1,e} - T_{w_2,e}\right) \\ 0 \\ \dot{m}_{eri} - \dot{m}_{ero} \\ k_{eh}(h_g - h_{2,e}) \\ \alpha_{ei1} A_{ei} \left(T_{r_1,e} - T_{w_1,e}\right) + Q \\ k_{ew}(T_{w_1,e} - T_{w_2,e}) \\ \dot{m}_{ero} \end{bmatrix} \quad \textbf{(20)}$$

$$\begin{bmatrix} z_{11} & z_{12} & 0 & 0 & 0 & z_{16} & z_{17} \\ z_{21} & z_{22} & z_{23} & 0 & 0 & 0 & z_{27} \\ z_{31} & z_{32} & 0 & 0 & 0 & z_{36} & z_{37} \\ z_{41} & z_{42} & z_{43} & 0 & 0 & 0 & z_{47} \\ z_{51} & 0 & z_{54} & 0 & 0 & 0 & 0 \\ z_{61} & 0 & z_{65} & 0 & 0 & 0 & 0 \\ 0 & z_{72} & 0 & 0 & 0 & z_{76} & z_{77} \end{bmatrix} \begin{bmatrix} \dot{L_{1,e}} \\ \dot{P}_e \\ \dot{h}_{2,e} \\ \dot{T}_{w1} \\ \dot{T}_{e,w2} \\ \dot{\overline{\gamma}}_e \\ \dot{m}_{int,e} \end{bmatrix}$$

$$= \begin{bmatrix} \dot{m}_{eri}\,(h_{eri} - h_{1,e}) + \alpha_{i1,e} A_{i,e} L_{1,e} \left(T_{e,w1} - T_{e,r1}\right) \\ -\dot{m}_{ero}\,(h_{r2,e} - h_g) + \alpha_{i2,e} A_{i,e} L_{2,e} \left(T_{e,w2} - T_{e,r2}\right) \\ \dot{m}_{eri} \\ -\dot{m}_{ero} \\ \alpha_{i1,e} A_{i,e} \left(T_{r_1,e} - T_{w_1,e}\right) + Q_1 \\ \alpha_{i2,e} A_{i,e} \left(T_{r_2,e} - T_{w_2,e}\right) + Q_2 \\ k_{eg}(\overline{\gamma}_e - \overline{\gamma}_{e,total}) \end{bmatrix} \quad \textbf{(21)}$$

Table 2: SMB evaporator *Z* matrix elements

	TP	TP+SH
z_{12}	$A_{CS,e}\frac{L_{1,e}}{L_{total,e}}\left(\rho_{1,e}\frac{dh_{1,e}}{dP}-1\right)$	$A_{CS,e}\frac{L_{1,e}}{L_{total,e}}\left(\rho_{1,e}\frac{dh_{1,e}}{dP}-1\right)$
z_{16}	$A_{CS,e}\frac{L_{1,e}}{L_{total,e}}\rho_{1,e}\frac{dh_{1,e}}{d\bar{\gamma}_e}$	$A_{CS,e}\frac{L_{1,e}}{L_{total,e}}\rho_{1,e}\frac{dh_{1,e}}{d\bar{\gamma}_e}$
z_{17}	0	$\left(h_{g,e}-h_{1,e}\right)$
z_{21}	1	0
z_{22}	0	$-A_{CS,e}\frac{L_{2,e}}{L_{total,e}}$
z_{23}	0	$A_{CS,e}\frac{L_{2,e}}{L_{total,e}}\rho_{2,e}$
z_{27}	0	$\left(h_{2,e}-h_{g,e}\right)$
z_{31}	0	$A_{CS,e}\rho_{1,e}$
z_{32}	$A_{CS,e}\frac{L_{1,e}}{L_{total,e}}\frac{d\rho_{1,e}}{dP}$	$A_{CS,e}\frac{L_{1,e}}{L_{total,e}}\frac{d\rho_{1,e}}{dP}$
z_{36}	$A_{CS,e}\frac{L_{1,e}}{L_{total,e}}\frac{d\rho_{1,e}}{d\bar{\gamma}_e}$	$A_{CS,e}\frac{L_{1,e}}{L_{total,e}}\frac{d\rho_{1,e}}{d\bar{\gamma}_e}$
z_{37}	0	1
z_{41}	0	$-A_{CS,e}\frac{L_{2,e}}{L_{total,e}}$
z_{42}	0	$A_{CS,e}\frac{L_{2,e}}{L_{total,e}}\frac{d\rho_{2,e}}{dP}$
z_{43}	1	$A_{CS,e}\frac{L_{2,e}}{L_{total,e}}\frac{d\rho_{2,e}}{dh_{2,e}}$
z_{47}	0	-1
z_{51}	$(C_P\rho A)_{W,e}\left(\frac{T_{w_1,e}-T_{int,e}}{L_{1,e}}\right)$	$(C_P\rho A)_{W,e}\left(\frac{T_{w_1,e}-T_{w_2,e}}{L_{1,e}}\right)$
z_{54}	$(C_P\rho A)_{W,e}$	$(C_P\rho A)_{W,e}$
z_{61}	0	$(C_P\rho A)_{W,e}\left(\frac{T_{int,e}-T_{w_2,e}}{L_{1,e}}\right)$

Table 2: Continued

	TP	TP+SH
z_{65}	1	$(C_P \rho A)_{W,e}$
z_{72}	$\frac{d\bar{\gamma}_{total,e}}{dP}$	$\frac{d\bar{\gamma}_{total,e}}{dP}$
z_{76}	0	-1
z_{77}	1	0

As in the condenser model, the vector x for the condenser can be expressed in the form $x = [L_{2,c} \quad L_{c,3} \quad P_c \quad h_{3,c} \quad T_{w_1,c} \quad T_{w_2,c} \quad T_{w_3,c} \quad \bar{\gamma}_c]^T$, where $h_{3,c} = \frac{1}{2}(h_{cro} + h_f)$. Equations (22) and (23) show the state space representation of the condenser of condition 1 and condition 2 shown in Figure 10. $\dot{T}_{c,w1} = k_{c,w}(T_{w_2,c} - T_{w_1,c})$ in the system model was used to insure smooth switching between the appearance and disappearance of the first superheated region. To be noted, $\overline{\gamma}_{c,total}$ in the system matrix was calculated based on Equation (17), while $\overline{\gamma}_c$ is the integration of $\dot{\overline{\gamma}}_c$ at each time step. The interface mass flow rate between the superheated vapor region and the two-phase region, $\dot{m}_{int1,c}$, and the interface mass flow rate between the two-phase region and the subcooled liquid region, $\dot{m}_{int2,c}$ are also calculated in the governing equations. The z matrix elements are listed in Table 3.

$$\begin{bmatrix} z_{11} & z_{12} & 0 & 0 & 0 & 0 & 0 & 0 & z_{19} & 0 \\ 0 & z_{22} & 0 & 0 & 0 & 0 & 0 & 0 & z_{29} & z_{2,10} \\ 0 & 0 & z_{33} & z_{34} & 0 & 0 & 0 & 0 & 0 & z_{3,10} \\ z_{41} & z_{42} & z_{43} & 0 & 0 & 0 & 0 & z_{48} & z_{49} & 0 \\ z_{51} & 0 & z_{53} & 0 & 0 & 0 & 0 & z_{58} & z_{59} & z_{5,10} \\ 0 & z_{62} & 0 & z_{64} & 0 & 0 & 0 & 0 & 0 & z_{6,10} \\ z_{71} & z_{72} & 0 & 0 & z_{75} & 0 & 0 & 0 & 0 & 0 \\ z_{81} & z_{82} & 0 & 0 & 0 & z_{86} & 0 & 0 & 0 & 0 \\ 0 & z_{92} & 0 & 0 & 0 & 0 & z_{97} & 0 & 0 & 0 \\ 0 & 0 & z_{10,3} & 0 & 0 & 0 & 0 & z_{10,8} & z_{10,9} & 0 \end{bmatrix} \begin{bmatrix} \dot{L}_{2,c} \\ \dot{L}_{3,c} \\ \dot{P}_c \\ \dot{h}_{3,c} \\ \dot{T}_{w_1,c} \\ \dot{T}_{w_2,c} \\ \dot{T}_{w_3,c} \\ \dot{\bar{\gamma}}_c \\ \dot{m}_{int1,c} \\ \dot{m}_{int2,c} \end{bmatrix} \quad \textbf{(22)}$$

$$= \begin{bmatrix} 0 \\ \dot{m}_{cri}(h_{cri} - h_{2,c}) + \alpha_{i2,c} A_{i,c} L_{2,c} (T_{w_2,c} - T_{r_2,c}) \\ -\dot{m}_{cro}(h_{cro} - h_{3,c}) + \alpha_{i3,c} A_{i,c} L_{3,c} (T_{w_3,c} - T_{r_3,c}) \\ k_{cg}(\overline{\gamma}_c - \overline{\gamma}_{c,total}) \\ \dot{m}_{cri} \\ \dot{m}_{cro} \\ k_{cw}(T_{w_2,c} - T_{w_1,c}) \\ \alpha_{i2,c} A_{i,c}(T_{r2,c} - T_{w_2,c}) + \alpha_o A_o(T_a - T_{w_2,c}) \\ \alpha_{i3,c} A_{i,c}(T_{r3,c} - T_{w_3,c}) + \alpha_o A_o(T_a - T_{w_3,c}) \\ \dot{m}_{cri} \end{bmatrix}$$

$$\begin{bmatrix} z_{11} & z_{12} & 0 & 0 & 0 & 0 & 0 & 0 & z_{19} & 0 \\ 0 & z_{22} & 0 & 0 & 0 & 0 & 0 & 0 & z_{29} & z_{2,10} \\ 0 & 0 & z_{33} & z_{34} & 0 & 0 & 0 & 0 & 0 & z_{3,10} \\ z_{41} & z_{42} & z_{43} & 0 & 0 & 0 & 0 & z_{48} & z_{49} & 0 \\ z_{51} & 0 & z_{53} & 0 & 0 & 0 & 0 & z_{58} & z_{59} & z_{5,10} \\ 0 & z_{62} & 0 & z_{64} & 0 & 0 & 0 & 0 & 0 & z_{6,10} \\ z_{71} & z_{72} & 0 & 0 & z_{75} & 0 & 0 & 0 & 0 & 0 \\ z_{81} & z_{82} & 0 & 0 & 0 & z_{86} & 0 & 0 & 0 & 0 \\ 0 & z_{92} & 0 & 0 & 0 & 0 & z_{97} & 0 & 0 & 0 \\ 0 & 0 & z_{10,3} & 0 & 0 & 0 & 0 & z_{10,8} & z_{10,9} & 0 \end{bmatrix} \begin{bmatrix} \dot{L}_{2,c} \\ \dot{L}_{3,c} \\ \dot{P}_c \\ \dot{h}_{3,c} \\ \dot{T}_{w_1,c} \\ \dot{T}_{w_2,c} \\ \dot{T}_{w_3,c} \\ \dot{\bar{\gamma}}_c \\ \dot{m}_{int1,c} \\ \dot{m}_{int2,c} \end{bmatrix} \quad \textbf{(23)}$$

$$= \begin{bmatrix} \dot{m}_{cri}\left(h_{cri} - h_{1,c}\right) + \alpha_{i1,c}A_{i,c}L_{1,c}\left(T_{w_1,c} - T_{r_1,c}\right) - 0.5A_{CS,c}\dfrac{L_{1,c}}{L_{total,c}}\rho_{1,c}\dfrac{dh_{cri}}{dt} \\ \alpha_{i2,c}A_{i,c}L_{2,c}(T_{w_2,c} - T_{r_2,c}) \\ -\dot{m}_{cro}(h_{cro} - h_{3,c}) + \alpha_{i3,c}A_{i,c}\dfrac{L_{3,c}}{L_{total,c}}(T_{w_3,c} - T_{r_3,c}) \\ \dot{m}_{cri} - A_{CS,c}L_{1,c}\dfrac{d\rho_{1,c}}{dh_{cri}}\dfrac{dh_{cri}}{dt} \\ 0 \\ -\dot{m}_{cro} \\ \alpha_{i1,c}A_{i,c}\left(T_{r_1,c} - T_{w_2,c}\right) + \alpha_o A_o\left(T_a - T_{w_2,c}\right) \\ \alpha_{i2,c}A_{i,c}\left(T_{r_2,c} - T_{w_2,c}\right) + \alpha_o A_o\left(T_a - T_{w_2,c}\right) \\ \alpha_{i3,c}A_{i,c}\left(T_{r_3,c} - T_{w_3,c}\right) + \alpha_o A_o\left(T_a - T_{w_3,c}\right) \\ k_{cg}(\overline{\gamma}_c - \overline{\gamma}_{c,total}) \end{bmatrix}$$

Table 3: SMB condenser *Z* matrix elements

	TP+SL	SH+TP+SL
z_{11}	1	$A_{CS,c}\dfrac{L_{1,c}}{L_{total,c}}\left(0.5\rho_{1,c}\dfrac{dh_g}{dP} - 1\right)$
z_{12}	1	0
z_{19}	0	$\left(h_{g,c} - h_{1,c}\right)$
z_{23}	$A_{CS,c}\dfrac{L_{2,c}}{L_{total,c}}\left(\rho_{2,c}\dfrac{dh_{2,c}}{dP} - 1\right)$	$A_{CS,c}\dfrac{L_{2,c}}{L_{total,c}}\left(\rho_{2,c}\dfrac{dh_{2,c}}{dP} - 1\right)$
z_{28}	$A_{CS,c}\dfrac{L_{2,c}}{L_{total,c}}\rho_{2,c}\dfrac{dh_{2,c}}{d\bar{\gamma}_c}$	$A_{CS,c}\dfrac{L_{2,c}}{L_{total,c}}\rho_{2,c}\dfrac{dh_{2,c}}{d\bar{\gamma}_c}$
z_{29}	$\left(h_{f,c} - h_{2,c}\right)$	$\left(h_{2,c} - h_{g,c}\right)$
$z_{2,10}$	0	$\left(h_{f,c} - h_{2,c}\right)$
z_{33}	$-A_{CS,c}\dfrac{L_{3,c}}{L_{total,c}}$	$-A_{CS,c}\dfrac{L_{3,c}}{L_{total,c}}$
z_{34}	$A_{CS,c}\dfrac{L_{3,c}}{L_{total,c}}\rho_{3,c}$	$A_{CS,c}\dfrac{L_{3,c}}{L_{total,c}}\rho_{3,c}$
$z_{3,10}$	$h_{3,c} - h_{f,c}$	$h_{3,c} - h_{f,c}$

Table 3: Continued

	TP+SL	SH+TP+SL
z_{41}	0	$-A_{CS,c}\rho_{1,c}$
z_{42}	0	$-A_{CS,c}\rho_{1,c}$
z_{43}	$\frac{d\bar{\gamma}_{total,c}}{dP}$	$A_{CS,c}\frac{L_{1,c}}{L_{total,c}}\frac{d\rho_{1,c}}{dh_{cri}}$
z_{48}	-1	0
z_{49}	0	1
z_{51}	$A_{CS,c}\rho_{2,c}$	$A_{CS,c}\rho_{2,c}$
z_{53}	$A_{CS,c}\frac{L_{2,c}}{L_{total,c}}\frac{d\rho_{2,c}}{dP}$	$A_{CS,c}\frac{L_{2,c}}{L_{total,c}}\frac{d\rho_{2,c}}{dP}$
z_{58}	$A_{CS,c}\frac{L_{2,c}}{L_{total,c}}\frac{d\rho_{2,c}}{d\bar{\gamma}_c}$	$A_{CS,c}\frac{L_{2,c}}{L_{total,c}}\frac{d\rho_{2,c}}{d\bar{\gamma}_c}$
z_{59}	0	-1
$z_{5,10}$	1	1
z_{62}	$A_{CS,c}\rho_{3,c}$	$A_{CS,c}\rho_{3,c}$
z_{64}	$A_{CS,c}\frac{L_{3,c}}{L_{total,c}}\frac{d\rho_{3,c}}{dh_{3,c}}$	$A_{CS,c}\frac{L_{3,c}}{L_{total,c}}\frac{d\rho_{3,c}}{dh_{3,c}}$
$z_{6,10}$	-1	-1
z_{71}	0	$-(C_P\rho A)_{W,c}\left(\frac{T_{w_1,c}-T_{int1,c}}{L_{1,c}}\right)$
z_{72}	0	$-(C_P\rho A)_{W,c}\left(\frac{T_{w_1,c}-T_{int1,c}}{L_{1,c}}\right)$
z_{75}	1	$(C_P\rho A)_{W,c}$
z_{81}	$(C_P\rho A)_{W,c}\left(\frac{T_{w_2,c}-T_{int2,c}}{L_{3,c}}\right)$	$-(C_P\rho A)_{W,c}\left(\frac{T_{int1,c}-T_{int2,c}}{L_{2,c}}\right)$ $+(C_P\rho A)_{W,c}\left(\frac{T_{w_2,c}-T_{int2,c}}{L_{2,c}}\right)$
z_{82}	0	$-(C_P\rho A)_{W,c}\left(\frac{T_{int1,c}-T_{int2,c}}{L_{2,c}}\right)$

Table 3: Continued

	TP+SL	SH+TP+SL
z_{86}	$(C_P \rho A)_{W,c}$	$(C_P \rho A)_{W,c}$
z_{92}	$(C_P \rho A)_{W,c}\left(\frac{T_{w_3,c} - T_{int2,c}}{L_{3,c}}\right)$	$-(C_P \rho A)_{W,c}\left(\frac{T_{int2,c} - T_{w_3,c}}{L_{3,c}}\right)$
z_{97}	$(C_P \rho A)_{W,c}$	$(C_P \rho A)_{W,c}$
$z_{10,3}$	$\frac{d\bar{\gamma}_{total,c}}{dP}$	$\frac{d\bar{\gamma}_{total,c}}{dP}$
$z_{10,8}$	0	-1
$z_{10,9}$	1	0

The SMB model has ability to handle the disappearance and appearance of fluid regions by switching between different MB models. During system start-up or shut-down, the absence of a fluid region drives the region length to zero, thus causing the governing equations to become singular. To prevent simulation failure, appropriate switching criteria must be met during the fluid phase region change.

Mckinley and Alleyne [39] proposed the void fraction switching scheme which is used in the evaporator model. Switching criteria are defined in Table 4. The model switches from the evaporator with both two-phase fluid region and superheated vapor region (TP+SH) to two phase region only (TP) when the superheated vapor region length, L_{e2} , is close to zero and the time derivative of L_{e2} is less than zero. The model switches from evaporator with two-phase region only (TP) to both two-phase region and superheated vapor in the evaporator (TP+V) when the time derivative of mean void fraction, $\dot{\bar{\gamma}}_e$, is greater than zero, which indicates the presence of

superheated vapor in the evaporator. A minimum threshold length, L_{eps} is a pre-defined value as a percentage of the total tube length to provide numerical stability.

Table 4: Evaporator switching criteria

TP→TP+SH	TP←TP+SH
$\dot{\overline{\gamma}}_e > 0$	$L_{e2} \leq L_{eps} L_{e,total}$
$\frac{L_{e1}}{L_{e,total}}\left(\overline{\gamma}_e - \overline{\gamma}_{e,total}\right) > L_{eps}^2$	$\dot{L}_{e2} < 0$

In the condenser, the model switches from the condition where only two-phase fluid and subcooled liquid (TP+SL) is present to all the fluid phase regions (SH+TP+SL) are in the condenser by comparing inlet refrigerant enthalpy, h_{cri} with the saturated vapor enthalpy. An enthalpy tolerance, h_{eps}, is added to the saturated vapor enthalpy based on Bonilla et al. [43] to reduce chattering. Table 5 summaries the condenser switching criteria.

Table 5: Condenser switching criteria

TP+SL→SH+TP+SL	TP+SL ← SH+TP+SL
$h_{cri} \geq h_g + h_{eps}$	$h_{cri} \leq h_g + h_{eps}$
$\frac{L_{c2}}{L_{c,total}}\left(\overline{\gamma}_c - \overline{\gamma}_{c,total}\right) > L_{eps}^2$	

In the MB model, the wall temperature at the interfaces between regions varies along with the sizes of the regions. The wall temperature at the interface were calculated as a weighted mean of the wall temperatures in the two-phase and superheated regions (or two-phase and

subcooled regions) to consider the varying sizes of the region (i.e., $T_{w,int} = \frac{L_2}{L_{total}} T_{w,1} + \frac{L_1}{L_{total}} T_{w,2}$) [38]. Pressure was assumed to be the same in the combined heat exchanger.

As listed in Equation (24), the total evaporator outlet mass flow equals to the condenser inlet mass flow rate. While the total evaporator outlet refrigerant energy equals to the condenser inlet refrigerant energy as shown in Equation (25). Including Equations (24) and (25) with the evaporator and condenser model derivation, the combined heat exchanger can be put in the form as Equation (26). State vectors within the evaporator at each instance of time are: $x_{e_n} = \begin{bmatrix} L_{1,e_n} & h_{1,e_n} & T_{w_1,e_n} & T_{w_2,e_n} & \overline{\gamma}_{e_n} \end{bmatrix}$. The condenser state vector is $x_c = [L_{2,c} \quad L_{3,c} \quad h_{cr3} \quad T_{w_1,c} \quad T_{w_2,c} \quad T_{w_3,c} \quad \overline{\gamma}_c]$. f_{e_n} and f_c are defined as evaporator and condition f vectors. Detailed mathematical presentations are shown in Appendix.

$$\sum_{j=1}^{n} \dot{m}_{ero,j} = \dot{m}_{cri} \tag{24}$$

$$\sum_{j=1}^{n} h_{ero,j} \dot{m}_{ero,j} = \dot{m}_{cri} h_{cri} \tag{25}$$

$$\begin{bmatrix} Z_{e_1,1} & Z_{e_1,2} & 0 & 0 & 0 & 0 & 0 \\ Z_{e_2,1} & 0 & Z_{e_2,2} & 0 & 0 & 0 & 0 \\ Z_{e_3,1} & 0 & 0 & Z_{e_3,2} & 0 & 0 & 0 \\ Z_{e_4,1} & 0 & 0 & 0 & Z_{e_4,2} & 0 & 0 \\ \vdots & 0 & 0 & 0 & 0 & \ddots & 0 \\ Z_{e_n,1} & 0 & 0 & 0 & 0 & Z_{e_n,2} & 0 \\ Z_{c_1} & Z_{c_2,1} & Z_{c_2,2} & Z_{c_2,4} & \dots & Z_{c_2,n} & Z_{c_3} \end{bmatrix} \begin{bmatrix} \dot{P} \\ \dot{x}_{e_1} \\ \dot{x}_{e_2} \\ \dot{x}_{e_3} \\ \vdots \\ \dot{x}_{e_n} \\ \dot{x}_c \end{bmatrix} = \begin{bmatrix} f_{e_1} \\ f_{e_2} \\ f_{e_3} \\ f_{e_4} \\ \vdots \\ f_{e_n} \\ f_c \end{bmatrix} \tag{26}$$

The simulation used Equation (26) as the general governing equation for the combined heat exchanger. With the setup in Equation (26), the simulation has feasibility of choosing any

number of evaporators to be included in the system. Detailed calculations of block Z matrixes are shown in the Appendix.

With n numbers of evaporators included in the model, the computational speed of the model became important. Figure 11 shows the real time factor of the combined heat exchanger model running on a standard desktop computer. The real-time factor is defined as computational time over length of simulated time. A selected number of evaporators were tested. The figure reveals the real-time factor from two evaporators for up to 60 evaporators in parallel. A trend can be discovered from the plotted line. From the plot, the real time factor can be predicted for up to hundreds of evaporators.

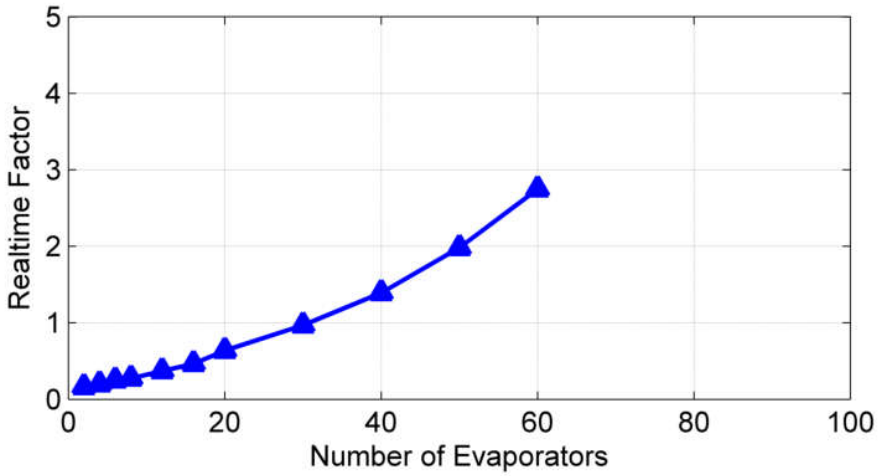

Figure 11: Number of evaporators vs. computational time

2.5. Multi-evaporator Pumped Two-Phase System

To simulate a real-case scenario, heat exchanger pressure was set to 760 kPa, and the saturated temperature of the refrigerant (R134a) was 30 °C. These specific testing conditions were selected based on real operating conditions for a small-scale electronics-cooling

application. The surface temperature of most silicon-based electronics must be maintained under 85 °C for safety. Some data center applications would like to have a surface temperature below 40°C. A 30 °C refrigerant temperature should be adequate to cover most applications. The heat flux on each evaporator was set to 495 Watts as a typical heat load. Refrigerant mass flow rate on one evaporator was set to be 0.003 kg/s. This value demonstrates one leading characteristic of a two-phase cooling system, reduced mass flow rate. The parameters chosen in this case are presented as those for a study case. Any realistic physical parameters and operating conditions can be used in the designed model. The simulation parameters chosen are based on the prototype PTP cooling system for server bank shown in Figure 12 with the parameters in Table 6.

Figure 12: Prototype PTP cooling system for server banks

Table 6: Key parameters used in the simulation

Description	Symbol	Value
Evaporator Mass [kg]	$Mass_e$	0.05
Evaporator Internal Area [m^2]	$A_{i,e}$	0.1
Evaporator External Area [m^2]	$A_{o,e}$	0.75
Evaporator Cross-section Area [m^2]	$A_{cs,e}$	$7.5e^{-5}$
Evaporator Tube Diameter [m]	d_e	$5e^{-3}$
Condenser Mass [kg]	$Mass_c$	1
Condenser Internal Area [m^2]	$A_{i,c}$	0.275
Condenser External Area [m^2]	$A_{o,c}$	2.8
Condenser Cross-section Area [m^2]	$A_{cs,c}$	$5.1e^{-5}$
Evaporator Tube Diameter [m]	d_c	$8.1e^{-3}$

Changes in heat load are typical in electronics applications. To test system performance, multiple heat load step changes were applied to each evaporator. The system response is presented in Figure 13. Heat exchanger pressure, wall temperature, superheat, evaporator exit quality, and refrigerant mass flow rate were all plotted. The initial system operating condition was chosen to be at a high quality level, 0.98, at the outlet of each evaporator. With 5% of normial heat flux step, the evaporator outlet showed 7 °C of superheat. Each evaporator showed its own ability to switch between the two-phase and superheated regions. Wall temperatures increased significantly with the presense of superheated vapor, which urged an effective control method to to avoid superheat and maintain wall temperature. While heat load step change was only applied to one evaporator, the remaining three evaporators also showed the presence of superheat with increased wall temperatures. Coupled dynamics were observed between multiple evaporators. A pump-speed step change also was simulated, shown in Figure 14. Total valve refrigerant mass flow rate changed along with the pump refrigerant mass flow rate. With the pump speed step change, the system pressure changed correspondingly which indicated the

possibility of using a variable speed pump to regulate system pressure. During the step changes, the system response time was observed to be around 50 seconds to 100 seconds. This is due to the constant reservoir between the pump and valves. With fluid condition changes in the pump or heat exchangers, the valves' response time is slower due to the lack of dynamics in the constant reservoir. In real-time applications, system without a constant reservoir or with a temperature controlled and pressure controlled surge tank will have faster valve responses.

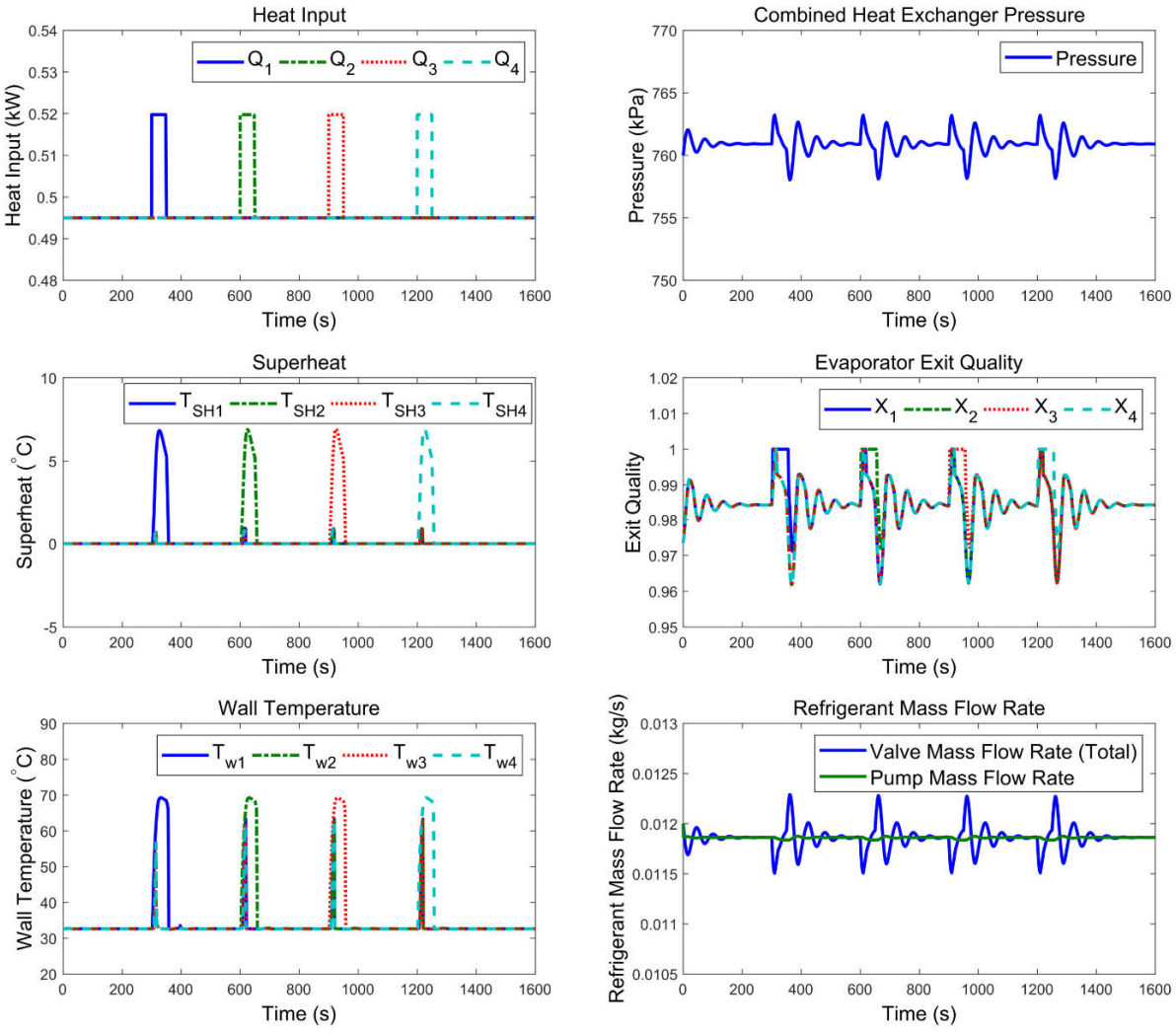

Figure 13: System response for changes in external heat flux

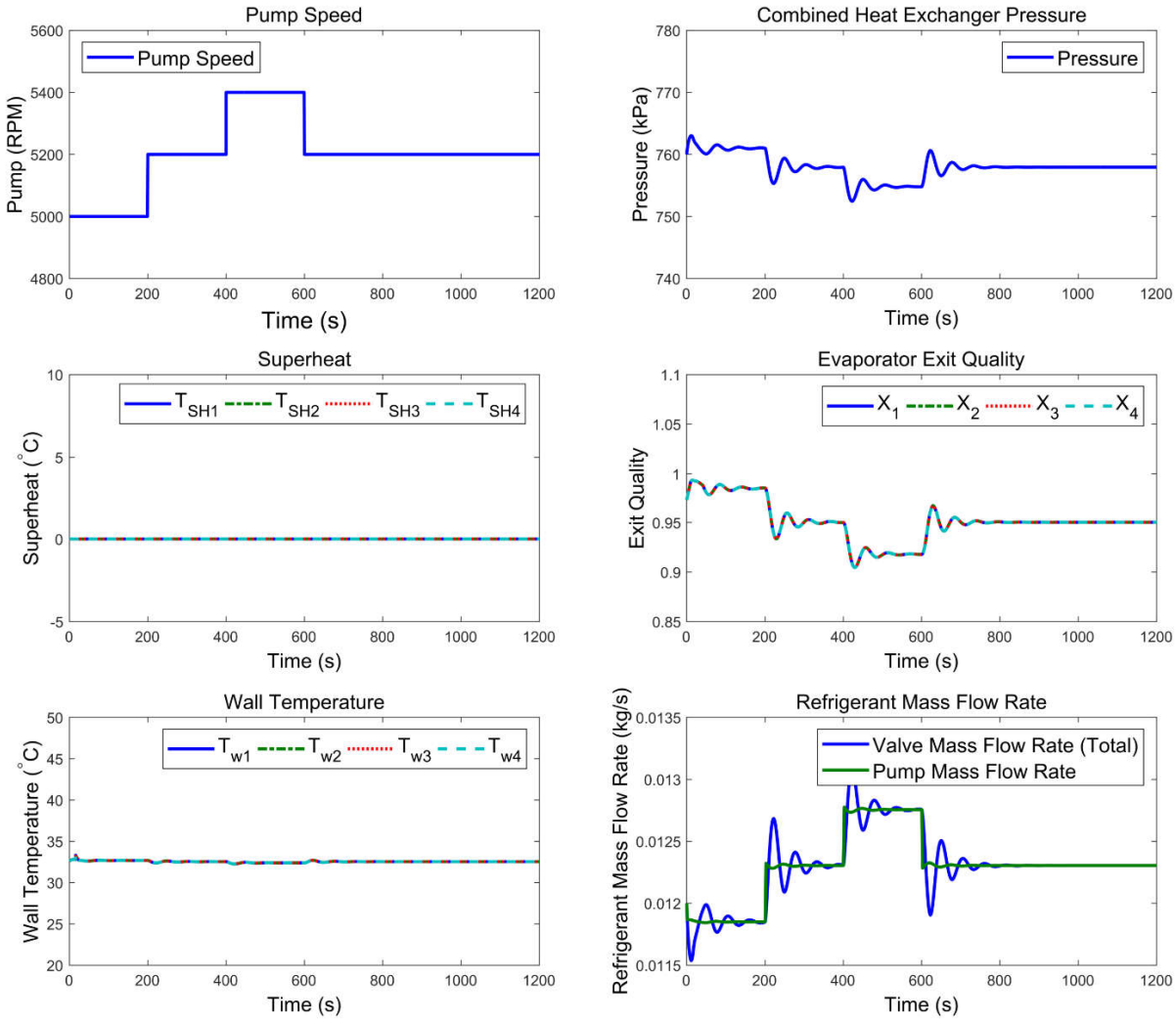

Figure 14: System response with pump-speed step change

3. CONTROL ARCHITECTURE DESIGN FOR MULTI-EVAPORATOR PUMPED TWO-PHASE SYSTEM

With a proper dynamic PTP system model in place, we were able to examine the control architecture of the multi-evaporator PTP system. The essential goal of using PTP cooling is to maintain constant chip temperature during system operation.

In normal operating conditions, the heat exchanger refrigerant temperature is always the saturated temperature under current system pressure, as the exit quality is always constrained to be less than one. In addition to the two-phase wall temperature and pressure dependency, multi-evaporator systems have the natural behavior of coupled dynamics. A system can be represented in the form of Equation (27).The variable $y(s)$ represents the system output, and $u(s)$ represents the system input. $G(s)$ is the system transfer function. In the current four-evaporator PTP system, $y(s)$ is $[T_{w1} \quad T_{w2} \quad T_{w3} \quad T_{w3} \quad P]^T$, which is the refrigerant wall temperature and heat exchanger pressure of the evaporators. $u(s)$ is the system input signals, $[v_1 \quad v_2 \quad v_3 \quad v_4 \quad \omega_p]^T$, which corresponds to valve opening positions and pump speed. Equation (28) is the detailed system transfer function to relate inputs to outputs. Step tests were performed on each individual actuator and variable-speed pump and on valves to solve the static-system gain matrix of $G(s)$. $G(0)$ in Equation (29) is the static gain matrix of current system parameters. It is calculated by doing step changes of each input and correlating inputs and outputs based on Equation (28).

$$y(s) = G(s)u(s) \tag{27}$$

$$\begin{bmatrix} T_{w1} \\ T_{w1} \\ T_{w1} \\ T_{w1} \\ P \end{bmatrix} = \begin{bmatrix} G_{11} & G_{12} & G_{13} & G_{14} & G_{15} \\ G_{21} & G_{22} & G_{23} & G_{24} & G_{25} \\ G_{31} & G_{32} & G_{33} & G_{34} & G_{35} \\ G_{41} & G_{42} & G_{43} & G_{44} & G_{45} \\ G_{51} & G_{52} & G_{53} & G_{54} & G_{55} \end{bmatrix} \begin{bmatrix} v_1 \\ v_1 \\ v_1 \\ v_1 \\ \omega_p \end{bmatrix} \quad \textbf{(28)}$$

$$G(0) = \begin{bmatrix} -3.45 & 0.02 & 0.02 & 0.02 & -0.00069 \\ 0.02 & -3.45 & 0.02 & 0.02 & -0.00061 \\ 0.02 & 0.02 & -3.45 & 0.02 & -0.00069 \\ 0.02 & 0.02 & 0.02 & -3.45 & -0.00069 \\ 0.44 & 0.44 & 0.44 & 0.44 & -0.015 \end{bmatrix} \quad \textbf{(29)}$$

In order to be used in the analysis, $G(0)$ was scaled based on expected magnitudes of disturbances and reference changes, on the allowed magnitude of each input signal, and on the allowed deviation of each input, as shown in Equations (30) and (31). The scaled $G_s(0)$ is presented in Equation (32).

$$y = \frac{\hat{y}}{\hat{e}_{max}} \quad \textbf{(30)}$$

$$u = \frac{\hat{u}}{\hat{u}_{max}} \quad \textbf{(31)}$$

In these equations, a hat ($\widehat{\ }$) shows that the variables are in their unscaled units: $\hat{e}_{max}$ is the largest allowed control error, $\hat{u}_{max}$ is the largest allowed input change.

$$G_s(0) = \begin{bmatrix} -1.8 & 0.01 & 0.01 & 0.01 & -0.03 \\ 0.01 & -1.8 & 0.01 & 0.01 & -0.03 \\ 0.01 & 0.01 & -1.8 & 0.01 & -0.03 \\ 0.01 & 0.01 & 0.01 & -1.8 & -0.03 \\ 0.7 & 0.7 & 0.7 & 0.7 & -2.01 \end{bmatrix} \quad \textbf{(32)}$$

Any matrix G may be decomposed into its singular value decomposition, as shown in Equations (33) to (36). The condition number of a matrix is defined as the ratio between the maximum and minimum singular values. For the current PTP system, the condition number was 2.1, as shown in Equation (37). The condition number can be used as an input-output

controllability measure. The calculated condition number was less than 10. The system was not ill-conditioned.

$$G = U\Sigma V^H \tag{33}$$

$$U = \begin{bmatrix} -0.2452 & 0.0000 & 0.8660 & 0.866 & -0.4358 \\ -0.2452 & 0.1892 & -0.2887 & 0.7943 & -0.4358 \\ -0.2452 & -0.7825 & -0.2887 & -0.2333 & -0.4358 \\ -0.2452 & 0.5932 & 0.2887 & 0.5610 & -0.4358 \\ 0.8715 & 0.0000 & 0.0000 & 0.0000 & -0.4903 \end{bmatrix} \tag{34}$$

$$\Sigma = \begin{bmatrix} 2.7 & 0 & 0 & 0 & 0 \\ 0 & 1.8 & 0 & 0 & 0 \\ 0 & 0 & 1.8 & 0 & 0 \\ 0 & 0 & 0 & 1.8 & 0 \\ 0 & 0 & 0 & 0 & 1.3 \end{bmatrix} \tag{35}$$

$$V^H = \begin{bmatrix} 0.3857 & 0 & -0.8660 & 0 & 0.3182 \\ 0.3857 & -0.1892 & 0.2887 & -0.7943 & 0.3182 \\ 0.3857 & 0.7825 & 0.2887 & 0.2333 & 0.3182 \\ 0.3857 & -0.5932 & -0.2887 & 0.5610 & 0.3182 \\ -0.6363 & -0.0000 & -0.0000 & -0.0000 & 0.7714 \end{bmatrix} \tag{36}$$

$$\gamma(G) \triangleq \frac{\bar{\sigma}(G)}{\underline{\sigma}(G)} = \frac{2.7}{1.3} = 2.1 \tag{37}$$

Bristol [46] showed that the relative gain array (RGA) provides a measure of interactions between inputs and outputs. The RGA for the current system is calculated in Equation (38) with the pairing in Table 7. The selected pairing had an RGA matrix close to identity. Refrigerant wall temperatures could be controlled by each valve. Heat exchanger pressure could be controlled by the variable-speed pump.

$$RGA \quad \Lambda(G) = \begin{bmatrix} 0.9942 & -0.000 & -0.000 & -0.000 & 0.0058 \\ -0.000 & 0.9942 & -0.000 & -0.000 & 0.0058 \\ -0.000 & -0.000 & 0.9942 & -0.000 & 0.0058 \\ -0.000 & -0.000 & -0.000 & 0.9942 & 0.0058 \\ 0.0058 & 0.0058 & 0.0058 & 0.0058 & 0.9769 \end{bmatrix} \tag{38}$$

Table 7: Input and output pairing

Inputs	Outputs
Valve 1	T_{w_1}
Valve 2	T_{w_2}
Valve 3	T_{w_3}
Valve 4	T_{w_4}
Pump	P

3.1. Decoupled PI Controllers

In two-phase refrigerant cooling, as the refrigerant in the evaporators is always saturated boiling, the refrigerant temperature is the saturated temperature of the system pressure. Maintaining a constant system pressure is as important as maintaining constant chip temperature. Thus, as shown in the pairing in Table 7, inlet valve feedback controls were combined with a pump feedback control to maintain constant system temperature and pressure.

Multi-evaporator system has the natural behavior of coupling between the evaporators. To solve the coupling issues in the multi-evaporator PTP system, a decoupling matrix was utilized along with the controllers. The term "decoupling" refers to diagonal decoupling, which means each input/output is independent. In PTP cooling, a decoupling matrix separates the coupled interactions multiple evaporators in parallel and the coupled behavior between refrigerant wall temperatures and pressures. $G(0)$ is the system gain matrix of the system transfer function. $G^{-1}(0)$ is the inverse of the system gain matrix.

$$G^{-1}(0) = \begin{bmatrix} -0.29 & -0 & -0 & -0 & 0.0132 \\ -0 & -0.29 & -0 & -0 & 0.0132 \\ -0 & -0 & -0.29 & -0 & 0.0132 \\ -0 & -0 & -0 & -0.29 & 0.0132 \\ -8.38 & -8.38 & -8.38 & -8.38 & -64.57 \end{bmatrix} \quad \textbf{(39)}$$

Proportional-integral (PI) controllers are commonly used in VCC cooling. PTP systems and VCC systems have similar nonlinearity issues and coupled dynamics, so PI controllers are considered to be a promising approach in PTP cooling. Surface wall temperature was used as the feedback signal to a PI valve controller to maintain a constant chip temperature. The valve gradually changed inlet mass flow rate to compensate for the oscillations detected in the system. A controller schematic is shown in Figure 15**.**

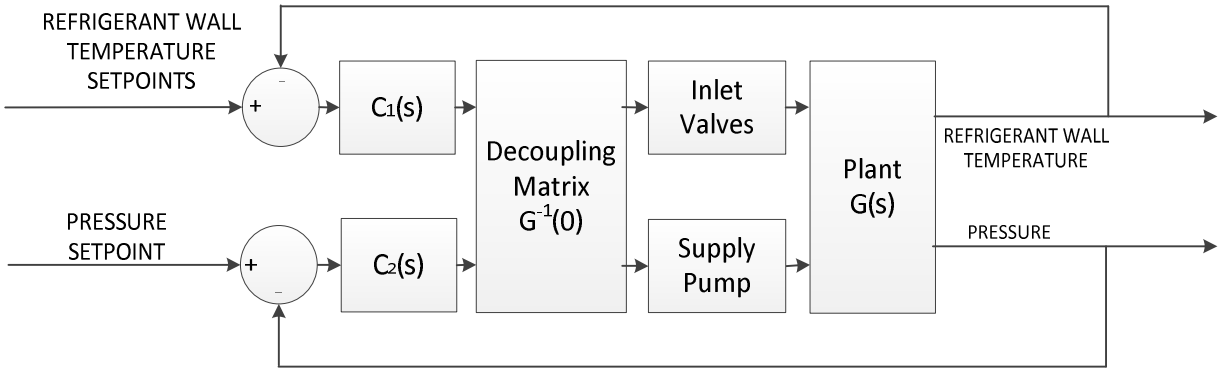

Figure 15: Controller schematic

Figure 16 shows a system test of 10% heat increase in each evaporator. The system pressure was maintained at a constant value during the heat changes. In this server-bank-cooling application, the evaporator size was relatively small, resulting in a short disturbance response time. Because of a high evaporator-exit quality initial condition and the wall temperatures changes were small before the appearance of superheats, the decoupled two-phase control architecture was not enough to compensate for the rapidly increasing wall temperatures with the appearance of superheats. During the heat step increase on evaporator 1, superheat was only observed on evaporator 1. This demonstrated the functionality of the decoupling matrix in the control architecture. However, the system was still at risk for CHF, with 10% heat load impulses.

A superheat of 5 °C could result in a 70 °C evaporator wall temperature. The system showed different evaporator superheats at the same level of heat load step changes. This is due to when the wall temperature feedback control was regulating mass flow rate to compensate the increased wall temperature, it also changed the evaporator exit vapor quality. Evaporator 2, 3, 4 were at a different exit quality condition during the heat step changes comparing with initial condition. Thus, simple decoupled PI controllers were determined to be insufficient in PTP cooling for CHF avoidance.

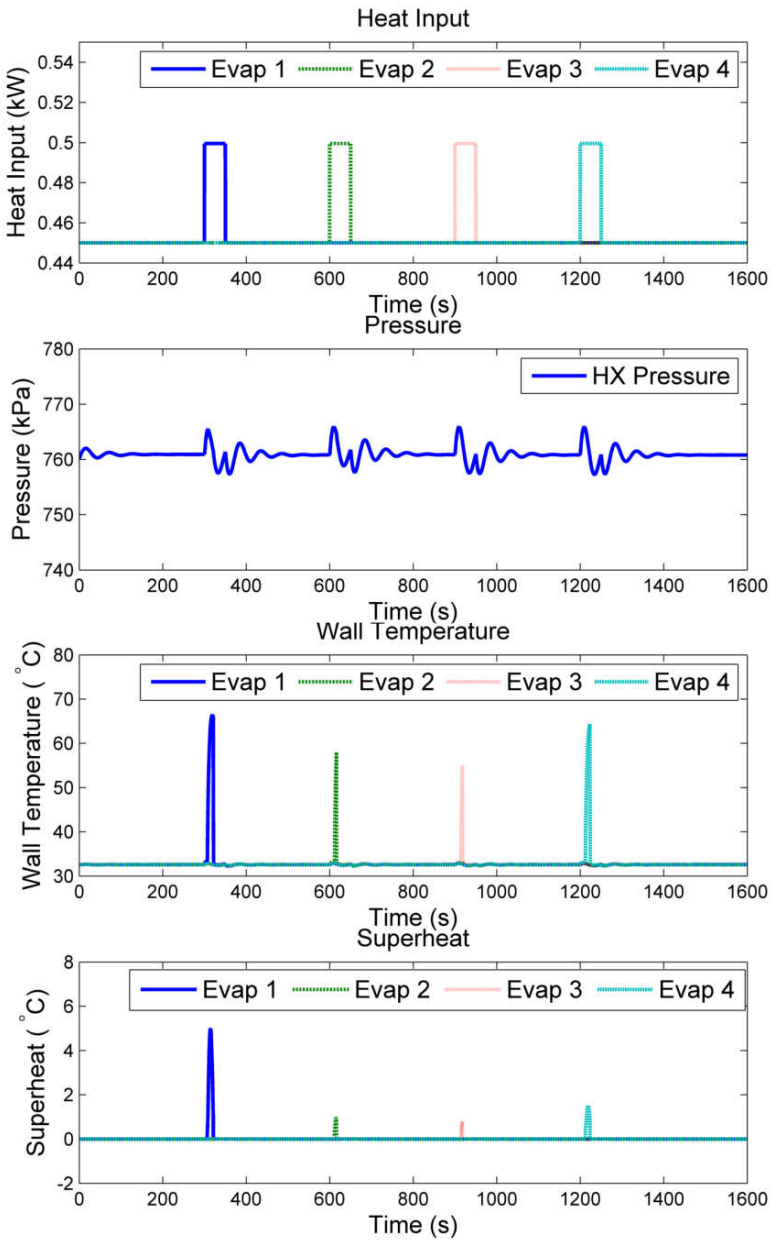

Figure 16: PTP system with decoupled PI controllers under heat load disturbances

The decoupled PI controllers were shown to be successful in decoupling the dynamics between multiple evaporators but still have limitations in CHF avoidance. This is due to the fact that before the appearance of superheat, the refrigerant temperature is always the saturated temperature of the system pressure regardless of the vapor quality. With the pump feedback

controller, $C_2(s)$, regulating the system pressure, the refrigerant wall temperature fluctuation is relatively small when only two-phase fluid is in the evaporator. The wall temperature feedback controller, $C_1(s)$, does not have enough feedback signal. Thus, extra control techniques were needed in combination with the decoupled PI controllers to solve the issues in PTP cooling. Two control architectures are proposed and compared here to solve the problems experienced in different load conditions.

3.2. Decoupled PI Controllers with Estimated Exit quality Feedback

In two-phase cooling, refrigerant temperature is always the saturated temperature of the pressure (i.e., superheat is zero at saturated boiling). As a result, neither wall temperature nor superheat is a good parameter to indicate CHF. A direct indicator is vapor quality. The two-phase vapor quality x defined as a function of enthalpy h is as follows:

$$x = \frac{h - h_f}{h_{fg}} \tag{40}$$

where h_f is the saturated liquid enthalpy, and h_{fg} is the fluid enthalpy of vaporization.

However, two-phase vapor quality is not a measurable parameter. For two-phase saturated conditions, temperature is constant for any quality values for a given pressure. An exit quality estimation method is proposed in the controller design.

Condenser outlet is always subcooled liquid to ensure safe operation of the pump. The energy balance equation for the condenser is given by the following:

$$\dot{q}_{cond} = \dot{m}_c(h_{cri} - h_{cro}) = c_p\dot{m}_w(T_{wo} - T_{wi}) \tag{41}$$

where $\dot{q}_{cond}$ is heat removed by the condenser, which is the same as the energy increased on the external water side based on energy conservation. $\dot{m}_c$ and $\dot{m}_w$ are the mass flow rate of the

refrigerant and external fluid flow rate, respectively. c_P is the specific heat of the external fluid. h_{cri} and h_{cro} are the condenser inlet and outlet enthalpy, respectively. Condenser outlet enthalpy can be obtained by refrigerant property mapping using condenser outlet refrigerant temperature and pressure measurements, as shown in Equation (42). T_{wo} and T_{wi} are the external fluid outlet and inlet temperatures.

$$h_{cro} = h(P_C\ , T_{cro}\ ) \tag{42}$$

Combining Equation (41) and (42), h_{cri} can be calculated as,

$$h_{cri} = \frac{c\dot{m}_w(T_{wo} - T_{wi})}{\dot{m}_c} + h(P_C\ , T_{cro}\ ) \tag{43}$$

From the system schematic, the evaporator exit lines were shown to merge into the condenser inlet. The average estimated evaporator exit quality can be expressed by the following:

$$x_{est} = \frac{\left(h_{cri} - h_f\right)}{h_{fg}} \tag{44}$$

An estimated evaporator exit quality feedback control is proposed with the decoupled PI control architecture. The schematic of the control architecture is shown in Figure 17. In such a control architecture, the estimated exit quality PI controller ($C_3(s)$) maintains a high exit quality to utilize more latent heat of vaporization as well as avoiding CHF, while the PI pressure feedback controller ($C_2(s)$) and refrigerant wall temperature feedback controllers ($C_1(s)$) gives the system the ability to resist a sudden appearance of superheat.

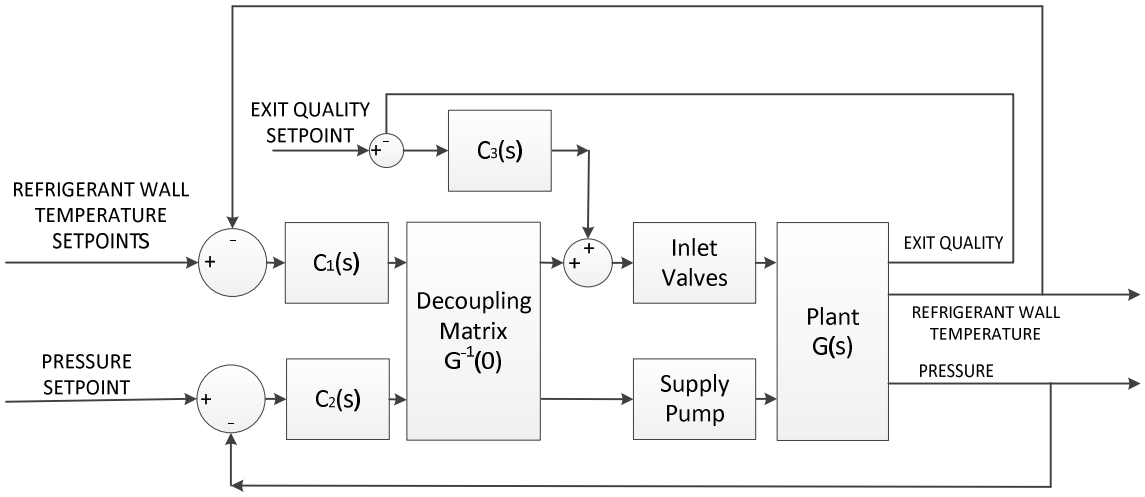

Figure 17: Decoupled PI controllers with estimated evaporator exit quality feedback control architecture

Figure 18 showed the system response with heat load disturbances when the proposed decoupled PI controllers with estimated exit quality feedback control architecture was applied to the system. With the same amount of heat load disturbances in Figure 16, superheat was not observed during the disturbances, refrigerant wall temperatures were kept constant. With estimated exit quality feedback, controller $C_3(s)$ regulated the inlet valves to compensate the increasing heat flux. With the simplicity of PI controllers, the control architecture has the potential to be widely used in server bank cooling.

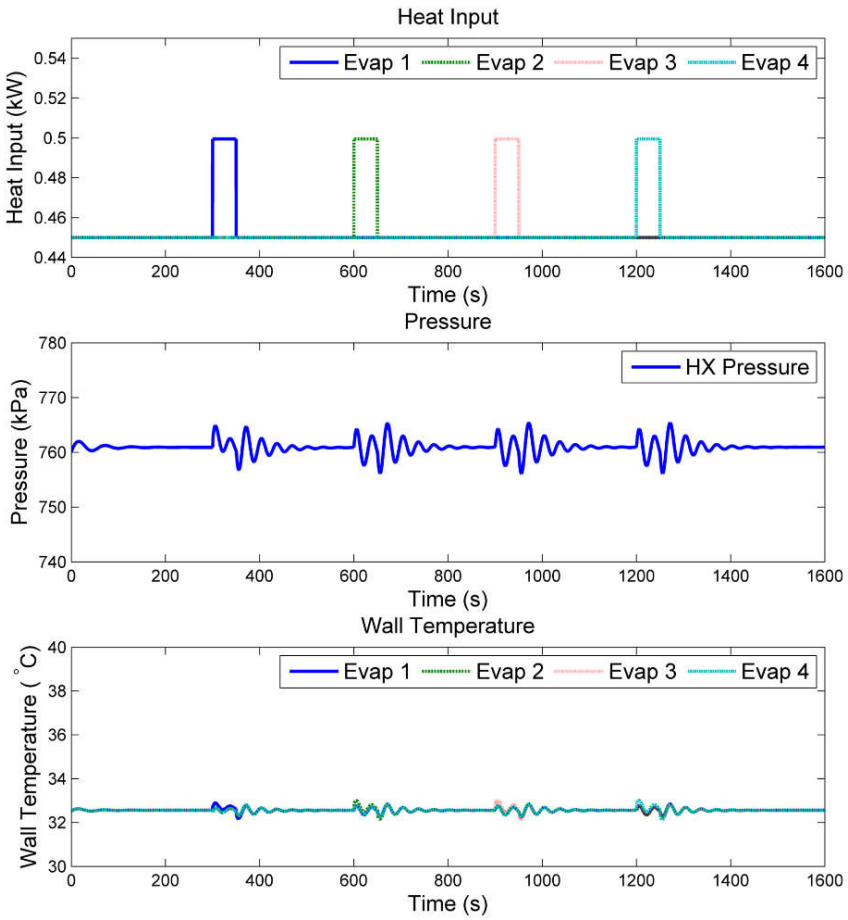

Figure 18: PTP system with decoupled PI controllers with estimated evaporator exit quality feedback control under heat load disturbances

3.3. Decoupled PI Controllers with Heat flux Feedforward

In most applications, heat flux changes are unpredictable. However, in some cases, heat flux can be a known parameter to the system, such as a system where the heat load can be measure by a power transducer. With a known heat flux, valves can be controlled to maintain the exit quality, while the decoupled PI controllers can still be robust enough to maintain system pressure and wall temperature. Figure 19 presents a schematic of decoupled PI controllers with

heat flux feedforward, where $C_1(s)$ and $C_2(s)$ are simple PI controller and $C_3(s)$ is a feedforward controller.

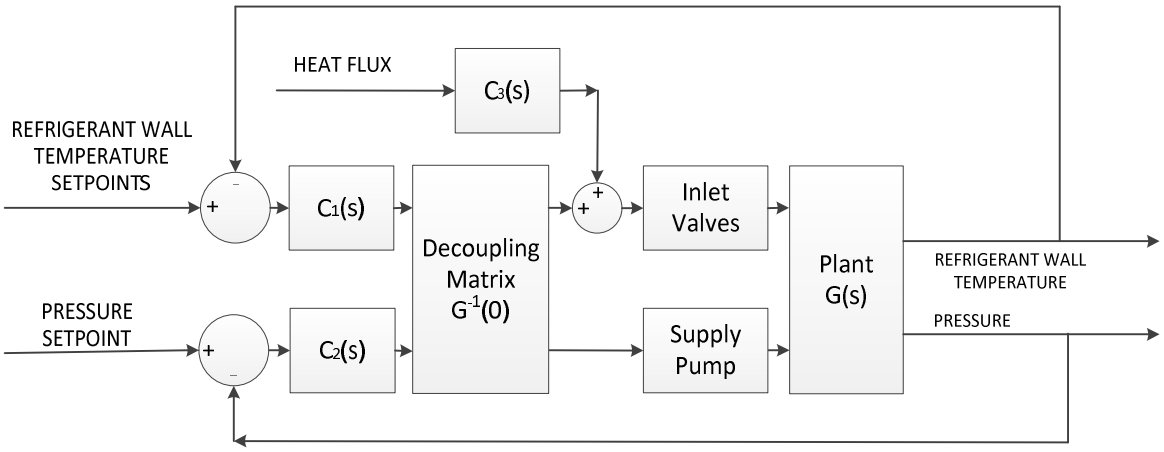

Figure 19: Decoupled PI controllers with heat flux feedforward control architecture

3.4. Comparison of Control Architectures

To demonstrate the performance of the proposed control architectures, decoupled PI controllers with estimated evaporator exit quality feedback control and decoupled PI controllers with heat flux feedforward control were tested under different heat load conditions with heat step changes. Decoupled PI controller with exact evaporator exit quality feedback control was tested together as a comparison with decoupled PI controller with estimated evaporator exit quality feedback control.

The initial system condition was set to an exit quality of 0.9 at each evaporator outlet. Thus, a small perturbation of heat load change could have pushed the system to face CHF. The evaporators are given an evenly distributed heat load at 450 Watts, 250 Watts, and 90 Watts to represent high heat load, medium heat load and low heat load conditions, as shown in Figure 20.

Evaporator 1 was given 10% of maximum heat load step changes during the high heat load, medium heat load and low heat load condition. All the evaporators were set up symmetrically with identical physical parameters. Because the setup of the evaporators was the same, heat impulses on evaporator 1 can represent heat flux changes on any evaporator.

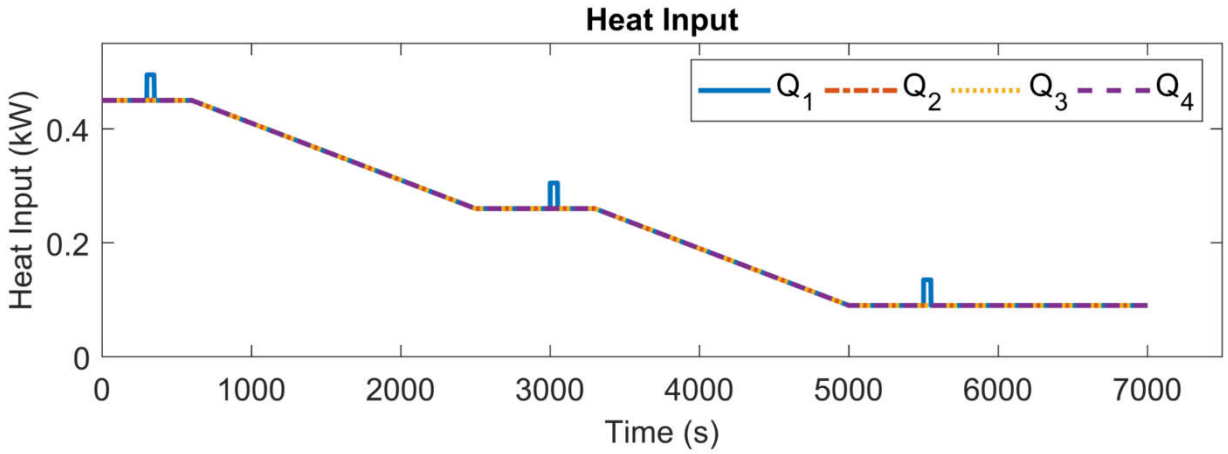

Figure 20: Evenly distributed head loads - PTP

The exit quality setpoint was set to 0.9 in the cases using exact quality feedback and heat flux feedforward control. For system operation safety, the estimated average exit quality setpoint for estimated evaporator exit quality was set to 0.8.

The system pressures are plotted in Figure 21. Both the proposed control architectures showed good performance in maintaining constant system pressure. During the heat impulses, the pressure fluctuations were less than 10 kPa with the tested control architectures. The decoupled PI controller with estimated evaporator exit quality feedback control showed a slightly higher pressure fluctuation the first heat step change comparing with the other control

architecture due to the estimated average exit quality setpoint change during as shown in subplot (a) of Figure 21.

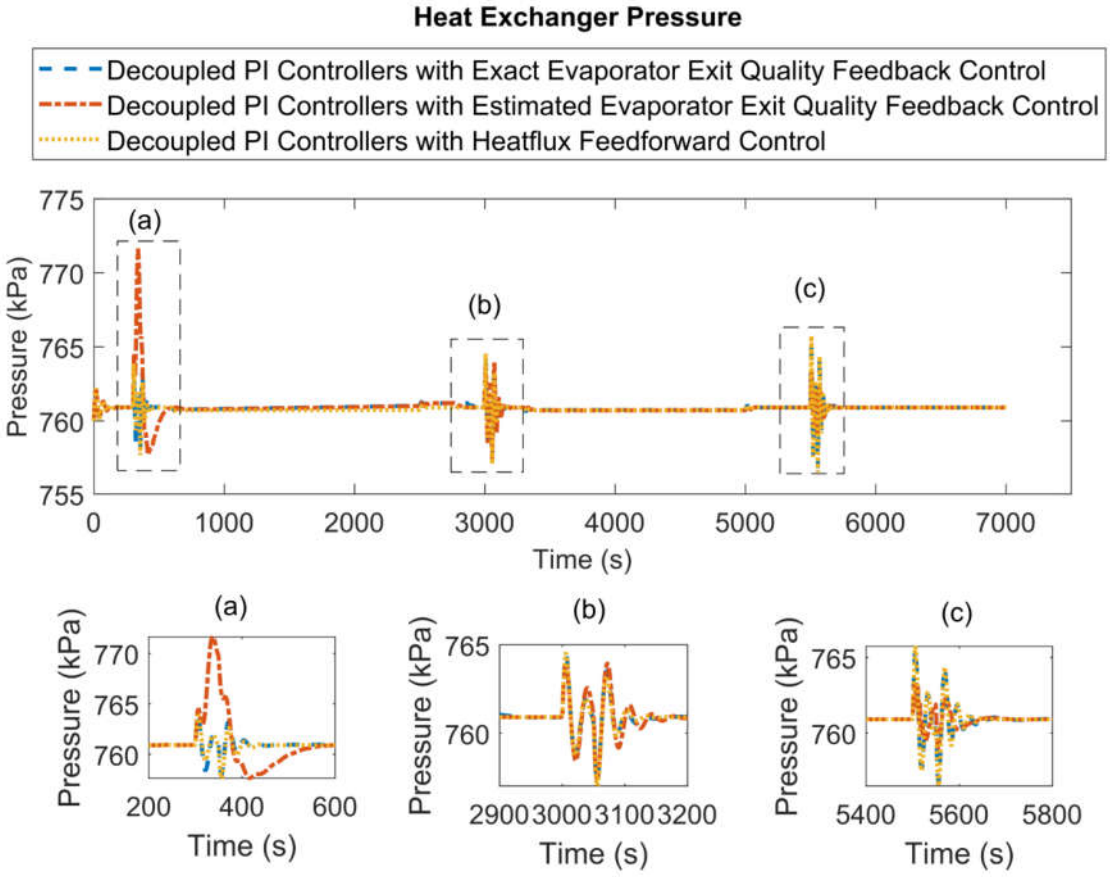

Figure 21: System pressures under evenly distributed heat loads - PTP

Wall temperatures are plotted in Figure 22. Both the proposed control architectures showed the ability to maintain constant wall temperatures. With each control architecture, the wall temperature fluctuations all fell within 1 °C. The enlarged plots of the wall temperatures during the heat load step changes were included in Figure 23. The differences in the refrigerant wall temperatures using decoupled PI controller with estimated evaporator exit quality feedback control and decoupled PI controller with heat flux feedforward control are relatively small. When

using the estimated evaporator exit quality as the feedback signal, the wall temperature performance was same as using the exact evaporator exit quality as the feedback signal.

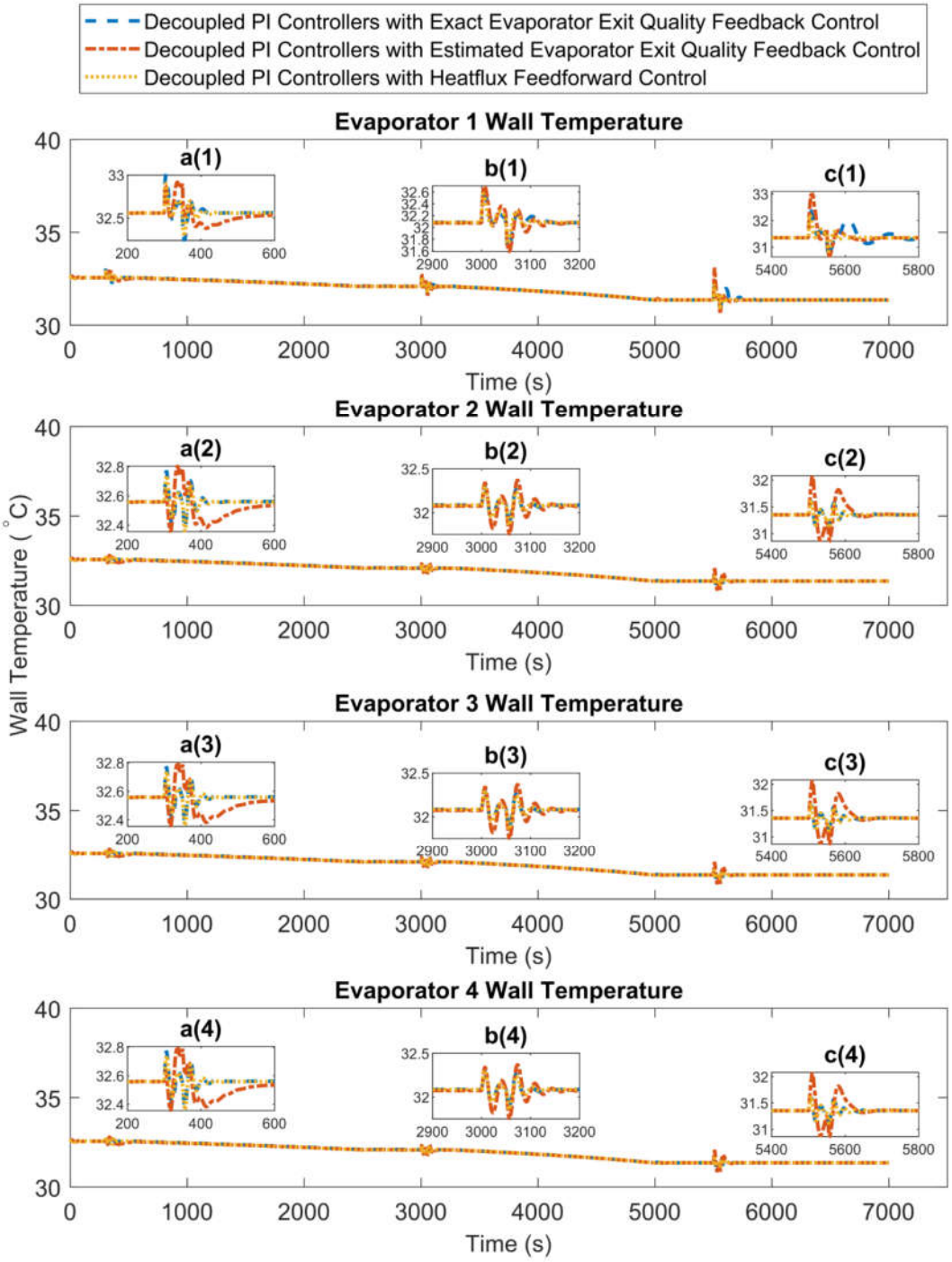

Figure 22: Wall temperatures under evenly distributed heat loads - PTP

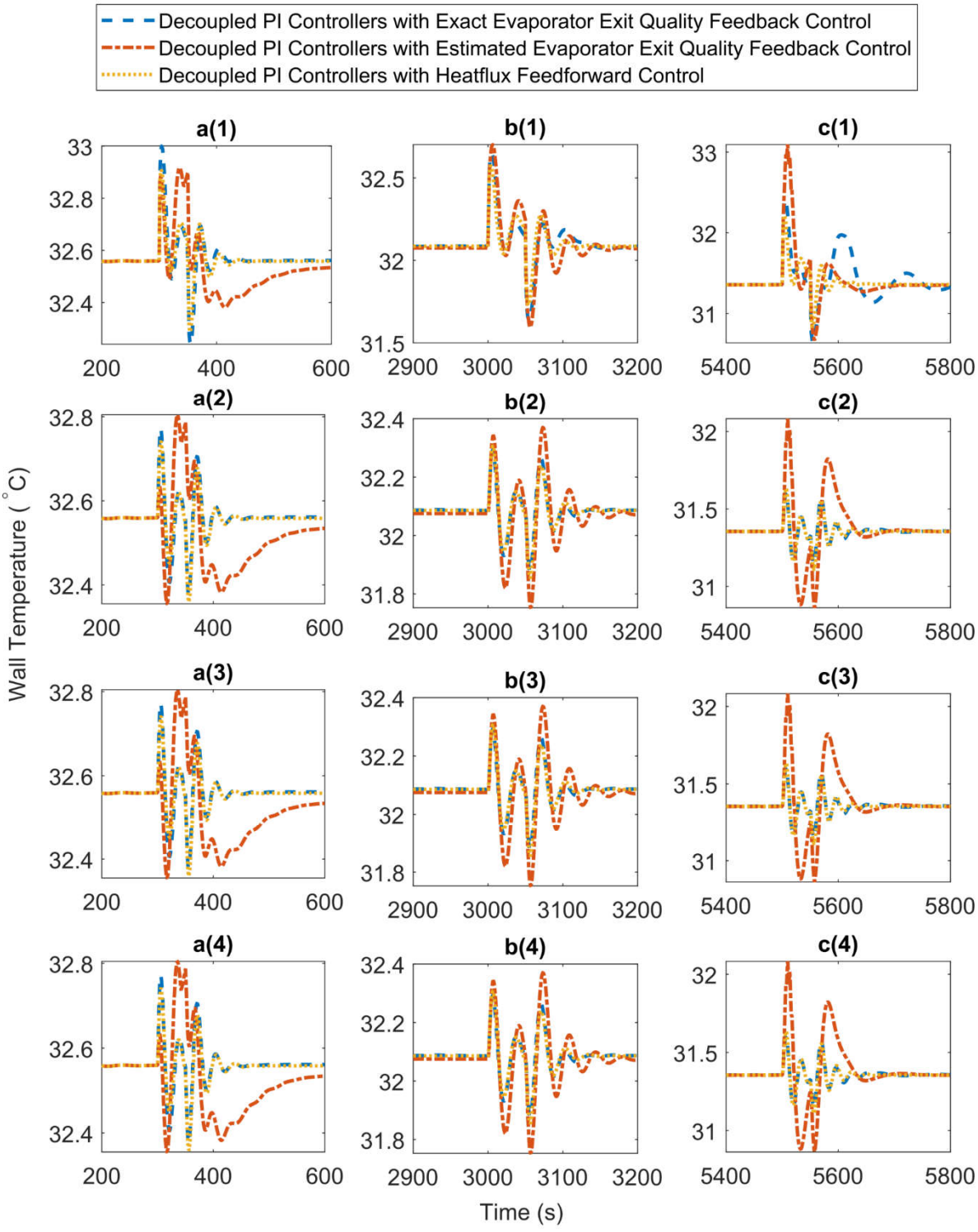

Figure 23: Enlarged wall temperatures under evenly distributed heat loads - PTP

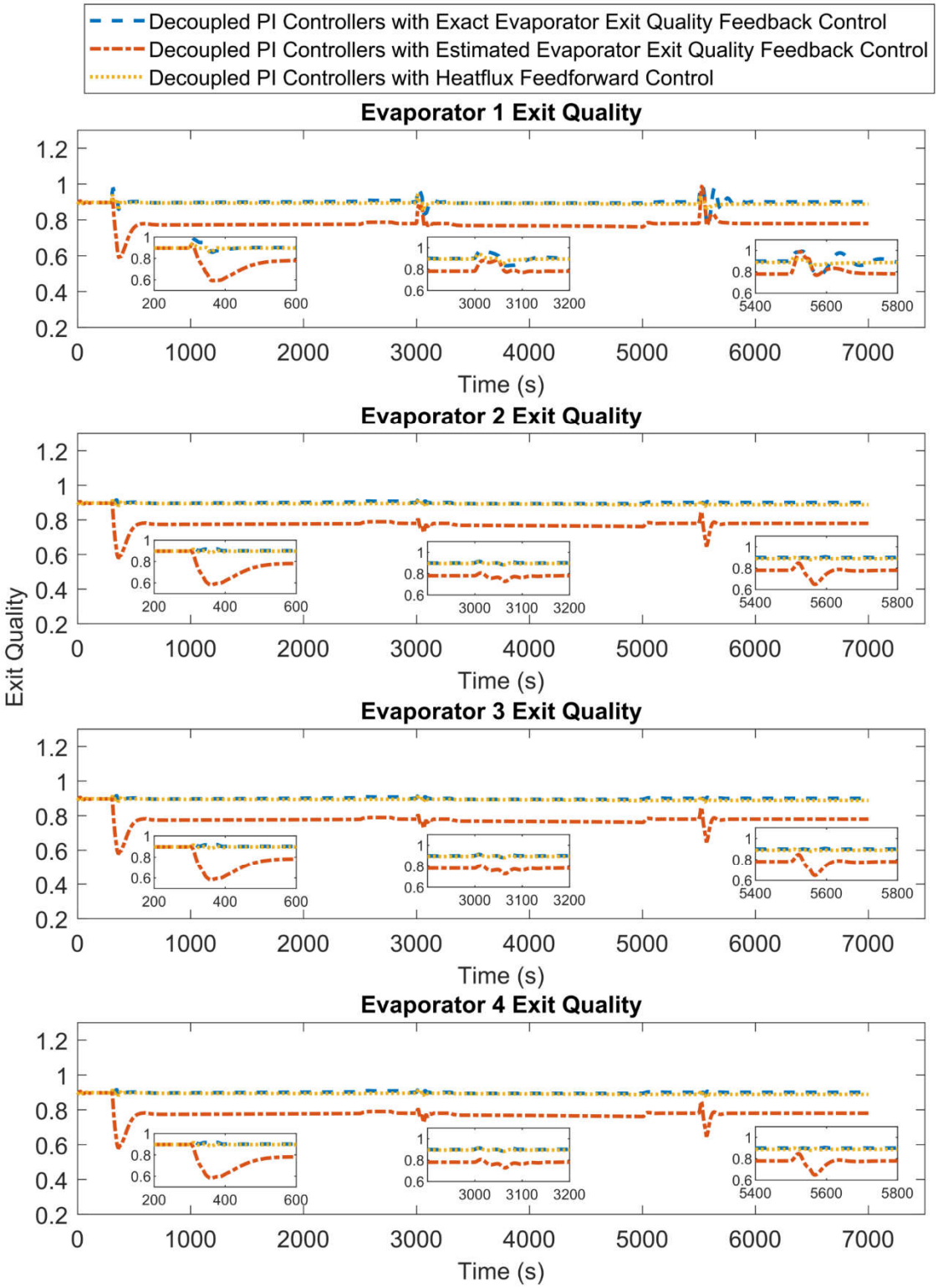

Figure 24: Evaporator exit qualities under evenly distributed heat loads - PTP

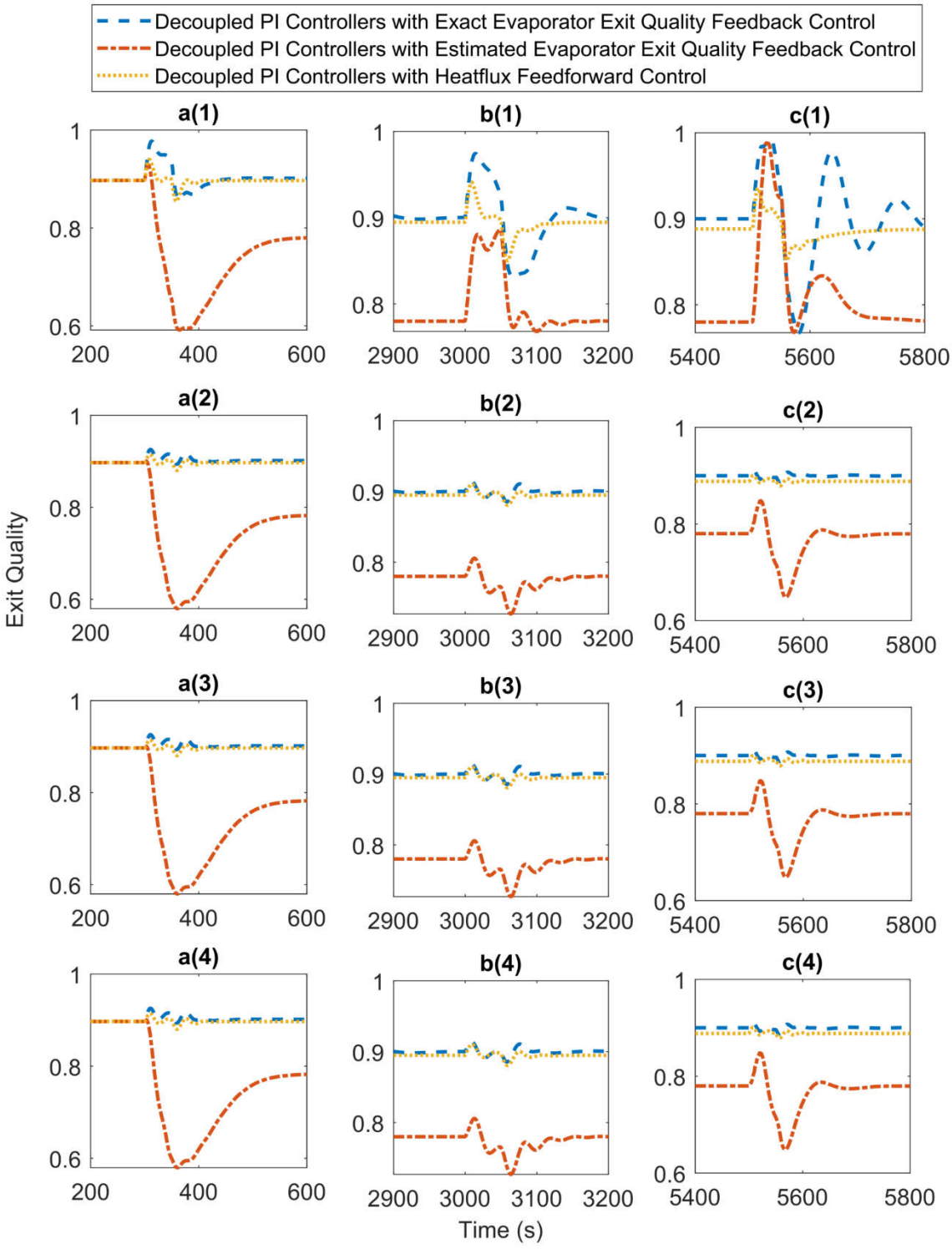

Figure 25: Enlarged evaporator exit qualities under evenly distributed heat loads - PTP

Evaporator exit qualities are plotted in Figure 24 with an enlarged plot during heat load step changes in Figure 25. The proposed decoupled PI controller with estimated evaporator exit quality feedback and decoupled PI controller with heat flux feedforword control effectively maintained the evaporator exit quality at the desired level. During the heat load step changes, the fluctuation of the exit quality was the highest at the low heat condition due to the increased system sensitivity of low heat load on the system as shown in Figure 25 subplot c(1). Comparing decoupled PI controller with estimated exit quality feedback control with decoupled PI controller with exact quality feedback control, the evaporator exit quality fluctuation was higher when using the estimated evaporator exit quality method. To compensate the estimated evaporator exit quality uncertainty when using the estimated evaporator exit quality method, the estimated evaporator exit quality setpoint needs to be lower than the exact exit quality setpoint. In the decouple PI controller with heat flux feedforward control, the control efforts can be separated into two main types, feedforward control signals to maintain exit quality and decoupled PI controllers to maintain constant operating pressure and evaporator wall temperature. When the system pressure is well maintained, having the evaporator exit quality under control can ensure the wall temperature stays in a safe operation rage. Control gains were tuned so that the heat flux forward control signal was the dominant control effort in the control architecture to maintain the evaporator exit quality.

The evaporator exit qualities, when using the decoupled PI controllers with estimated exit quality feedback, are of particular interest. The comparison between the exact exit qualities and the estimated exit quality is plotted in Figure 26. In the subplots (a), (b) and (c), the estimated exit quality was found to be very close to the exact exit qualities. When the multi-evaporator

PTP system is exposed to evenly distributed heat loads, using the estimated evaporator exit method can keep the system away from CHF.

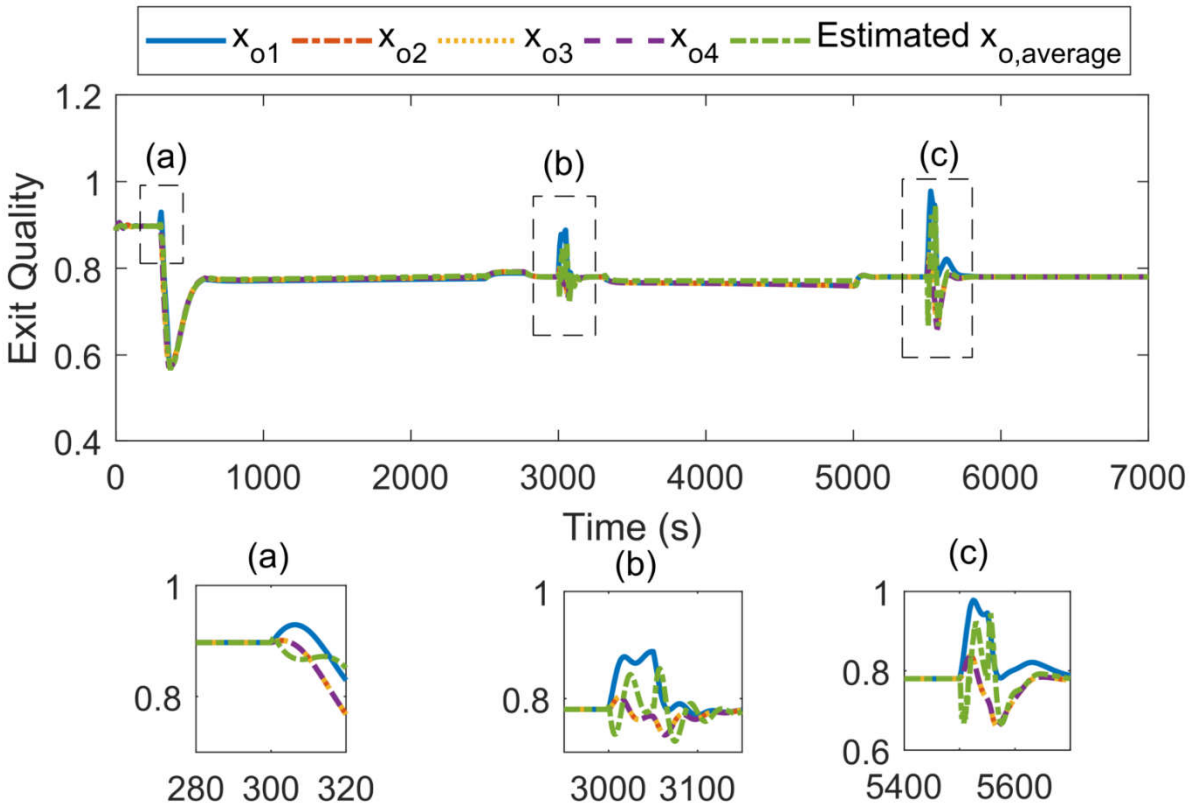

Figure 26: Comparison between exact evaporator exit qualities and estimated exit quality, heat load 1 - PTP

The previous tests were conducted with all the evaporators under evenly distributed heat loads. To explore the performance of the control architectures further, the control architectures were examined again under unevenly distributed heat load conditions, as shown in Figure 27. The heat load on evaporator 1 was at high load, medium load, and low load with 10% maximum heat impulses, while heat loads on evaporators 2, 3, and 4 were kept constant.

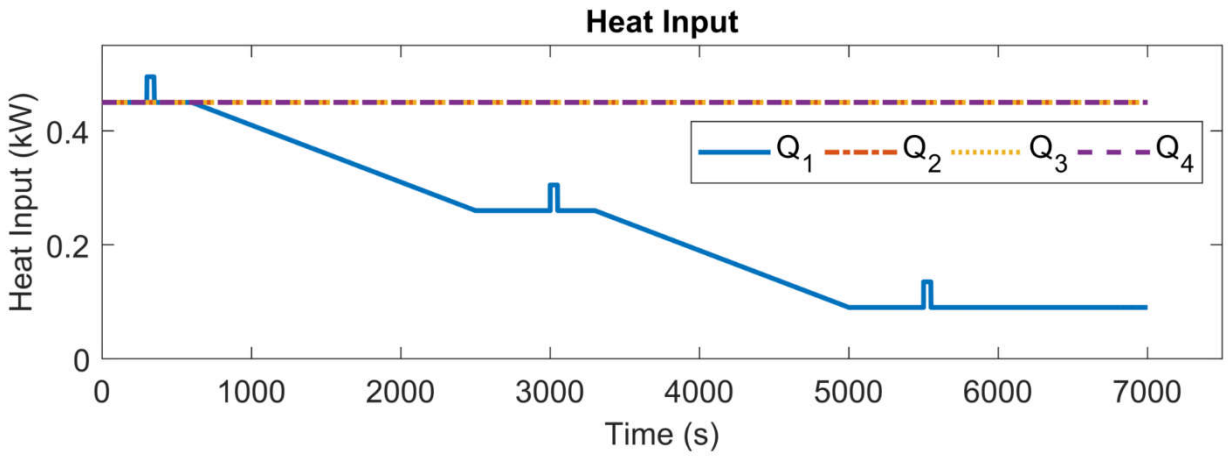

Figure 27: Unevenly distributed heat loads - PTP

Figure 28 shows the system pressures under unevenly distributed heat loads when using the decoupled PI controller with exact evaporator exit quality feedback control, the decoupled PI controller with estimated evaporator average exit quality feedback control, and the decoupled PI controller with heat flux feedforward control. The proposed control architecture with estimated evaporator average exit quality and the control architecture with heat flux feedforward showed good performance in maintaining constant system pressure during all levels of heat loads. The pressure performance during heat load step changes when using the estimated evaporator average exit quality is the same as using the exact evaporator exit quality as the feedback signal as shown in Figure 28 subplot b and c. The increased pressure fluctuation in Figure 28 subplot (a) is only due to estimated evaporator average exit quality setpoint changed from 0.9 to 0.8.

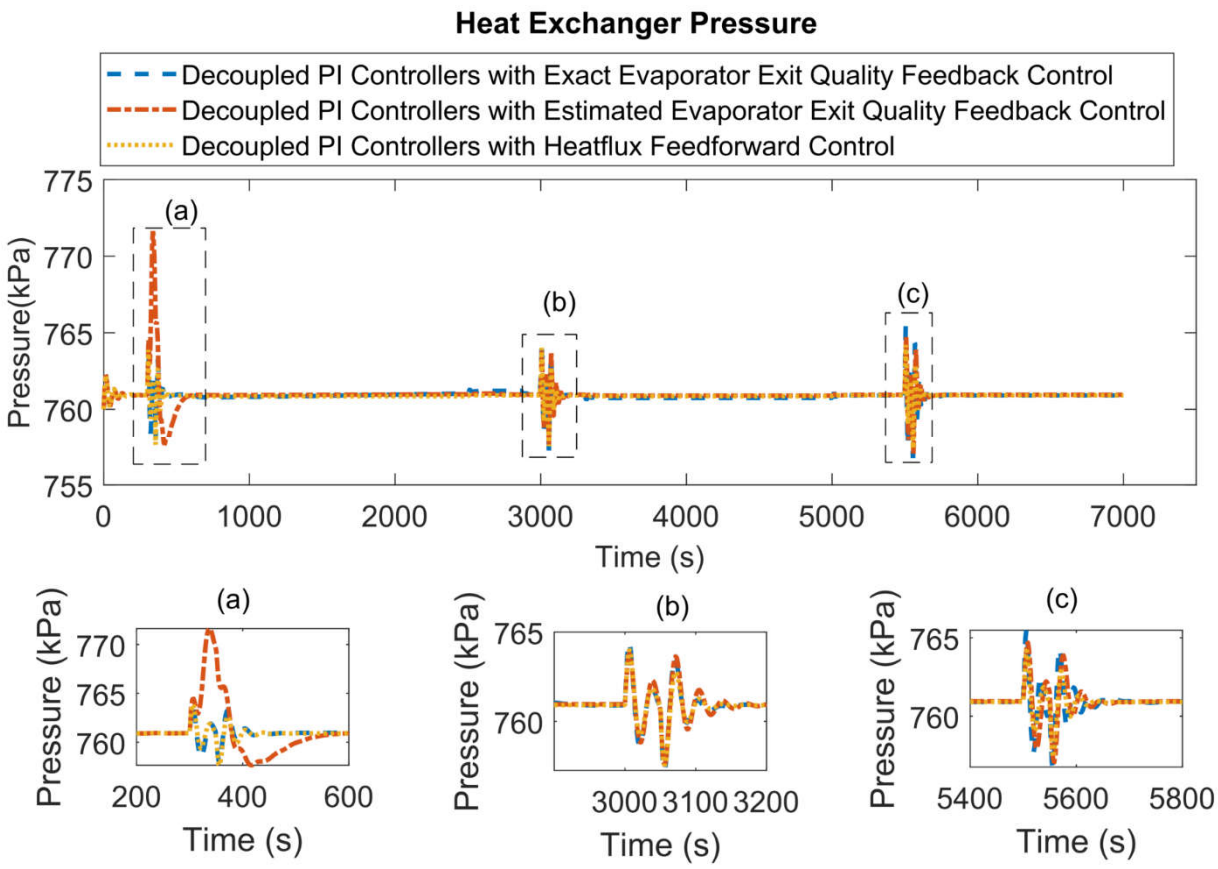

Figure 28: System pressures 2 under unevenly distributed heat loads - PTP

Wall temperatures of the evaporators under unevenly distributed heat loads are plotted in Figure 29 with the enlarged view during heat step changes in Figure 30. On evaporator 1, the tested decoupled PI controllers with exact evaporator exit quality feedback control, the decoupled PI controllers with estimated evaporator average exit quality feedback control and the decoupled PI controllers with heat flux feedforward control showed the ability to maintain constant wall temperatures. With each control architecture, the refrigerant wall temperature fluctuations all fell within 1 °C.

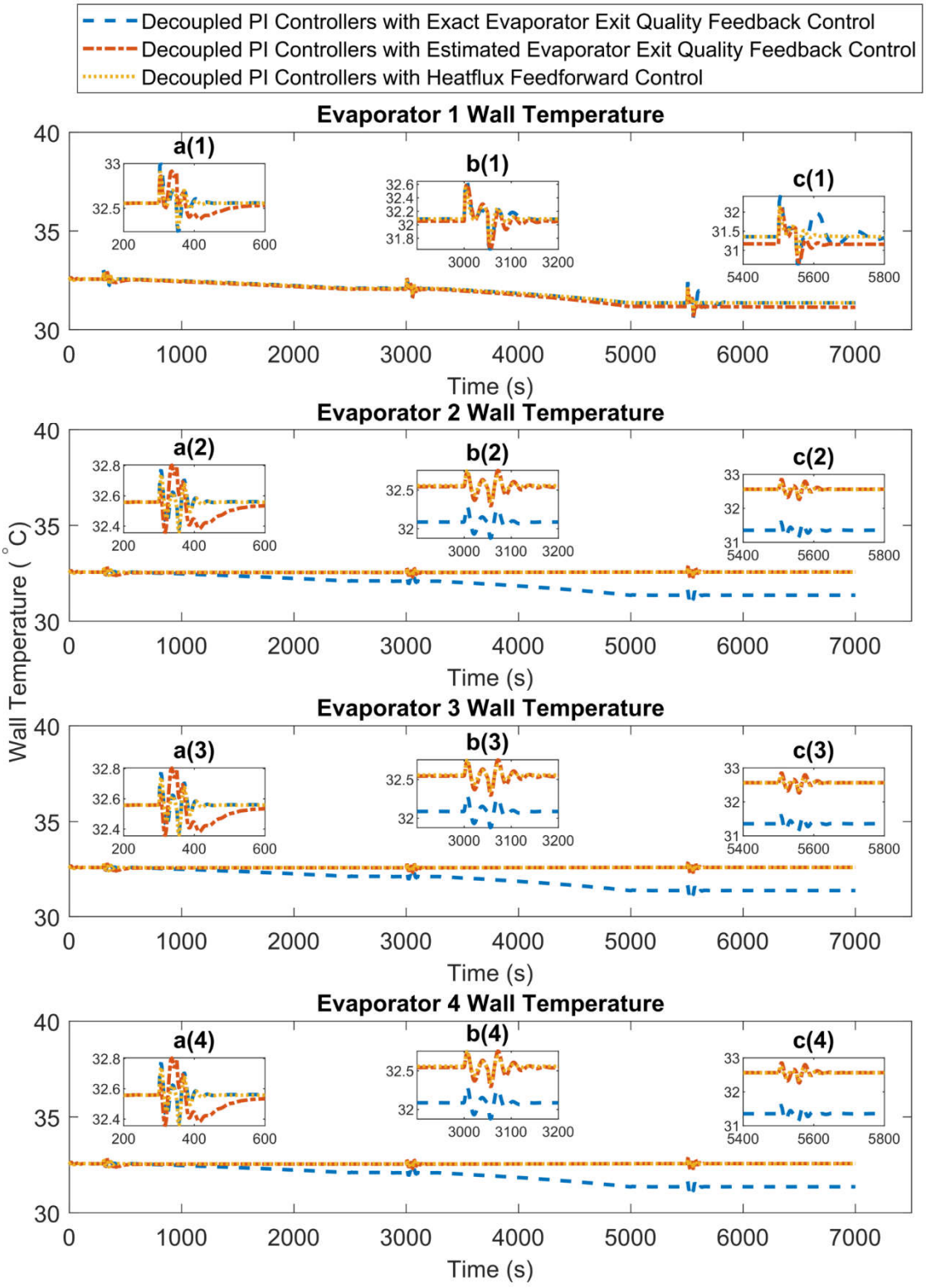

Figure 29: Wall temperatures under unevenly distributed heat loads - PTP

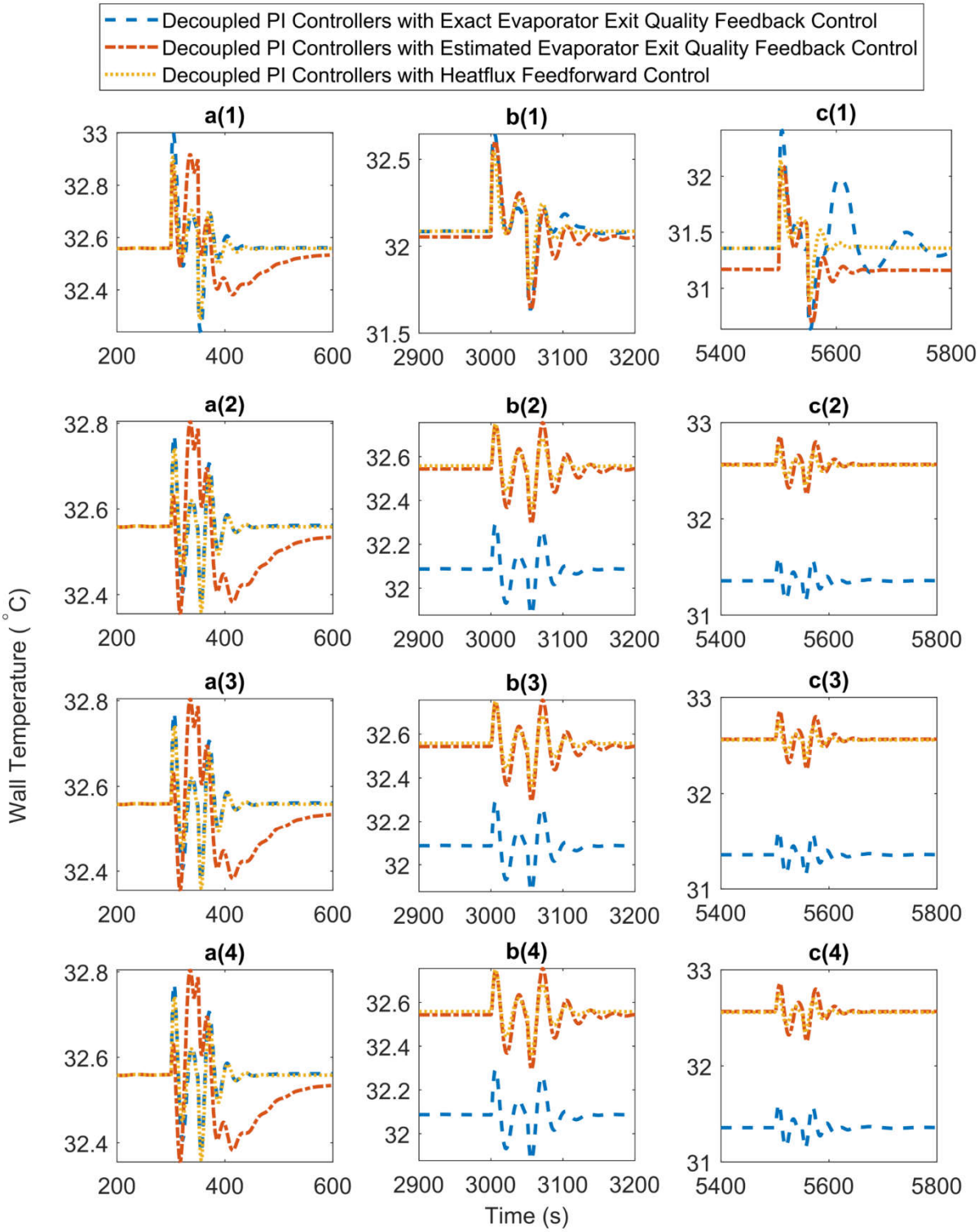

Figure 30: Enlarged wall temperatures under unevenly distributed heat loads - PTP

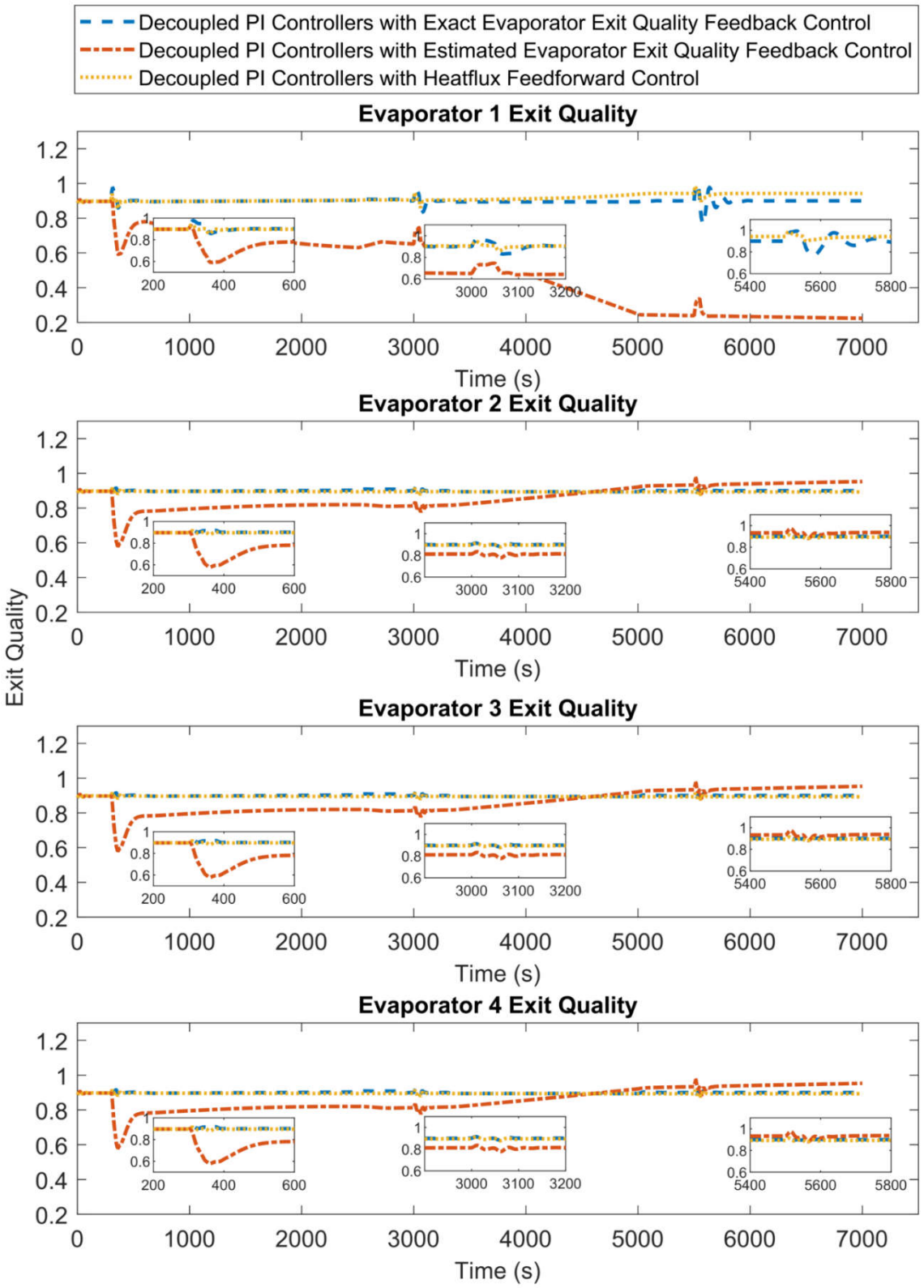

Figure 31: Evaporator exit qualities under unevenly distributed heat loads - PTP

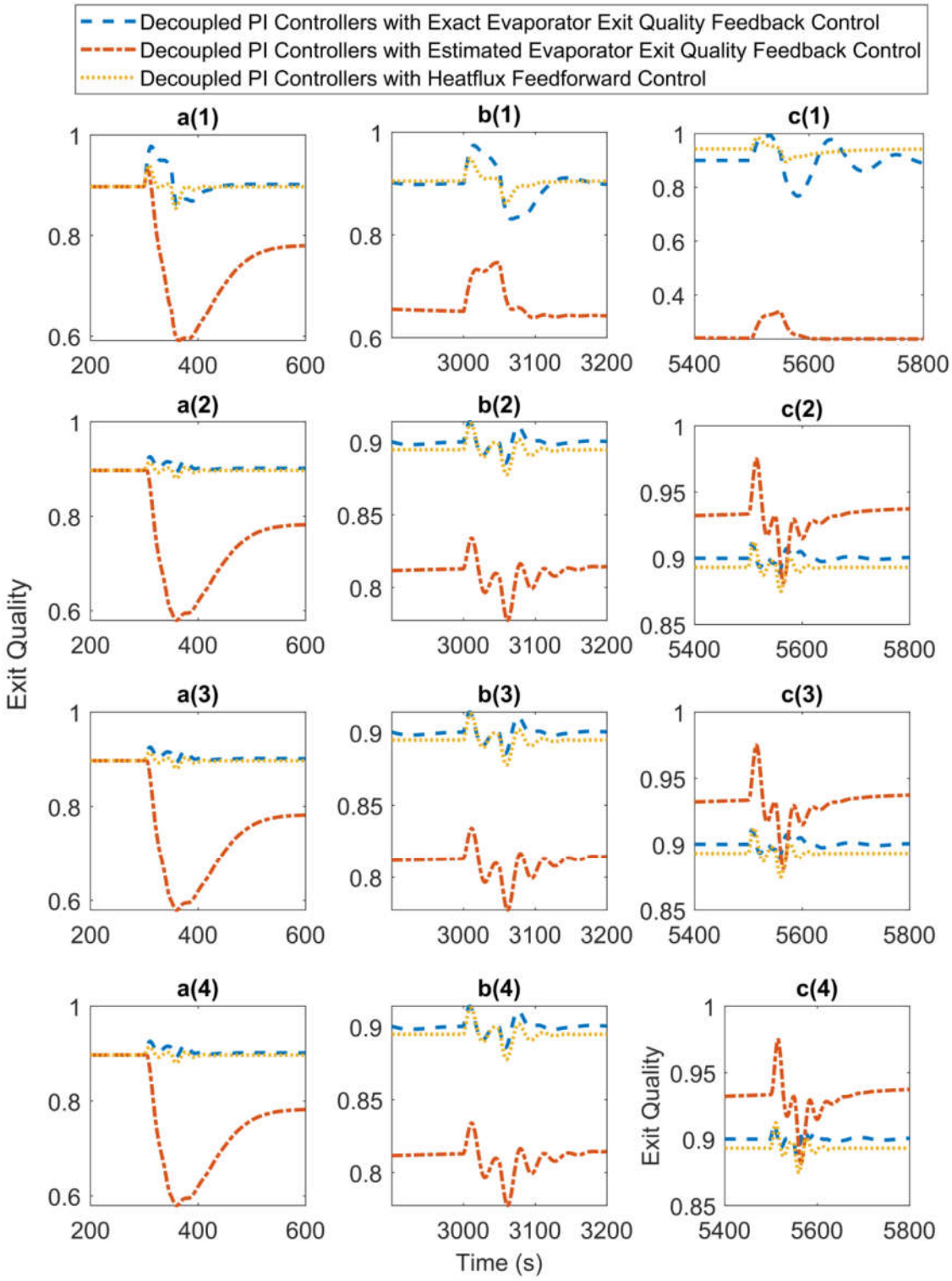

Figure 32: Enlarged evaporator exit qualities under unevenly distributed heat loads - PTP

Evaporator exit qualities and the enlarged views during heat load step changes are plotted in Figure 31 and Figure 32. Decoupled PI controllers with heat flux feedforward control effectively maintained the exit qualities at 0.9 at steady state conditions. The estimated average evaporator exit quality setpoint was set to 0.8 for safe operation in the case of using decoupled PI controllers with estimated average evaporator exit quality feedback control. Evaporator exit qualities deviated when using the estimated average evaporator exit quality. Evaporator 1 was showing a lower level of exit quality when evaporator 1 was given a lower level of heat load. While the exit quality of evaporator 2, 3, and 4 were showing a slightly increasing trend.

The exit qualities when using decoupled PI controllers with estimated exit quality feedback control, are of particular interest. Figure 33 plots a detailed comparison between exact exit qualities and estimated exit quality under unevenly distributed heat load. The estimated exit quality was maintained well at 0.8. The exact exit quality on evaporator 1 decreased while evaporator 1 was given at a lower heat load. In the meantime, the exact exit qualities of evaporator 2 and 3, are slightly above 0.8. This result was due to fact that all the evaporator inlet valves were using the same estimated average exit quality feedback signal and wall temperature fluctuations were very small very the system pressure is well maintained. The evaporator with the higher heat load tended to have an exit quality lower than the estimated value, while the evaporator with the lower heat load had an exit quality higher than the estimated value.

With a system of largely uneven heat load distribution, the gains of the refrigerant wall temperature feedback control should be tuned with a larger value, such that the control signals for the valves from the refrigerant wall temperature feedback control can compensate for the unevenly distributed heat loads.

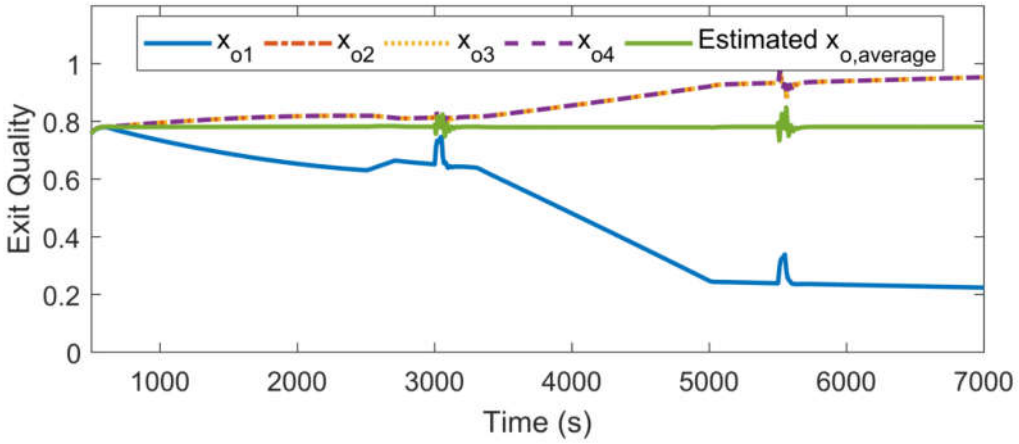

Figure 33: Comparison between exact exit qualities and estimated exit quality under unevenly distributed heat loads – PTP

In a PTP system with a large number of evaporators in parallel, the worst-case scenario of unevenly distributed heat loads is when one evaporator is under low heat load and the remaining evaporators are under high heat loads. The estimated average evaporator exit quality setpoint should be chosen based on the worst-case scenario. By properly choosing the setpoint and gains of the control architecture, all the exit qualities can be maintained to avoid CHF.

The valves are controlled by two controllers in the proposed decoupled PI controllers with estimated evaporator exit quality feedback control, the wall temperature feedback controller and the estimated exit quality feedback controller. However, with unevenly distributed heat loads, the deviation of exit quality values between multiple evaporators which will affect the system's tolerance of heat load disturbances. The balance between the wall temperature feedback controller and the estimated exit quality feedback controller need to be determined by specific system operating condition.

4. INTEGRATED PUMPED TWO-PHASE SYSTEM WITH VAPOR COMPRESSION CYCLE SYSTEM

In most existing data centers, air-cooling systems serve as the major way to maintain desired operating conditions. In a typical air-cooling system, air blows into the server to remove the heat conducted to a heat sink by the chips. The air, in turn, is cooled by chilled water, which is maintained lower than the ambient temperature to produce sufficient heat transfer. Thus, data centers always have centralized chillers which is a vapor compression cycle (VCC) system. The pumped two-phase (PTP) system can be integrated with the existing VCC system. Other than using chilled water to remove heat from the condenser, the PTP condenser can be integrated with the VCC evaporator to have the benefit of direct refrigerant-to-refrigerant cooling. With such a system integration, the new cooling scheme not only improves cooling efficiency but also reduces energy consumption and equipment costs by eliminating water loop between PTP and VCC.

Figure 34 is a schematic of a multi-evaporator PTP system integrated with a VCC system. The multi-evaporator PTP system here deploys the same schematic as discussed in the previous chapter. Four evaporators are placed in parallel in the system. The PTP condenser is integrated with the VCC evaporator to be a refrigerant-to-refrigerant heat exchanger.

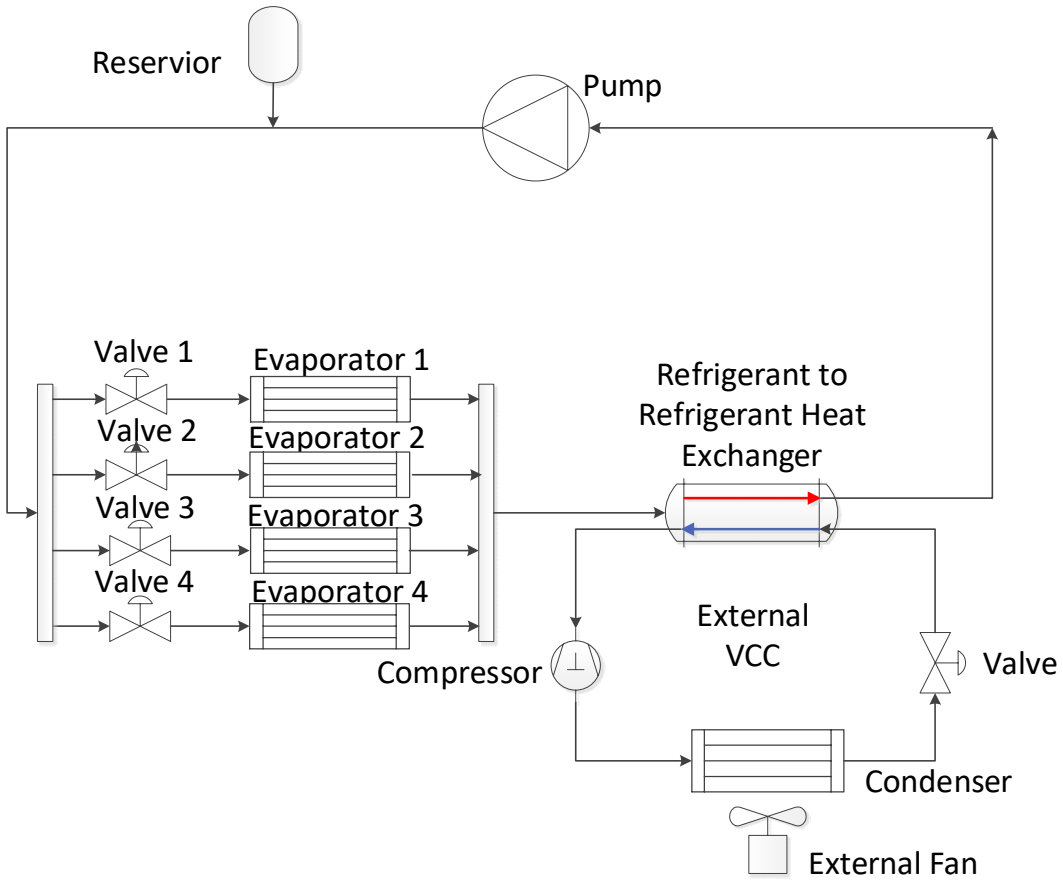

Figure 34: Integrated PTP-VCC system model

The VCC has four major components: compressor, condenser, expansion valve, and evaporator. An ideal VCC involves four processes: 1) isentropic compression in a compressor, 2) isobaric heat rejection in a condenser, 3) isenthalpic expansion in an expansion valve, and 4) isobaric heat absorption in an evaporator. Figure 35 shows a pressure-enthalpy diagram of a PTP-VCC system. In the VCC, the first step of the thermodynamic cycle starts in the compressor. It turns the low-pressure, gaseous refrigerant into a high-pressure, high-temperature gas by adding energy to the refrigerant (Process 1 to 2). Then, the refrigerant goes into the condenser, where heat exchange happens with the secondary fluid (usually water or air). Heat is

rejected to the secondary fluid as the refrigerant condenses into a high-pressure liquid (Process 2 to 3). Safety equipment usually is placed after the condenser to ensure that the refrigerant is in the saturated liquid condition before entering the valve. Isenthalpic valve throttling happens in Process 3 to 4, where the saturated liquid refrigerant enters an expansion valve and expands to a low-pressure, low-temperature, two-phase fluid. As the two-phase fluid passes through the evaporator, heat energy is absorbed from the zone as the refrigerant boils. The refrigerant evaporates into a low-pressure superheated vapor when leaving the evaporator. The cycle restarts with the compressor. In Process 4 to 1, the VCC evaporator is integrated with the PTP condenser to remove the heat from the PTP condenser. In the VCC system, the degree of superheat is a crucial factor for safe compressor operation. Superheat is defined as the temperature difference between the evaporator outlet temperature and evaporator-pressure saturation temperature.

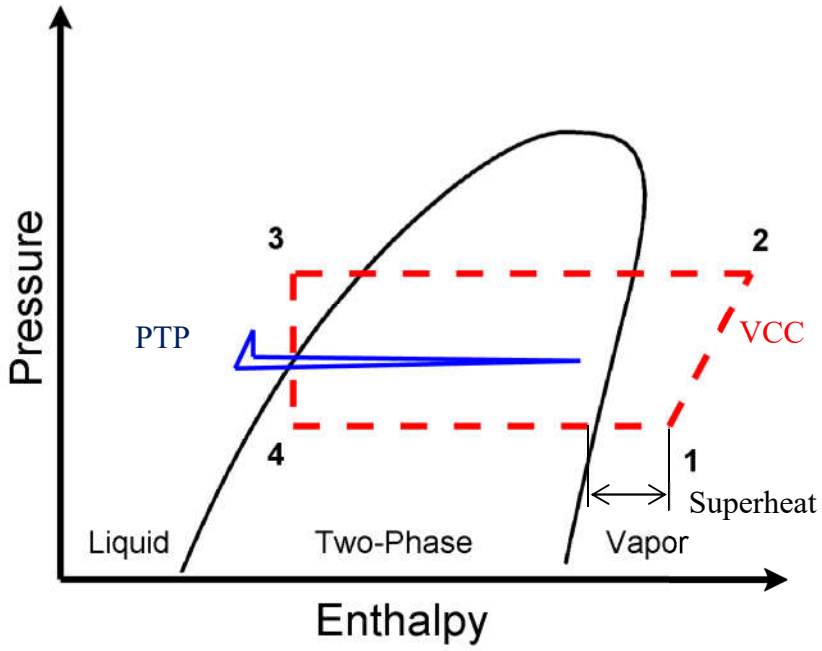

Figure 35: Pressure-Enthalpy diagram of a PTP-VCC system

4.1. Integrated Refrigerant-to-Refrigerant Heat Exchanger

Based on the previous modeling method, the PTP heat exchangers were modeled together as a combined heat exchanger. The main challenge of integrating the PTP and VCC is to add the VCC evaporator to the PTP combined heat exchanger. The combined heat exchanger was remodeled to add the refrigerant-to-refrigerant heat exchanger condenser feature.

The refrigerants on the PTP condenser and VCC evaporator were considered to be coflow. The PTP condenser and VCC evaporator shared the same refrigerant wall temperatures. Inside the PTP condenser, the refrigerant was separated into three regions: superheated vapor, two-phase fluid, and subcooled liquid. Inside the VCC evaporator, the refrigerant was separated into two regions: two-phase fluid and superheated vapor. The switched moving boundary (SMB) method was used to model the heat exchanger to handle the appearance and disappearance of the superheated vapor region on both the PTP side and the VCC side.

Considering the fluid conditions inside the PTP condenser, when the PTP system is in normal operating conditions with an evaporator exit quality less than 1, the PTP condenser has two-phase fluid and subcooled liquid regions. Otherwise, the PTP condenser has all three fluid-phase regions if CHF occurs. VCC cycles require superheated vapor at the outlet of the VCC evaporator to prevent vapor from entering the compressor and potentially causing cavity in the compressor. Under normal operating conditions, the VCC evaporator has two-phase fluid and superheated vapor regions. In abnormal operating conditions, the VCC evaporator only has a two-phase fluid region when it loses superheat.

Refrigerant wall temperature is a crucial parameter to be calculated inside the model. Heat-transfer coefficients are determined largely by the fluid phases on both sides of the heat

exchangers, further determining the refrigerant wall temperatures. Thus, the length of each region is also a significant factor contributing to refrigerant wall temperatures.

To consider the fluid phase condition and length of each region inside the refrigerant-to-refrigerant heat exchanger, seven conditions can happen in the refrigerant-to-refrigerant heat exchanger, presented in Figure 36 to Figure 41. The total heat exchanger length on the PTP condenser and VCC evaporator were the same. $L_{PTP,1}$, $L_{PTP,2}$, and $L_{PTP,3}$ represent the fluid-region length of superheated vapor, two-phase fluid, and subcooled liquid in the PTP condenser. $L_{VCC,1}$ and $L_{VCC,2}$ represent the fluid-region length of the two-phase fluid and superheated vapor in the VCC evaporator. The PTP condenser and VCC evaporator shared the same refrigerant wall temperatures of T_{w1}, T_{w2}, T_{w3}, and T_{w4}. The conditions are summarized in Table 8.

Table 8: Refrigerant-to-refrigerant heat Exchanger fluid region conditions

	PTP Condenser	VCC Evaporator	Length Criteria
Condition 1	SH + TP + SC	TP	N/A
Condition 2	TP + SC	TP	N/A
Condition 3	TP + SC	TP + SC	$L_{VCC,1} < L_{PTP,2}$
Condition 4	TP + SC	TP + SC	$L_{VCC,1} > L_{PTP,2}$
Condition 5	SH + TP + SC	TP + SC	$L_{VCC,1} < L_{PTP,1}$
Condition 6	SH + TP + SC	TP + SC	$L_{PTP,1} < L_{VCC,1} < L_{PTP,2}$
Condition 7	SH + TP + SC	TP + SC	$L_{VCC,1} > L_{PTP,1} + L_{PTP,2}$

The derivation of governing equations still follows the conservation of mass (Equation (10)), the conservation of refrigerant energy (Equation (11)), and the conservation of refrigerant wall energy (Equation (12)).

Conditions within the refrigerant-to-refrigerant heat exchanger at each instant of time are represented by the state vector in Equation (45). The variable $h_{VCC,o}$ represents the outlet enthalpy of the VCC evaporator. P_{VCC} is the pressure of the VCC evaporator. The variable $\overline{\gamma}_{VCC}$ is the mean void fraction of the VCC evaporator. The variable $h_{PTP,o}$ represents the outlet enthalpy of the PTP evaporator. P_{PTP} is the pressure of the PTP condenser. Finally, the variable $\overline{\gamma}_{PTP}$ is the mean void fraction of the PTP condenser.

$$x_{r2r} = \tag{45}$$

$$[P_{VCC} \quad L_{VCC,1} \quad h_{VCC,o} \quad \overline{\gamma}_{VCC} \quad \dots$$

$$\dots \quad L_{PTP,2} \quad L_{PTP,3} \quad P_{PTP} \quad h_{PTP,o} \quad T_{w1} \quad T_{w2} \quad T_{w3} \quad T_{w4} \quad \overline{\gamma}_{PTP}]$$

$$\begin{bmatrix} z_{11} & z_{12} & z_{13} & 0 & 0 & 0 & 0 & 0 & 0 & 0 & 0 & 0 & 0 \\ z_{21} & z_{22} & z_{23} & 0 & 0 & 0 & 0 & 0 & 0 & 0 & 0 & 0 & 0 \\ z_{31} & z_{32} & z_{33} & 0 & 0 & 0 & 0 & 0 & 0 & 0 & 0 & 0 & 0 \\ z_{41} & 0 & 0 & 4_{54} & 0 & 0 & 0 & 0 & 0 & 0 & 0 & 0 & 0 \\ 0 & 0 & 0 & 0 & z_{55} & 0 & z_{57} & 0 & 0 & 0 & 0 & 0 & 0 \\ 0 & 0 & 0 & 0 & z_{65} & z_{66} & z_{67} & z_{68} & 0 & 0 & 0 & 0 & 0 \\ 0 & 0 & 0 & 0 & z_{75} & z_{76} & z_{77} & z_{78} & 0 & 0 & 0 & 0 & 0 \\ 0 & 0 & 0 & 0 & z_{85} & z_{86} & z_{87} & z_{88} & 0 & 0 & 0 & 0 & 0 \\ 0 & 0 & 0 & 0 & z_{95} & z_{96} & 0 & 0 & z_{99} & 0 & 0 & 0 & 0 \\ 0 & 0 & 0 & 0 & z_{10,5} & z_{10,6} & 0 & 0 & 0 & z_{10,10} & 0 & 0 & 0 \\ 0 & 0 & 0 & 0 & z_{11,5} & z_{11,6} & 0 & 0 & 0 & 0 & z_{11,11} & 0 & 0 \\ 0 & 0 & 0 & 0 & z_{12,5} & z_{12,6} & 0 & 0 & 0 & 0 & 0 & z_{12,12} & 0 \\ 0 & 0 & 0 & 0 & 0 & 0 & z_{13,7} & 0 & 0 & 0 & 0 & 0 & z_{13,13} \end{bmatrix} \begin{bmatrix} \dot{P}_{VCC} \\ \dot{L}_{VCC,1} \\ \dot{h}_{VCC,o} \\ \dot{\overline{\gamma}}_{VCC} \\ \dot{L}_{PTP,2} \\ \dot{L}_{PTP,3} \\ \dot{P}_{PTP} \\ \dot{h}_{PTP,o} \\ \dot{T}_{w1} \\ \dot{T}_{w2} \\ \dot{T}_{w3} \\ \dot{T}_{w4} \\ \dot{\overline{\gamma}}_{PTP} \end{bmatrix}$$

$$= \begin{bmatrix} \dot{m}_{VCC,i} - \dot{m}_{VCC,o} \\ f_{VCC,1} \\ f_{VCC,2} \\ f_{VCC,1} \\ f_{PTP,1} \\ f_{PTP,2} \\ f_{PTP,3} \\ k_{VCC}(\overline{\gamma}_{VCC} - \overline{\gamma}_{VCC,total}) \\ \dot{m}_{PTP,i} - \dot{m}_{PTP,o} \\ f_{w1} \\ f_{w2} \\ f_{w3} \\ f_{w4} \\ k_{PTP}(\overline{\gamma}_{PTP} - \overline{\gamma}_{PTP,total}) \end{bmatrix} \quad \textbf{(46)}$$

The governing matrix of the VCC evaporator and PTP condenser is shown in Equation (46). Details about the f vectors are discussed in the following section. $f_{VCC,1}$ represents the refrigerant energy conservation in two-phase region of the VCC evaporator, while $f_{VCC,2}$ represents the refrigerant energy conservation in the superheated vapor region of the VCC evaporator. $f_{PTP,1}$ is the refrigerant energy conservation in superheated vapor region of the PTP condenser. $f_{PTP,2}$ is the refrigerant energy conservation in the two-phase fluid region of the PTP condenser. $f_{PTP,3}$ is the refrigerant energy conservation in the subcooled liquid region of the PTP condenser. f_{w1}, f_{w2}, f_{w3}, and f_{w4} are the corresponding wall energy conservations. Table 9 lists the parameters used in the f vector expressions.

Table 9: Parameters used in the expressions of PTP-VCC integrated heat exchanger f vectors

Symbol	Description
$\alpha_{VCC,i1}$	Heat-transfer coefficient between tube wall and VCC evaporator two-phase fluid
$\alpha_{VCC,i2}$	Heat-transfer coefficient between tube wall and VCC evaporator superheated vapor
$\alpha_{PTP,i1}$	Heat-transfer coefficient between tube wall and PTP condenser superheated vapor
$\alpha_{PTP,i2}$	Heat-transfer coefficient between tube wall and PTP condenser two-phase fluid
$\alpha_{PTP,i3}$	Heat-transfer coefficient between tube wall and PTP condenser subcooled liquid
$T_{VCC,r1}$	Refrigerant temperature of VCC evaporator two-phase fluid
$T_{VCC,r2}$	Refrigerant temperature of VCC evaporator superheated vapor
$T_{PTP,r1}$	Refrigerant temperature of PTP condenser superheated vapor
$T_{PTP,r2}$	Refrigerant temperature of PTP condenser two-phase fluid
$T_{PTP,r3}$	Refrigerant temperature of PTP condenser subcooled liquid

In Condition 1, the PTP condenser has three phase regions, while the VCC evaporator has only one two-phase region, as shown in Figure 36. The top tube represents the PTP condenser, and the bottom tube is the VCC evaporator. In this condition, the change of length in each region in the PTP condenser does not have major effects on the heat-transfer coefficients on both sides on the walls. Refrigerant wall conservations were performed on L_1, L_2, and L_3. Detailed expressions of the f vector are presented in Table 10.

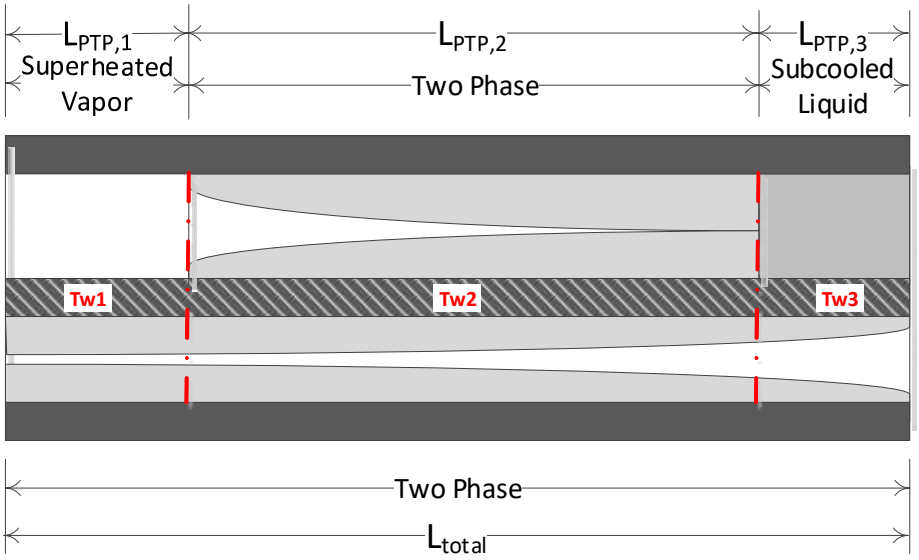

Figure 36: Refrigerant-to-refrigerant heat exchanger - Condition 1

Table 10: Refrigerant-to-refrigerant heat exchanger f vector - Condition 1

$f_{VCC,1}$	$\dot{m}_{VCC,i}h_{VCC,i} - \dot{m}_{VCC,o}h_{VCC,o} + \alpha_{VCC,i1}A_{VCC,i}\left(\frac{L_{PTP,1}}{L_{total}}\right)(T_{w1} - T_{VCC,r1}) + \alpha_{VCC,i1}A_{VCC,i}\left(\frac{L_{PTP,2}}{L_{total}}\right)(T_{w2} - T_{VCC,r1}) + \alpha_{VCC,i1}A_{VCC,i}\left(\frac{L_{PTP,3}}{L_{total}}\right)(T_{w3} - T_{VCC,r1})$
$f_{VCC,2}$	0
$f_{PTP,1}$	$\dot{m}_{PTP,o}(h_{PTP,g} - h_{PTP,o}) + \alpha_{PTP,i1}A_{PTP,i}\left(\frac{L_{PTP,1}}{L_{total}}\right)(T_{w1} - T_{PTP,r1})$
$f_{PTP,2}$	$\dot{m}_{PTP,in}(h_{PTP,in} - h_{PTP,g}) + \alpha_{PTP,i2}A_{PTP,i}\left(\frac{L_{PTP,2}}{L_{total}}\right)(T_{w2} - T_{PTP,r2})$
$f_{PTP,3}$	$\dot{m}_{PTP,in}h_{PTP,g} - \dot{m}_{PTP,o}h_{PTP,f} + \alpha_{PTP,i3}A_{PTP,i}\left(\frac{L_{PTP,3}}{L_{total}}\right)(T_{w3} - T_{PTP,r3})$
f_{w1}	$\alpha_{VCC,i1}A_{VCC,i}(T_{VCC,r1} - T_{w1}) + \alpha_{PTP,i1}A_{PTP,i}(T_{PTP,r1} - T_{w1})$
f_{w2}	$\alpha_{VCC,i1}A_{VCC,i}(T_{VCC,r1} - T_{w2}) + \alpha_{PTP,i2}A_{c,i}(T_{PTP,r2} - T_{w2})$
f_{w3}	$\alpha_{VCC,i1}A_{VCC,i}(T_{VCC,r1} - T_{w3}) + \alpha_{PTP,i3}A_{c,i}(T_{PTP,r3} - T_{w3})$
f_{w4}	0

In Condition 2, the PTP condenser has two phase regions, while the VCC evaporator has only one two-phase region, as shown in Figure 37. Refrigerant wall conservations were performed on $L_{PTP,2}$ and $L_{PTP,3}$. Detailed expressions of f vector are presented in Table 11.

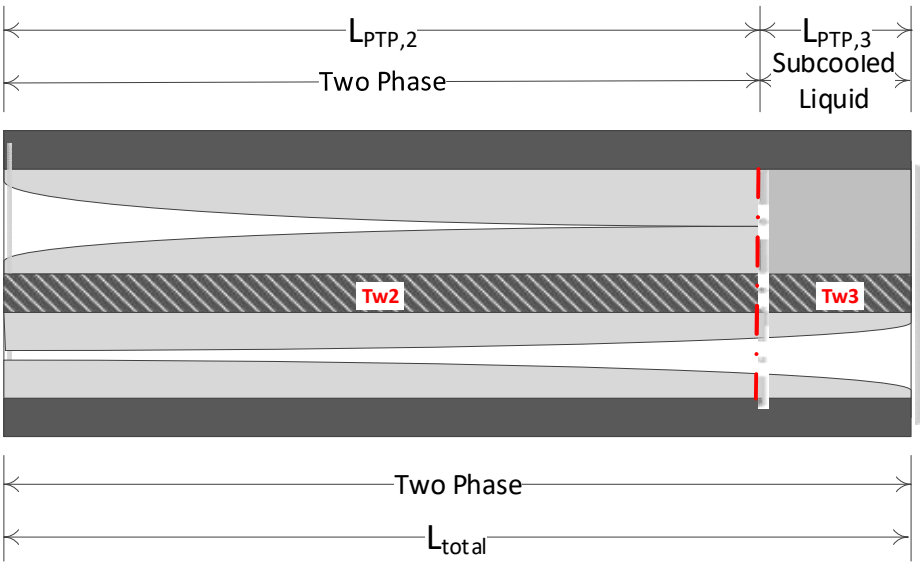

Figure 37: Refrigerant-to-refrigerant heat exchanger - Condition 2

Table 11: Refrigerant-to-refrigerant heat exchanger f vector - Condition 2

$f_{VCC,1}$	$\dot{m}_{VCC,i}h_{VCC,i} - \dot{m}_{VCC,o}h_{VCC,o} + A_{VCC,i}\left(\frac{L_{PTP,2}}{L_{total}}\right)(T_{w2} - T_{VCC,r1}) + \alpha_{VCC,i1}A_{VCC,i}\left(\frac{L_{PTP,3}}{L_{total}}\right)(T_{w3} - T_{VCC,r1})$
$f_{VCC,2}$	0
$f_{PTP,1}$	0
$f_{PTP,2}$	$\dot{m}_{PTP,i}(h_{PTP,i} - h_{PTP,g}) + \alpha_{PTP,i2}A_{PTP,i}\left(\frac{L_{PTP,2}}{L_{total}}\right)(T_{w2} - T_{PTP,r2})$
$f_{PTP,3}$	$\dot{m}_{PTP,i}h_g - \dot{m}_{PTP,o}h_{PTP,f} + \alpha_{PTP,i3}A_{PTP,i}\left(\frac{L_{PTP,3}}{L_{total}}\right)(T_{w3} - T_{PTP,r3})$
f_{w1}	0
f_{w2}	$\alpha_{VCC,i1}A_{VCC,i}(T_{VCC,r1} - T_{w2}) + \alpha_{PTP,i2}A_{c,i}(T_{PTP,r2} - T_{w2})$
f_{w3}	$\alpha_{VCC,i1}A_{VCC,i}(T_{VCC,r1} - T_{w3}) + \alpha_{PTP,i3}A_{c,i}(T_{PTP,r3} - T_{w3})$
f_{w4}	0

When the PTP condenser has only two-phase region and the VCC evaporator has a two-phase region and a superheated vapor region, the length of each region affects the fluid phase on both sides of T_{w3}. When the length of the two-phase region in VCC evaporator $L_{VCC,1}$ is less than the length of the two-phase region in PTP condenser $L_{PTP,2}$, T_{w3} has a two-phase fluid region on both the PTP condenser side and the VCC evaporator side. When the length of the two-phase region in VCC evaporator $L_{VCC,1}$ is greater than the length of the two-phase region in PTP condenser $L_{PTP,2}$, T_{w3} has a two-phase fluid region on the PTP condenser side and superheated vapor on the VCC evaporator side. The heat-transfer coefficients are dramatically different when the region length changed. Therefore, when performing wall temperature conservation, the length difference must be calculated separately.

In Condition 3, the PTP condenser has a two-phase region and a subcooled liquid region, while the VCC evaporator has a two-phase region and a superheated vapor region, as shown in Figure 38. In Condition 3, the length of the two-phase region in VCC evaporator, $L_{VCC,1}$, is less than the length of the two-phase region in PTP condenser $L_{PTP,2}$. Refrigerant wall conservations are performed on $L_{VCC,1}$, $L_{PTP,2} - L_{VCC,1}$, and $L_{PTP,3}$. T_{w3} had two-phase fluid on the PTP condenser side and superheated vapor on the VCC evaporator side. Detailed expressions of the f vector are presented in Table 12.

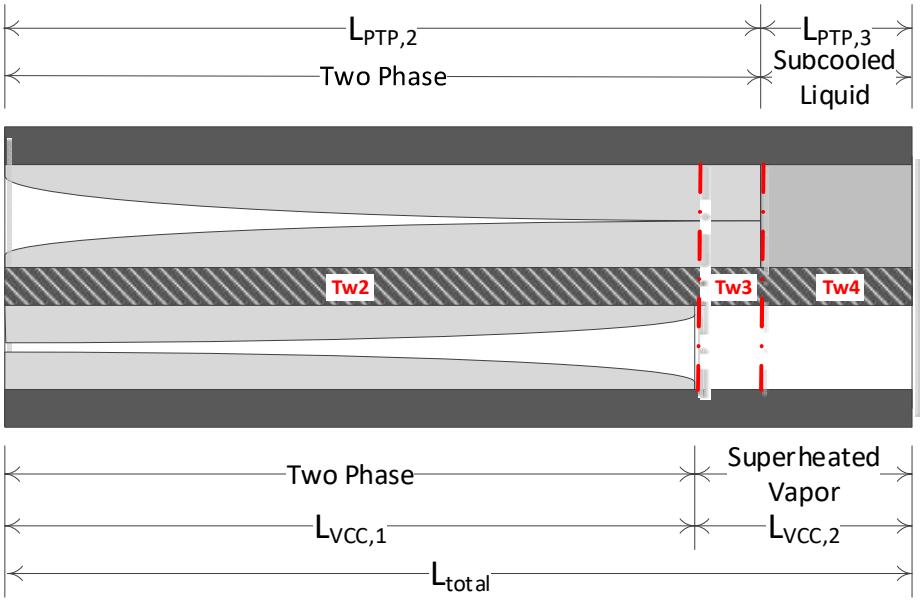

Figure 38: Refrigerant-to-refrigerant heat exchanger - Condition 3

Table 12: Refrigerant-to-refrigerant heat exchanger f vector - Condition 3

$f_{VCC,1}$	$\dot{m}_{VCC,i}h_{VCC,i} - \dot{m}_{VCC,o}h_{VCC,g} + \alpha_{VCC,i1}A_{VCC,i}\left(\frac{L_{PTP,2}}{L_{total}}\right)\left(T_{w2} - T_{VCC,r1}\right)$
$f_{VCC,2}$	$\dot{m}_{VCC,o}\left(h_{VCC,g} - h_{VCC,o}\right) + \alpha_{VCC,i2}A_{VCC,i}\left(\frac{L_{PTP,2} - L_{VCC,1}}{L_{total}}\right)\left(T_{w3} - T_{VCC,r2}\right)$ $+ \alpha_{VCC,i1}A_{VCC,i}\left(\frac{L_{PTP,3}}{L_{total}}\right)\left(T_{w4} - T_{VCC,r2}\right)$
$f_{PTP,1}$	0
$f_{PTP,2}$	$\dot{m}_{PTP,in}\left(h_{PTP,in} - h_{PTP,g}\right) + \alpha_{PTP,i2}A_{PTP,i}\left(\frac{L_{PTP,2}}{L_{total}}\right)\left(T_{w2} - T_{PTP,r2}\right)$ $+ \alpha_{PTP,i2}A_{c,i}\left(\frac{L_{PTP,2} - L_{VCC,1}}{L_{total}}\right)\left(T_{w3} - T_{PTP,r2}\right)$
$f_{PTP,3}$	$\dot{m}_{PTP,i}h_{PTP,g} - \dot{m}_{PTP,o}h_{PTP,f} + \alpha_{PTP,i3}A_{PTP,i}\left(\frac{L_{PTP,3}}{L_{total}}\right)\left(T_{w3} - T_{PTP,r3}\right)$
f_{w1}	0
f_{w2}	$\alpha_{VCC,i1}A_{VCC,i}\left(T_{VCC,r1} - T_{w2}\right) + \alpha_{VCC,i2}A_{VCC,i}\left(T_{VCC,r2} - T_{w2}\right)$
f_{w3}	$\alpha_{VCC,i2}A_{VCC,i}\left(T_{VCC,r2} - T_{w3}\right) + \alpha_{VCC,i2}A_{VCC,i}\left(T_{VCC,r2} - T_{w3}\right)$
f_{w4}	$\alpha_{VCC,i2}A_{VCC,i}\left(T_{VCC,r2} - T_{w4}\right) + \alpha_{VCC,i3}A_{VCC,i}\left(T_{VCC,r3} - T_{w4}\right)$

In Condition 4, the PTP condenser has a two-phase region and a subcooled liquid region, while the VCC evaporator has a two-phase region and a superheated vapor region, as shown in Figure 39. In Condition 4, the length of the two-phase region in VCC evaporator $L_{VCC,1}$ is greater than length of the two-phase region in PTP condenser $L_{PTP,2}$. T_{w3} has two-phase fluid on both the PTP condenser side and the VCC evaporator side. Detailed expressions of the f vector are presented in Table 13.

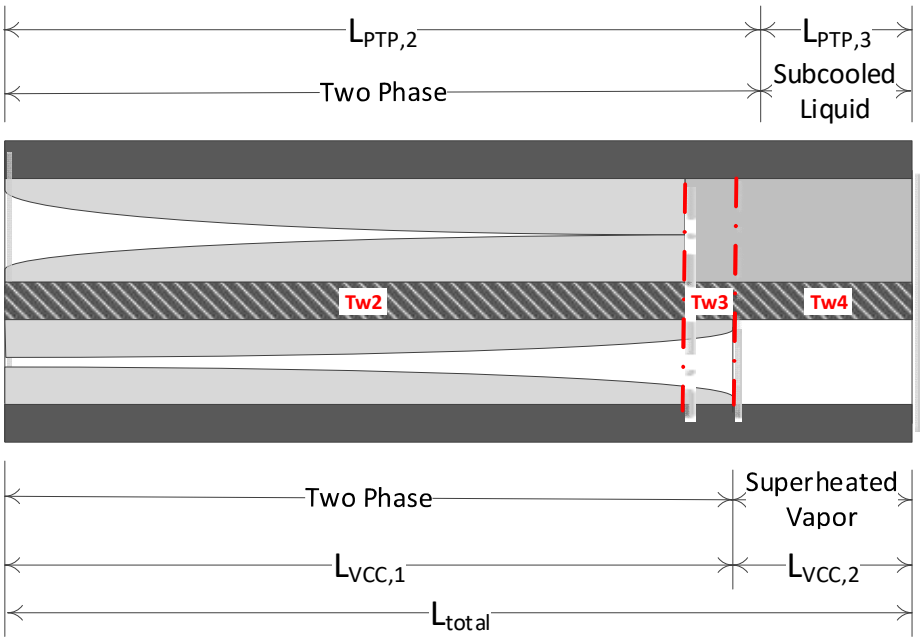

Figure 39: Refrigerant-to-refrigerant heat exchanger - Condition 4

Table 13: Refrigerant-to-refrigerant heat exchanger f vector - Condition 4

$f_{VCC,1}$	$\dot{m}_{VCC,i}h_{VCC,i} - \dot{m}_{VCC,o}h_{VCC,g} + \alpha_{VCC,i1}A_{VCC,i}\left(\frac{L_{PTP,2}}{L_{total}}\right)(T_{w2} - T_{VCC,r1}) + \alpha_{VCC,i1}A_{VCC,i}\left(\frac{L_{VCC,1} - L_{PTP,2}}{L_{total}}\right)(T_{w3} - T_{VCC,r1})$
$f_{VCC,2}$	$\dot{m}_{VCC,o}(h_{VCC,g} - h_{VCC,o}) + \alpha_{VCC,i1}A_{VCC,i}\left(\frac{L_{VCC,2}}{L_{total}}\right)(T_{w4} - T_{VCC,r2})$
$f_{PTP,1}$	0

Table 13: Continued

$f_{PTP,2}$	$\dot{m}_{PTP,in}\left(h_{PTP,in} - h_{PTP,g}\right) + \alpha_{PTP,i2}A_{PTP,i}\left(\frac{L_{PTP,2}}{L_{total}}\right)\left(T_{w2} - T_{PTP,r2}\right) + \alpha_{PTP,i2}A_{PTP,i}\left(\frac{L_{VCC,1} - L_{PTP,2}}{L_{total}}\right)\left(T_{w3} - T_{PTP,r2}\right)$
$f_{PTP,3}$	$\dot{m}_{PTP,i}h_{PTP,g} - \dot{m}_{PTP,o}h_{PTP,f} + \alpha_{PTP,i3}A_{PTP,i}\left(\frac{L_{PTP,3}}{L_{total}}\right)\left(T_{w3} - T_{PTP,r3}\right)$
f_{w1}	0
f_{w2}	$\alpha_{VCC,i1}A_{VCC,i}\left(T_{VCC,r1} - T_{w2}\right) + \alpha_{PTP,i2}A_{PTP,i}\left(T_{PTP,r2} - T_{w2}\right)$
f_{w3}	$\alpha_{VCC,i1}A_{VCC,i}\left(T_{VCC,r1} - T_{w3}\right) + \alpha_{PTP,i3}A_{PTP,i}\left(T_{PTP,r3} - T_{w3}\right)$
f_{w4}	$\alpha_{VCC,i2}A_{VCC,i}\left(T_{VCC,r2} - T_{w4}\right) + \alpha_{PTP,i3}A_{PTP,i}\left(T_{PTP,r3} - T_{w4}\right)$

When the PTP condenser has superheated vapor, two-phase fluid, and subcooled liquid regions and the VCC evaporator has a two-phase region and a superheated vapor region, the length of each fluid region changes, and T_{w2} and T_{w3} encounter different fluid regions on both sides. Thus, the PTP condenser with three phase regions and the VCC evaporator with two fluid regions are separated into three subconditions.

In Condition 5, as shown in Figure 40, the PTP condenser has superheated vapor, two-phase fluid, and subcooled liquid regions, and the VCC evaporator has a two-phase region and a superheated vapor region. The length of the two-phase region in VCC evaporator $L_{VCC,1}$ is less than the length of the superheated region in PTP condenser $L_{PTP,1}$. T_{w2} has superheated vapor on the PTP condenser side with two-phase fluid on the VCC evaporator side. T_{w3} has two-phase fluid on the PTP condenser side with superheated vapor on the VCC evaporator side. The f vectors are summarized in Table 14.

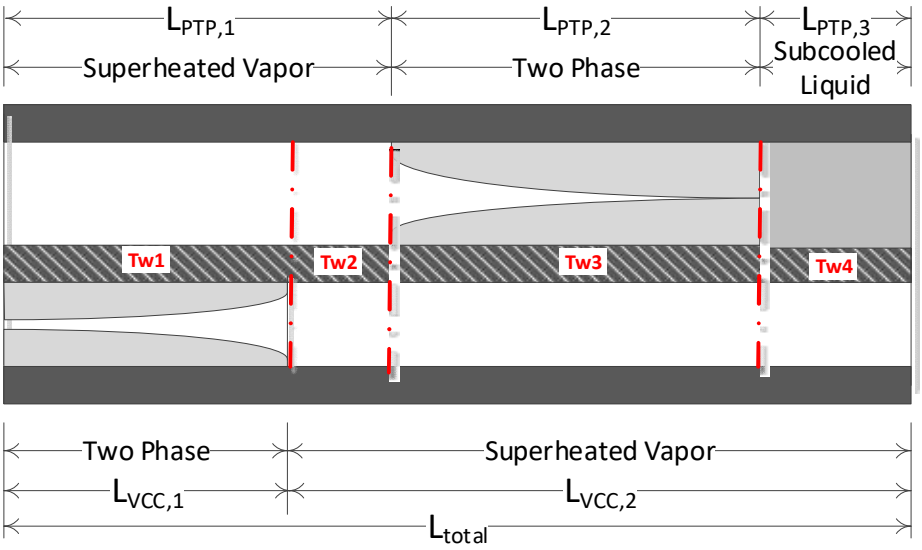

Figure 40: Refrigerant-to-refrigerant heat exchanger - Condition 5

Table 14: Refrigerant-to-refrigerant heat exchanger f vector - Condition 5

$f_{VCC,1}$	$\dot{m}_{VCC,i}h_{VCC,i} - \dot{m}_{VCC,o}h_{VCC,g} + \alpha_{VCC,i1}A_{VCC,i}\left(\frac{L_{VCC,1}}{L_{total}}\right)(T_{w1} - T_{VCC,r1})$
$f_{VCC,2}$	$\dot{m}_{VCC,o}(h_{VCC,g} - h_{VCC,o}) + \alpha_{VCC,i2}A_{VCC,i}\left(\frac{L_{PTP,1} - L_{VCC,1}}{L_{total}}\right)(T_{w2} - T_{VCC,r2}) + \alpha_{VCC,i2}A_{VCC,i}\left(\frac{L_{PTP,2}}{L_{total}}\right)(T_{w3} - T_{VCC,r2}) + \alpha_{VCC,i2}A_{VCC,i}\left(\frac{L_{PTP,3}}{L_{total}}\right)(T_{w4} - T_{VCC,r2})$
$f_{PTP,1}$	$\dot{m}_{PTP,o}(h_{PTP,g} - h_{PTP,o}) + \alpha_{PTP,i1}A_{PTP,i}\left(\frac{L_{VCC,1}}{L_{total}}\right)(T_{w1} - T_{PTP,r1}) + \alpha_{PTP,i1}A_{PTP,i}\left(\frac{L_{PTP,1} - L_{VCC,1}}{L_{total}}\right)(T_{w2} - T_{PTP,r1})$
$f_{PTP,2}$	$\dot{m}_{PTP,i}(h_{PTP,i} - h_{PTP,g}) + \alpha_{PTP,i2}A_{PTP,i}\left(\frac{L_{PTP,2}}{L_{total}}\right)(T_{w3} - T_{PTP,r2})$
$f_{PTP,3}$	$\dot{m}_{PTP,i}h_{PTPg} - \dot{m}_{PTP,o}h_{PTP,f} + \alpha_{PTP,i3}A_{PTP,i}\left(\frac{L_{PTP,3}}{L_{total}}\right)(T_{w4} - T_{PTP,r3})$
f_{w1}	$\alpha_{VCC,i1}A_{VCC,i}(T_{VCC,r1} - T_{w1}) + \alpha_{PTP,i1}A_{PTP,i}(T_{PTP,r1} - T_{w1})$
f_{w2}	$\alpha_{VCC,i2}A_{VCC,i}(T_{VCC,r2} - T_{w2}) + \alpha_{PTP,i1}A_{PTP,i}(T_{PTP,r1} - T_{w2})$
f_{w3}	$\alpha_{VCC,i2}A_{VCC,i}(T_{VCC,r2} - T_{w3}) + \alpha_{PTP,i2}A_{PTP,i}(T_{PTP,r2} - T_{w3})$
f_{w4}	$\alpha_{VCC,i2}A_{VCC,i}(T_{VCC,r2} - T_{w3}) + \alpha_{PTP,i3}A_{PTP,i}(T_{PTP,r3} - T_{w3})$

In Condition 6, as shown in Figure 41, the PTP condenser has superheated vapor, two-phase fluid, and subcooled liquid regions, and the VCC evaporator has a two-phase region and a superheated vapor region. The length of the two-phase region in VCC evaporator $L_{VCC,1}$ is greater than the length of the superheated region in PTP condenser $L_{PTP,1}$ and less than the length of the two-phase region in PTP condenser $L_{PTP,2}$. T_{w2} has two-phase fluid on both the PTP condenser side and the VCC evaporator side. T_{w3} has two-phase fluid on the PTP condenser side and superheated vapor on the VCC evaporator side. The f vectors are summarized in Table 15.

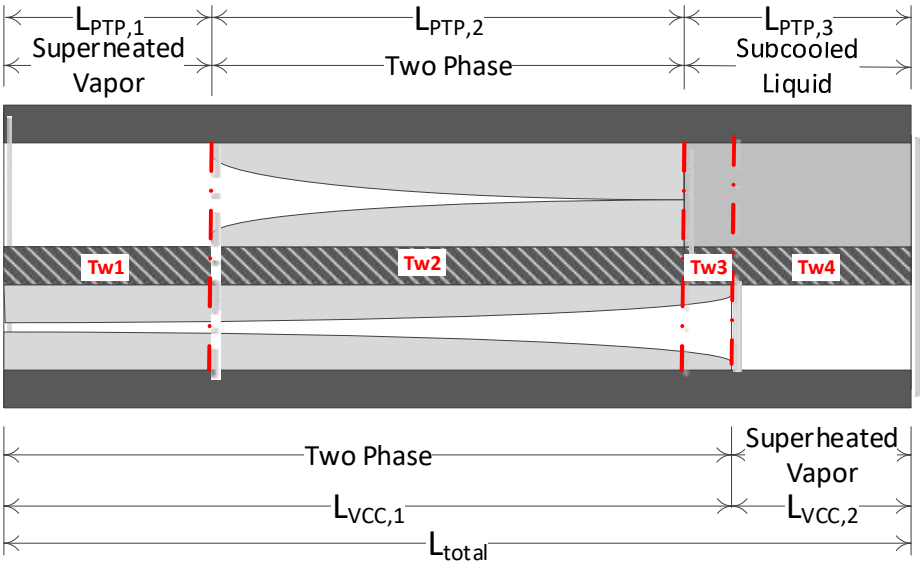

Figure 41: Refrigerant-to-refrigerant heat exchanger - Condition 6

Table 15: Refrigerant-to-refrigerant heat exchanger f vector - Condition 6

$f_{VCC,1}$	$\dot{m}_{VCC,i}h_{VCC,i} - \dot{m}_{VCC,o}h_{VCC,g} + \alpha_{VCC,i1}A_{VCC,i}\left(\frac{L_{PTP,1}}{L_{total}}\right)(T_{w1} - T_{VCC,r1}) + \alpha_{VCC,i1}A_{VCC,i}\left(\frac{L_{VCC,1} - L_{PTP,1}}{L_{total}}\right)(T_{w2} - T_{VCC,r1})$
$f_{VCC,2}$	$\dot{m}_{VCC,o}(h_{VCC,g} - h_{VCC,o}) + \alpha_{VCC,i2}A_{VCC,i}\left(\frac{L_{VCC,2} - L_{PTP,3}}{L_{total}}\right)(T_{w3} - T_{VCC,r2}) + \alpha_{VCC,i2}A_{VCC,i}\left(\frac{L_{PTP,3}}{L_{total}}\right)(T_{w4} - T_{VCC,r2})$
$f_{PTP,1}$	$\dot{m}_{PTP,o}(h_{PTP,g} - h_{PTP,o}) + \alpha_{PTP,i1}A_{PTP,i}\left(\frac{L_{PTP,1}}{L_{total}}\right)(T_{w1} - T_{PTP,r1})$
$f_{PTP,2}$	$\dot{m}_{PTP,i}(h_{PTP,i} - h_{PTP,g}) + \alpha_{PTP,i2}A_{PTP,i}\left(\frac{L_{VCC,1} - L_{PTP,1}}{L_{total}}\right)(T_{w2} - T_{PTP,r2}) + \alpha_{PTP,i3}A_{PTP,i}\left(\frac{L_{VCC,2} - L_{PTP,3}}{L_{total}}\right)(T_{w3} - T_{PTP,r3})$
$f_{PTP,3}$	$\dot{m}_{PTP,i}h_{PTP,g} - \dot{m}_{PTP,o}h_{PTP,f} + \alpha_{PTP,i3}A_{PTP,i}\left(\frac{L_{PTP,3}}{L_{total}}\right)(T_{w4} - T_{PTP,r3})$
f_{w1}	$\alpha_{VCC,i1}A_{VCC,i}(T_{VCC,r1} - T_{w1}) + \alpha_{PTP,i1}A_{PTP,i}(T_{PTP,r1} - T_{w1})$
f_{w2}	$\alpha_{VCC,i1}A_{VCC,i}(T_{VCC,r1} - T_{w2}) + \alpha_{PTP,i2}A_{PTP,i}(T_{PTP,r2} - T_{w2})$
f_{w3}	$\alpha_{VCC,i2}A_{VCC,i}(T_{VCC,r2} - T_{w3}) + \alpha_{PTP,i2}A_{PTP,i}(T_{PTP,r2} - T_{w3})$
f_{w4}	$\alpha_{VCC,i2}A_{VCC,i}(T_{VCC,r2} - T_{w3}) + \alpha_{PTP,i3}A_{PTP,i}(T_{PTP,r3} - T_{w3})$

In Condition 7, as shown in Figure 42, the PTP condenser has superheated vapor, two-phase fluid, and subcooled liquid regions, and the VCC evaporator has a two-phase region and a superheated vapor region. The length of the two-phase region in VCC evaporator $L_{VCC,1}$ is greater than the length of the superheated region in PTP condenser $L_{PTP,1}$ plus the length of the two-phase region in PTP condenser L_2. T_{w2} has two-phase fluid on both the PTP condenser side and the VCC evaporator side. T_{w3} has subcooled liquid on the PTP condenser side and two-phase fluid on the VCC evaporator side. The f vectors are summarized in Table 16.

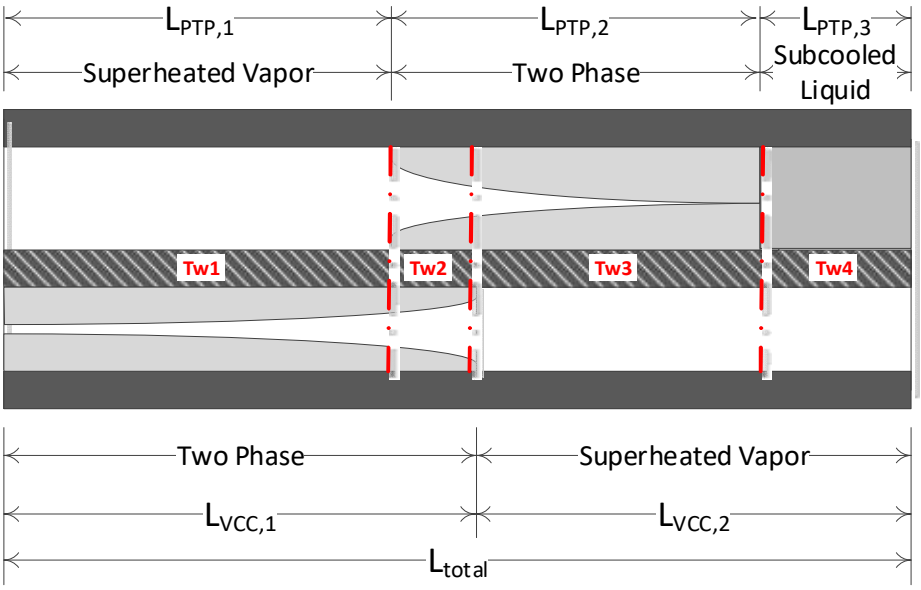

Figure 42: Refrigerant-to-refrigerant heat exchanger - Condition 7

Table 16: Refrigerant-to-refrigerant heat exchanger f vector- Condition 7

$f_{VCC,1}$	$\dot{m}_{VCC,i}h_{VCC,i} - \dot{m}_{VCC,o}h_{VCC,g} + \alpha_{VCC,i1}A_{VCC,i}\left(\frac{L_{PTP,1}}{L_{total}}\right)(T_{w1} - T_{VCC,r1}) + \alpha_{VCC,i2}A_{VCC,i}\left(\frac{L_{PTP,2}}{L_{total}}\right)(T_{w2} - T_{VCC,r1}) + \alpha_{VCC,i2}A_{VCC,i}\left(\frac{L_{VCC,1} - L_{PTP,1} - L_{PTP,2}}{L_{total}}\right)(T_{w3} - T_{VCC,r1})$
$f_{VCC,2}$	$\dot{m}_{VCC,o}(h_{VCC,g} - h_{VCC,o}) + \alpha_{VCC,i2}A_{VCC,i}\left(\frac{L_{PTP}}{L_{total}}\right)(T_{w4} - T_{VCC,r2})$
$f_{PTP,1}$	$\dot{m}_{PTP,o}(h_{PTP,g} - h_{PTP,o}) + \alpha_{PTP,i1}A_{PTP,i}\left(\frac{L_{PTP,1}}{L_{total}}\right)(T_{w1} - T_{PTP,r1})$
$f_{PTP,2}$	$\dot{m}_{PTP,i}(h_{PTP,in} - h_{PTP,g}) + \alpha_{PTP,i2}A_{PTP,i}\left(\frac{L_{PTP,2}}{L_{total}}\right)(T_{w2} - T_{PTP,r2})$
$f_{PTP,3}$	$\dot{m}_{PTP,i}h_g - \dot{m}_{PTP,o}h_{PTP,f} + \alpha_{PTP,i3}A_{PTP,i}\left(\frac{L_{VCC,1} - L_{PTP,1} - L_{PTP,2}}{L_{total}}\right)(T_{w3} - T_{PTP,r3}) + \alpha_{PTP,i3}A_{PTP,i}\left(\frac{L_{VCC,2}}{L_{total}}\right)(T_{w4} - T_{PTP,r3})$
f_{w1}	$\alpha_{VCC,i1}A_{VCC,i}(T_{VCC,r1} - T_{w1}) + \alpha_{PTP,i1}A_{PTP,i}(T_{PTP,r1} - T_{w1})$

Table 16: Continued

f_{w2}	$\alpha_{VCC,i1}A_{VCC,i}(T_{VCC,r1}-T_{w2})+\alpha_{PTP,i2}A_{PTP,i}(T_{PTP,r2}-T_{w2})$
f_{w3}	$\alpha_{VCC,i1}A_{VCC,i}(T_{VCC,r1}-T_{w3})+\alpha_{PTP,i3}A_{PTP,i}(T_{PTP,r3}-T_{w3})$
f_{w4}	$\alpha_{VCC,i2}A_{VCC,i}(T_{VCC,r2}-T_{w3})+\alpha_{PTP,i3}A_{PTP,i}(T_{PTP,r3}-T_{w4})$

The state vector in the integrated refrigerant-to-refrigerant combined heat exchanger was expanded to Equation (47) with the corresponding u vector in Equation (48). The governing matrix of the integrated PTP-VCC heat exchanger was updated as Equation (49), with n representing the numbers of PTP evaporators in parallel.

$$x = [P \quad x_{e,1} \quad x_{e,2} \quad x_{e,3} \quad \dots \quad x_{e,n} \quad x_{r2r}] \tag{47}$$

$$u = [x_{e,1} \quad x_{e,2} \quad x_{e,3} \quad \dots \quad x_{e,n} \quad x_{r2r}] \tag{48}$$

$$\begin{bmatrix} Z_{e_1,1} & Z_{e_1,2} & 0 & 0 & 0 & 0 & 0 \\ Z_{e_2,1} & 0 & Z_{e_2,2} & 0 & 0 & 0 & 0 \\ Z_{e_3,1} & 0 & 0 & Z_{e_3,2} & 0 & 0 & 0 \\ Z_{e_4,1} & 0 & 0 & 0 & Z_{e_4,2} & 0 & 0 \\ \vdots & 0 & 0 & 0 & 0 & \ddots & 0 \\ Z_{e_n,1} & 0 & 0 & 0 & 0 & Z_{e_n,2} & 0 \\ Z_{r_1} & Z_{r_2,1} & Z_{r_2,2} & Z_{r,4} & \dots & Z_{r_2,n} & Z_{r_3} \end{bmatrix} \begin{bmatrix} \dot{P} \\ \dot{x}_{e,1} \\ \dot{x}_{e,2} \\ \dot{x}_{e,3} \\ \vdots \\ \dot{x}_{e,n} \\ \dot{x}_{r2r} \end{bmatrix} = \begin{bmatrix} f_{e,1} \\ f_{e,2} \\ f_{e,3} \\ f_{e,4} \\ \vdots \\ f_{e,n} \\ f_{r2r} \end{bmatrix} \tag{49}$$

4.2. Integrated System Performance Test

A pump-speed step test was performed as shown in Figure 43 and Figure 44. Figure 43 is the PTP data including pump speeds, PTP system pressures, superheats, exit qualities, wall temperatures, and mass flow rates. The mass flow rates increased with a pump-speed step increase. The exit qualities and wall temperatures decreased with an increase of mass flow rate, as did the PTP heat exchanger pressure. Figure 44 is the VCC data including VCC evaporator and condenser pressures, superheats, and mass flow rates. With the pump step increase, same fluid phase condition was maintained on the PTP side. With the same fluid phase condition and

only 10 kPa of PTP system pressure change, the heat transfer coefficient change was also relatively small. So small fluctuations were observed during the step change, and the changes of steady state values were within 3% with a 10% pump speed step.

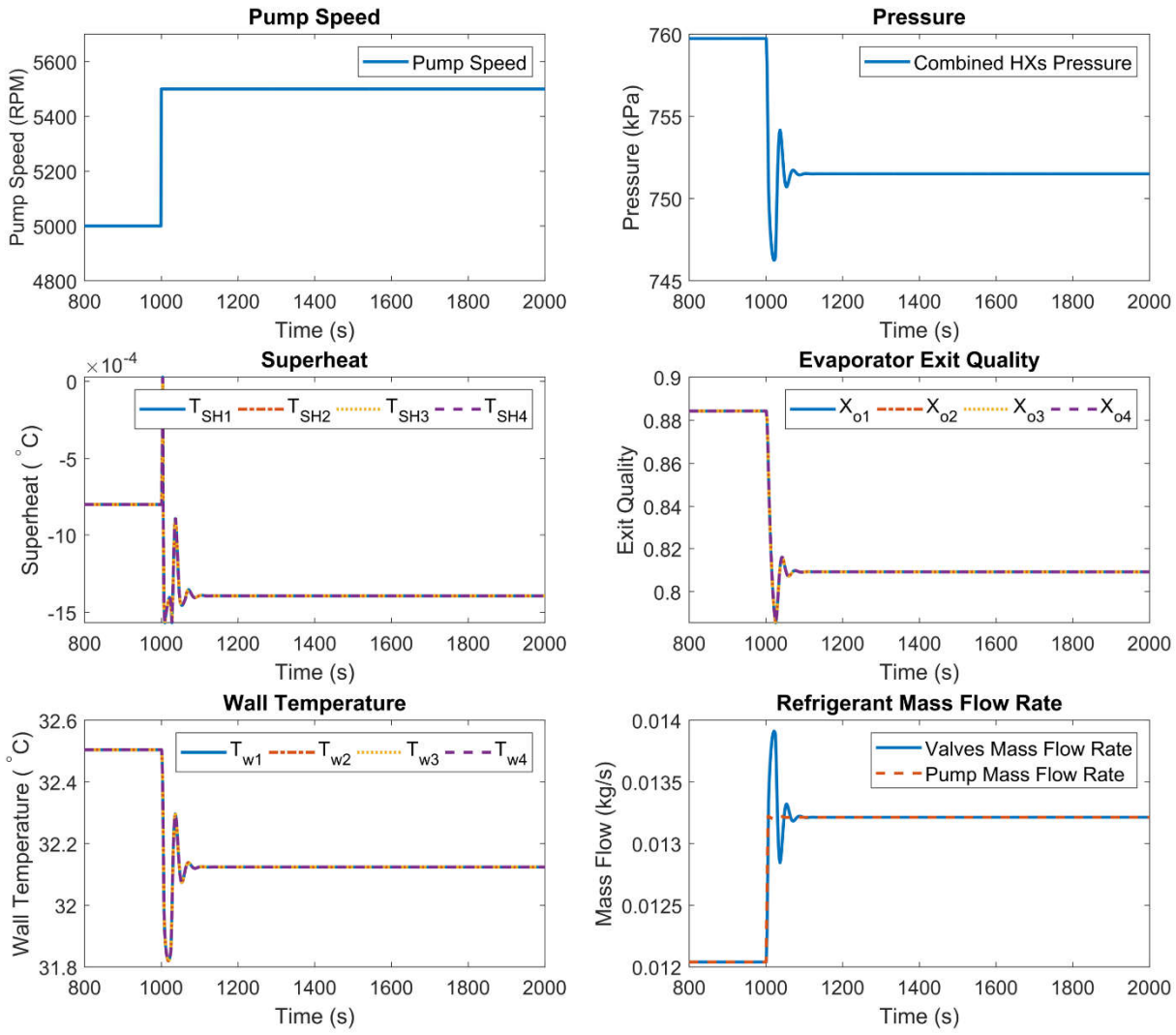

Figure 43: Pump-speed step test - PTP data

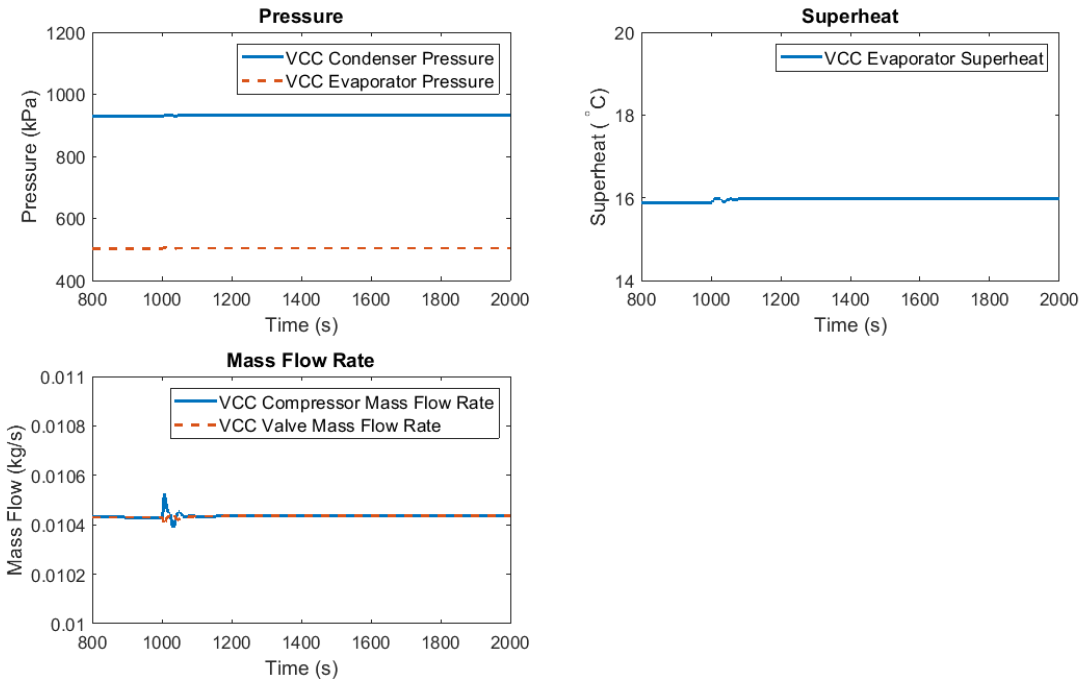

Figure 44: Pump-speed step test - VCC data

Figure 45 and Figure 46 plot the heat load step tests. Figure 45 shows the PTP data including pressures, superheats, exit qualities, wall temperatures, and mass flow rates. Heat loads were given a 20% step increases on each evaporator. The initial system condition was set up with an exit quality closed to 0.9. A heat load step increase of 20%, superheats were observed at the PTP evaporator outlets. High wall temperatures were observed with the appearance of superheated vapor. Figure 46 shows the VCC data including VCC evaporator and condenser pressures, superheats, and mass flow rates. With the heat load step increase, the heat rejected to the VCC side increased, resulting an increase of VCC superheat and slightly fluctuating VCC pressures.

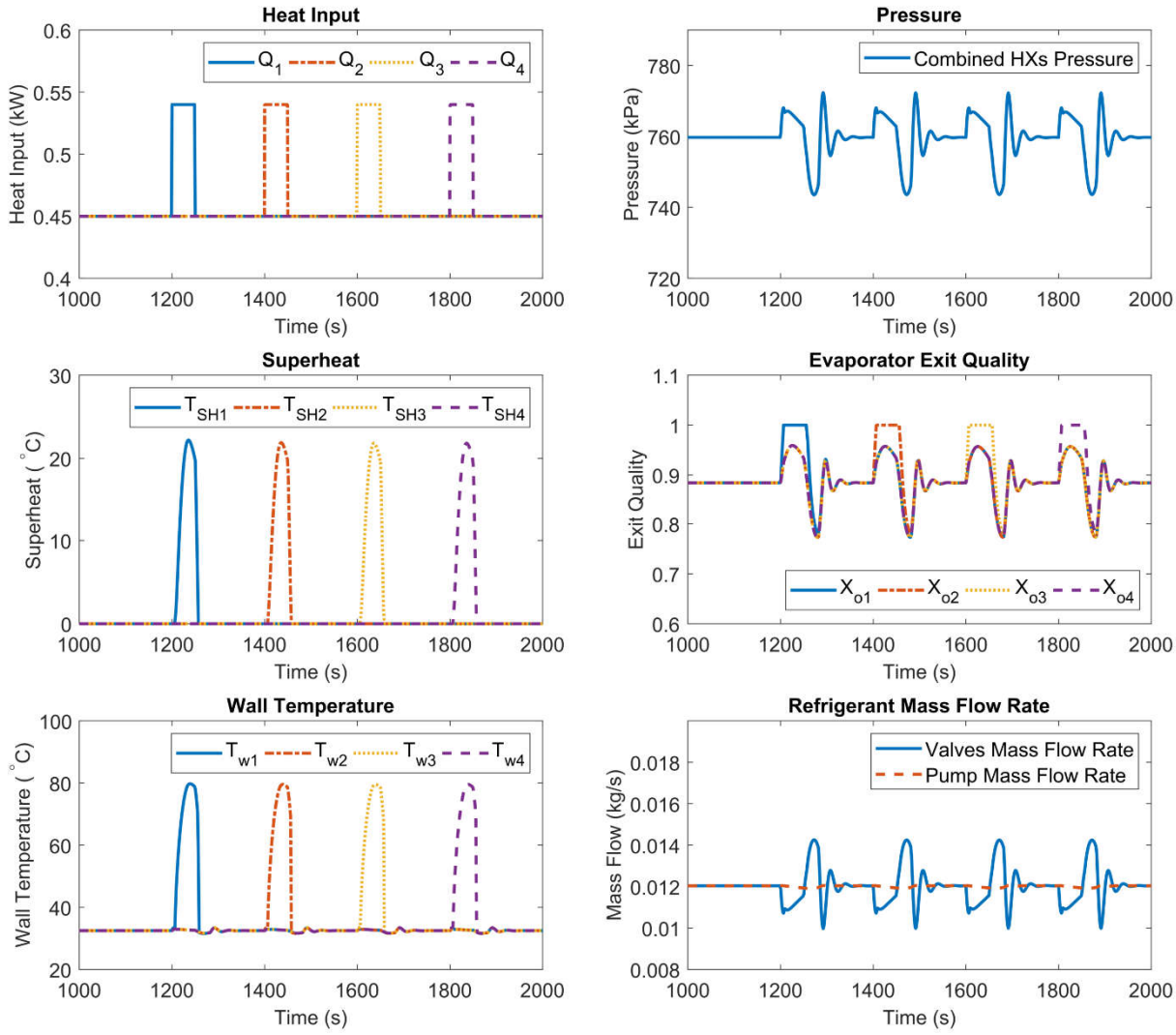

Figure 45: Heat step test - PTP data

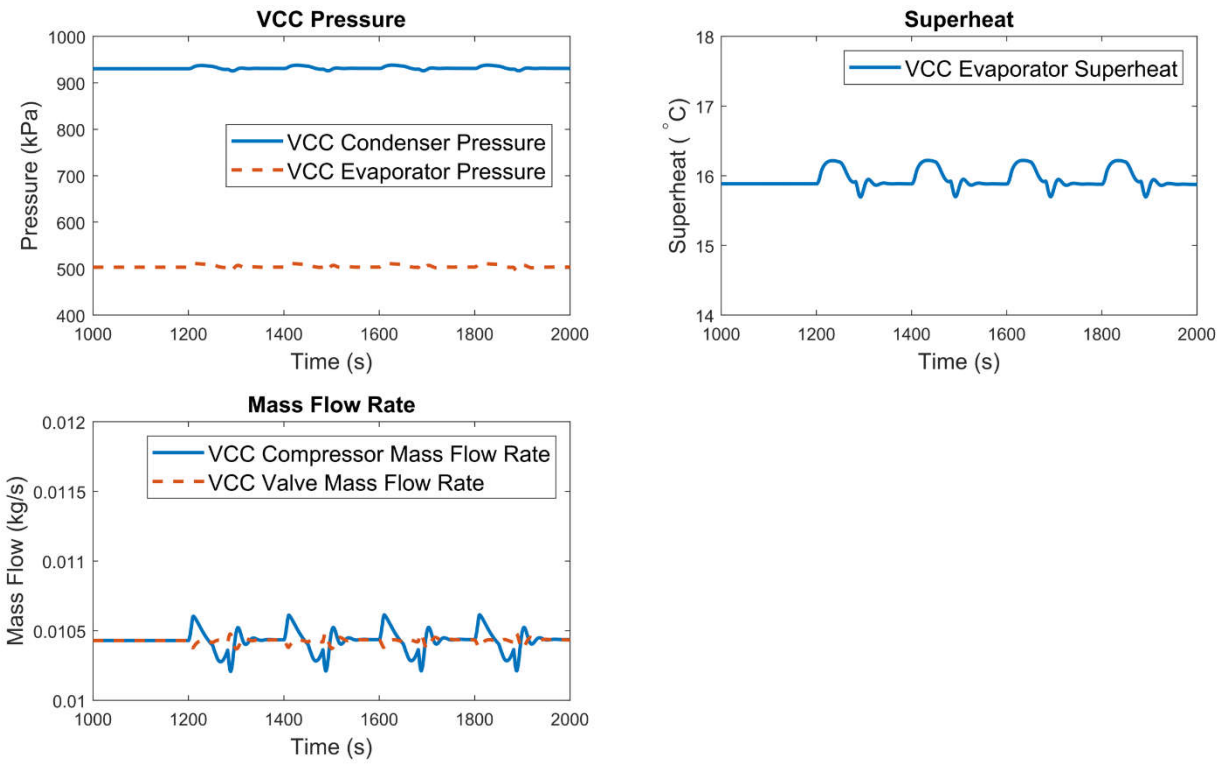

Figure 46: Heat step test - VCC data

The PTP-VCC integrated system was given a 10% VCC compressor step test, shown in Figure 47 and Figure 48. PTP system pressure, evaporator exit qualities, wall temperatures, and mass flow rates from the PTP side are plotted in Figure 47. Compressor speed, VCC evaporator and condenser pressures, superheats, and mass flow rates from the VCC side are plotted in Figure 48. With a 10% VCC compressor step increase, the VCC system pressure differential increased, as did superheats and mass flow rates. Because of the increased heat capacity on the VCC side, pressures, exit qualities, and wall temperatures of the PTP system experienced a step decrease. The mass flow rates of the PTP system increased to compensate for the increased heat capacity on the VCC side.

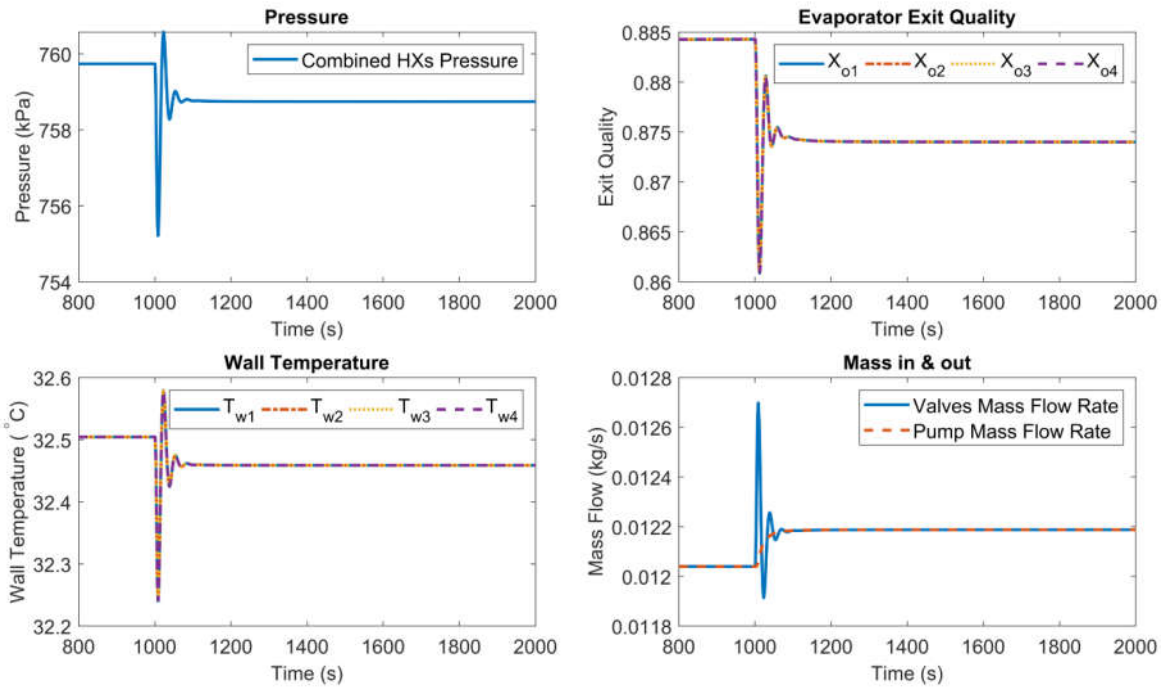

Figure 47: Compressor step test - PTP data

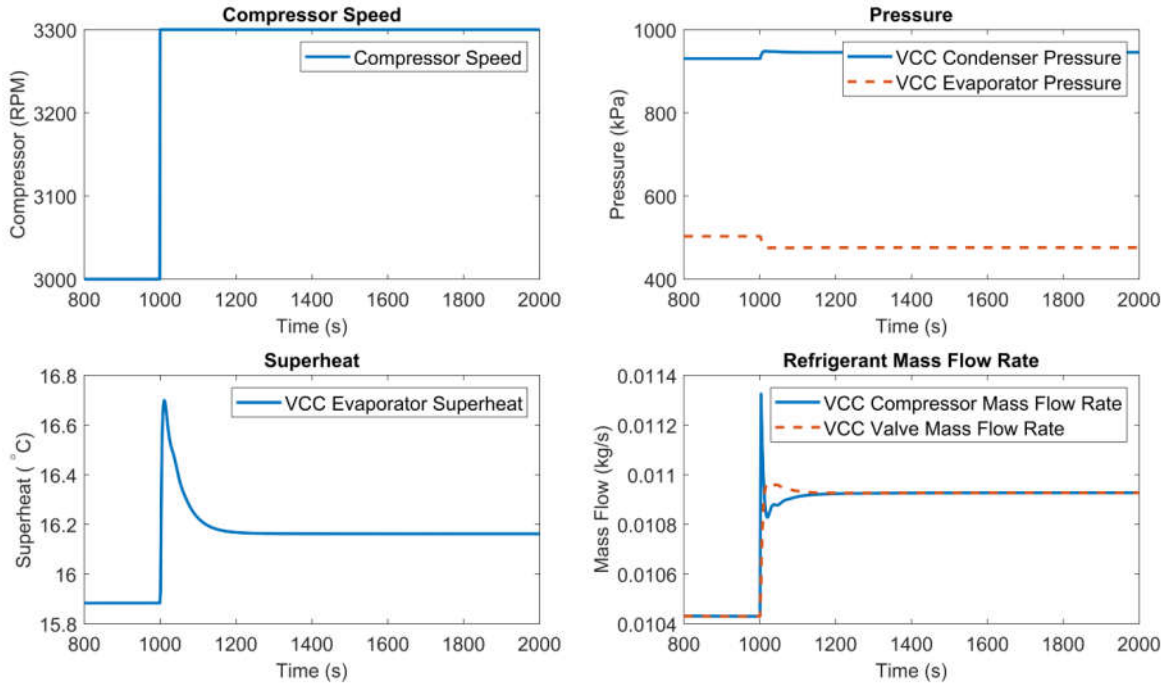

Figure 48: Compressor step test - VCC data

From the above system step tests, system couplings can be observed on the PTP-VCC system. Changes on one side could affect system conditions on the other side. Control architectures that can maintain both cycles at constant operating conditions with external fluctuations are important in the operation of an integrated PTP-VCC system.

5. CONTROL ARCHTECTURE DESIGN OF PUMPED TWO-PHASE AND VAPOR COMPRESSION INTEGRATED SYSTEM

The integrated pumped two-phase (PTP) and vapor compression cycle (VCC) system has a refrigerant-to-refrigerant heat exchanger that increases the coupled dynamics in the system because of shared refrigerant wall temperatures and heat-transfer coefficients.

The PTP system was deployed with the same control architecture as discussed in the Chapter 3 for avoiding critical heat flux (CHF) and maintaining stable refrigerant wall temperatures. For the VCC, superheat needs to be controlled at a constant level to avoid liquid entering the compressor and causing cavity in the compressor. A constant evaporating pressure is also required for stable system operation.

Superheat in a VCC is calculated as the evaporator outlet temperature minus the saturated temperature of evaporator pressure, as shown in Equation (50). From Equation (50), we notice that superheat and evaporating pressure have a coupled relationship. $G(s)_2$ represents the transfer function correlating valve opening position and compressor speed to evaporator superheat and pressure. A similar decoupling matrix found by the inverse of the static gain of $G(s)_2$ was used on the VCC to solve the thermally coupled behavior of superheat and evaporator pressure, as shown in Equation (52). PI controllers were used with the decoupling matrix on the VCC side to maintain constant operating conditions. Figure 49 shows the control architecture applied on the PTP-VCC integrated system.

$$T_{SH} = T_{ero} - T_{sat} \tag{50}$$

$$\begin{bmatrix} T_{SH} \\ P_{evap} \end{bmatrix} = G(s)_2 \begin{bmatrix} u_v \\ \omega_k \end{bmatrix} \quad \textbf{(51)}$$

$$G^{-1}(0)_2 = \begin{bmatrix} -0.084 & 4.3 \\ -0.0044 & -1.282 \end{bmatrix} \quad \textbf{(52)}$$

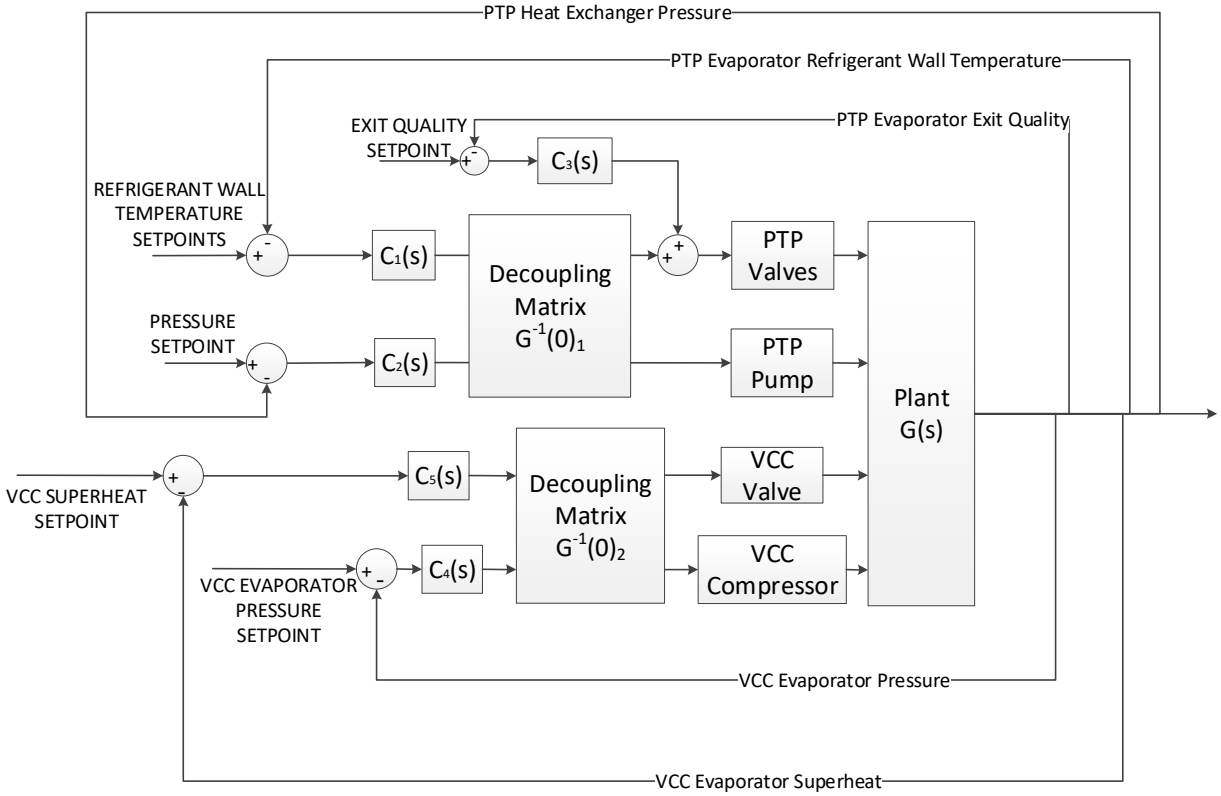

Figure 49: Control architecture for integrated PTP-VCC system

5.1. Cycle Decoupling

The control architecture reduces the coupled dynamics between PTP pressure and refrigerant wall temperatures, as well as the superheat and evaporator pressure in the VCC. The decoupling behavior between the PTP cycle and VCC has yet to be addressed.

Intuitively, the volume of the heat exchanger can affect the speed of pressure dynamics. In modeling procedures, the volume of a heat exchanger is calculated as the length of the heat

exchanger multiplied by the cross-sectional area as shown in Equation (53). To study the effect of cross-sectional area on the time scale of dynamics of the refrigerant-to-refrigerant heat exchanger, a few test cases were conducted with different groups of cross-sectional areas.

$$V = A_{CS} \cdot L \tag{53}$$

The system was tested using the original PTP condenser cross-section area, five times the original cross-section area, and 10 times the original cross-section area. PTP controllers were used to regulate the pressure and refrigerant wall temperatures, the VCC valve was kept at a constant value, and the compressor was given a step increase. At 10 times the PTP condenser cross-section area, the magnitude of the oscillation was the largest, and the initial cross-section area showed the smallest oscillation. The frequency at the initial cross-section area was much faster than 10 times the PTP condenser cross-section area. Intuitively, this group of test means that increasing the PTP condenser volume could increase the coupling between the PTP cycle and the VCC.

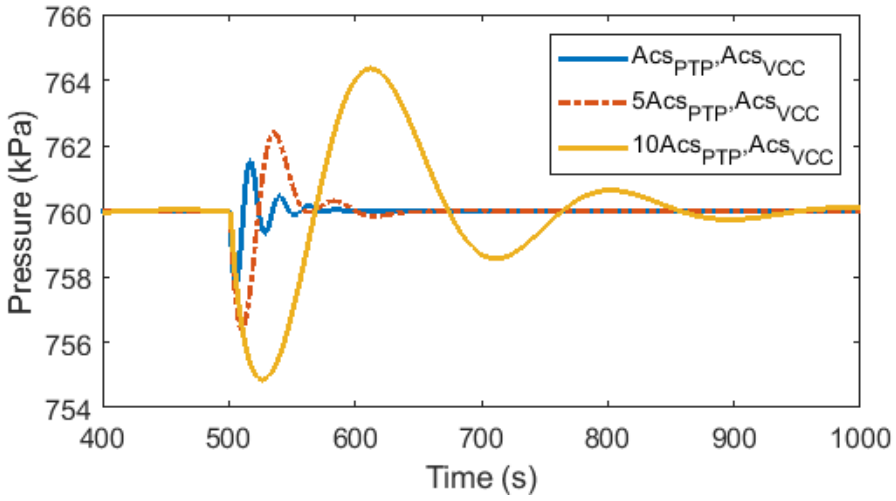

Figure 50: PTP pressure comparisons under different PTP condenser cross-sectional areas

Under the conditions of the initial PTP condenser cross-sectional area, the VCC evaporator cross-section area was increased to 10 times the original value to compare with the initial VCC evaporator cross-section area. PTP controllers were used to regulate the pressure and refrigerant wall temperatures, the VCC valve was kept at a constant value, and compressor was given a step increase. Figure 51 shows the test results. With the same compressor step change, increasing the external VCC evaporator cross-sectional area showed reduced coupling behavior between the two cycles.

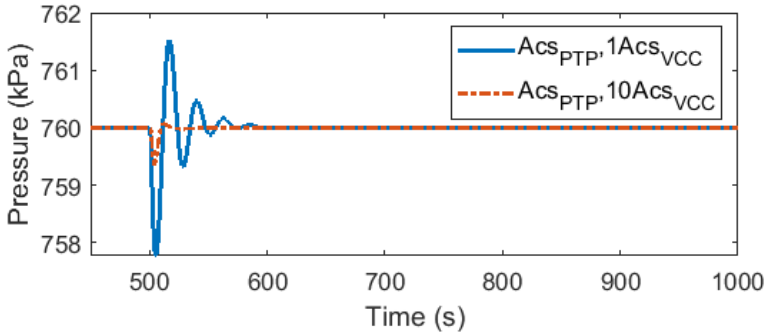

Figure 51: PTP pressure comparisons under different VCC evaporator cross-sectional areas

To validate the effect of cross-sectional area on system time scale further, both VCC evaporator cross-sectional area and PTP condenser cross-sectionalal area were changed together. Figure 52 presents three cases: the initial PTP condenser cross-sectional area and the initial VCC evaporator cross-sectionalal area, 5 times the initial PTP condenser cross-sectional area and the initial VCC evaporator cross-sectional area, the initial PTP condenser cross-sectional area and 10 times the initial VCC evaporator cross-sectional area . PTP controllers were used to regulate the pressure and refrigerant wall temperatures, the VCC compressor was kept at a constant value, and the valve was given a step change, as shown in Figure 52. With the initial PTP condenser

cross-sectional area and 10 times the initial VCC evaporator cross-sectional area, the magnitude and frequency of the oscillation were the smallest among the three test cases.

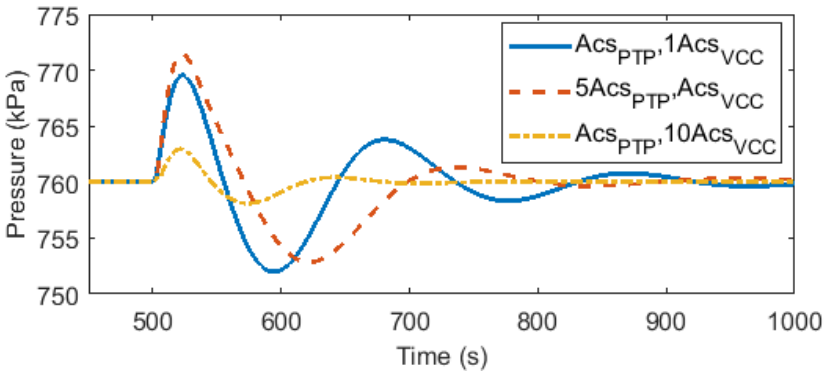

Figure 52: PTP pressure comparisons under different PTP condenser cross-sectional area conditions and VCC evaporator cross-sectional area conditions

The VCC evaporator cross-sectional area was increased further to 20 times the initial value and 30 times the initial value. At 800s to 850s in Figure 53, heat load impulses were applied to the system, and PTP pressure dynamics were plotted. Significant improvement was observed with 10 times the initial VCC evaporator cross-sectional area. However, the improvement was minimum when increasing the cross-sectional area to 20 times the initial value or more.

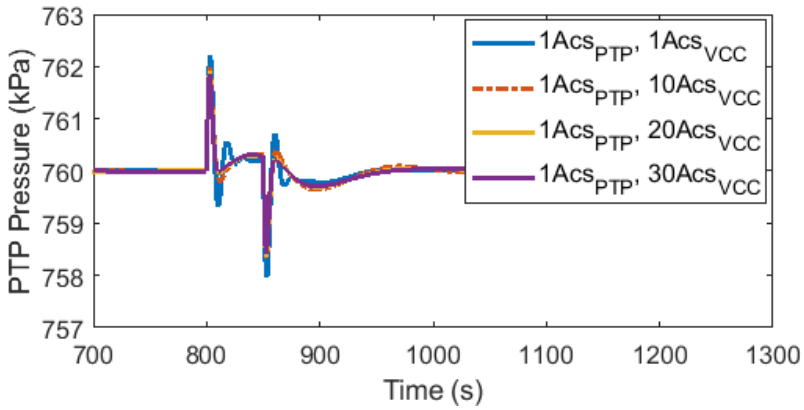

Figure 53: PTP pressure comparisons under large VCC evaporator cross-sectional areas

VCC evaporator superheat and VCC evaporator pressure with the initial PTP condenser cross-sectional area and 10 times the initial VCC evaporator cross-sectional area are compared in Figure 54 and Figure 55. At 3500s, heat impulses were given to the system at a medium load condition. At 6000s, heat impulses were given to the system at a low load condition. Improvement of the magnitude and frequency of the oscillations was observed with 10 times the initial VCC evaporator cross-sectional area.

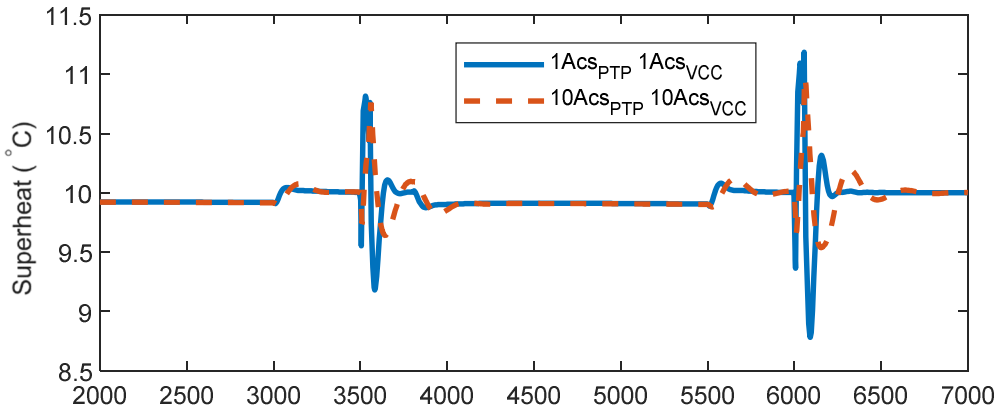

Figure 54: Evaporator superheat comparisons with different VCC evaporator cross-sectional areas

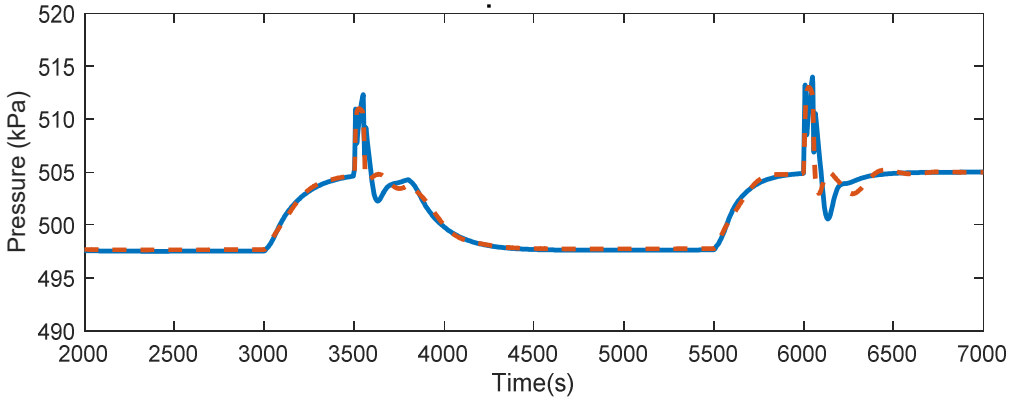

Figure 55: Evaporator pressure comparisons with different VCC evaporator cross-sectional areas

The conclusion can be drawn that a small PTP condenser volume and a relatively large VCC evaporator volume can help with the coupling between the PTP cycle and VCC in an integrated system. This conclusion can be used as a general guideline when designing an integrated PTP-VCC system.

5.2. Time-Scale Separation Analysis

Given the conclusions drawn in the previous section, further mathematical analysis was needed of the time-scale separation of the PTP cycle and the VCC. The lumped-parameter model developed for integrated heat exchangers (detailed in previous sections) is highly nonlinear. A linear model was needed for analyzing the behavior between the two cycles.

5.2.1. Combined Heat Exchanger

The heat exchanger models developed previously are in the form of Equation (54). Assuming $Z(x,u)$ is invertible, Equation (54) can be rearranged in the form of Equation (55).

$$Z(x,u)\cdot\dot{x} = f(x,u) \tag{54}$$

$$\dot{x} = Z(x,u)^{-1}f(x,u) = g(x,u) \tag{55}$$

A local linearization was performed assuming $x = x_0 + \delta x$ and neglecting high-order terms, so Equation (55) can be presented as Equation (56). Expanding $\left[\frac{\partial g}{\partial x}\Big|_{x_0,u_0}\right]$ and $\left[\frac{\partial g}{\partial u}\Big|_{x_0,u_0}\right]$, Equation (56) can be denoted as Equation (57). Using F_x and F_u to represent $\left[\frac{\partial g}{\partial x}\Big|_{x_0,u_0}\right]$ and $\left[\frac{\partial g}{\partial u}\Big|_{x_0,u_0}\right]$, Equation (58) has a similar form of $\dot{x} = Ax + Bu$. This form can be denoted as Equation (59) using the substitution in Equations (60), (61), (62), and (63).

$$\dot{x} = \left[\frac{\partial g}{\partial x}\Big|_{x_0,u_0}\right](x - x_0) + \left[\frac{\partial g}{\partial u}\Big|_{x_0,u_0}\right](u - u_0) \quad \textbf{(56)}$$

$$\dot{x} = \left[Z|_{x_0,u_0}\right]^{-1}\left[\frac{\partial f}{\partial x}\Big|_{x_0,u_0}\right](x - x_0) + \left[Z|_{x_0,u_0}\right]^{-1}\left[\frac{\partial f}{\partial u}\Big|_{x_0,u_0}\right](u - u_0) \quad \textbf{(57)}$$

$$\dot{x} = Z^{-1}F_x(x - x_0) + Z^{-1}F_u(u - u_0) \quad \textbf{(58)}$$

$$\dot{x} = A\delta x + B\delta u \quad \textbf{(59)}$$

$$A = Z^{-1}F_x \quad \textbf{(60)}$$

$$B = Z^{-1}F_u \quad \textbf{(61)}$$

$$F_x = \frac{\partial f}{\partial x}\Big|_{x_0,u_0} \quad \textbf{(62)}$$

$$F_u = \frac{\partial f}{\partial u}\Big|_{x_0,u_0} \quad \textbf{(63)}$$

Equation (64) is listed as the nonlinear output equations. With the substitution in Equation (67) and (68), the linearized version is denoted as Equation (65), which the standard form is as Equation (66).

$$y = g(x, u) \quad \textbf{(64)}$$

$$\delta y = G_x\delta x + G_u\delta u \quad \textbf{(65)}$$

$$\delta y = C\delta x + D\delta u \quad \textbf{(66)}$$

$$C = G_x = \frac{\partial g}{\partial x}\Big|_{x_0,u_0} \quad \textbf{(67)}$$

$$D = G_u = \frac{\partial g}{\partial u}\Big|_{x_0,u_0} \quad \textbf{(68)}$$

The linearization was performed based on the enthalpy-switching system governing equations. The x state is listed in Equation (69). Because the linearization was based on the condition that only two-phase fluid is in the PTP evaporators, two-phase and subcooled liquid in

the condenser, and two-phase and superheated vapor are in the VCC evaporators, the mean void fractions and evaporator two-phase zone lengths were not included in the x states.

$$x = [h_{PTP,ero}\ \ T_{PTP,ew1}\ \ \dot{m}_{PTP,eri}\ \ \dots \tag{69}$$

$$L_{PTP,c2}\ \ L_{PTPc3}\ \ h_{PTP,cro}\ \ T_{w1}\ \ T_{w2}\ \ T_{w3}\ \ T_{w4}\ \ \ P_{VCC}\ ]$$

The input vector u is defined as in Equation (70). In the evaporators, the inlet mass flow rates, the inlet enthalpies, and the heat load on the evaporators are included as inputs. Because the condenser inlet mass flow rate times inlet enthalpy is the sum of the evaporator outlet mass flow rate times enthalpy, the condenser inlet mass flow rate and enthalpy were not considered in the input vector. The condenser outlet mass flow rate was accounted in the input vector. As for the external VCC evaporator, the inlet and outlet mass flow rate and inlet enthalpy were considered in the input vector.

$$u = [\dot{m}_{PTP,eri}\ \ h_{PTP,eri}\ Q\ \dots\ \dot{m}_{PTP,cro}\ \ \dot{m}_{VCC,eri}\ \ \dot{m}_{VCC,ero}\ h_{VCC,eri}] \tag{70}$$

The output vector g is listed as in Equation (74). Evaporator outlet enthalpy, two-phase zone refrigerant wall temperatures, PTP heat exchanger pressure, condenser outlet enthalpy and temperature, external VCC evaporator enthalpy, and outlet temperature and pressure were chosen as output parameters.

$$g = [h_{PTP,ero}\ \ T_{PTP,ew1}\ \ P_{PTP}\ \ h_{PTP,cro}\ \ T_{PTP,cro}\ \ h_{VCC,ero}\ \ T_{VCC,ero}\ \ P_{VCC}] \tag{71}$$

$f(x,u)$ vector is presented in detail in Table 17 with j respresenting the j[th] evaporator in parallel.

Table 17: f vector for linearization

$f(7j-6)$	$\dot{m}_{PTP,eri}(j)h_{PTP,eri}(j) + \alpha_{PTP,ei1}(i)A_{PTP,ei}\left(T_{PTP,ew1}(j) - T_{PTP,er1}(j)\right)$
$f(7j-5)$	0
$f(7j-4)$	$\dot{m}_{PTP,eri}(j)$

Table 17: Continued

$f(7j-3)$	$\alpha_{PTP,ei1}(j)A_{PTP,ei}\left(T_{PTP,ew1}(j)-T_{PTP,er1}(j)\right)+Q(j)$	
$f(7j-2)$	0	
$f(7j-1)$	0	
$f(7j)$	0	
$f(7n+1)$	$L_{PTP,c2} \geq L_{VCC,e1}$	$-\dot{m}_{PTP,cro}h_{PTP,f}+$ $\alpha_{PTP,ci2}A_{PTP,ci}\left(\frac{L_{VCC,e1}}{L_{total}}\right)(T_{w2}-$ $T_{PTP,cr2})+\alpha_{PTP,ci2}A_{PTP,ci}\left(\frac{L_{PTP,c2}-L_{VCC,e1}}{L_{total}}\right)(T_{w3}-$ $T_{PTP,cr2})$
	$L_{PTP,c2} \geq L_{VCC,e1}$	$-\dot{m}_{PTP,cro}h_{PTP,f}+$ $\alpha_{PTP,ci2}A_{PTP,ci}\left(\frac{L_{PTP,c2}}{L_{total}}\right)(T_{w2}-T_{PTP,cr2})$
$f(7n+2)$	0	
$f(7n+3)$	$L_{PTP,c2} \geq L_{VCC,e1}$	$\dot{m}_{PTP,cro}h_{PTP,f}-\dot{m}_{PTP,cro}h_{PTP,cro}+$ $\alpha_{PTP,ci3}A_{PTP,ci}\left(\frac{L_{PTP,c3}}{L_{total}}\right)(T_{w4}-T_{PTP,cr3})$
	$L_{PTP,c2} < L_{VCC,e1}$	$\dot{m}_{PTP,cro}h_{PTP,f}-\dot{m}_{PTP,cro}h_{PTP,cro}+$ $\alpha_{PTP,ci2}A_{PTP,ci}\left(\frac{L_{VCC,e1}-L_{PTP,c2}}{L_{total}}\right)(T_{w3}-T_{PTP,cr3})+$ $\alpha_{PTP,ci3}A_{PTP,ci}\left(\frac{L_{VCC,e2}}{L_{total}}\right)(T_{w4}-T_{PTP,cr3})$
$f(7n+4)$	$-\dot{m}_{PTP,cro}$	
$f(7n+5)$	0	
$f(7n+6)$	$\alpha_{PTP,ci2}A_{PTP,ci}\left(T_{PTP,cr2}-T_{w2}\right)+\alpha_{VCC,Ei1}A_{VCC,ei}\left(T_{VCC,er1}-T_{w2}\right)$	
$f(7n+7)$	$L_{PTP,c2} \geq L_{VCC,e1}$	$\alpha_{PTP,ci2}A_{PTP,ci}\left(T_{PTP,cr2}-T_{w3}\right)+$ $\alpha_{VCC,ei2}A_{VCC,ei}\left(T_{VCC,er2}-T_{w3}\right)$
	$L_{PTP,c2} < L_{VCC,e1}$	$\alpha_{PTP,ci3}A_{PTP,ci}\left(T_{PTP,cr3}-T_{w3}\right)$ $+\alpha_{VCC,ei1}A_{VCC,ei}\left(T_{VCC,er1}-T_{w3}\right)$
$f(7n+8)$	$\alpha_{PTP,ci3}A_{PTP,ci}\left(T_{PTP,cr3}-T_{w4}\right)+\alpha_{VCC,ei2}A_{VCC,ei}\left(T_{VCC,er2}-T_{w4}\right)$	
$f(7n+9)$	0	

Table 17: Continued

$f(7n+10)$	0	
$f(7n+11)$	0	
$f(7n+12)$	$L_{PTP,c2} \geq L_{VCC,e1}$	$\dot{m}_{VCC,eri} h_{VCC,eri} - \dot{m}_{VCC,ero} h_{VCC,g} + \alpha_{VCC,ei1} A_{VCC,ei} \left(\frac{L_{VCC,e1}}{L_{total}}\right) \left(T_{w2} - T_{VCC,er1}\right)$
	$L_{PTP,c2} < L_{VCC,e1}$	$\dot{m}_{VCC,eri} h_{VCC,exRi} - \dot{m}_{VCC,ero} h_{VCC,g} + \alpha_{VCC,ei1} A_{VCC,ei} \left(\frac{L_{PTP,c2}}{L_{total}}\right) \left(T_{w3} - T_{VCC,er1}\right) + \alpha_{VCC,ei1} A_{VCC,ei} \left(\frac{L_{VCC,e1} - L_{PTP,c2}}{L_{total}}\right) \left(T_{w4} - T_{VCC,er1}\right)$
$f(7n+13)$	$L_{PTP,c2} \geq L_{VCC,e1}$	$\dot{m}_{VCC,eri}\left(h_{VCC,g} - h_{VCC,ero}\right) + \alpha_{VCC,ei2} A_{VCC,ei} \left(\frac{L_{PTP,c2} - L_{VCC,e1}}{L_{total}}\right) \left(T_{w3} - T_{VCC,er2}\right) + \alpha_{VCC,ei1} A_{VCC,ei} \left(\frac{L_{PTP,c3}}{L_{total}}\right) \left(T_{w4} - T_{VCC,er2}\right)$
	$L_{PTP,c2} < L_{VCC,e1}$	$\dot{m}_{VCC,ero}\left(h_{VCC,g} - h_{VCC,ero}\right) + \alpha_{VCC,ei2} A_{VCC,ei} \left(\frac{L_{VCC,e2}}{L_{total}}\right) \left(T_{w4} - T_{VCC,er2}\right)$
$f(7n+14)$	$\dot{m}_{VCC,eri} - \dot{m}_{VCC,ero}$	
$f(7n+15)$	0	
$f(7n+16)$	0	

F_x matrix elements are listed in Table 18. The evaporator and the first region in the condenser are two-phase fluid, which is a combination of saturated liquid and saturated vapor. The two-phase fluid region properties, $\rho_{PTP,f,g}$, $h_{PTP,f,g}$, and the refrigerant temperatures $T_{PTP,er1}$ and $T_{PTP,cr2}$ are only a function of the PTP heat exchanger pressure. The same rule applies to the VCC evaporator two-phase zone. In the condenser subcooled region, the average refrigerant properties were calculated as $T_{PTP,cr3} = T(P_{PTP}, h_{PTP,cr3})$ and $\rho_{PTP,cr3} =$

$T(P, h_{PTP,cr3})$. However, because $h_{PTP,cr3} = \frac{h_{PTP,g}+h_{PTP,cro}}{2}$, $T_{PTP,cr3} \approx \frac{T_{sat}(P_{PTP})+T(P_{PTP},h_{PTP,cro})}{2}$, for the partial derivatives of $T_{PTP,cr3}$, the approximations $\frac{\partial T_{PTP,cr3}}{\partial P_{PTP}} = \frac{1}{2}\left(\frac{dT_{sat}}{dP_{PTP}} + \frac{\partial T_{PTP,cro}}{\partial P_{PTP}}|_{h_{PTP,cr3}}\right)$ and $\frac{\partial T_{PTP,cr3}}{\partial h_{PTP,cro}} = \frac{1}{2}\left(\frac{\partial T_{PTP,cr3}}{\partial h_{PTP,cr3}}|_{P_{PTP}}\right)$ were used. Similarly, the partial derivatives in the VCC evaporators were calculated as $\frac{\partial T_{VCC,ero}}{\partial P_{VCC}} = \frac{1}{2}\left(\frac{dT_{sat}}{dP_{VCC}} + \frac{dT_{VCC,ero}}{dP_{VCC}}\right)$, $\frac{\partial T_{VCC,er2}}{\partial h_{VCC,ero}} = \frac{1}{2}\left(\frac{\partial T_{VCC,er2}}{\partial h_{VCC,er2}}|_{P_{VCC}}\right)$.

The partial derivatives of the heat-transfer coefficient with respect to the state were not included in the derivation because the system is not expected to experience large system condition changes and because the linearization was performed locally. F_u is listed in Table 19.

Table 18: F_x matrix elements

$\frac{\partial f(7j-6)}{\partial T_{PTP,ew}}$	$F_x(7j-6,7j-4)$	$\alpha_{PTP,ei1}(j)A_{PTP,ei}$	
$\frac{\partial f(7j-6)}{\partial P_{PTP}}$	$F_x(7j-6,7n+11)$	$-\alpha_{PTP,ei1}(j)A_{PTP,ei}\left(\frac{dT_{sat}}{dP_{PTP}}\right)$	
$\frac{\partial f(7j-3)}{\partial T_{PTP,ew}}$	$F_x(7j-4,7j-4)$	$-\alpha_{PTP,ei1}(j)A_{PTP,ei}$	
$\frac{\partial f(7j-3)}{\partial P_{PTP}}$	$F_x(7j-4,7n+11)$	$-\alpha_{PTP,ei1}(j)A_{PTP,ei}\left(\frac{dT_{sat}}{dP_{PTP}}\right)$	
$\frac{\partial f(7n+1)}{\partial L_{PTP,c2}}$	$F_x(7n+1,7n+1)$	$L_{PTP,c2} \geq L_{VCC,e1}$	$\alpha_{PTP,ci2}A_{PTP,ci}\left(\frac{1}{L_{total}}\right)(T_{w3}-T_{PTP,cr2})$
		$L_{PTP,c2} < L_{VCC,e1}$	$\alpha_{PTP,ci2}A_{PTP,ci}\left(\frac{1}{L_{total}}\right)(T_{w2}-T_{PTP,cr2})$

Table 18: Continued

$\frac{\partial f(7n+1)}{\partial T_{w2}}$	$F_x(7n+1,7n+5)$	$L_{PTP,c2} \geq L_{VCC,e1}$	$\alpha_{PTP,ci2} A_{PTP,ci} \left(\frac{L_{VCC,e1}}{L_{total}}\right)$
		$L_{PTP,c2} \geq L_{VCC,e1}$	$\alpha_{PTP,ci2} A_{PTP,ci} \left(\frac{L_{PTP,c2}}{L_{total}}\right)$
$\frac{\partial f(7n+1)}{\partial T_{w3}}$	$F_x(7n+1,7n+6)$	$L_{PTP,c2} \geq L_{VCC,e1}$	$\alpha_{PTP,ci2} A_{PTP,ci} \left(\frac{L_{PTP,c2} - L_{VCC,e1}}{L_{total}}\right)$
		$L_{PTP,c2} < L_{VCC,e1}$	0
$\frac{\partial f(7n+1)}{\partial P_{PTP}}$	$F_x(7n+1,7n+11)$	$-\dot{m}_{PTP,cro} \frac{dh_{PTP,f}}{dP_{PTP}} + \alpha_{PTP,ci2} A_{PTP,ci} \left(\frac{L_{PTP,c2}}{L_{total}}\right) \left(-\frac{dT_{sat}}{dP_{PTP}}\right)$	
$\frac{\partial f(7n+1)}{\partial L_{VCC,e1}}$	$F_x(7n+1,7n+12)$	$L_{PTP,c2} \geq L_{VCC,e1}$	$\alpha_{PTP,ci2} A_{PTP,ci} \left(\frac{L_{PTP,c2}}{L_{total}}\right) (T_{w2} - T_{PTP,cr2}) - \alpha_{PTP,ci2} A_{PTP,ci} \left(\frac{L_{PTP,c2}}{L_{total}}\right) (T_{w3} - T_{PTP,cr2})$
		$L_{PTP,c2} < L_{VCC,e1}$	0
$\frac{\partial f(7n+3)}{\partial L_{PTP,c2}}$	$F_x(7n+3,7n+1)$	$L_{PTP,c2} \geq L_{VCC,e1}$	0
		$L_{PTP,c2} < L_{VCC,e1}$	$-\alpha_{PTP,ci3} A_{PTP,ci} \left(\frac{1}{L_{total}}\right) (T_{w3} - T_{PTP,cr3})$
$\frac{\partial f(7n+3)}{\partial L_{PTP,c3}}$	$F_x(7n+3,7n+2)$	$L_{PTP,c2} \geq L_{VCC,e1}$	$\alpha_{PTP,ci3} A_{PTP,ci} \left(\frac{1}{L_{total}}\right) (T_{w4} - T_{PTP,cr3})$
		$L_{PTP,c2} < L_{VCC,e1}$	0
$\frac{\partial f(7n+3)}{\partial h_{PTP,cro}}$	$F_x(7n+3,7n+3)$	$-\dot{m}_{PTP,cro} + \alpha_{PTP,ci3} A_{PTP,ci} \left(\frac{L_{PTP,c3}}{L_{total}}\right) \left(-\frac{0.5 dT_{PTP,cro}}{dh_{PTPcro}}\right)$	

Table 18: Continued

$\frac{\partial f(7n+3)}{\partial T_{w3}}$	$F_x(7n+3,7n+6)$	$L_{PTP,c2} \geq L_{VCC,e1}$	0
		$L_{PTP,c2} < L_{VCC,e1}$	$\alpha_{PTP,ci3} A_{PTP,ci} \left(\frac{L_{VCC,e1} - L_{PTP,c2}}{L_{total}}\right)$
$\frac{\partial f(7n+3)}{\partial T_{w4}}$	$F_x(7n+3,7n+7)$	$L_{PTP,c2} \geq L_{VCC,e1}$	$\alpha_{PTP,ci3} A_{PTP,ci} \left(\frac{L_{PTP,c3}}{L_{total}}\right)$
		$L_{PTP,c2} < L_{VCC,e1}$	$\alpha_{PTP,ci3} A_{PTP,ci} \left(\frac{L_{VCC,e2}}{L_{total}}\right)$
$\frac{\partial f(7n+3)}{\partial P_{PTP}}$	$F_x(7n+3,7n+11)$	$\dot{m}_{PTP,cro} \frac{dh_{PTP,f}}{dP_{PTP}} + \alpha_{PTP,ci3} A_{PTP,ci} \left(\frac{L_{PTP,c3}}{L_{total}}\right) (-0.5) (\frac{dT_{sat}}{dP_{PTP}} + \frac{dT_{PTP,cro}}{dP_{PTP}})$	
$\frac{\partial f(7n+3)}{\partial L_{VCC,e1}}$	$F_x(7n+3,7n+12)$	$L_{PTP,c2} \geq L_{VCC,e1}$	0
		$L_{PTP,c2} < L_{VCC,e1}$	$\alpha_{PTP,ci3} A_{PTP,ci} \left(\frac{1}{L_{total}}\right) (T_{w3} - T_{PTP,cr3}) - \alpha_{PTP,ci3} A_{PTP,ci} \left(\frac{1}{L_{total}}\right) (T_{w4} - T_{PTP,cr3})$
$\frac{\partial f(7n+6)}{\partial T_{w2}}$	$F_x(7n+6,7n+5)$	$-\alpha_{PTP,ci2} A_{PTP,ci} - \alpha_{VCC,ei1} A_{VCC,ei}$	
$\frac{\partial f(7n+6)}{\partial P_{PTP}}$	$F_x(7n+6,7n+11)$	$\alpha_{PTP,ci2} A_{PTP,ci} \frac{dT_{sat}}{dP_{PTP}}$	
$\frac{\partial f(7n+6)}{\partial P_{VCC}}$	$F_x(7n+6,7n+16)$	$\alpha_{VCC,ei1} A_{VCC,ei} \frac{dT_{sat}}{dP_{VCC}}$	
$\frac{\partial f(7n+7)}{\partial h_{PTP,cro}}$	$F_x(7n+7,7n+3)$	$L_{PTP,c2} \geq L_{VCC,e1}$	0
		$L_{PTP,c2} < L_{VCC,e1}$	$\alpha_{PTP,ci3} A_{PTP,ci} \frac{dT_{PTP,cro}}{dh_{PTP,cro}}$

Table 18: Continued

$\frac{\partial f(7n+7)}{\partial T_{w3}}$	$F_x(7n+7,7n+6)$	$L_{PTP,c2} < L_{VCC,e1}$	$-\alpha_{PTP,ci2}A_{PTP,ci} - \alpha_{VCC,ei2}A_{VCC,ei}$
		$L_{PTP,c2} < L_{VCC,e1}$	$-\alpha_{PTP,ci3}A_{PTP,ci} - \alpha_{VCC,ei1}A_{VCC,ei}$
$\frac{\partial f(7n+7)}{\partial P}$	$F_x(7n+7,7n+11)$	$L_{PTP,c2} < L_{VCC,e1}$	$\alpha_{PTP,ci2}A_{PTP,ci}\frac{dT_{sat}}{dP_{PTP}}$
		$L_{PTP,c2} < L_{VCC,e1}$	$\alpha_{PTP,ci3}(0.5)\left(\frac{dT_{sat}}{dP_{PTP}} + \frac{dT_{PTP,cro}}{dP_{PTP}}\right)$
$\frac{\partial f(7n+7)}{\partial h_{VCC,eri}}$	$F_x(7n+7,7n+13)$	$L_{PTP,c2} < L_{VCC,e1}$	$0.5\alpha_{VCC,ei2}A_{VCC,ei}\left(\frac{dT_{VCC,ero}}{dh_{VCC,ero}}\right)$
		$L_{PTP,c2} < L_{VCC,e1}$	0
$\frac{\partial f(7n+7)}{\partial P_{VCC}}$	$F_x(7n+7,7n+16)$	$L_{PTP,c2} < L_{VCC,e1}$	$\alpha_{VCC,ei2}A_{VCC,ei}(0.5)\left(\frac{dT_{sat}}{dP_{VCC}} + \frac{dT_{VCC,ero}}{dP_{VCC}}\right)$
		$L_{PTP,c2} < L_{VCC,e1}$	$\alpha_{VCC,ei1}A_{VCC,ei}\left(\frac{dT_{sat}}{dP_{VCC}}\right)$
$\frac{\partial f(7n+8)}{\partial h_{PTP,cro}}$	$F_x(7n+8,7n+3)$	$0.5\alpha_{PTP,ci3}A_{PTP,ci}\left(\frac{dT_{PTP,cro}}{dh_{PTP,cro}}\right)$	
$\frac{\partial f(7n+8)}{\partial T_{w4}}$	$F_x(7n+8,7n+7)$	$-\alpha_{PTP,ci3}A_{PTP,ci} - \alpha_{VCC,ei2}A_{VCC,ei}$	
$\frac{\partial f(7n+8)}{\partial P_{PTP}}$	$F_x(7n+8,7n+11)$	$\alpha_{PTP,ci3}A_{PTP,ci}(0.5)\left(\frac{dT_{sat}}{dP_{PTP}} + \frac{dT_{PTP,cro}}{dP_{PTP}}\right)$	
$\frac{\partial f(7n+8)}{\partial h_{VCC,ero}}$	$F_x(7n+8,7n+13)$	$\alpha_{VCC,ei2}A_{VCC,ei}(0.5)\left(\frac{dT_{VCC,ero}}{dh_{VCC,ero}}\right)$	
$\frac{\partial f(7n+8)}{\partial P_{VCC}}$	$F_x(7n+8,7n+16)$	$\alpha_{VCC,ei2}A_{VCC,ei}(0.5)\left(\frac{dT_{sat}}{dP_{VCC}} + \frac{dT_{VCC,ero}}{dP_{VCC}}\right)$	

Table 18: Continued

$\frac{\partial f(7n+12)}{\partial L_{PTP,c2}}$	$F_x(7n+12,7n+1)$	$L_{PTP,c2} \geq L_{VCC,e1}$	0
		$L_{PTP,c2} < L_{VCC,e1}$	$\alpha_{VCC,ei1}A_{VCC,ei}\left(\frac{1}{L_{total}}\right)(T_{w2}-T_{VCC,er1}) - \alpha_{VCC,ei1}A_{VCC,ei}\left(\frac{1}{L_{total}}\right)(T_{w3}-T_{VCC,er1})$
$\frac{\partial f(7n+12)}{\partial T_{w2}}$	$F_x(7n+12,7n+5)$	$L_{PTP,c2} \geq L_{VCC,e1}$	$\alpha_{VCC,ei1}A_{VCC,ei}\left(\frac{L_{VCC,e1}}{L_{total}}\right)$
		$L_{PTP,c2} < L_{VCC,e1}$	$\alpha_{VCC,ei1}A_{VCC,ei}\left(\frac{L_{PTP,c2}}{L_{total}}\right)$
$\frac{\partial f(7n+12)}{\partial T_{w3}}$	$F_x(7n+12,7n+6)$	$L_{PTP,c2} \geq L_{VCC,e1}$	0
		$L_{PTP,c2} < L_{VCC,e1}$	$\alpha_{VCC,ei1}A_{VCC,ei}\left(\frac{L_{VCC,e1}-L_{PTP,c2}}{L_{total}}\right)$
$\frac{\partial f(7n+12)}{\partial L_{VCC,e1}}$	$F_x(7n+12,7n+12)$	$L_{PTP,c2} \geq L_{VCC,e1}$	$\alpha_{VCC,ei1}A_{VCC,ei}\left(\frac{1}{L_{total}}\right)(T_{w2}-T_{VCC,er1})$
		$L_{PTP,c2} < L_{VCC,e1}$	$\alpha_{VCC,ei1}A_{VCC,ei}\left(\frac{1}{L_{total}}\right)(T_{w3}-T_{VCC,er1})$
$\frac{\partial f(7n+12)}{\partial P_{VCC}}$	$F_x(7n+12,7n+16)$	$L_{PTP,c2} \geq L_{VCC,e1}$	$-\dot{m}_{VCC,ero}\frac{dh_{VCC,g}}{dP_{VCC}} + \alpha_{VCC,ei1}A_{VCC,ei}\left(\frac{L_{VCC,e1}}{L_{total}}\right)\left(-\frac{dT_{sat}}{dP_{VCC}}\right)$
		$L_{PTP,c2} < L_{VCC,e1}$	$-\dot{m}_{VCC,ero}\frac{dh_{VCC,g}}{dP_{VCC}} + \alpha_{VCC,ei1}A_{VCC,ei}\left(\frac{L_{PTP,c2}}{L_{total}}\right)\left(-\frac{dT_{sat}}{dP_{VCC}}\right) - \alpha_{VCC,ei1}A_{VCC,ei}\left(\frac{L_{PTP,c2}-L_{VCC,e1}}{L_{total}}\right)\left(-\frac{dT_{sat}}{dP_{VCC}}\right)$

Table 18: Continued

$\frac{\partial f(7n+13)}{\partial L_{PTP,c2}}$	$F_x(7n+13,7n+1)$	$L_{PTP,c2} \geq L_{VCC,e1}$	$\alpha_{VCC,ei2} A_{VCC,ei} \left(\frac{1}{L_{total}}\right)(T_{w3} - T_{VCC,er2})$
		$L_{PTP,c2} < L_{VCC,e1}$	0
$\frac{\partial f(7n+13)}{\partial L_{PTP,c3}}$	$F_x(7n+13,7n+2)$	$L_{PTP,c2} \geq L_{VCC,e1}$	$\alpha_{VCC,ei2} A_{VCC,ei} \left(\frac{1}{L_{total}}\right)(T_{w4} - T_{VCC,er2})$
		$L_{PTP,c2} < L_{VCC,e1}$	0
$\frac{\partial f(7n+13)}{\partial T_{w3}}$	$F_x(7n+13,7n+6)$	$L_{PTP,c2} \geq L_{VCC,e1}$	$\alpha_{VCC,ei2} A_{VCC,ei} \left(\frac{L_{PTP,c2} - L_{VCC,e1}}{L_{total}}\right)$
		$L_{PTP,c2} < L_{VCC,e1}$	0
$\frac{\partial f(7n+13)}{\partial T_{w4}}$	$F_x(7n+13,7n+7)$	$L_{PTP,c2} \geq L_{VCC,e1}$	$\alpha_{VCC,ei2} A_{VCC,ei} \left(\frac{L_{PTP,c3}}{L_{total}}\right)$
		$L_{PTP,c2} < L_{VCC,e1}$	$\alpha_{VCC,ei2} A_{VCC,ei} \left(\frac{L_{VCC,e1} - L_{PTP,c2}}{L_{total}}\right)$
$\frac{\partial f(7n+13)}{\partial L_{VCC,e1}}$	$F_x(7n+13,7n+12)$	$L_{PTP,c2} \geq L_{VCC,e1}$	$-\alpha_{VCC,ei2} A_{VCC,ei} \left(\frac{1}{L_{total}}\right)(T_{w3} - T_{VCC,er2})$
		$L_{PTP,c2} < L_{VCC,e1}$	$-\alpha_{VCC,ei2} A_{VCC,ei} \left(\frac{1}{L_{total}}\right)(T_{w4} - T_{VCC,er2})$

Table 18: Continued

$\frac{\partial f(7n+13)}{\partial h_{VCC,ero}}$	$F_x(7n+13,7n+13)$	$L_{PTP,c2} \geq L_{VCC,e1}$	$-\dot{m}_{VCC,ero} + \alpha_{VCC,ei2} A_{VCC,ei} \left(\frac{L_{PTP,c2} - L_{VCC,e1}}{L_{total}}\right) \left(-0.5 \frac{dT_{VCC,ero}}{dh_{VCC,ero}}\right) + \alpha_{VCC,ei2} A_{VCC,ei} \left(\frac{L_{PTP,c3}}{L_{total}}\right) \left(-0.5 \frac{dT_{VCC,ero}}{dh_{VCC,ero}}\right)$
		$L_{PTP,c2} < L_{VCC,e1}$	$-\dot{m}_{VCC,ero} + \alpha_{VCC,ei2} A_{VCC,ei} \left(\frac{L_{VCC,e2}}{L_{total}}\right) \left(-0.5 \frac{dT_{sat}}{dP_{VCC}}\right)$
$\frac{\partial f(7n+13)}{\partial P_{VCC}}$	$F_x(7n+13,7n+16)$	$L_{PTP,c2} \geq L_{VCC,e1}$	$\dot{m}_{VCC,ero} \frac{dh_{VCC,g}}{dP_{VCC}} + \alpha_{VCC,ei2} A_{VCC,ei} \left(\frac{L_{PTP,c2} - L_{VCC,e1}}{L_{total}}\right) + (-0.5) \left(\frac{dT_{sat}}{dP_{VCC}} + \frac{dT_{VCC,ero}}{dP_{VCC}}\right) + \alpha_{VCC,ei2} A_{VCC,ei} \left(\frac{L_{PTP,c3}}{L_{total}}\right) (-0.5) \left(\frac{dT_{sat}}{dP_{VCC}} + \frac{dT_{VCC,ero}}{dP_{VCC}}\right)$
		$L_{PTP,c2} < L_{VCC,e1}$	$\dot{m}_{VCC,ero} \frac{dh_{VCC,g}}{dP_{VCC}} + \alpha_{VCC,ei2} A_{VCC,ei} \left(\frac{L_{VCC,e2}}{L_{total}}\right) (-0.5) \left(\frac{dT_{sat}}{dP_{VCC}} + \frac{dT_{VCC,ero}}{dP_{VCC}}\right)$

Table 19: F_u matrix elements

$\frac{\partial f(7j-6)}{\partial \dot{m}_{PTP,eri}}$	$F_u(7j-6,3j-2)$	$h_{PTP,eri}(j) + \frac{d\alpha_{PTP,ei1}(j)}{d\dot{m}_{PTP,eri}(j)} A_{PTP,ei} \left(T_{PTP,ew1}(j) - T_{PTP,er1}(j)\right)$
$\frac{\partial f(7j-6)}{\partial h_{PTP,eri}}$	$F_u(7j-6,3j-1)$	$\dot{m}_{PTP,eri}(j) + \frac{d\alpha_{PTP,ei1}(j)}{dh_{PTP,eri}(j)} A_{PTP,ei} \left(T_{PTP,ew1}(j) - T_{PTP,er1}(j)\right)$
$\frac{\partial f(7j-6)}{\partial Q}$	$F_u(7j-6,3j)$	$\frac{d\alpha_{PTP,ei1}(j)}{dQ(j)} A_{PTP,ei} \left(T_{PTP,ew1}(j) - T_{PTP,er1}(j)\right)$

Table 19: Continued

$\frac{\partial f(7j-4)}{\partial \dot{m}_{PTP,eri}}$	$F_u(7j-4,3j-2)$	1	
$\frac{\partial f(7j-3)}{\partial \dot{m}_{PTP,eri}}$	$F_u(7j-3,3j-2)$	$\alpha_{PTP,ei1}(j)A_{PTP,ei}\left(T_{PTP,ew1}(j)-T_{PTP,er1}(j)\right)$	
$\frac{\partial f(7j-3)}{\partial h_{PTP,eri}}$	$F_u(7j-3,3j-1)$	$\frac{d\alpha_{PTP,ei1}(j)}{dh_{PTP,eri}(j)}A_{PTP,ei}\left(T_{PTP,ew1}(j)-T_{PTP,er1}(j)\right)$	
$\frac{\partial f(7j-3)}{\partial Q}$	$F_u(7j-3,3i)$	1	
$\frac{\partial f(7n+1)}{\partial \dot{m}_{PTP,cro}}$	$F_u(7n+1,3n+1)$	$-h_{PTP,f}$	
$\frac{\partial f(7n+3)}{\partial \dot{m}_{PTP,cro}}$	$F_u(7n+3,3n+1)$	$h_{PTP,f}-h_{PTP,cro}$	
$\frac{\partial f(7n+6)}{\partial \dot{m}_{VCC,eri}}$	$F_u(7n+6,3n+2)$	$\frac{d\alpha_{VCC,ei1}}{d\dot{m}_{VCC,eri}}A_{VCC,ei}\left(T_{VCC,er1}-T_{w2}\right)$	
$\frac{\partial f(7n+6)}{\partial h_{VCC,eri}}$	$F_u(7n+6,3n+4)$	$\frac{d\alpha_{VCC,ei1}}{dh_{VCC,eri}}A_{VCC,ei}\left(T_{VCC,er1}-T_{w2}\right)$	
$\frac{\partial f(7n+7)}{\partial \dot{m}_{VCC,eri}}$	$F_u(7n+7,3n+2)$	$L_{PTP,c2} \geq L_{VCC,e1}$	$\frac{d\alpha_{VCC,ei1}}{d\dot{m}_{VCC,eri}}A_{VCC,ei}\left(T_{VCC,er1}-T_{w3}\right)$
		$L_{PTP,c2} < L_{VCC,e1}$	0
$\frac{\partial f(7n+7)}{\partial \dot{m}_{VCC,ero}}$	$F_u(7n+7,3n+3)$	$L_{PTP,c2} \geq L_{VCC,e1}$	0
		$L_{PTP,c2} < L_{VCC,e1}$	$\frac{d\alpha_{VCC,ei2}}{d\dot{m}_{VCC,ero}}A_{VCC,ei}\left(T_{VCC,er2}-T_{w3}\right)$
$\frac{\partial f(7n+7)}{\partial h_{VCC,eri}}$	$F_u(7n+7,3n+4)$	$L_{PTP,c2} \geq L_{VCC,e1}$	$\frac{d\alpha_{VCC,ei2}}{dh_{VCC,eri}}A_{VCC,ei}\left(T_{VCC,er1}-T_{w3}\right)$
		$L_{PTP,c2} < L_{VCC,e1}$	0
$\frac{\partial f(7n+8)}{\partial \dot{m}_{VCC,ero}}$	$F_u(7n+8,3n+3)$	$\frac{d\alpha_{VCC,ei2}}{d\dot{m}_{VCC,ero}}A_{VCC,ei}\left(T_{VCC,er2}-T_{w4}\right)$	

Table 19: Continued

$\frac{\partial f(7n+12)}{\partial \dot{m}_{VCC,eri}}$	$F_u(7n+12,3n+2)$	$L_{PTP,c2} \geq L_{VCC,e1}$	$h_{VCC,eri} + \frac{d\alpha_{VCC,ei1}}{d\dot{m}_{VCC,eri}} A_{VCC,ei} \left(\frac{L_{VCC,e1}}{L_{total}}\right) (T_{w2} - T_{VCC,er1})$
		$L_{PTP,c2} < L_{VCC,e1}$	$h_{VCC,eri} + \frac{d\alpha_{VCC,ei1}}{d\dot{m}_{VCC,eri}} A_{VCC,ei} \left(\frac{L_{PTP,c2}}{L_{total}}\right) (T_{w2} - T_{VCC,er1}) + \frac{d\alpha_{VCC,ei1}}{d\dot{m}_{VCC,eri}} A_{VCC,ei} \left(\frac{L_{VCC,e1} - L_{PTP,c2}}{L_{total}}\right) (T_{w3} - T_{VCC,er1})$
$\frac{\partial f(7n+12)}{\partial \dot{m}_{VCC,ero}}$	$F_u(7n+12,3n+3)$	$L_{PTP,c2} \geq L_{VCC,e1}$	$-h_{VCC,g} + \frac{d\alpha_{VCC,ei1}}{d\dot{m}_{VCC,ero}} A_{VCC,ei} \left(\frac{L_{VCC,e1}}{L_{total}}\right) (T_{w2} - T_{VCC,er1})$
		$L_{PTP,c2} < L_{VCC,e1}$	$-h_{VCC,g} + \frac{d\alpha_{VCC,ei1}}{d\dot{m}_{VCC,ero}} A_{VCC,ei} \left(\frac{L_{PTP,c2}}{L_{total}}\right) (T_{w2} - T_{VCC,er1}) + \frac{d\alpha_{VCC,ei1}}{d\dot{m}_{VCC,ero}} A_{VCC,ei} \left(\frac{L_{VCC,e1} - L_{PTP,c2}}{L_{total}}\right) (T_{w3} - T_{VCC,er1})$
$\frac{\partial f(7n+12)}{\partial h_{VCC,eri}}$	$F_u(7n+12,3n+4)$	$L_{PTP,c2} \geq L_{VCC,e1}$	$\dot{m}_{VCC,eri} + \frac{d\alpha_{VCC,ei1}}{dh_{VCC,eri}} A_{VCC,ei} \left(\frac{L_{VCC,e1}}{L_{total}}\right) (T_{w2} - T_{VCC,er1})$
		$L_{PTP,c2} < L_{VCC,e1}$	$\dot{m}_{VCC,eri} + \frac{d\alpha_{VCC,ei1}}{dh_{VCC,eri}} A_{VCC,ei} \left(\frac{L_{PTP,c2}}{L_{total}}\right) (T_{w2} - T_{VCC,er1}) + \frac{d\alpha_{VCC,ei1}}{dh_{VCC,eri}} A_{VCC,ei} \left(\frac{L_{VCC,e1} - L_{PTP,c2}}{L_{total}}\right) (T_{w3} - T_{VCC,er1})$

Table 19: Continued

$\frac{\partial f(7n+13)}{\partial \dot{m}_{VCC,ero}}$	$F_u(7n+13,3n+3)$	$L_{PTP,c2} \geq L_{VCC,e1}$	$(h_{VCCC,g} - h_{VCC,ero}) + \frac{d\alpha_{VCC,ei2}}{d\dot{m}_{VCC,ero}} A_{VCC,ei} \left(\frac{L_{PTP,c2} - L_{VCC,e1}}{L_{total}}\right)(T_{w3} - T_{VCC,er2}) + \frac{d\alpha_{VCC,ei2}}{d\dot{m}_{VCC,ero}} A_{VCC,ei} \left(\frac{L_{PTP,c3}}{L_{total}}\right)(T_{w4} - T_{VCC,er2})$
		$L_{PTP,c2} < L_{VCC,e1}$	$(h_{VCC,g} - h_{VCC,ero}) + \frac{d\alpha_{VCC,ei2}}{d\dot{m}_{VCC,ero}} A_{VCC,ei} \left(\frac{L_{PTP,c3}}{L_{total}}\right)(T_{w4} - T_{VCC,er2})$
$\frac{\partial f(7n+14)}{\partial \dot{m}_{VCC,eri}}$	$F_u(7n+14,3n+2)$	1	
$\frac{\partial f(7n+14)}{\partial \dot{m}_{VCC,ero}}$	$F_u(7n+14,3n+3)$	1	

The matrix elements g_x are listed in Table 20. The element of g_u equals zero because the output does not relate directly to the inputs.

Table 20: G_x matrix elements

$\frac{\partial g(3j-2)}{\partial h_{PTP,ero}}$	$G_x(3i-2,7j-5)$	1
$\frac{\partial g(3j-1)}{\partial T_{PTP,ew}}$	$G_x(3j-1,7j-4)$	1
$\frac{\partial g(3n)}{\partial P_{PTP}}$	$G_x(3n,7n+11)$	1
$\frac{\partial g(3n+1)}{\partial h_{VCC,ero}}$	$G_x(3n+1,7n+13)$	1
$\frac{\partial g(3n+2)}{\partial h_{PTP,cro}}$	$G_x(3n+2,7n+3)$	$\frac{dT_{PTP,cro}}{dh_{PTP,cro}}$
$\frac{\partial g(3n+2)}{\partial P_{PTP}}$	$G_x(3n+2,7n+11)$	$\frac{dT_{PTP,cro}}{dP_{PTP}}$

Table 20: Continued

$\frac{\partial g(3n+3)}{\partial P_{PTP}}$	$G_x(3n+3,7n+13)$	1
$\frac{\partial g(3n+4)}{\partial h_{VCC,ero}}$	$G_x(3n+4,7n+13)$	$\frac{dT_{VCC,ero}}{dh_{VCC,ero}}$
$\frac{\partial g(3n+4)}{\partial P_{VCC}}$	$G_x(3n+4,7n+16)$	$\frac{dT_{VCC,ero}}{dP_{VCC}}$
$\frac{\partial g(3n+5)}{\partial P_{VCC}}$	$G_x(3n+5,7n+16)$	1

The eigenvalues of the A matrix in the state-space model provide information about stability and the relative speed of response. A large-magnitude eigenvalue is "faster" than a small-magnitude eigenvalue. λ_1 is the eigenvalue of A matrix with the original cross-sectional areas. λ_2 is the eigenvalue of A matrix with 10 times the VCC evaporator original cross-sectional area. Equations (72) and (73) list the eigenvalues in the two cases. The smallest absolute eigenvalue in the VCC evaporator cross-sectional area at 10 times the original was smaller than the original case, resulting in a slower system response. Increasing the volume of the VCC evaporator resulted in slower eigenvalues. By doing this, the disturbance in the PTP cycle could be separated by increasing the volume of the VCC evaporator.

$$\lambda_1 = \begin{bmatrix} -68.036 \\ -43.276 \\ -5.7499 + 0.83934i \\ -5.7499 - 0.83934i \\ -3.3544 \\ -2.6103 \\ -0.4663 \\ -0.09782 \\ -0.01284 \\ -0.007983 \\ 0 \end{bmatrix} \quad \textbf{(72)}$$

$$\lambda_2 = \begin{bmatrix} -14.583 \\ -5.4524 + 1.5698i \\ -5.4524 - 1.5698i \\ -3.3544 \\ -2.3085 \\ -1.0203 \\ -0.40808 \\ -0.37825 \\ -0.011859 \\ -0.001236 \\ 0 \end{bmatrix} \quad \textbf{(73)}$$

5.2.2. Valve, Pump, Compressor Linearization

Valves, pump, and compressor were defined by equation $y = f(u)$. A local linearization was given as $y = Du$. The matrix *D* was found by correlating inputs to outputs.

The inlets of the valves in the PTP cycle were connected to the constant reservoir. Thus, the pressure and enthalpy feeding into the valves were not considered in the inputs. The inputs and outputs are defined in Equations (74) and (75), where D is defined in Equation (76). The evaluation of the matrix yields the following values in Equation (77):

$$u_v = [u_v \quad P_{vo}]^T \quad \textbf{(74)}$$

$$y_v = [\dot{m}_v \quad h_{vo}]^T \quad \textbf{(75)}$$

$$\frac{\partial f}{\partial u} = D = \begin{bmatrix} d_{11} & d_{12} \\ 0 & 0 \end{bmatrix} \quad \textbf{(76)}$$

$$D = \begin{bmatrix} 0.0006 & -0.000439 \\ 0 & 0 \end{bmatrix} \quad \textbf{(77)}$$

The outlets of the pump in the PTP cycle also were connected to the constant reservoir. Thus, the pump outlet pressure was not considered in the pump inputs. The inputs and outputs of the pump model are defined in Equations (78) and (79), where D is defined in Equation (80). The evaluation of the matrix yields the following values in Equation (81):

$$u_p = [\omega_p \quad P_{pi} \quad h_{pi}]^T \tag{78}$$

$$y_p = [\dot{m}_p \quad h_{po}]^T \tag{79}$$

$$\frac{\partial f}{\partial u} = D = \begin{bmatrix} d_{11} & d_{12} & d_{13} \\ 0 & d_{22} & d_{23} \end{bmatrix} \tag{80}$$

$$D = \begin{bmatrix} 0.000024 & -1.2e^{-6} & -0.00027 \\ 0 & -0.45 & 1.02 \end{bmatrix} \tag{81}$$

For the VCC valve model, the value inputs and outputs are defined in Equations (82) and (83), where matrix D is presented in Equation (84). The evaluation of the matrix yields the following values in Equation (85):

$$u_v = [u_v \quad P_{vi} \quad P_{vi} \quad h_{vi}]^T \tag{82}$$

$$y_v = [\dot{m}_v \quad h_{vo}]^T \tag{83}$$

$$\frac{\partial f}{\partial u} = D = \begin{bmatrix} d_{11} & d_{12} & d_{13} & d_{14} \\ 0 & 0 & 0 & d_{24} \end{bmatrix} \tag{84}$$

$$D = \begin{bmatrix} 0.0002 & 0.000013 & -0.0019872 & -1.13e^{-5} \\ 0 & 0 & 0 & 1 \end{bmatrix} \tag{85}$$

In the VCC compressor model, the value inputs and outputs are defined in Equations (86) and (87), where matrix D is presented in Equation (88). The evaluation of the matrix yields the following values in Equation (89):

$$u_k = [\omega_k \quad P_{ki} \quad P_{ko} \quad h_{ki}]^T \tag{86}$$

$$y_k = [\dot{m}_k \quad h_{k,o}]^T \tag{87}$$

$$\frac{\partial f}{\partial u} = D = \begin{bmatrix} d_{11} & d_{12} & d_{13} & d_{14} \\ 0 & d_{22} & d_{23} & d_{24} \end{bmatrix} \tag{88}$$

$$\frac{\partial f}{\partial u} = D = \begin{bmatrix} 3.35e^{-6} & 2e^{-6} & 2e^{-7} & -0.0000446 \\ 0 & -0.09 & 0.048 & 1.12 \end{bmatrix} \tag{89}$$

The linearization of the VCC condenser was similar to that of the combined heat exchanger. Details are not included; the overall system model can be found by appropriately defining the component model inputs in terms of system input and component output. This procedure can be done numerically by using algorithms available in MATLAB.

Figure 56 presents the eigenvalue comparison of the system with the initial PTP condenser cross-sectional area and the initial VCC evaporator cross-sectional area and the initial PTP condenser cross-sectional area and 10 times the initial VCC evaporator cross-sectional area. The eigenvalues close to the origin reveal that increasing the volume of the external VCC evaporator could slow down the coupling between the PTP and VCC.

λ_1 is the eigenvalue of A matrix with the original cross-sectional area. λ_2 is the eigenvalue of A matrix with 10 times the VCC evaporator original cross-sectional area. The eigenvalues are listed in Equations (90) and (91).

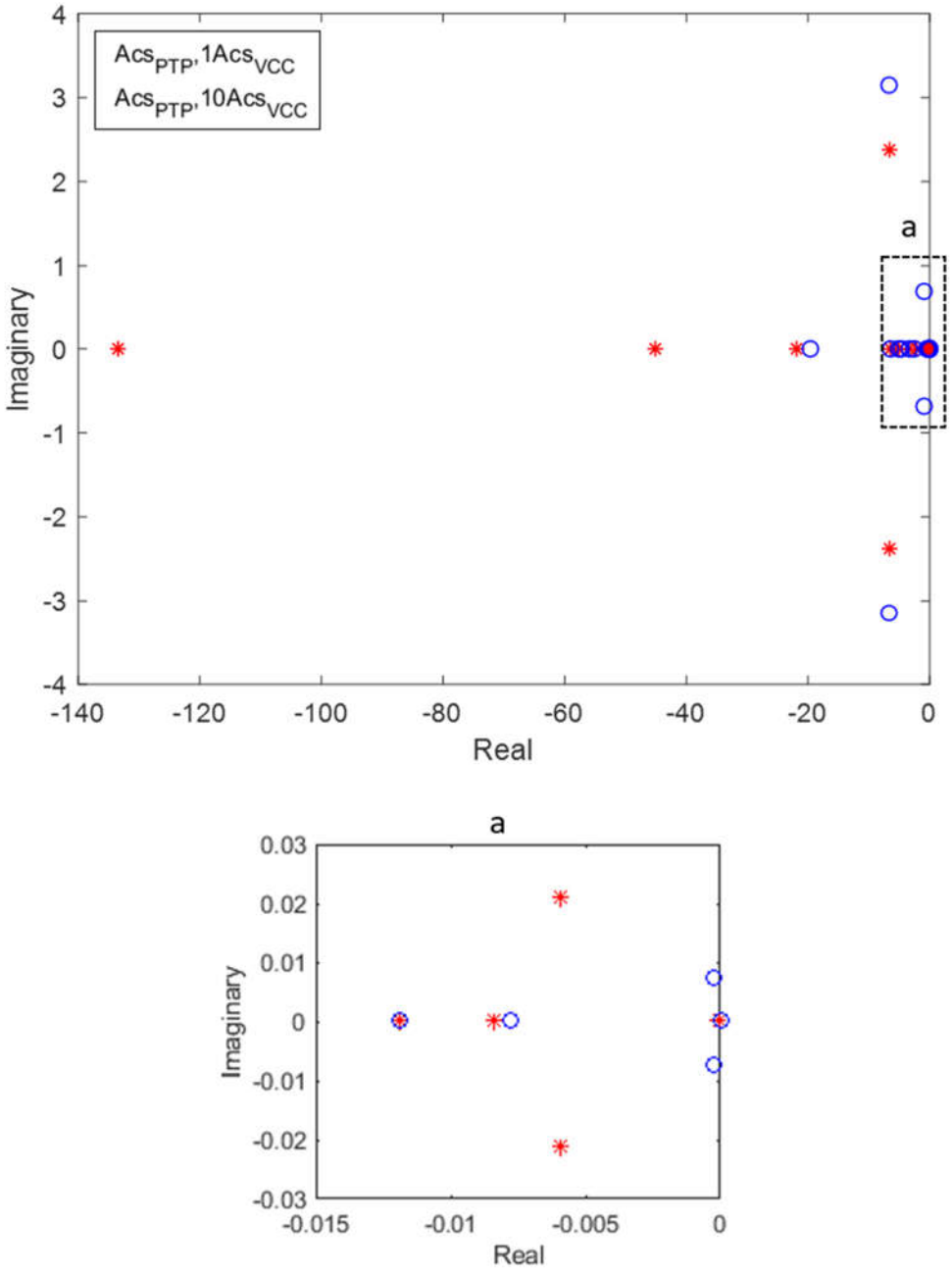

Figure 56: Comparison of eigenvalues

$$\lambda_1 = \begin{bmatrix} -133.45 \\ -45.111 \\ -21.867 \\ -6.5816 + 2.378i \\ -6.5816 - 2.378i \\ -6.4529 \\ -5.0869 \\ -5.0494 \\ -2.1495 \\ -0.464 \\ -0.30831 \\ -0.21968 \\ -0.13449 \\ -0.088951 \\ -0.0059107 + 0.021182i \\ -0.0059107 - 0.021182i \\ -0.0081869 \\ 0 \end{bmatrix} \quad \textbf{(90)}$$

$$\lambda_2 = \begin{bmatrix} -19.618 \\ -6.6764 + 3.1484i \\ -6.6764 - 3.1484i \\ -6.4521 \\ -5.103 \\ -4.6598 \\ -2.5245 \\ -0.92544 + 0.6831i \\ -0.92544 - 0.6831i \\ -0.44185 \\ -0.30725 \\ -0.21943 \\ -0.13529 \\ -0.088935 \\ -0.000264 + 0.007163i \\ -0.000264 - 0.007163i \\ -0.0075039 \\ 0 \end{bmatrix} \quad \textbf{(91)}$$

To verify that the model fidelity is not compromised significantly by linearization procedure, the linearized model was compared with the nonlinear model with the same heat load step changes. Pressure and wall temperatures are plotted in Figure 58 and Figure 59. Althrough

there are small differences between the nonliner model and the linearized model, the linearized model adequately follows the transient response of the nonlinear system model.

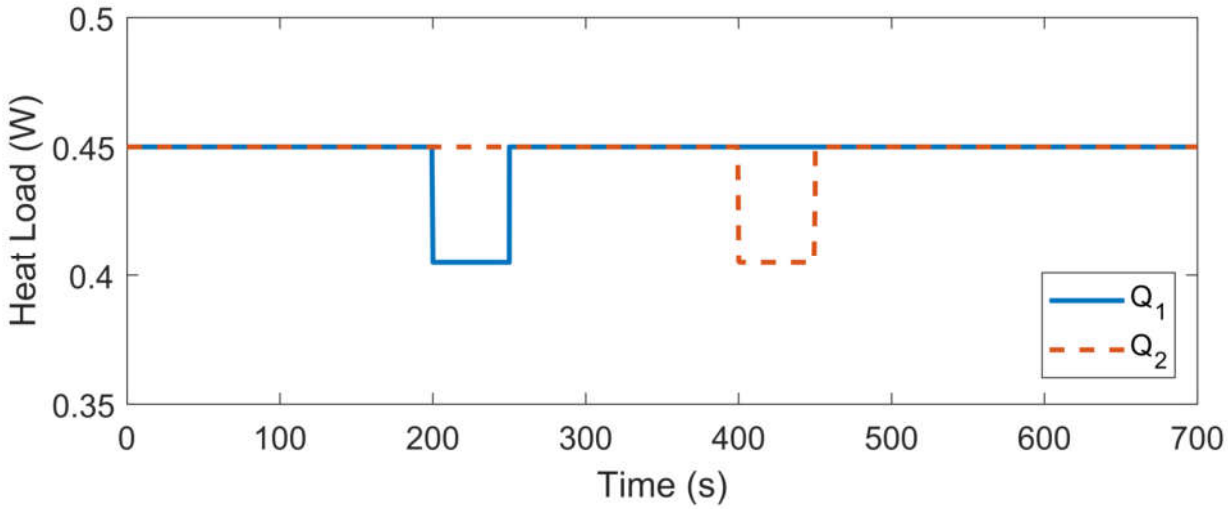

Figure 57: Heat loads step changes on nonlinear and linearized model

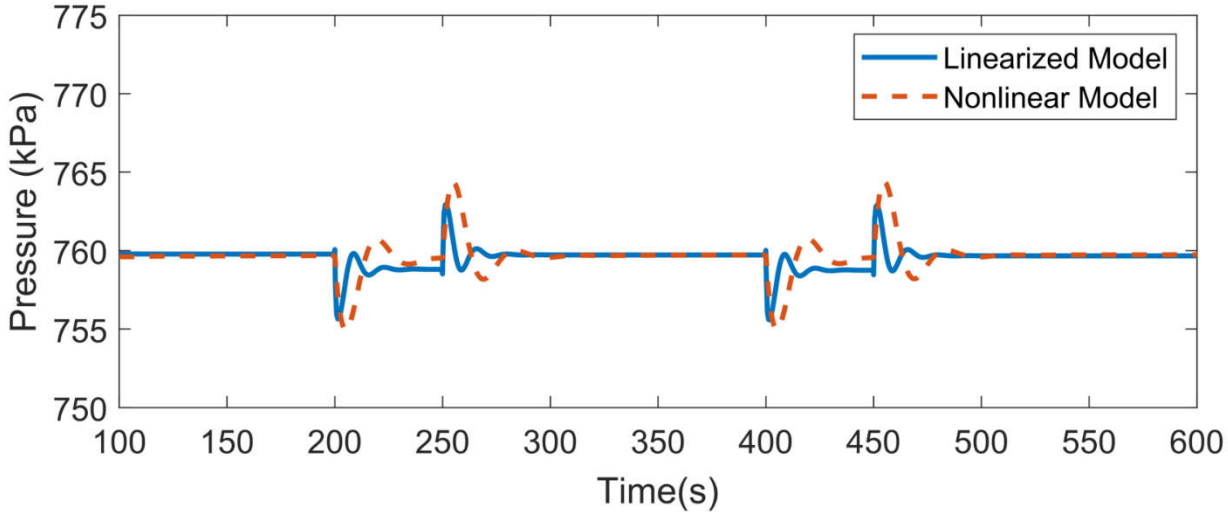

Figure 58: Pressure comparison of nonlinear model and linearized model

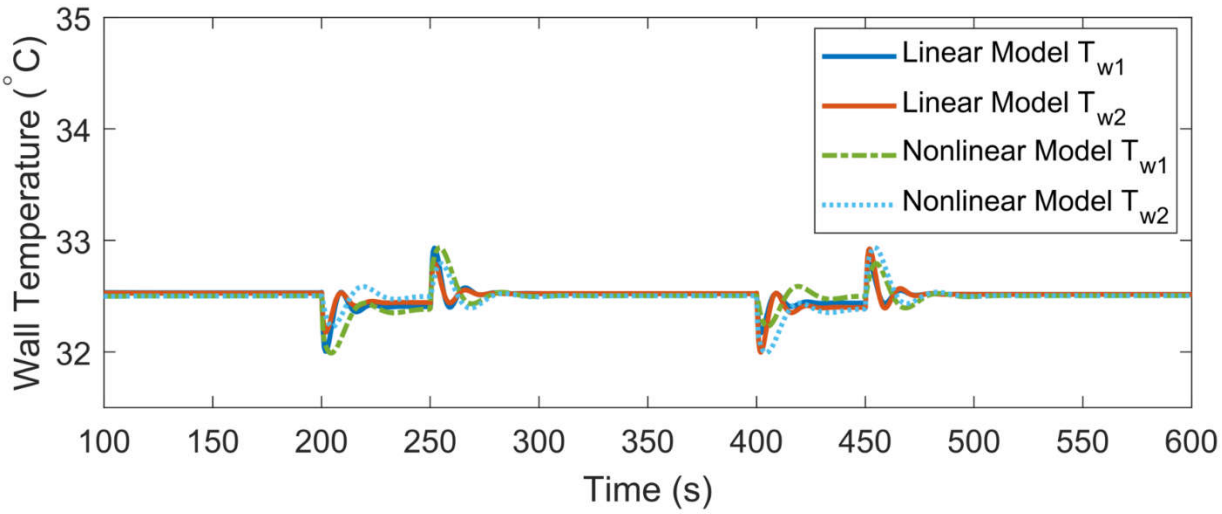

Figure 59: Wall temperatures comparison of nonlinear model and linearized model

5.3. Control Architecture Comparison

Two control architectures for PTP-VCC system are compared in this section. On the PTP side, decoupled PI controllers with estimated evaporator exit quality feedback control were adopted in the control architecture while decoupled PI controllers were used on the VCC side to maintain constant VCC evaporator pressure and superheat. The control architecture schematic is shown in Figure 60, where PI controllers were used in $C_1(s)$ to $C_5(s)$. The exact evaporator exit quality was used as the feedback signal for $C_3(s)$ in the control architecture to test alongside with in the proposed control architecture as a comparison to test the effectiveness of estimating evaporator exit quality. The other tested control architecture used heat flux feedforward controller to replace the estimated evaporator exit quality feedback controller in the PTP-VCC as shown in Figure 61 where $C_3(s)$ represents the heat flux feedforwad controller**.**

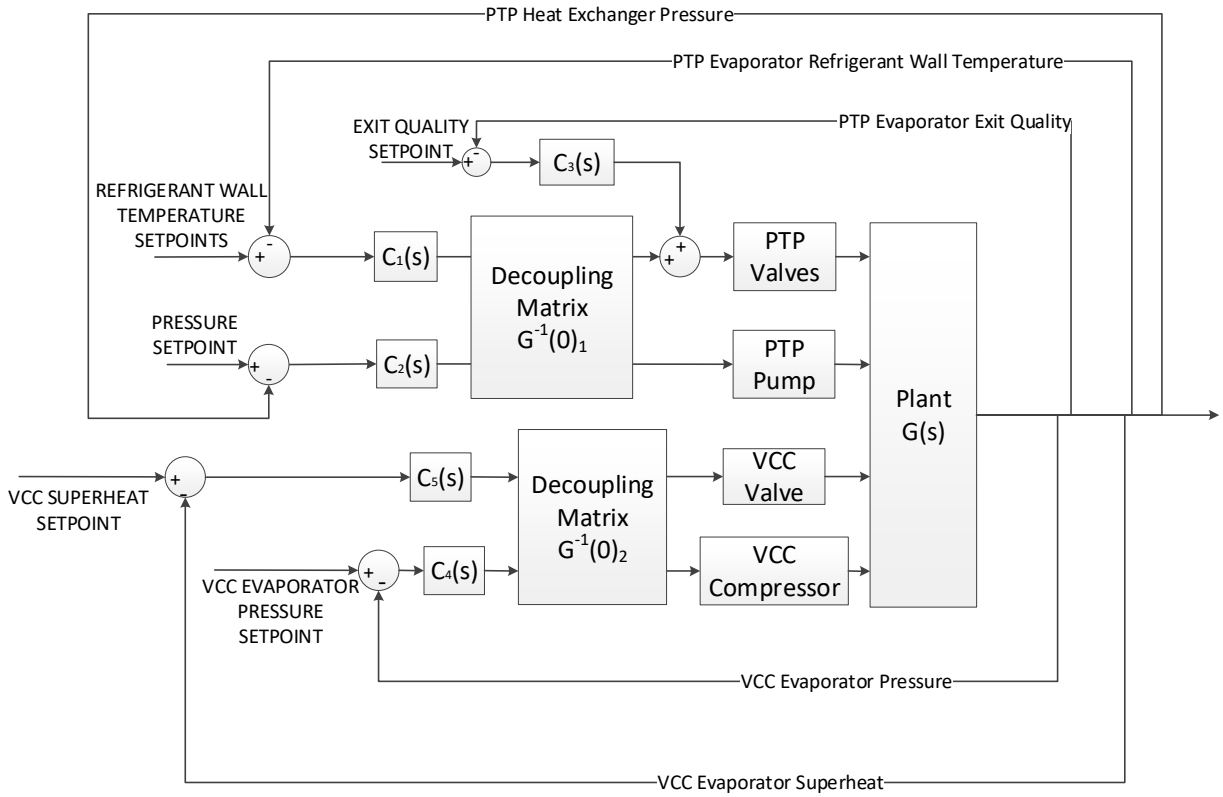

Figure 60: Control architecture with estimated evaporator exit quality feedback for integrated PTP-VCC system

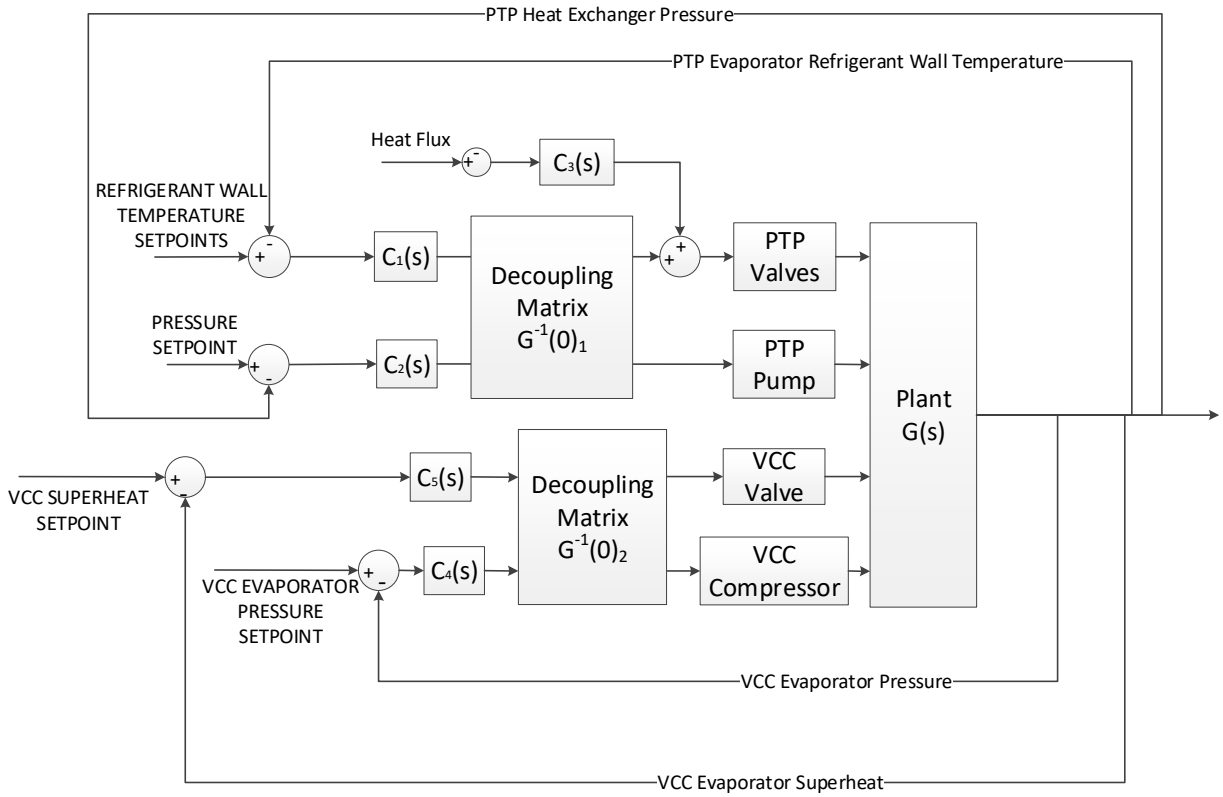

Figure 61: Control architecture with heat flux feedforward for integrated PTP-VCC system

The PTP-VCC system was tested with evenly distributed heat loads at 450 Watts, 250 Watts and 90 Watts to represent high heat load, medium heat load, and low heat load conditions. 10% of maximum heat load step changes are given to evaporator 1. Figure 62 shows the heat loads. All the evaporators were set up symmetrically with identical physical parameters. Heat load step changes on evaporator 1 can represent heat load changes on any evaporator.

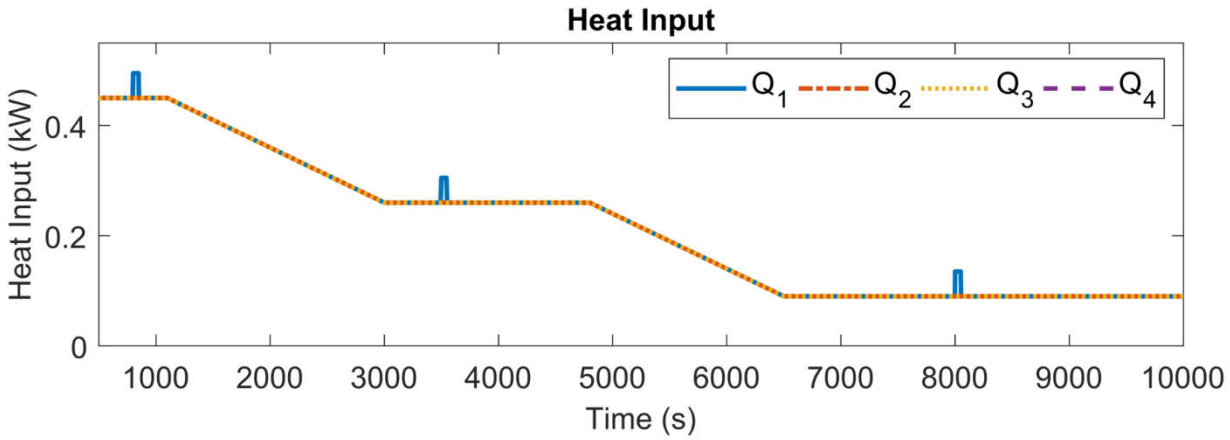

Figure 62: Evenly distributed heat load - PTP-VCC

The PTP system pressures of the tested control architectures are plotted in Figure 63. All the control architectures showed good performance in maintaining constant system pressure. Larger pressure fluctuation was observed at the lower heat load condition due to increased system sensibility at a low heat load condition.

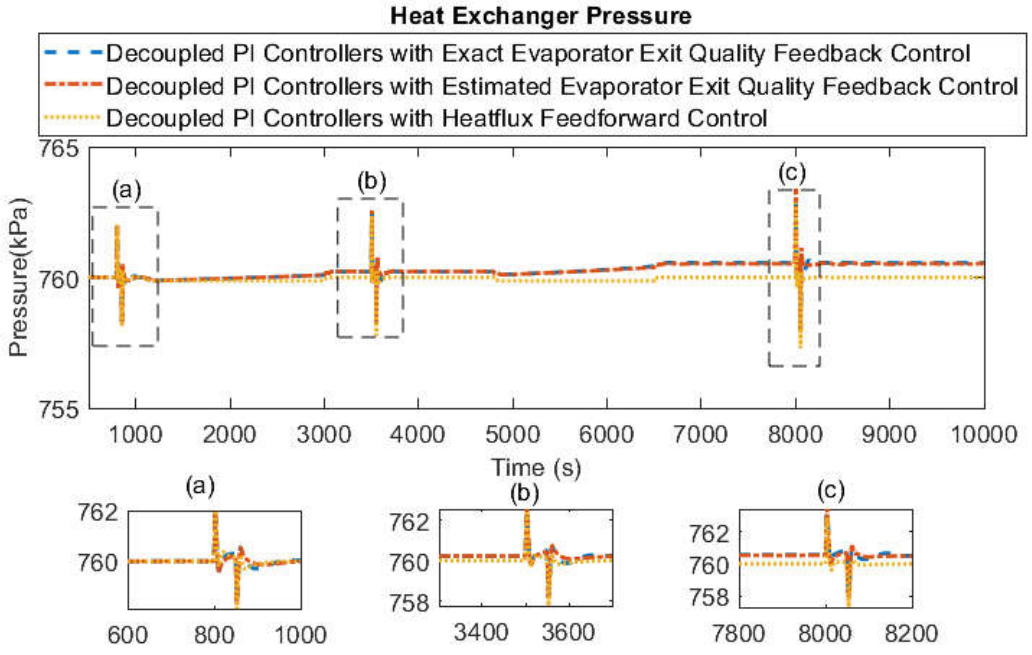

Figure 63: PTP system pressure under evenly distributed heat load - PTP-VCC

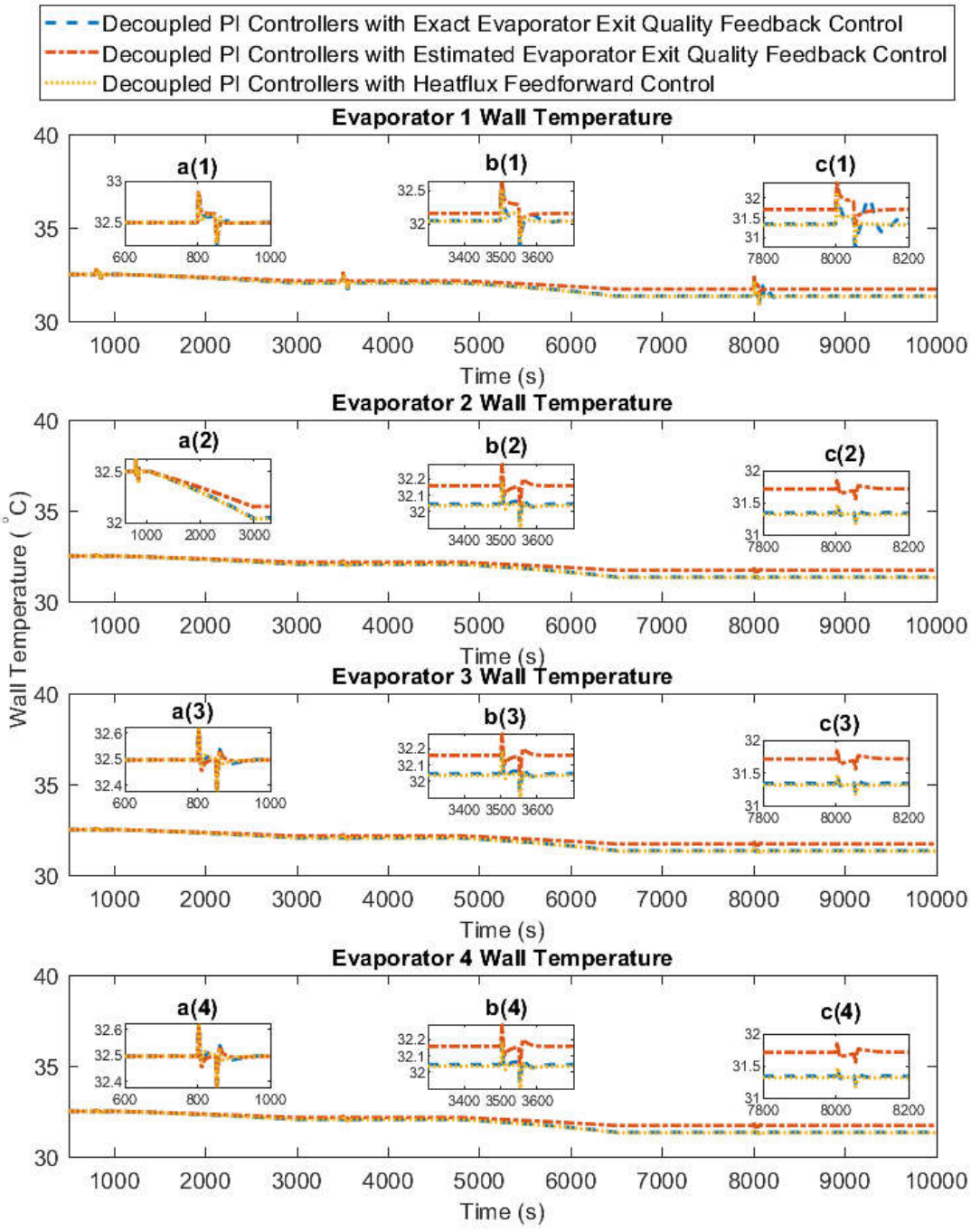

Figure 64: PTP wall temperatures under evenly distributed heat loads – PTP-VCC

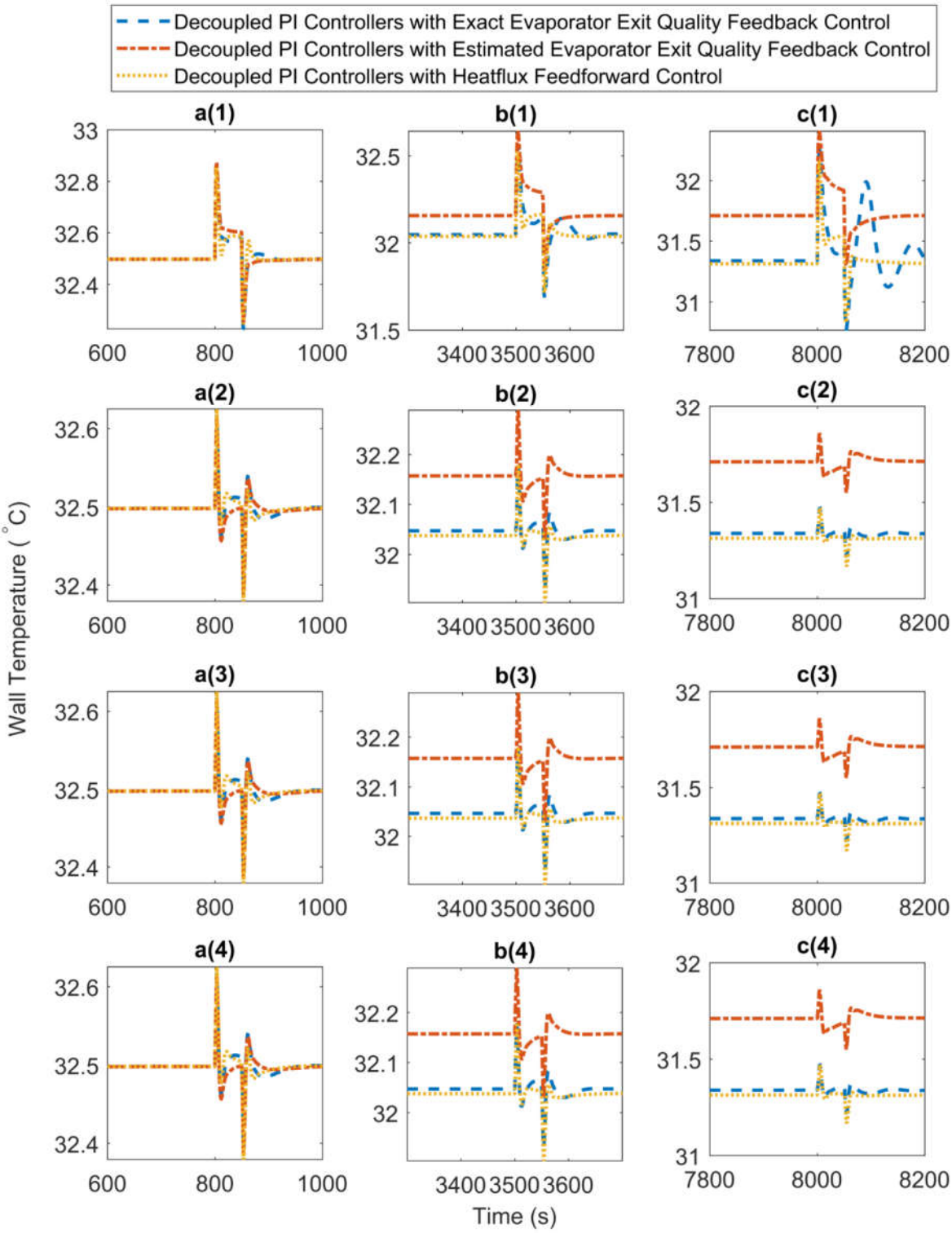

Figure 65: Enlarged PTP wall temperatures under evenly distributed heat loads – PTP-VCC

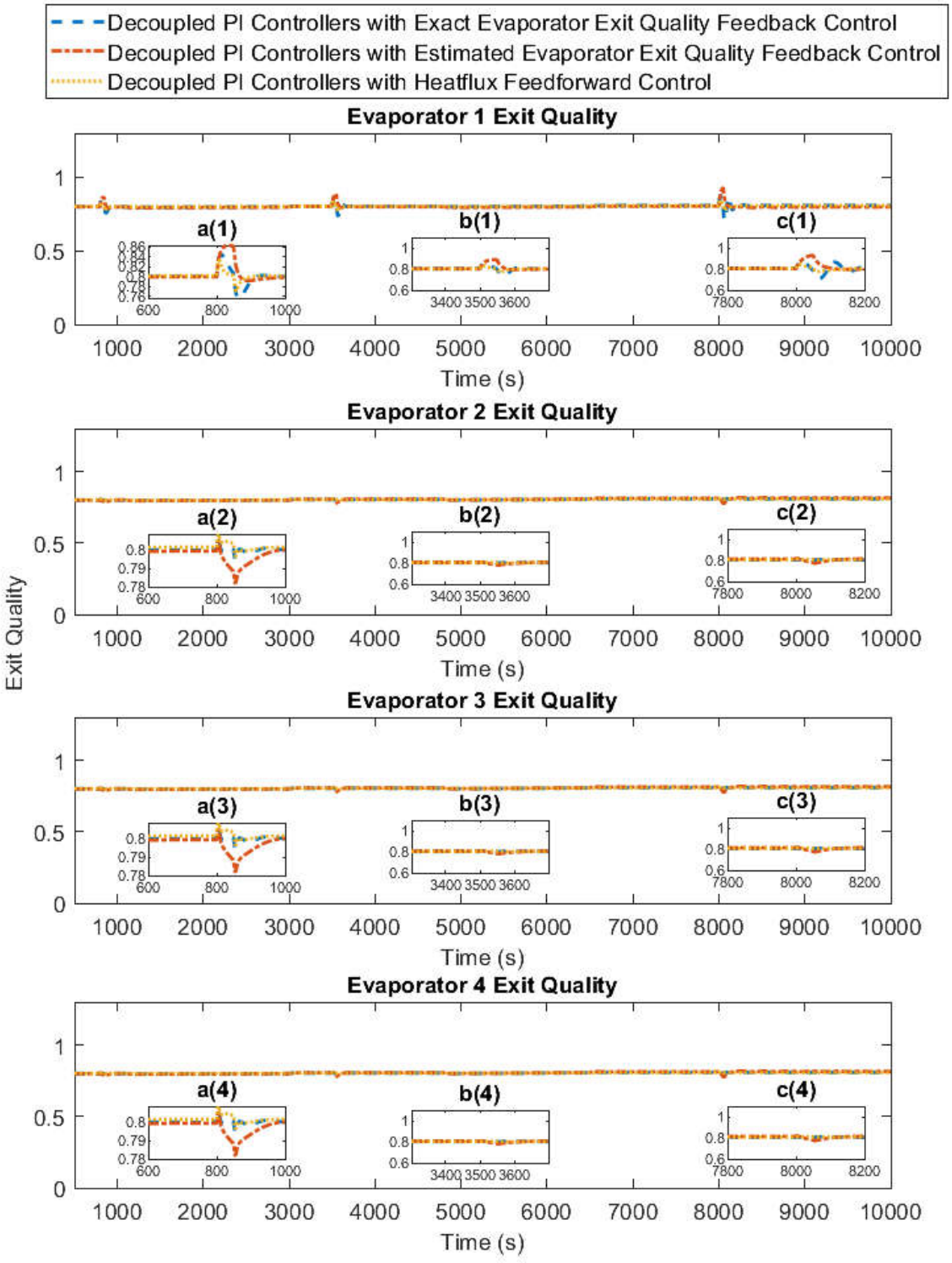

Figure 66: PTP evaporator exit qualities under evenly distributed heat loads - PTP-VCC

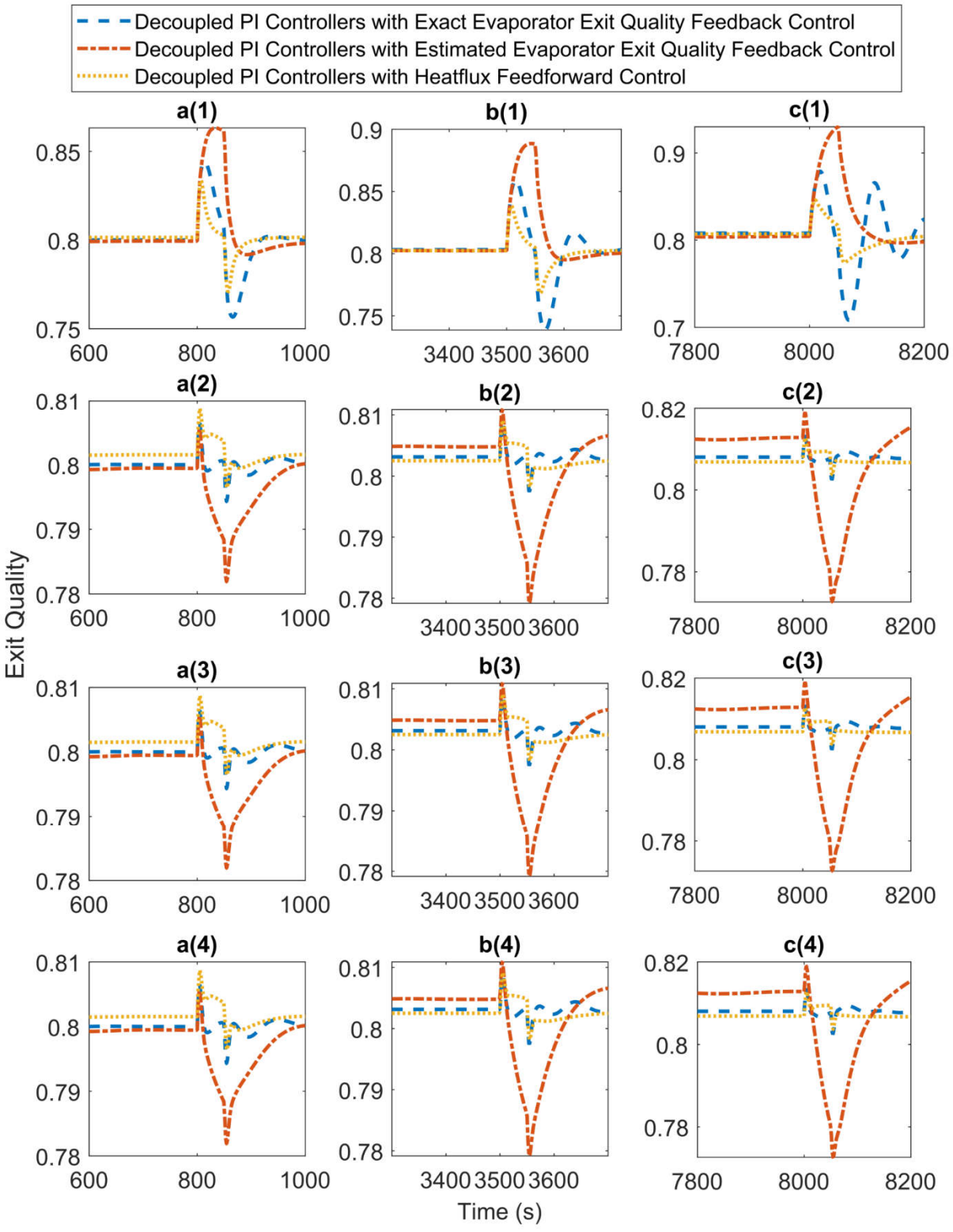

Figure 67: Enlarged PTP evaporator exit qualities under evenly distributed heat loads - PTP-VCC

PTP wall temperatures are plotted in Figure 64. An enlarged views during the heat step changes are plotted in Figure 65. All the tested control architectures showed the ability to maintain constant PTP wall temperatures.

PTP evaporator exit qualities are plotted in Figure 66 with an enlarged view during heat step changes in Figure 67. The exit quality setpoint was set to be 0.8. The exit qualities when using the estimated evaporator average exit quality in the control are of particular interest. The comparison between the exact exit qualities and the estimated exit quality is plotted in Figure 68. The estimated exit quality was very close to the exact exit qualities when the system has evenly distributed heat loads on the evaporators.

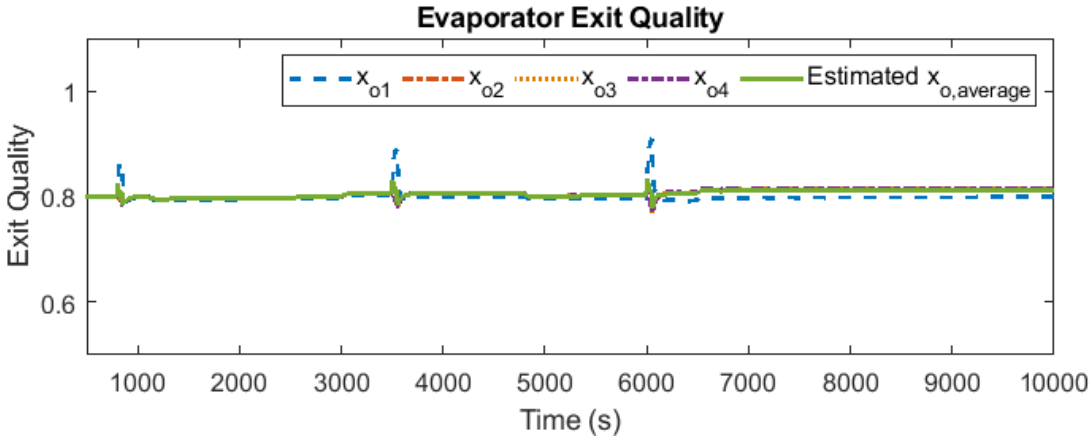

Figure 68: Comparison between evaporator exact exit qualities and estimated exit quality under evenly distributed heat loads - PTP-VCC.

The VCC evaporator and condenser pressures are plotted in Figure 69. In all the three test cases, the VCC evaporator and condenser pressures showed the same results. With decreasing heat load, the VCC evaporator pressures were well maintained at a constant value. The condenser pressures were regulated by the compressor to maintain system performance. VCC superheat is plotted in Figure 70. The superheats in the three test cases were kept at 10 °C. Small

oscillations were observed in low heat load conditions due increasing system sensitivity under low heat load condition.

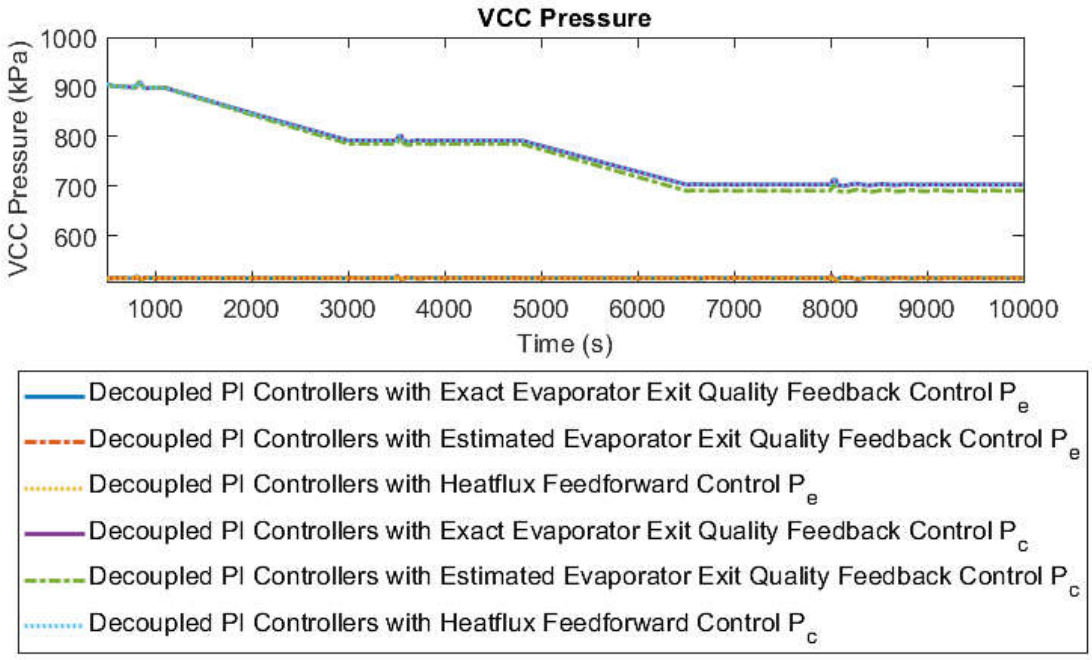

Figure 69: VCC pressure under evenly distributed heat loads

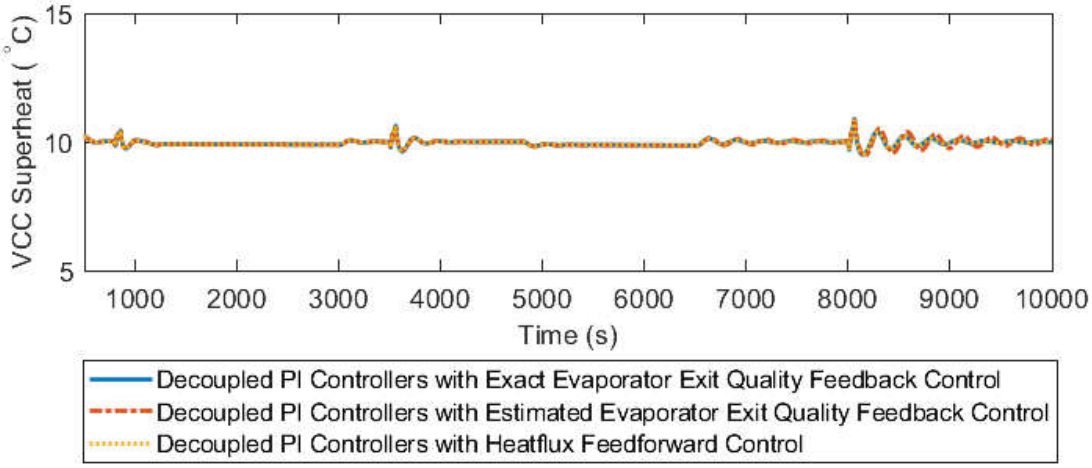

Figure 70: VCC superheat under evenly distributed heat loads

The cases were tested again under unevenly distributed heat loads shown in Figure 71. Evaporator 1 was given different heat loads at high load condition, medium load condition and low load condition while the heat loads on evaporator 2, 3 and 4 remain constant. Figure 72 plots the system pressures with the control architectures. All the control architectures showed good performance in maintaining constant system pressure. At steady state, the system pressure was well maintained at 760 kPa. During the heat impulses, the magnitude of the oscillations was slightly higher at the low heat load condition because of the increased sensitivity of low heat loads.

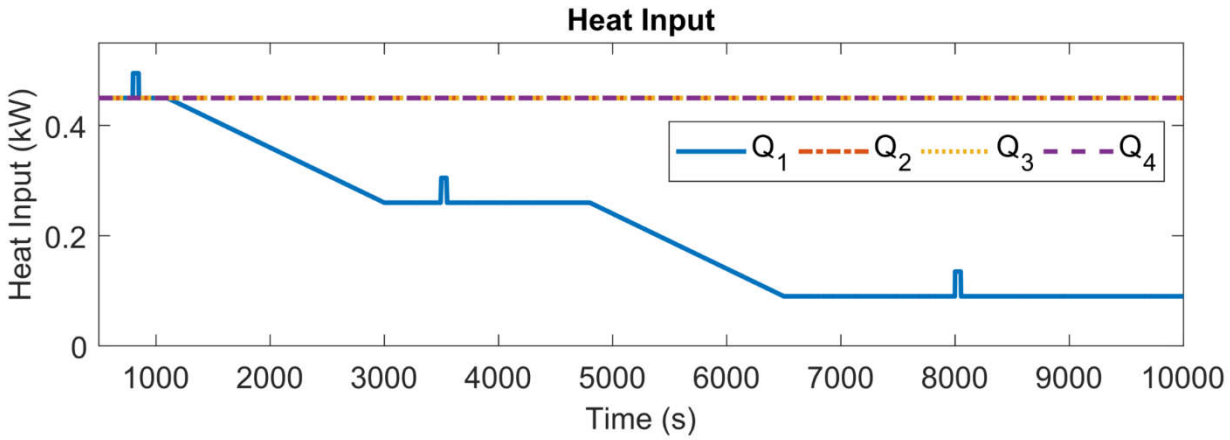

Figure 71: Unevenly distributed heat loads - PTP-VCC

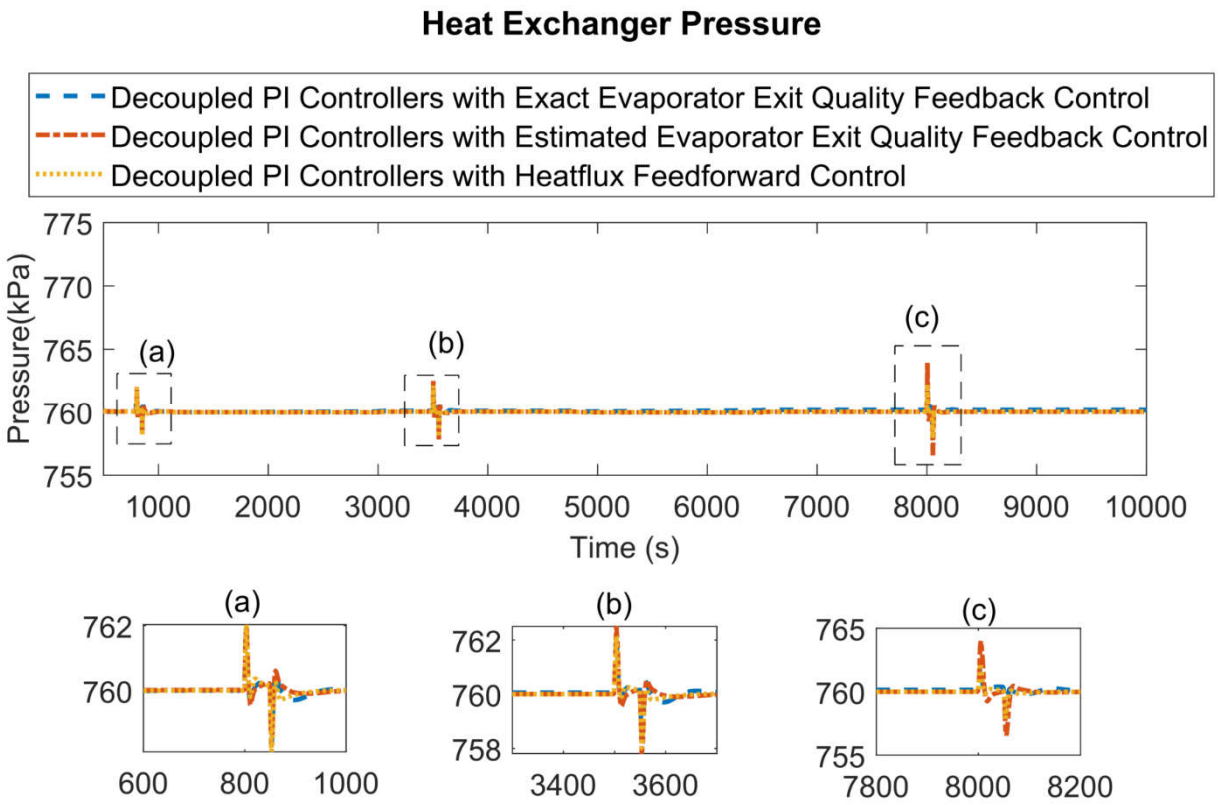

Figure 72: PTP system pressures under unevenly distributed heat loads - PTP-VCC.

Evaporator wall temperatures are shown in Figure 73 to compare different control architectures. The enlarged view of evaporator wall temperatures during the heat load step changes were plotted in Figure 74. Both the decoupled PI controllers with estimated evaporator average exit quality feedback control architecture and decoupled PI controllers with heat flux feedforward control architecture maintain constant wall temperatures and avoid CHF. On Evaporators 2, 3, and 4, the wall temperatures were stable at a setpoint of 32.5 °C. On evaporator 1, the wall temperature difference between using estimated average evaporator exit quality as feedback and using exit evaporator exit quality as feedback signal was less than 0.3 °C. During the heat load step changes, temperature fluctuations were observed on all evaporators. With each control architecture, the temperature fluctuations all fell within 1 °C.

Evaporator exit qualities are plotted in Figure 75. The enlarged views of evaporator exit quality during heat load changes are present in Figure 76. Both the decoupled PI controllers with estimated evaporator average exit quality feedback control architecture and decoupled PI controllers with heat flux feedforward control architecture effectively maintained exit quality at 0.8 under steady state conditions. During the heat impulses, the exit quality changes were less than 0.1 under all heat load conditions. On Evaporator 1, the exit quality in Case 2 decreased while heat load decreased.

The estimated exit quality was well maintained at 0.8, while Evaporator 1 exit quality increased with heat load and Evaporator 2, 3, and 4 exit qualities slightly increased above 0.8 as shown in Figure 77. This result was caused by the uneven distribution of the heat loads. The evaporator with higher heat load tended to have an exit quality lower than the estimated value, while the evaporator with lower heat load had an exit quality higher than the estimated value. This result was due to fact that all the evaporator inlet valves were using the same estimated average exit quality feedback signal. With a system of largely uneven heat distribution, the gains of the refrigerant wall temperature feedback should be tuned with a larger value, in which the control signals of the valves from the refrigerant wall feedback control compensate for the uneven distribution of the heat loads. In a PTP system with a large number of evaporators in parallel, the worst-case scenario of uneven heat load distribution is one evaporator with a high heat load and the remaining ones with low heat loads. By properly choosing the setpoint and gains of the control architecture, all the exit qualities can be maintained to avoid CHF.

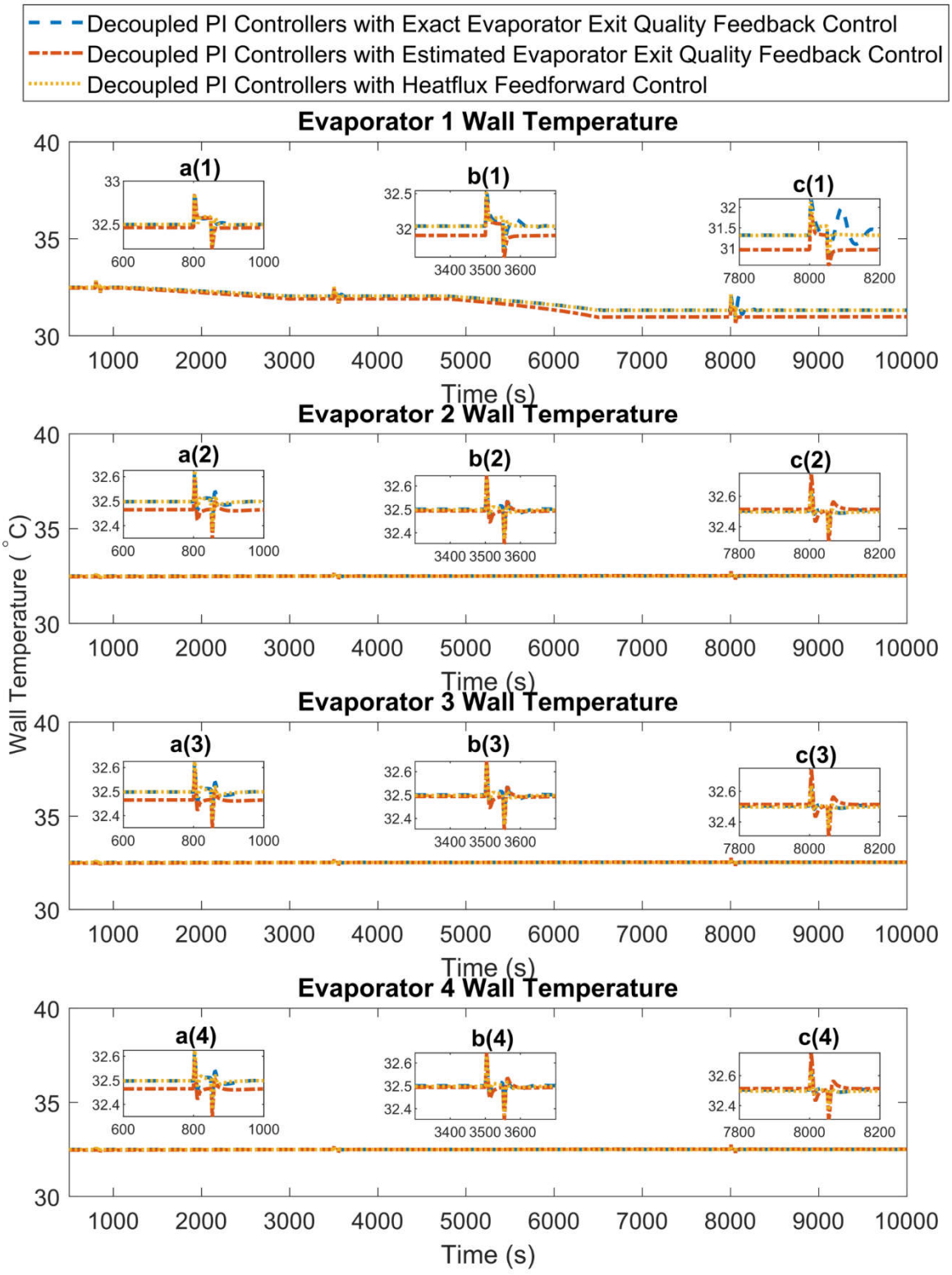

Figure 73: PTP wall temperatures under unevenly distributed heat loads - PTP-VCC.

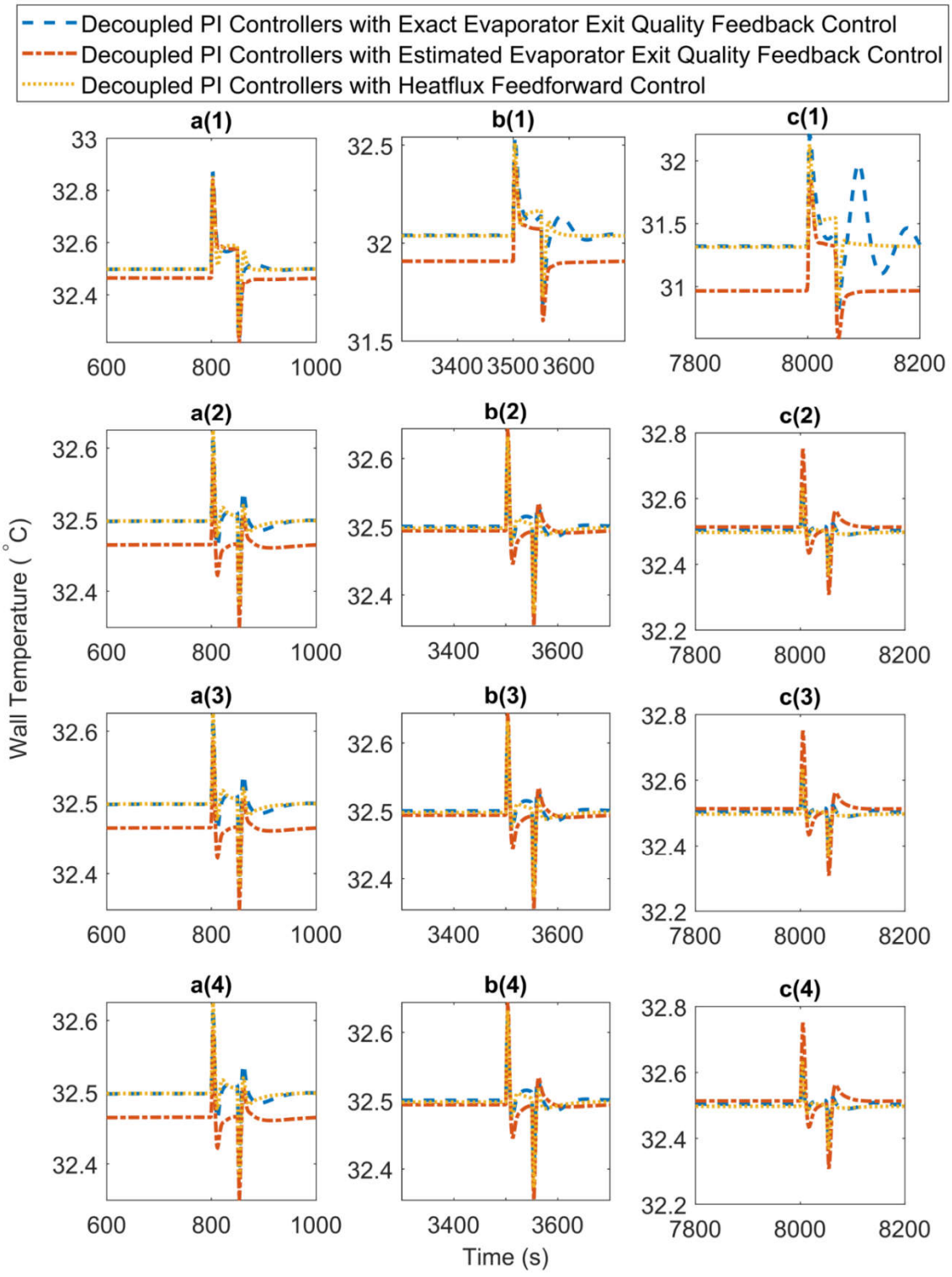

Figure 74: Enlarged PTP wall temperatures under unevenly distributed heat loads - PTP-VCC.

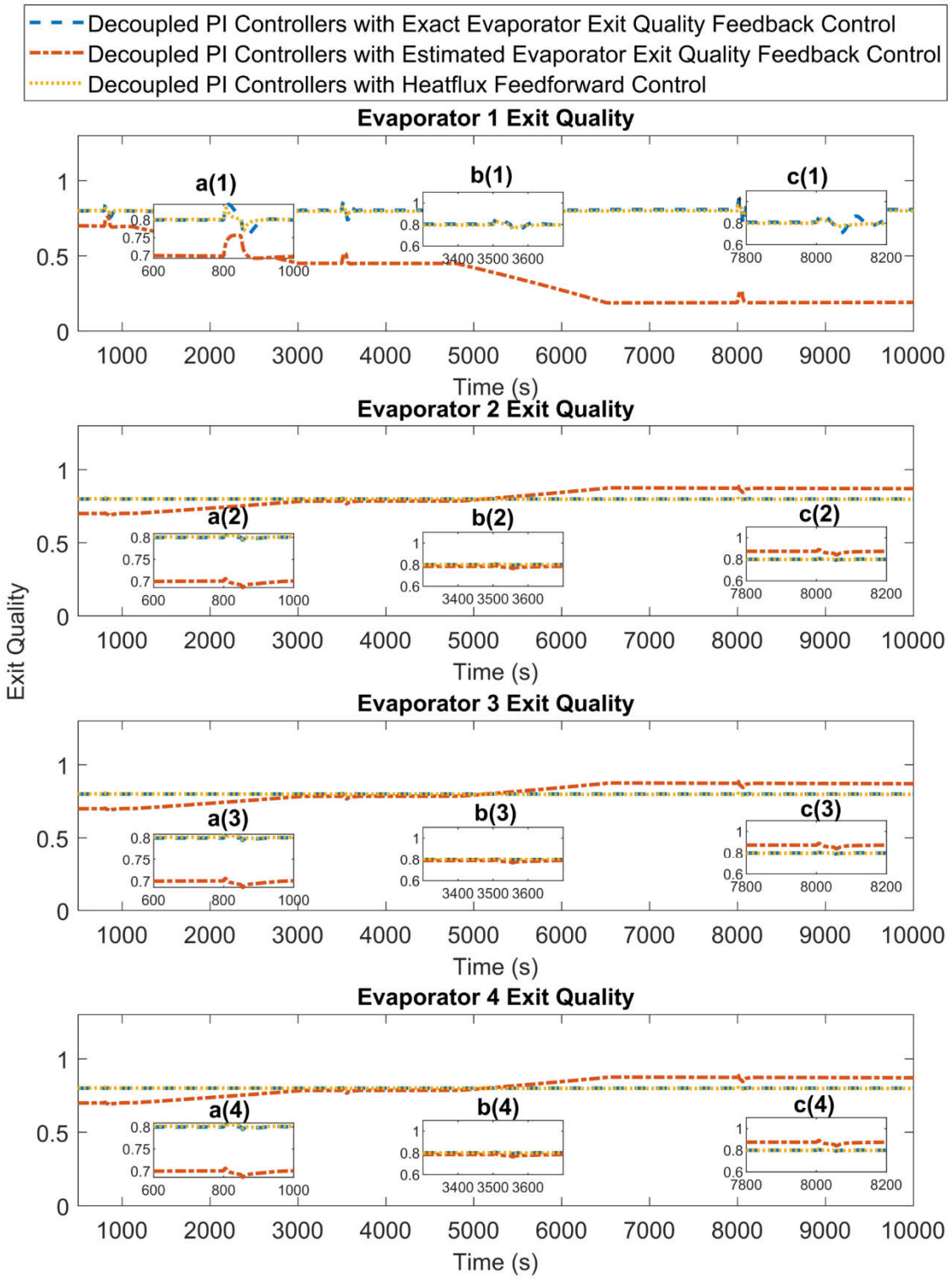

Figure 75: PTP evaporator exit qualities under unevenly distributed heat loads - PTP-VCC

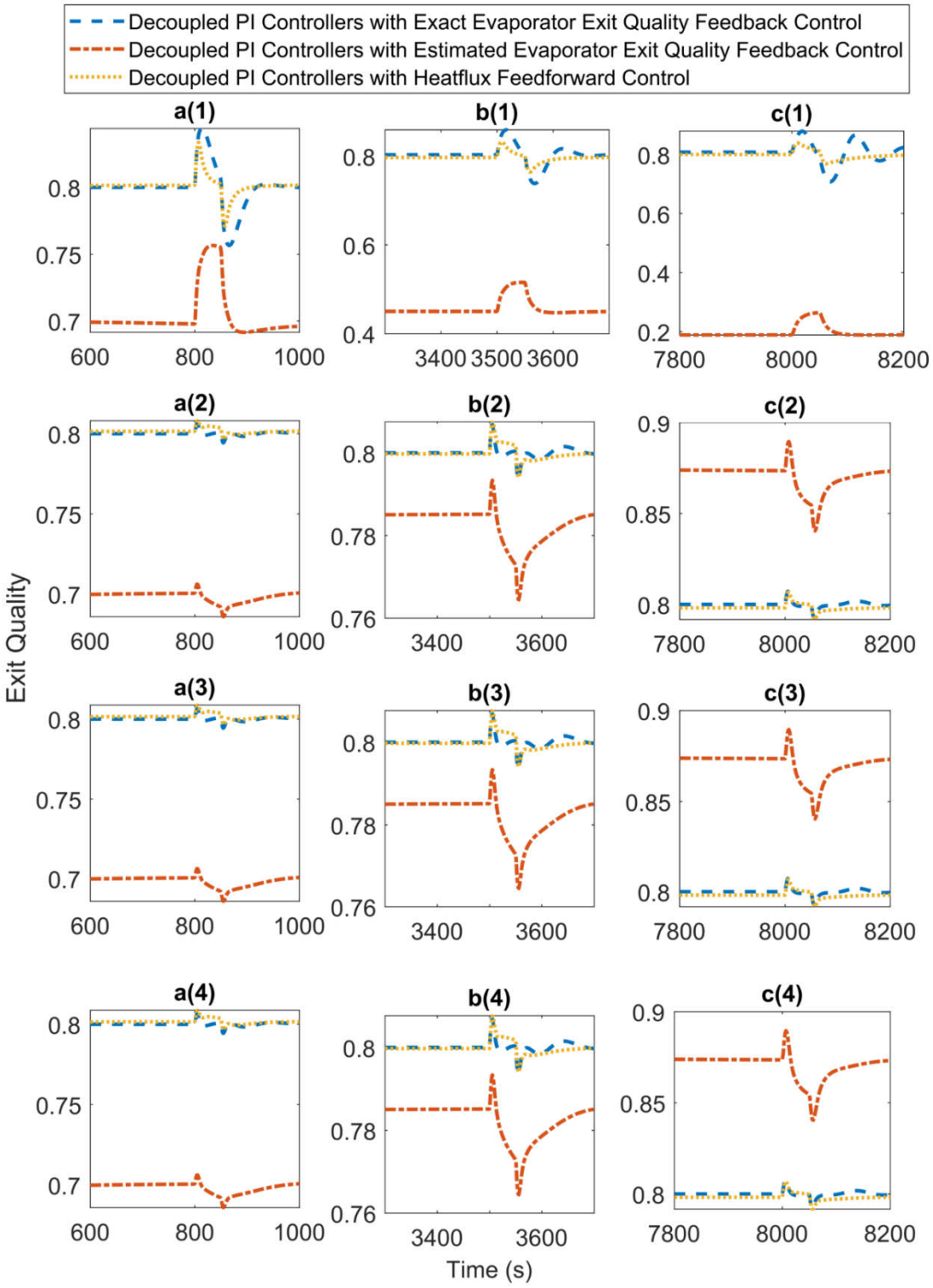

Figure 76: Enlarged PTP evaporator exit qualities under unevenly distributed heat loads - PTP-VCC

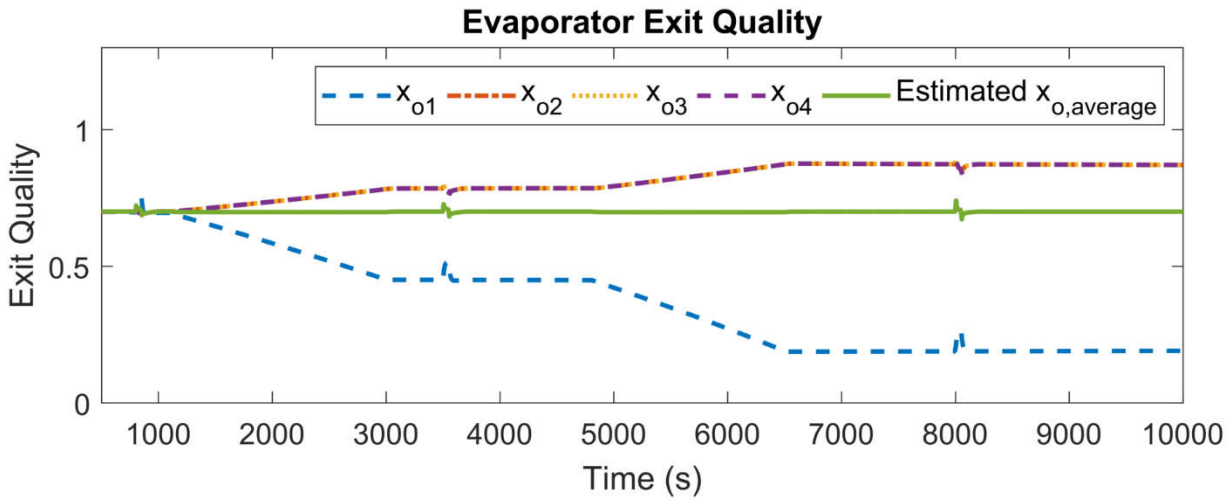

Figure 77: Comparison between exact exit qualities and estimated exit quality under unevenly distributed heat loads
- PTP-VCC

The VCC evaporator and condenser pressures are plotted in Figure 78. In the test cases, the VCC evaporator and condenser pressures showed the same results. With decreased heat load, the VCC evaporator pressures were well maintained at a constant value. The condenser pressures were regulated by the compressor to maintain system performance. VCC superheat is plotted in Figure 79. The superheats in the three test cases were kept at 10 °C.

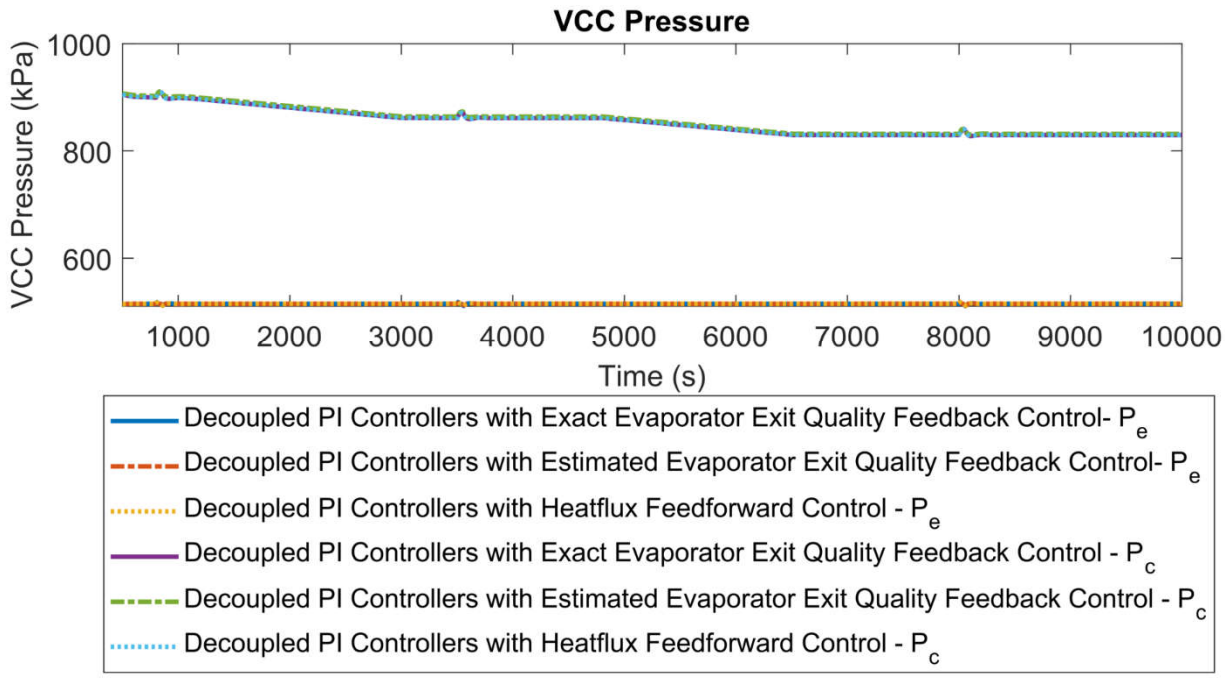

Figure 78: VCC pressures quality under unevenly distributed heat loads - PTP-VCC

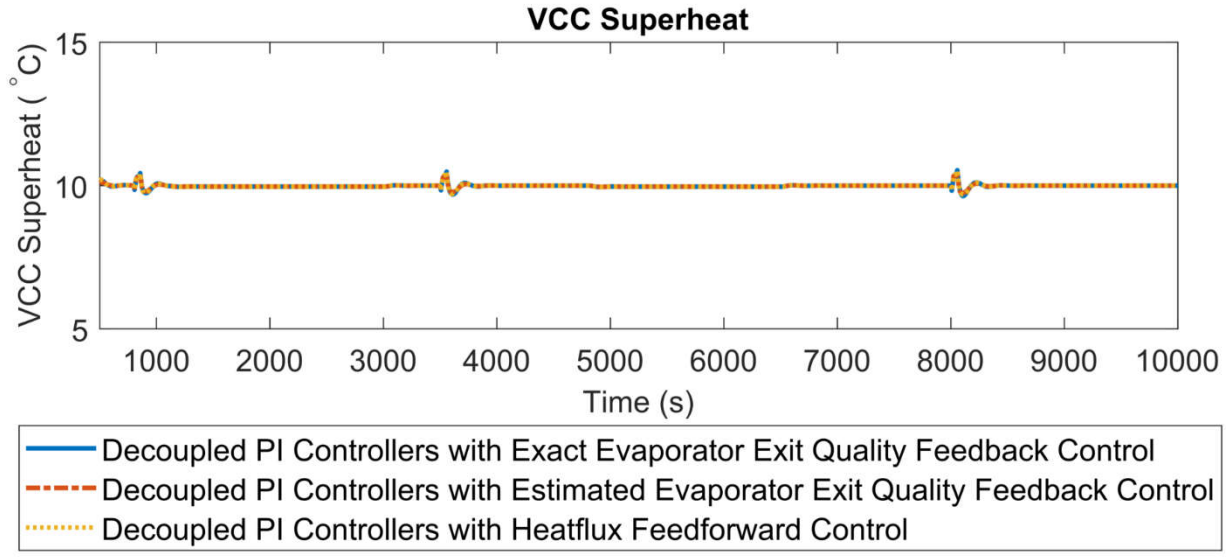

Figure 79: VCC superheats quality under unevenly distributed heat loads - PTP-VCC

6. CONCLUSION

6.1. Summary of Research Contribution

This dissertation presents dynamics modeling and control architecture design for a multi-evaporator pumped two-phase (PTP) system with an integration of a vapor compression cycle (VCC). The primary contributions include (1) model development and simulation of a control-oriented multi-evaporator PTP cooling system; (2) control architecture design for multi-evaporator PTP cooling system for variable heat load conditions; (3) model development and simulation of an integrated multi-evaporator PTP system and VCC; (4) control architecture design for integrated multi-evaporator PTP system and VCC with variable heat load conditions.

(1) Dynamic modeling for multi-evaporator PTP cooling system

PTP system schematics were studied and tested to find the appropriate system setup to keep the advantages of two-phase cooling while favoring controller implementation. With the valves before each evaporator, refrigerant flow can be controlled to compensate different load conditions without causing clogging. The evaporators and condenser were modeled together (unconventionally) to overcome the issue of lacking mass flow rate components in between. Both the moving boundary (MB) and finite control volume (FCV) methods were tested. The FCV method can provide more spatial detail about system conditions, while the MB method has a faster real-time factor with more evaporators in parallel. With the switched moving boundary (SMB) method, the combined heat exchanger model revealed the ability to handle a large number of evaporators in parallel within a reasonable timeframe.

(2) Control architecture design for multi-evaporator PTP cooling system

The system schematic was designed to be suitable for applying control architectures for CHF avoidance. Simple Proportional-Integral (PI) controllers are not sufficient for PTP systems to ensure CHF avoidance. Two control architectures were proposed and compared. Decoupled Proportion-Integral (PI) controllers with estimated evaporator exit feedback control and decoupled PI controllers with heat flux feedforward showed promising results under different load conditions. These approaches ensure system operational safety with high exit quality. However, heat flux cannot be predicted in a majority of cases, and feedback control is easier than feedforward control in application. These two reasons make decoupled PI controllers with estimated evaporator exit feedback control more suitable for most applications.

The decoupled control architecture consists of valve feedback controllers, a pump-speed feedback controller, and a decoupling matrix to compensate for coupled dynamics among multiple evaporators. A key design of this architecture is using the estimated evaporator exit quality to suppress superheat to heat load disturbances. This control architecture has significant practical applications. With certain temperature and pressure measurements, the PTP cooling system becomes robust to 110% maximum external heat loads. Furthermore, this control architecture allows the system to operate with high exit qualities and good energy efficiency.

(3) Dynamic modeling for integrated multi-evaporator PTP-VCC system

The multi-evaporator PTP system was integrated with a VCC that provides the necessary heat rejection for the PTP condenser. The VCC evaporator was used to remove the heat from the PTP condenser. Thus, the condenser in the combined heat exchanger was modeled as a refrigerant-to-refrigerant heat exchanger. A multi-evaporator PTP-VCC system was developed to study the interaction dynamics among the two cycles to provide a more intuitive for design.

(4) Control architecture design for integrated multi-evaporator PTP-VCC system

The same decoupled control architecture was applied on the PTP cycle. A separate control architecture was implemented on the VCC to maintain constant superheat and evaporating pressure. A time-scale separation analysis was performed to identify the physical mechanism for the coupling between the two cycles.

A linearized dynamic system model was derived to identify the dynamic modes and their associated time scales. Increasing the volume of the VCC evaporator can help reduce the pressure interaction between the two cycles.

6.2. Future Research

The control architectures were successful in the simulation test cases, and we anticipate that they could be applied directly to the prototype system. Further experimental validation is needed to determine the effectiveness of the estimated exit quality feedback control with valves and pump feedback control.

REFERENCES

[1] S. Garimella *et al.*, "Thermal Challenges in Next-Generation Electronic Systems," *IEEE Transactions on Components and Packaging Technologies,* vol. 31, no. 4, pp. 801-815, 2008. doi: 10.1109/TCAPT.2008.2001197

[2] A. Shehabi, S. Smith, and D. Sartor, "United States Data Center Energy Usage Report," Lawrence Berkeley National Laboratory, 2016, Available: http://eta-publications.lbl.gov/sites/default/files/lbnl-1005775_v2.pdf.

[3] J. Lee and I. Mudawar, "Low-Temperature Two-Phase Microchannel Cooling for High-Heat-Flux Thermal Management of Defense Electronics," *IEEE Transactions on Components and Packaging Technologies,* vol. 32, no. 2, pp. 453-465, 2009. doi: 10.1109/TCAPT.2008.2005783

[4] D. B. Tuckerman, "High-performance heat sinking for VLSI," *IEEE Electron Device Letters,* vol. 2, no. 5, pp. 126-129, May. 1981. doi: 10.1109/EDL.1981.25367

[5] T. Brunschwiler, "Heat-removal performance scaling of interlayer cooled chip stacks," in *12th IEEE Intersociety Conference on Thermal and Thermomechanical Phenomena in Electronic Systems*, Las Vegas, NV, USA, 2010, pp. 1-12. doi: 10.1109/ITHERM.2010.5501254

[6] M. M. Ohadi, S. V. Dessiatoun, K. Choo, M. Pecht, and J. V. Lawler, "A comparison analysis of air, liquid, and two-phase cooling of data centers," in *28th Annual IEEE Semiconductor Thermal Measurement and Management Symposium (SEMI-THERM)*, 2012, pp. 58-63. doi: 10.1109/STHERM.2012.6188826

[7] R. Schmidt, "Packaging of New Servers, Energy Efficiency Aspects," presented at the 1st Berkeley Symposium on Energy Efficient Electronics, 2009. Available: https://e3s-center.berkeley.edu/wp-content/uploads/2017/07/RogerSchmidt.pdf

[8] T. Jomard, U. Eckes, E. Touvier, and M. Lallemand, "Modelling of the two-phase cooling of a power semiconductor and its associated evaporators," in *Eighth Annual IEEE Semiconductor Thermal Measurement and Management Symposium*, 1992, pp. 20-24. doi: 10.1109/STHERM.1992.172848

[9] P. H. Desai and G. Wiegner, "Evaluation of Freon modules for power electronics designed for a locomotive traction drive," *IEEE Transactions on Industry Applications,* vol. 26, no. 3, pp. 394-400, 1990. doi: 10.1109/28.55968

[10] I. Mudawar, "Direct-immersion cooling for high power electronic chips," in *Intersociety Conference on Thermal Phenomena in Electronic Systems*, 1992, pp. 74-84. doi: 10.1109/ITHERM.1992.187743

[11] G. N. Dulnev, V. A. Korablyev, and A. V. Sharkov, "Evaporation cooling of high power electronic devices," *IEEE Transactions on Components, Packaging, and Manufacturing Technology: Part A,* vol. 19, no. 3, pp. 431-434, 1996. doi: 10.1109/95.536845

[12] B. Agostini, M. Fabbri, J. E. Park, L. Wojtan, J. R. Thome, and B. Michel, "State of the Art of High Heat Flux Cooling Technologies," *Heat Transfer Engineering,* vol. 28, no. 4, pp. 258-281, April 2007. doi: 10.1080/01457630601117799

[13] I. Mudawar, "Assessment of high-heat-flux thermal management schemes," *IEEE Transactions on Components and Packaging Technologies,* vol. 24, no. 5, pp. 122-141, Jun. 2001. doi: 10.1109/6144.926375

[14] Y.-Y. Hsu and R. W. Graham, *Transport processes in boiling and two-phase systems, including near-critical fluids*. La Grange Park, Ill., USA : American Nuclear Society, 1986.

[15] R. Hannemann, J. Marsala, and M. Pitasi, "Pumped Liquid Multiphase Cooling," in *Proceedings of IMECE04 2004 ASME International Mechanical Engineering Congress and Exposition*, Anaheim, California, USA, 2004, no. 47071, pp. 469-473. doi: 10.1115/IMECE2004-60669

[16] S. Trutassanawin, "Experimental Investigation of a Miniature-Scale Refrigeration System for Electronics Cooling," *IEEE Transactions on Components and Packaging Technologies,* vol. 29, no. 3, pp. 678-687, 2006. doi: 10.1109/tcapt.2006.881762

[17] R. Mongia *et al.*, "Small scale refrigeration system for electronics cooling within a notebook computer," in *Thermal and Thermomechanical Proceedings 10th Intersociety Conference on Phenomena in Electronics Systems*, San Diego, CA, USA, 2006. doi: 10.1109/ITHERM.2006.1645421

[18] J. B. Marcinichen, J. R. Thome, and B. Michel, "Cooling of microprocessors with micro-evaporation: A novel two-phase cooling cycle," *International Journal of Refrigeration,* vol. 33, no. 7, pp. 1264-1276, 2010. doi: 10.1016/j.ijrefrig.2010.06.008

[19] J. Marcinichen, J. Olivier, d. O. V, and J. Thome, "A review of on-chip micro-evaporation: Experimental evaluation of liquid pumping and vapor compression driven cooling systems and control," *Applied Energy,* vol. 92, pp. 147-161, 2012. doi: 10.1016/j.apenergy.2011.10.030

[20] D. Wu, J. B. Marcinichen, and J. R. Thome, "Experimental evaluation of a controlled hybrid two-phase multi-microchannel cooling and heat recovery system driven by liquid

pump and vapor compressor," *International Journal of Refrigeration,* vol. 36, no. 2, pp. 375-389, Mar. 2013. doi: 10.1016/j.ijrefrig.2012.11.011

[21] A. Heydari, "Miniature vapor compression refrigeration systems for active cooling of high performance computers," presented at the ITherm 2002. Eighth Intersociety Conference on Thermal and Thermomechanical Phenomena in Electronic Systems, San Diego, CA, USA, 2002. doi: 10.1109/ITHERM.2002.1012480

[22] R. Zhou *et al.*, "The steady-state modeling and optimization of a refrigeration system for high heat flux removal," *Applied Thermal Engineering,* vol. 30, no. 16, pp. 2347-2356, November 2010. doi: 10.1016/j.applthermaleng.2010.05.023

[23] R. Zhou *et al.*, "The Steady-State Modeling and Static System Design of a Refrigeration System for High Heat Flux Removal," no. 48715, pp. 1607-1616, 2008. doi: 10.1115/IMECE2008-69074

[24] J. Catano, T. Zhang, J. T. Wen, M. K. Jensen, and Y. Peles, "Vapor compression refrigeration cycle for electronics cooling – Part I: Dynamic modeling and experimental validation," *International Journal of Heat & Mass Transfer,* vol. 66, pp. 911-921, Nov. 2013. doi: 10.1016/j.ijheatmasstransfer.2013.06.075

[25] J. Catano, F. Lizarralde, T. Zhang, J. T. Wen, M. K. Jensen, and Y. Peles, "Vapor compression refrigeration cycle for electronics cooling – Part II: gain-scheduling control for critical heat flux avoidance," *International Journal of Heat & Mass Transfer,* Article vol. 66, pp. 922-929, Nov. 2013. doi: 10.1016/j.ijheatmasstransfer.2013.06.074

[26] T. Zhang, J. Catano, R. Zhou, and J. T. Wen, "Dynamic Modeling of Refrigeration Cycle for Electronics Cooling," in *ASME 2008 International Mechanical Engineering Congress*

and Exposition, 2008, no. 48715, pp. 1587-1596, Volume 10: Heat Transfer, Fluid Flows, and Thermal Systems, Parts A, B, and C. doi: 10.1115/IMECE2008-69047

[27] Z. Yang, D. T. Pollock, and J. T. Wen, "Gain-scheduling control of vapor compression cycle for transient heat-flux removal," *Control Engineering Practice,* vol. 39, pp. 67-89, June 2015. doi: 10.1016/j.conengprac.2015.02.004

[28] K. Kelkar, S. Patankar, S. Kang, M. Iyengar, and R. Schmidt, "Computational method for generalized analysis of pumped two-phase cooling systems and its application to a system used in data-center environments," in *12th IEEE Intersociety Conference on Thermal and Thermomechanical Phenomena in Electronic Systems*, 2010, pp. 1-11. doi: 10.1109/ITHERM.2010.5501416

[29] L. Chen, "Enthalpy-based system-model for pumped two-phase cooling systems," presented at the 15th IEEE Intersociety Conference on Thermal and Thermomechanical Phenomena in Electronic Systems (ITherm), Las Vegas, NV, USA, 2016. doi: 10.1109/ITHERM.2016.7517629

[30] B. P. Rasmussen, "Dynamic modeling for vapor compression systems—Part I: Literature review," *HVAC & R Research,* vol. 18, no. 5, p. 934, Sep. 2012. doi: 10.1080/10789669.2011.582916

[31] J. Nyers and G. Stoyan, "A dynamical model adequate for controlling the evaporator of a heat pump," *International journal of refrigeration,* vol. 17, no. 2, pp. 101-108, 1994. doi: 10.1016/0140-7007(94)90050-7

[32] X. Jia, C. P. Tso, P. K. Chia, and P. Jolly, "A distributed model for prediction of the transient response of an evaporator," *International Journal of Refrigeration,* vol. 18, no. 5, pp. 336-342, 1995. doi: 10.1016/0140-7007(95)00015-4

[33] X. Jia, C. P. Tso, P. Jolly, and Y. W. Wong, "Distributed steady and dynamic modelling of dry-expansion evaporators," *International Journal of Refrigeration,* vol. 22, no. 2, pp. 126-136, Mar. 1999. doi: 10.1016/S0140-7007(98)00043-7

[34] G. L. Wedekind, B. L. Bhatt, and B. T. Beck, "A system mean void fraction model for predicting various transient phenomena associated with two-phase evaporating and condensing flows," *International Journal of Multiphase Flow,* vol. 4, no. 1, pp. 97-114, 1978. doi: 10.1016/0301-9322(78)90029-0

[35] S. Bendapudi, J. Braun, and E. Groll, "A comparison of moving-boundary and finite-volume formulations for transients in centrifugal chillers," *International Journal of Refrigeration,* vol. 31, no. 8, pp. 1437-1452, 2008. doi: 10.1016/j.ijrefrig.2008.03.006

[36] E. Rodriguez and B. P. Rasmussen, "A comparison of modeling paradigms for dynamic evaporator simulations with variable fluid phases," *Applied Thermal Engineering,* vol. 112, pp. 1326-1342, Feb. 2017. doi: 10.1016/j.applthermaleng.2016.10.131

[37] M. Willatzen, N. B. O. L. Pettit, and L. Ploug-Sørensen, "A general dynamic simulation model for evaporators and condensers in refrigeration. Part I: moving-boundary formulation of two-phase flows with heat exchange," *International Journal of Refrigeration,* vol. 21, no. 5, pp. 398-403, Aug. 1998. doi: 10.1016/S0140-7007(97)00091-1

[38] W. Zhang and C. Zhang, "A generalized moving-boundary model for transient simulation of dry-expansion evaporators under larger disturbances," *International Journal of Refrigeration,* vol. 29, no. 7, pp. 1119-1127, Nov. 2006. doi: 10.1016/j.ijrefrig.2006.03.002

[39] T. L. McKinley and A. G. Alleyne, "An advanced nonlinear switched heat exchanger model for vapor compression cycles using the moving-boundary method," *International Journal of Refrigeration,* vol. 31, no. 7, pp. 1253-1264, Nov. 2008. doi: 10.1016/j.ijrefrig.2008.01.012

[40] B. Li and A. G. Alleyne, "A dynamic model of a vapor compression cycle with shut-down and start-up operations," *International Journal of Refrigeration,* Article vol. 33, no. 3, pp. 538-552, May. 2010. doi: 10.1016/j.ijrefrig.2009.09.011

[41] L. Cecchinato and F. Mancini, "An intrinsically mass conservative switched evaporator model adopting the moving-boundary method," *International Journal of Refrigeration,* vol. 35, pp. 349-364, Mar. 2012. doi: 10.1016/j.ijrefrig.2011.10.007

[42] H. Qiao, V. Aut, and R. Radermacher, "An Improved Moving Boundary Heat Exchanger Model with Pressure Drop," presented at the International Refrigeration an Air Conditioning Conference, 2014. Available: https://docs.lib.purdue.edu/iracc/1414/

[43] J. Bonilla, "Switching moving boundary models for two-phase flow evaporators and condensers," *Communications in Nonlinear Science and Numerical Simulation,* vol. 20, no. 3, pp. 743-768, Mar. 2015. doi: 10.1016/j.cnsns.2014.06.035

[44] B. P. Rasmussen, "Control-Oriented Modeling of Transcritical Vapor Compression Systems," M.S. Thesis, Dept. of Mech. and Ind. Eng, University of Illinois, Urbana, IL, 2012.

[45] E. W. Grald, "A moving-boundary formulation for modeling time-dependent two-phase flows," *International Journal of Heat and Fluid Flow,* vol. 13, no. 3, pp. 266-272, Sep. 1992. doi: 10.1016/0142-727X(92)90040-G

[46] E. Bristol, "On a new measure of interaction for multivariable process control," *IEEE Transactions on Automatic Control,* vol. 11, no. 1, pp. 133-134, 1966. doi: 10.1109/TAC.1966.1098266

APPENDIX

This appendix presents the detailed model derivation for switched moving boundary evaporator, switched moving boundary condenser and the multi-evaporator combined heat exchanger.

The governing Partial Differential Equations (PDE) of a heat exchanger is based on conservation of refrigerant mass as shown in Equation A-1, conservation of refrigerant energy as shown in Equation (2) and conservation of refrigerant wall energy as shown in Equation (3).

$$\frac{\partial(\rho A_{CS})}{\partial t} + \frac{\partial(\dot{m})}{\partial z} = 0 \quad \textbf{A-1}$$

$$\frac{\partial(\rho A_{CS} h - A_{CS} P)}{\partial t} + \frac{\partial(\dot{m} h)}{\partial z} = p_i \alpha_i (T_w - T_r) \quad \textbf{A-2}$$

$$(C_P \rho A)_W (\dot{T}_w) = \alpha_i A_i (T_w - T_r) + \alpha_o A_o (T_a - T_w) \quad \textbf{A-3}$$

Switch Moving Boundary Evaporator Model Derivation

Evaporator with Only Two-phase Fluid

When there is only two-phase fluid in the evaporator, the length of the two-phase region equals to the total length of the tube as,

$$L_1 = L_{total} \quad \textbf{A-4}$$

Integrating Equation A-1 along the tube length, conservation of mass for the refrigerant in the heat exchanger is calculated as,

$$\int_0^{L_1} \left[\frac{\partial(\rho A_{CS})}{\partial t} + \frac{\partial(\dot{m})}{\partial z} \right] dz \quad \textbf{A-5}$$

$$= \int_0^{L_1} \frac{\partial(\rho A_{CS})}{\partial t} dz + \int_0^{L_1} \frac{\partial(\dot{m})}{\partial z} dz$$

$$= A_{CS} \left[\int_0^{L_1} \frac{\partial}{\partial t} dz \right] + \dot{m}_{out} - \dot{m}_{in}$$

$$= A_{CS} \left[\frac{d}{dt} \int_0^{L_1} (\rho)\, dz \right] + \dot{m}_{out} - \dot{m}_{in}$$

$$= A_{CS} \left[\frac{d}{dt} (\rho_1 L_1) \right] + \dot{m}_{out} - \dot{m}_{in}$$

$$= A_{CS} [\dot{\rho}_1\, L_{total}] + \dot{m}_{out} - \dot{m}_{in}$$

$$= A_{CS} L_{total} \left(\left. \frac{d\rho_1}{dP} \right|_P \dot{P} + \left. \frac{d\rho_1}{dh} \right|_P \dot{h} \right) + \dot{m}_{out} - \dot{m}_{in}$$

Organizing Equation A-3, conservation of mass for the refrigerant in the heat exchanger has the form as,

$$A_{CS} L_{total} \left(\left. \frac{d\rho_1}{dP} \right|_P \dot{P} + \left. \frac{d\rho_1}{dh} \right|_P \dot{h} \right) = \dot{m}_{in} - \dot{m}_{out} \quad \textbf{A-6}$$

Integrating Equation A-2 part by part along the tube length,

$$\int_0^{L_1} \frac{\partial(\rho A_{CS} h)}{\partial t} dz \quad \textbf{A-7}$$

$$= A_{CS} \int_0^{L_1} \frac{\partial(\rho h)}{\partial t} dz$$

$$= A_{CS} \left[\frac{d}{dt} \int_0^{L_1} (\rho h) dz \right]$$

$$= A_{CS} \left[\frac{d}{dt} (\rho_1 h_1 L_1) \right]$$

$$= \frac{d(\rho_1 h_1)}{dt} A_{CS} L_{total}$$

$$= \frac{d\left(\rho_f h_f (1-\bar{\gamma}) + \rho_g h_g \bar{\gamma}\right)}{dt} A_{CS} L_{total}$$

$$\int_0^{L_1} \frac{\partial (A_{CS} P)}{\partial t} dz \qquad \textbf{A-8}$$

$$= A_{CS} \int_0^{L_1} \frac{\partial (P)}{\partial t} dz$$

$$= A_{CS} \left[\frac{d}{dt}(P L_{total})\right]$$

$$= A_{CS} L_{total} \dot{P}$$

$$\int_0^{L_1} \frac{\partial (\dot{m} h)}{\partial z} dz \qquad \textbf{A-9}$$

$$= \dot{m}_{out} h_{out} - \dot{m}_{in} h_{in}$$

$$\int_0^{L_1} p_i \alpha_i (T_w - T_r) dz \qquad \textbf{A-10}$$

$$= p_i \alpha_i (T_{w_1} - T_{r_1})$$

$$= \alpha_{i_1} A_i \frac{L_1}{L_{total}} \left(T_{w_1} - T_{r_1}\right)$$

$$= \alpha_{i_1} A_i \left(T_{w_1} - T_{r_1}\right)$$

Combining Equation A-7, A-8, A-9 and A-10, conservation of energy for the refrigerant in the two-phase only heat exchanger is represented as,

$$\left(\left(\frac{d\rho_1}{dP}\bigg|_h\right) h - 1\right) \dot{P} + \left[\left(h \left(\frac{d\rho_1}{dh}\bigg|_P\right) + \rho_1\right) \dot{h}\right] A_{CS} L_{total} \qquad \textbf{A-11}$$

$$= \dot{m}_{in} h_{in} - \dot{m}_{out} h_{out} + \alpha_{i_1} A_i \left(T_{w_1} - T_{r_1}\right)$$

Conservation of energy for the heat exchanger wall temperature is represented as,

$$(C_P \rho A)_W \left(\dot{T}_{w_1}\right) = \alpha_{i_1} A_i \left(T_{w_1} - T_{r_1}\right) + \alpha_o A_o \left(T_a - T_{w_1}\right) \qquad \textbf{A-12}$$

Evaporator with Two-phase Fluid and Superheated Vapor

When both two-phase fluid and superheated vapor are present in the evaporator, the two-phase region fluid properties can be presented as,

$$\rho_1 = \rho_f(1-\bar{\gamma}) + \rho_g(\bar{\gamma}) \quad \textbf{A-13}$$

$$\rho_1 h_1 = \rho_f h_f(1-\bar{\gamma}) + \rho_g h_g(\bar{\gamma}) \quad \textbf{A-14}$$

Superheated vapor region fluid properties can be presented as,

$$h_2 = \frac{h_{out} + h_g}{2}, \;\; T_{r_2} = T(P, h_2), \;\; \rho_2 = \rho(P, h_2) \quad \textbf{A-15}$$

The interface refrigerant mass flow rate between the two-phase fluid region and superheated vapor region is defined as $\dot{m}_{int}$. Integrating Equation A-1 along the tube length in the two-phase region, the conservation of refrigerant mass in two-phase region as be calculated as,

$$\int_0^{L_1} \left[\frac{\partial(\rho A_{CS})}{\partial t} + \frac{\partial(\dot{m})}{\partial z}\right] dz \quad \textbf{A-16}$$

$$= \int_0^{L_1} \frac{\partial(\rho A_{CS})}{\partial t} dz + \int_0^{L_1} \frac{\partial(\dot{m})}{\partial z} dz$$

$$= A_{CS}\left[\int_0^{L_1} \frac{\partial \rho}{\partial t} dz\right] + \dot{m}_{int} - \dot{m}_{in}$$

$$= A_{CS}\left[\frac{d}{dt}\int_0^{L_1} (\rho)\, dz\right] + \dot{m}_{int} - \dot{m}_{in}$$

$$= A_{CS}\left[\frac{d}{dt}(\rho_1 L_1)\right] + \dot{m}_{int} - \dot{m}_{in}$$

$$= A_{CS}\left[\frac{d}{dt}\left(\rho_f(1-\bar{\gamma})+\rho_g(\bar{\gamma})\right)L_1+\left(\rho_f(1-\bar{\gamma})+\rho_g(\bar{\gamma})\right)\dot{L}_1 - \rho_g\dot{L}_1\right]+\dot{m}_{int}-\dot{m}_{in}$$

$$= A_{CS}\left[\left(\dot{\rho}_f(1-\bar{\gamma})+\dot{\rho}_g(\bar{\gamma})+\dot{\bar{\gamma}}(\rho_f-\rho_g)\right)L_1 + \left(\rho_f(1-\bar{\gamma})+\rho_g(\bar{\gamma})\right)\dot{L}_1-\rho_g\dot{L}_1\right]+\dot{m}_{int} - \dot{m}_{in}$$

$$= A_{CS}\left[\left[\frac{d\rho_f}{dP}(1-\bar{\gamma})+\frac{d\rho_g}{dP}(\bar{\gamma})+\frac{d\bar{\gamma}}{dP}(\rho_g-\rho_f)\right]L_1\dot{P} + \left(\rho_f(1-\bar{\gamma})+\rho_g(\bar{\gamma})\right)\dot{L}_1-\rho_g\dot{L}_1\right]+\dot{m}_{int} - \dot{m}_{in}$$

$$= A_{CS}(1-\bar{\gamma})(\rho_g-\rho_f)\dot{L}_1 + \left[\frac{d\rho_f}{dP}(1-\bar{\gamma})+\frac{d\rho_g}{dP}(\bar{\gamma}) + \frac{d\bar{\gamma}}{dP}(\rho_g-\rho_f)\right]A_{CS}L_1\dot{P}+\dot{m}_{int}-\dot{m}_{in}$$

The final conservation of refrigerant mass in the two-phase can be presented as,

$$A_{CS}(1-\bar{\gamma})(\rho_g-\rho_f)\dot{L}_1+\left[\frac{d\rho_f}{dP}(1-\bar{\gamma})+\frac{d\rho_g}{dP}(\bar{\gamma})+\frac{d\bar{\gamma}}{dP}(\rho_g-\rho_f)\right]A_{CS}L_1\dot{P} = \dot{m}_{in}-\dot{m}_{int} \quad \textbf{A-17}$$

Integrating Equation (1) along the tube length in the superheated vapor region, the conservation of refrigerant mass for superheated vapor region as be calculated as,

$$\int_{L_1}^{L_{total}}\left[\frac{\partial(\rho A_{CS})}{\partial t}+\frac{\partial(\dot{m})}{\partial z}\right]dz \quad \textbf{A-18}$$

$$= \int_{L_1}^{L_{total}} \frac{\partial(\rho A_{CS})}{\partial t} dz + \int_{L_1}^{L_{total}} \frac{\partial(\dot{m})}{\partial z} dz$$

$$= A_{CS}\left[\int_{L_1}^{L_{total}} \frac{\partial \rho}{\partial t} dz\right] + \dot{m}_{out} - \dot{m}_{int}$$

$$= A_{CS}\left[\frac{d}{dt}\int_{L_1}^{L_{total}} (\rho)\, dz\right] + \dot{m}_{out} - \dot{m}_{int}$$

$$= A_{CS}\left[\frac{d}{dt}(\rho_2 L_2)\right] + \dot{m}_{out} - \dot{m}_{int}$$

$$= A_{CS}\left[\dot{\rho}_2 L_2 + \rho_2 \dot{L}_2 + \rho_g \dot{L}_1\right] + \dot{m}_{out} - \dot{m}_{int}$$

$$= A_{CS}\left[\dot{\rho}_2 L_2 - \rho_2 \dot{L}_1 + \rho_g \dot{L}_1\right] + \dot{m}_{out} - \dot{m}_{int}$$

$$= A_{CS}\left[\left[\left(\frac{d\rho_2}{dP}\Big|_{h_2}\right)\dot{P} + \left(\frac{d\dot{\rho_2}}{dh_2}\Big|_{P}\right)\dot{h}_2\right] L_2 + (\rho_g - \rho_2)\dot{L}_1\right] + \dot{m}_{out} - \dot{m}_{int}$$

$$= A_{CS}\left[\left[\left(\frac{d\rho_2}{dP}\Big|_{h_2}\right)\dot{P} + \left(\frac{d\rho_2}{dh_2}\Big|_{P}\right)\left(\frac{\dot{h}_{out} + \dot{h}_g}{2}\right)\right] L_2 + (\rho_g - \rho_2)\dot{L}_1\right] + \dot{m}_{out} - \dot{m}_{int}$$

$$= A_{CS}\left[\left[\left(\frac{d\rho_2}{dP}\Big|_{h_2}\right)\dot{P} + \frac{1}{2}\left(\frac{d\rho_2}{dh_2}\Big|_{P}\right)\dot{h}_{out} + \frac{1}{2}\left(\frac{d\rho_2}{dh_2}\Big|_{P}\right)\frac{dh_g}{dP}\dot{P}\right] L_2 + (\rho_g - \rho_2)\dot{L}_1\right] + \dot{m}_{out} - \dot{m}_{int}$$

$$= \left(\frac{d\rho_2}{dP}\Big|_{h_2} + \frac{1}{2}\left(\frac{d\rho_2}{dh_2}\Big|_{P}\right)\frac{dh_g}{dP}\right) A_{CS} L_2 \dot{P} + \frac{1}{2}\left(\frac{d\rho_2}{dh_2}\Big|_{P}\right) A_{CS} L_2 \dot{h}_{out} + (\rho_g - \rho_2) A_{CS} \dot{L}_1 + \dot{m}_{out} - \dot{m}_{int}$$

Based on Equation A-18, the conservation of refrigerant mass for superheated vapor region as be presented as,

$$\left[\left(\frac{\partial \rho_2}{\partial P}\Big|_{h_2}\right)+\frac{1}{2}\left(\frac{\partial \rho_2}{\partial h_2}\Big|_{P}\right)\frac{dh_g}{dP}\right]A_{CS}L_2\dot{P}+\frac{1}{2}\left(\frac{\partial \rho_2}{\partial h_2}\Big|_{P}\right)A_{CS}L_2\dot{h}_{out}+A_{CS}(\rho_g-\rho_2)\dot{L}_1 \quad \textbf{A-19}$$

$$=\dot{m}_{int}-\dot{m}_{out}$$

Adding Equation A-17 and A-19 together,

$$\left[\frac{d\rho_f}{\partial P}(1-\bar{\gamma}\,)+\frac{d\rho_g}{\partial P}(\bar{\gamma}\,)+\frac{d\bar{\gamma}}{\partial P}(\rho_g-\rho_f)\right]A_{CS}L_1\dot{P} \quad \textbf{A-20}$$

$$+\left[\left(\frac{\partial \rho_2}{\partial P}\Big|_{h_2}\right)+\frac{1}{2}\left(\frac{\partial \rho_2}{\partial h_2}\Big|_{P}\right)\frac{dh_g}{dP}\right]A_{CS}L_2\dot{P}+A_{CS}(1-\bar{\gamma}\,)(\rho_f-\rho_g)\dot{L}_1$$

$$+\frac{1}{2}\left(\frac{\partial \rho_2}{\partial h_2}\Big|_{P}\right)A_{CS}L_2\dot{h}_{out}+A_{CS}(\rho_g-\rho_2)\dot{L}_1=\dot{m}_{in}-\dot{m}_{out}$$

Rearranging Equation A-19, $\dot{m}_{int}$ can be presented as,

$$\dot{m}_{int}=\left[\left(\frac{\partial \rho_2}{\partial P}\Big|_{h_2}\right)+\frac{1}{2}\left(\frac{\partial \rho_2}{\partial h_2}\Big|_{P}\right)\frac{dh_g}{dP}\right]A_{CS}L_2\dot{P}+\frac{1}{2}\left(\frac{\partial \rho_2}{\partial h_2}\Big|_{P}\right)A_{CS}L_2\dot{h}_{out} \quad \textbf{A-21}$$

$$+A_{CS}(\rho_g-\rho_2)\dot{L}_1+\dot{m}_{out}$$

The conservation of refrigerant energy for two-phase region is calculated as,

$$\int_0^{L_1}\frac{\partial(\rho A_{CS}h)}{\partial t}dz \quad \textbf{A-22}$$

$$=A_{CS}\int_0^{L_1}\frac{\partial(\rho h)}{\partial t}dz$$

$$=A_{CS}\left[\frac{d}{dt}\int_0^{L_1}(\rho h)dz-\rho_g h_g\dot{L}_1\right]$$

$$=A_{CS}\left[\frac{d}{dt}\Big(\rho_f h_f(1-\bar{\gamma}\,)+\rho_g h_g(\bar{\gamma}\,)\Big)L_1-\rho_g h_g\dot{L}_1\right]$$

$$= \left(\frac{d(\rho_f h_f)}{dP}(1-\bar{\gamma}) + \frac{d(\rho_g h_g)}{dP}(\bar{\gamma}) + (\rho_g h_g - \rho_f h_f)\frac{d\bar{\gamma}}{dP} \right) A_{CS} L_1 \dot{P} + (1-\bar{\gamma})(\rho_f h_f - \rho_g h_g) A_{CS} \dot{L}_1$$

$$\int_0^{L_1} \frac{\partial (A_{CS} P)}{\partial t} dz \qquad \textbf{A-23}$$

$$= A_{CS} \int_0^{L_1} \frac{\partial (P)}{\partial t} dz$$

$$= A_{CS} \left[\frac{d}{dt}(P L_1) - P \dot{L}_1 \right]$$

$$= A_{CS} \dot{P} L_1$$

$$\int_0^{L_1} \frac{\partial (\dot{m} h)}{\partial z} dz \qquad \textbf{A-24}$$

$$= \dot{m}_{int} h_g - \dot{m}_{int} h_{in}$$

$$\int_0^{L_1} p_i \alpha_i (T_w - T_r) dz \qquad \textbf{A-25}$$

$$= p_i \alpha_i L_1 (T_{w_1} - T_{r_1})$$

$$= \alpha_{i_1} A_i \frac{L_1}{L_{total}} \left(T_{w_1} - T_{r_1} \right)$$

Combining Equation A-22, A-23, A-24 and A-25, conservation of refrigerant energy in the two-phase fluid region can be presented as,

$$\left(\frac{d(\rho_f h_f)}{dP}(1-\bar{\gamma}) + \frac{d(\rho_g h_g)}{dP}(\bar{\gamma}) + (\rho_g h_g - \rho_f h_f)\frac{d\bar{\gamma}}{dP} - 1\right) A_{CS} L_1 \dot{P} \quad \textbf{A-26}$$

$$+ (1-\bar{\gamma})(\rho_f h_f - \rho_g h_g) A_{CS} \dot{L}_1$$

$$= \dot{m}_{in} h_{in} - \dot{m}_{int} h_g + \alpha_{i_1} A_i \frac{L_1}{L_{total}} (T_{w_1} - T_{r_1})$$

Substituting Equation A-21 in to Equation A-26, conservation of refrigerant energy in the two-phase fluid region can be presented as,

$$\left(\frac{d(\rho_f h_f)}{dP}(1-\bar{\gamma}) + \frac{d(\rho_g h_g)}{dP}(\bar{\gamma}) + (\rho_g h_g - \rho_f h_f)\frac{d\bar{\gamma}}{dP} - 1\right) A_{CS} L_1 \dot{P} \quad \textbf{A-27}$$

$$+ h_g \left[\left(\frac{\partial \rho_2}{\partial P}\Big|_{h_2}\right) + \frac{1}{2}\left(\frac{\partial \rho_2}{\partial h_2}\Big|_{P}\right)\frac{dh_g}{dP}\right] A_{CS} L_2 \dot{P}$$

$$+ (1-\bar{\gamma})(\rho_f h_f - \rho_g h_g) A_{CS} \dot{L}_1 + A_{CS} h_g (\rho_g - \rho_2) \dot{L}_1$$

$$+ \frac{1}{2} h_g \left(\frac{\partial \rho_2}{\partial h_2}\Big|_{P}\right) A_{CS} L_2 \dot{h}_{out}$$

$$= \dot{m}_{in} h_{in} - \dot{m}_{out} h_g + \alpha_{i_1} A_i \frac{L_1}{L_{total}} (T_{w_1} - T_{r_1})$$

The conservation of refrigerant energy for superheated vapor region is calculated as,

$$\int_{L_1}^{L_{total}} \frac{\partial(\rho A_{CS} h)}{\partial t} dz \quad \textbf{A-28}$$

$$= A_{CS} \int_{L_1}^{L_{total}} \frac{\partial(\rho h)}{\partial t} dz$$

$$= A_{CS} \left[\frac{d}{dt}\int_{L_1}^{L_{total}} (\rho h) dz + \rho_g h_g \dot{L}_1\right]$$

$$= A_{CS} \left[\frac{d}{dt}(\rho_2 h_2 L_2) + \rho_g h_g \dot{L}_1\right]$$

$$= A_{CS}\left[\rho_2 h_2 \dot{L}_2 + \left(\dot{\rho}_2 h_2 + \rho_2 \dot{h}_2\right) L_2 + \rho_g h_g \dot{L}_1\right]$$

$$= A_{CS}\left[\left(\rho_g h_g - \rho_2 h_2\right)\dot{L}_1 + \left[\left(\frac{\partial \rho_2}{\partial P}\Big|_{h_2}\right)\dot{P} + \left(\frac{\partial \rho_2}{\partial h_2}\Big|_{P}\right)\dot{h}_2\right] h_2 L_2 + \rho_2 \dot{h}_2 L_2\right]$$

$$= A_{CS}\left[\left(\rho_g h_g - \rho_2 h_2\right)\dot{L}_1 + \left[\left(\frac{\partial \rho_2}{\partial P}\Big|_{h_2}\right)\dot{P} + \left(\frac{\partial \rho_2}{\partial h_2}\Big|_{P}\right)\left(\frac{\dot{h}_{out} + \dot{h}_g}{2}\right)\right]\left(\frac{h_{out} + h_g}{2}\right) L_2 + \rho_2\left(\frac{\dot{h}_{out} + \dot{h}_g}{2}\right) L_2\right]$$

$$= A_{CS}\left[\left(\rho_g h_g - \rho_2 h_2\right)\dot{L}_1 + \left[\left(\frac{\partial \rho_2}{\partial P}\Big|_{h_2}\right)\dot{P} + \left(\frac{\partial \rho_2}{\partial h_2}\Big|_{P}\right)\left(\frac{\dot{h}_{out}}{2} + \frac{1}{2}\frac{d\dot{h}_g}{dP}\dot{P}\right)\right]\left(\frac{h_{out} + h_g}{2}\right) L_2 + \rho_2\left(\frac{\dot{h}_{out}}{2} + \frac{1}{2}\frac{d\dot{h}_g}{dP}\dot{P}\right) L_2\right]$$

$$= A_{CS}(\rho_g h_g - \rho_2 h_2)\dot{L}_1 + \left[\left[\left(\frac{\partial \rho_2}{\partial P}\Big|_{h_2}\right) + \frac{1}{2}\left(\frac{\partial \rho_2}{\partial h_2}\Big|_{P}\right)\frac{dh_g}{dP}\right]h_2 + \frac{1}{2}\frac{dh_g}{dP}\rho_2\right]A_{CS}L_2\dot{P} + \frac{1}{2}\left[\left(\frac{\partial \rho_2}{\partial h_2}\Big|_{P}\right)h_2 + \rho_2\right]A_{CS}L_2\dot{h}_{out}$$

$$\int_{L_1}^{L_{total}} \frac{\partial (A_{CS}P)}{\partial t}\,dz \qquad \textbf{A-29}$$

$$= A_{CS}\int_{L_1}^{L_{total}} \frac{\partial (P)}{\partial t}\,dz$$

$$= A_{CS}\left[\frac{d}{dt}(PL_2) + P\dot{L}_1\right]$$

$$= A_{CS}\left[\dot{P}L_2 + P\dot{L}_2 + P\dot{L}_1\right]$$

$$= A_{CS}\left[\dot{P}L_2 - P\dot{L}_1 + P\dot{L}_1\right]$$

$$= A_{CS}L_2\dot{P}$$

$$\int_{L_1}^{L_{total}} \frac{\partial (\dot{m}h)}{\partial z}\,dz \qquad \textbf{A-30}$$

$$= \dot{m}_{out}h_{out} - \dot{m}_{int}h_g$$

$$\int_{L_1}^{L_{total}} p_i \alpha_{i_2}(T_{w_2} - T_{r_2})dz \qquad \textbf{A-31}$$

$$= p_i \alpha_{i_2} L_{total}\frac{L_2}{L_{total}}(T_{w_2} - T_{r_2})$$

$$= \alpha_{i_2} A_i \frac{L_2}{L_{total}}\left(T_{w_2} - T_{r_2}\right)$$

Combining Equation A-28, A-29, A-30 and A-31, conservation of refrigerant energy in the superheated vapor region can be presented as,

$$A_{CS}(\rho_g h_g - \rho_2 h_2)\dot{L}_1 + \left[\left[\left(\frac{\partial \rho_2}{\partial P}\Big|_{h_2}\right) + \frac{1}{2}\left(\frac{\partial \rho_2}{\partial h_2}\Big|_{P}\right)\frac{dh_g}{dP}\right]h_2 + \frac{1}{2}\frac{dh_g}{dP}\rho_2 - 1\right]A_{CS}L_2\dot{P}$$

$$+ \frac{1}{2}\left[\left(\frac{\partial \rho_2}{\partial h_2}\Big|_{P}\right)h_2 + \rho_2\right]A_{CS}L_2\dot{h}_{out} \qquad \textbf{A-32}$$

$$= \dot{m}_{int}h_g - \dot{m}_{out}h_{out} + \alpha_{i_2}A_i\frac{L_2}{L_{total}}(T_{w_2} - T_{r_2})$$

Substituting Equation A-21 into Equation A-32, conservation of refrigerant energy in the superheated vapor region can be presented as,

$$\left[\left[\left(\frac{\partial \rho_2}{\partial P}\Big|_{h_2}\right) + \frac{1}{2}\left(\frac{\partial \rho_2}{\partial h_2}\Big|_{P}\right)\frac{dh_g}{dP}\right]h_2 + \frac{1}{2}\frac{dh_g}{dP}\rho_2 - 1\right]A_{CS}L_2\dot{P}$$

$$- h_g\left[\left(\frac{\partial \rho_2}{\partial P}\Big|_{h_2}\right) + \frac{1}{2}\left(\frac{\partial \rho_2}{\partial h_2}\Big|_{P}\right)\frac{dh_g}{dP}\right]A_{CS}L_2\dot{P} + A_{CS}(\rho_g h_g - \rho_2 h_2)\dot{L}_1$$

$$- A_{CS}h_g(\rho_g - \rho_2)\dot{L}_1 + \frac{1}{2}\left[\left(\frac{\partial \rho_2}{\partial h_2}\Big|_{P}\right)h_2 + \rho_2\right]A_{CS}L_2\dot{h}_{out} \qquad \textbf{A-33}$$

$$- \frac{1}{2}h_g\left(\frac{\partial \rho_2}{\partial h_2}\Big|_{P}\right)A_{CS}L_2\dot{h}_{out}$$

$$= \dot{m}_{out}h_g - \dot{m}_{out}h_{out} + \alpha_{i_2}A_i\frac{L_2}{L_{total}}(T_{w_2} - T_{r_2})$$

Integrated conservation of refrigerant wall energy along the tube length in the two-phase fluid region, Equation A-3 can be presented as,

$$(C_P\rho A)_W\left(\dot{T}_{w_1} + \frac{T_{w_1} - T_{int}}{L_1}\dot{L}_1\right) = \alpha_{i_1}A_i(T_{w_1} - T_{r_1}) + \alpha_o A_o(T_a - T_{w_1}) \qquad \textbf{A-34}$$

Integrated conservation of refrigerant wall energy along the tube length in the superheated vapor region, Equation (3) can be presented as,

$$(C_P \rho A)_W \left(\dot{T}_{w_2} - \frac{T_{w_2} - T_{int}}{L_2} \dot{L}_2 \right) = \alpha_{i_2} A_i \left(T_{w_2} - T_{r_2} \right) + \alpha_o A_o \left(T_a - T_{w_2} \right) \quad \textbf{A-35}$$

Switch Moving Boundary Condenser Model Derivation

Condenser with Superheated Vapor, Two-phase Fluid and Subcooled Liquid

When all superheated vapor, two-phase fluid and subcooled liquid are present in the evaporator, the superheated vapor region fluid properties can be presented as,

$$h_1 = \frac{h_{in} + h_g}{2}, \;\; T_{r_1} = T(P, h_1), \;\; \rho_1 = \rho(P, h_1) \quad \textbf{A-36}$$

Two-phase fluid refrigerant properties can be expressed as,

$$\rho_2 = \rho_f (1 - \bar{\gamma}) + \rho_g (\bar{\gamma}) \quad \textbf{A-37}$$

$$\rho_2 h_2 = \rho_f h_f (1 - \bar{\gamma}) + \rho_g h_g (\bar{\gamma}) \quad \textbf{A-38}$$

Subcooled liquid region fluid properties can be presented as,

$$h_3 = \frac{h_{out} + h_f}{2}, \;\; T_{r_3} = T(P, h_3), \;\; \rho_3 = \rho(P, h_3) \quad \textbf{A-39}$$

The interface refrigerant mass flow rate between superheated vapor region and two-phase fluid region is defined as $\dot{m}_{int_1}$. While the interface refrigerant mass flow rate is defined as $\dot{m}_{int_2}$. Integrating Equation A-1 along the tube length in the superheated vapor region, the conservation of refrigerant mass for superheated vapor region as be calculated as,

$$\int_0^{L_1} \left[\frac{\partial (\rho A_{CS})}{\partial t} + \frac{\partial (\dot{m})}{\partial z} \right] dz \quad \textbf{A-40}$$

$$= \int_0^{L_1} \frac{\partial(\rho A_{CS})}{\partial t} dz + \int_0^{L_1} \frac{\partial(\dot{m})}{\partial z} dz$$

$$= A_{CS}\left[\int_0^{L_1} \frac{\partial \rho}{\partial t} dz\right] + \dot{m}_{int_1} - \dot{m}_{in}$$

$$= A_{CS}\left[\frac{d}{dt}\int_0^{L_1} (\rho)\, dz\right] + \dot{m}_{int_1} - \dot{m}_{in}$$

$$= A_{CS}\left[\frac{d}{dt}(\rho_1 L_1) - \rho_g \dot{L}_1\right] + \dot{m}_{int_1} - \dot{m}_{in}$$

$$= A_{CS}\left[\dot{\rho}_1 L_1 + \rho_1 \dot{L}_1 - \rho_g \dot{L}_1\right] + \dot{m}_{int_1} - \dot{m}_{in}$$

$$= A_{CS}\left[\left[\left(\frac{d\rho_1}{dP}\Big|_{h_1}\right)\dot{P} + \left(\frac{d\rho_1}{dh_1}\Big|_{P}\right)\dot{h}_1\right] L_1 + \rho_1 \dot{L}_1 - \rho_g \dot{L}_1\right] + \dot{m}_{int_1} - \dot{m}_{in}$$

$$= A_{CS}\left[\left[\left(\frac{d\rho_1}{dP}\Big|_{h_1}\right)\dot{P} + \left(\frac{d\rho_1}{dh_1}\Big|_{P}\right)\frac{\dot{h}_{in} + \dot{h}_g}{2}\right] L_1 + \rho_1 \dot{L}_1 - \rho_g \dot{L}_1\right] + \dot{m}_{int_1} - \dot{m}_{in}$$

$$= A_{CS}\left[\left[\left(\frac{d\rho_1}{dP}\Big|_{h_1}\right)\dot{P} + \frac{1}{2}\left(\frac{d\rho_1}{dh_1}\Big|_{P}\right)\dot{h}_{in} + \frac{1}{2}\left(\frac{d\rho_1}{dh_1}\Big|_{P}\right)\frac{dh_g}{dP}\dot{P}\right] L_1 + \rho_1 \dot{L}_1 - \rho_g \dot{L}_1\right] + \dot{m}_{int_1} - \dot{m}_{in}$$

$$= \left[\left(\frac{d\rho_1}{dP}\Big|_{h_1}\right) + \frac{1}{2}\left(\frac{d\rho_1}{dh_1}\Big|_{P}\right)\frac{dh_g}{dP}\right] A_{CS} L_1 \dot{P} + \frac{1}{2}\left(\frac{d\rho_1}{dh_1}\Big|_{P}\right) A_{CS} L_1 \dot{h}_{in} + (\rho_1 - \rho_g) A_{CS} \dot{L}_1$$

Based on Equation A-40, the conservation of refrigerant mass for superheated vapor region as be presented as,

$$\left[\left(\left.\frac{d\rho_1}{dP}\right|_{h_1}\right)+\frac{1}{2}\left(\left.\frac{d\rho_1}{dh_1}\right|_{P}\right)\frac{dh_g}{dP}\right]A_{CS}L_1\dot{P}+\frac{1}{2}\left(\left.\frac{d\rho_1}{dh_1}\right|_{P}\right)A_{CS}L_1\dot{h}_{in}+(\rho_1-\rho_g)A_{CS}\dot{L}_1 \quad \textbf{A-41}$$

$$=\dot{m}_{int_1}-\dot{m}_{in}$$

Integrating Equation A-1 along the tube length in the two-phase fluid region, the conservation of refrigerant mass for the two-phase fluid region as be calculated as,

$$\int_{L_1}^{L_1+L_2}\left[\frac{\partial(\rho A_{CS})}{\partial t}+\frac{\partial(\dot{m})}{\partial z}\right]dz \quad \textbf{A-42}$$

$$=\int_{L_1}^{L_1+L_2}\frac{\partial(\rho A_{CS})}{\partial t}dz+\int_{L_1}^{L_1+L_2}\frac{\partial(\dot{m})}{\partial z}dz$$

$$=A_{CS}\left[\int_{L_1}^{L_1+L_2}\frac{\partial\rho}{\partial t}dz\right]+\dot{m}_{int_2}-\dot{m}_{int_1}$$

$$=A_{CS}\left[\frac{d}{dt}\int_{L_1}^{L_1+L_2}(\rho)\,dz\right]+\dot{m}_{int_2}-\dot{m}_{int_1}$$

$$=A_{CS}\left[\frac{d}{dt}\int_{L_1}^{L_1+L_2}\left(\rho_f(1-\bar{\gamma})+\rho_g(\bar{\gamma})\right)dz+(\rho_g-\rho_f)\dot{L}_1-\rho_f\dot{L}_2\right]+\dot{m}_{int_2}-\dot{m}_{int_1}$$

$$=A_{CS}\left[\frac{d}{dt}\left(\left(\rho_f(1-\bar{\gamma})+\rho_g(\bar{\gamma})\right)L_2\right)+(\rho_g-\rho_f)\dot{L}_1-\rho_f\dot{L}_2\right]+\dot{m}_{int_2}-\dot{m}_{int_1}$$

$$=A_{CS}\left[\left(\rho_f(1-\bar{\gamma})+\rho_g(\bar{\gamma})\right)\dot{L}_2+\left(\dot{\rho}_f(1-\bar{\gamma})+\rho_f(1-\dot{\bar{\gamma}})+\dot{\rho}_g(\bar{\gamma})+\rho_g(\dot{\bar{\gamma}})\right)L_2+(\rho_g-\rho_f)\dot{L}_1-\rho_f\dot{L}_2\right]+\dot{m}_{int_2}-\dot{m}_{int_1}$$

$$= A_{CS}\Big[(\rho_g - \rho_f)\dot{L}_1 + (\rho_g - \rho_f)\bar{\gamma}\dot{L}_2 + \Big(\dot{\rho}_f(1-\bar{\gamma}) + \dot{\rho}_g(\bar{\gamma}) + (\rho_g - \rho_f)(\dot{\bar{\gamma}})\Big)L_2\Big] + \dot{m}_{int_2} - \dot{m}_{int_1}$$

$$= A_{CS}(\rho_g - \rho_f)\dot{L}_1 + A_{CS}(\rho_g - \rho_f)\bar{\gamma}\dot{L}_2 + \Big[\frac{d\rho_f}{\partial P}(1-\bar{\gamma}) + \frac{d\rho_g}{\partial P}(\bar{\gamma}) + \frac{d\bar{\gamma}}{\partial P}(\rho_g - \rho_f)\Big]A_{CS}L_2 + \dot{m}_{int_2} - \dot{m}_{int_1}$$

Based on Equation A-42, the conservation of refrigerant mass for superheated vapor region as be presented as,

$$A_{CS}(\rho_g - \rho_f)\dot{L}_1 + A_{CS}(\rho_g - \rho_f)\bar{\gamma}\dot{L}_2 \quad \textbf{A-43}$$
$$+\Big[\frac{d\rho_f}{\partial P}(1-\bar{\gamma}) + \frac{d\rho_g}{\partial P}(\bar{\gamma}) + \frac{d\bar{\gamma}}{\partial P}(\rho_g - \rho_f)\Big]A_{CS}L_2 = \dot{m}_{int_1} - \dot{m}_{int_2}$$

Integrating Equation (1) along the tube length in the subcooled liquid region, the conservation of refrigerant mass for subcooled liquid region as be calculated as,

$$\int_{L_1+L_2}^{L_{total}}\Big[\frac{\partial(\rho A_{CS})}{\partial t} + \frac{\partial(\dot{m})}{\partial z}\Big]dz \quad \textbf{A-44}$$

$$= \int_{L_1+L_2}^{L_{total}}\frac{\partial(\rho A_{CS})}{\partial t}dz + \int_{L_1+L_2}^{L_{total}}\frac{\partial(\dot{m})}{\partial z}dz$$

$$= A_{CS}\Big[\int_{L_1+L_2}^{L_{total}}\frac{\partial\rho}{\partial t}dz\Big] + \dot{m}_{out} - \dot{m}_{int_2}$$

$$= A_{CS}\left[\frac{d}{dt}\int_{L_1+L_2}^{L_{total}}(\rho)\,dz\right] + \dot{m}_{out} - \dot{m}_{int_2}$$

$$= A_{CS}\left[\frac{d}{dt}(\rho_3 L_3)\right] + \dot{m}_{out} - \dot{m}_{int_2}$$

$$= A_{CS}\left[\dot{\rho}_3 L_3 + \rho_3 \dot{L}_3 + \rho_f\left(\dot{L}_1 + \dot{L}_2\right)\right] + \dot{m}_{out} - \dot{m}_{int_2}$$

$$= A_{CS}\left[\dot{\rho}_3 L_3 - \rho_3\left(\dot{L}_1 + \dot{L}_2\right) + \rho_f\left(\dot{L}_1 + \dot{L}_2\right)\right] + \dot{m}_{out} - \dot{m}_{int_2}$$

$$= A_{CS}\left[\left[\left(\frac{d\rho_3}{dP}\Big|_{h_3}\right)\dot{P} + \left(\frac{d\rho_3}{dh_3}\Big|_{P}\right)\dot{h}_3\right]L_3 + \left(\rho_f - \rho_3\right)\left(\dot{L}_1 + \dot{L}_2\right)\right]$$
$$+ \dot{m}_{out} - \dot{m}_{int_2}$$

$$= A_{CS}\left[\left[\left(\frac{d\rho_3}{dP}\Big|_{h_3}\right)\dot{P} + \left(\frac{d\rho_3}{dh_3}\Big|_{P}\right)\left(\frac{\dot{h}_{out} + \dot{h}_f}{2}\right)\right]L_3\right.$$
$$\left. + \left(\rho_f - \rho_3\right)\left(\dot{L}_1 + \dot{L}_2\right)\right] + \dot{m}_{out} - \dot{m}_{int_2}$$

$$= A_{CS}\left[\left[\left(\frac{d\rho_3}{dP}\Big|_{h_3}\right)\dot{P} + \frac{1}{2}\left(\frac{d\rho_3}{dh_3}\Big|_{P}\right)\dot{h}_{out} + \frac{1}{2}\left(\frac{d\rho_3}{dh_3}\Big|_{P}\right)\frac{dh_f}{dP}\dot{P}\right]L_3\right.$$
$$\left. + \left(\rho_f - \rho_3\right)\left(\dot{L}_1 + \dot{L}_2\right)\right] + \dot{m}_{out} - \dot{m}_{int_2}$$

$$= \left(\left(\frac{d\rho_3}{dP}\Big|_{h_3}\right) + \frac{1}{2}\left(\frac{d\rho_3}{dh_3}\Big|_{P}\right)\frac{dh_f}{dP}\right)A_{CS}L_3\dot{P} + \frac{1}{2}\left(\frac{d\rho_3}{dh_3}\Big|_{P}\right)A_{CS}L_3\dot{h}_{out}$$
$$+ A_{CS}\left(\rho_f - \rho_3\right)\left(\dot{L}_1 + \dot{L}_2\right) + \dot{m}_{out} - \dot{m}_{int_2}$$

Based on Equation A-44, the conservation of refrigerant mass for subcooled liquid region can be presented as,

$$\left(\left(\frac{d\rho_3}{dP}\Big|_{h_3}\right)+\frac{1}{2}\left(\frac{d\rho_3}{dh_3}\Big|_{P}\right)\frac{dh_f}{dP}\right)A_{CS}L_3\dot{P}+\frac{1}{2}\left(\frac{d\rho_3}{dh_3}\Big|_{P}\right)A_{CS}L_3\dot{h}_{out} \quad \textbf{A-45}$$

$$+A_{CS}(\rho_f-\rho_3)(\dot{L}_1+\dot{L}_2)=\dot{m}_{int_2}-\dot{m}_{out}$$

Adding Equation A-41, A-43 and A-45 together and reorganizing the equation, the conservation of refrigerant mass in the heat exchanger can be presented as,

$$\left[\left(\frac{d\rho_1}{dP}\Big|_{h_1}\right)+\frac{1}{2}\left(\frac{d\rho_1}{dh_1}\Big|_{P}\right)\frac{dh_g}{dP}\right]A_{CS}L_1\dot{P} \quad \textbf{A-46}$$

$$+\left[\frac{d\rho_f}{\partial P}(1-\bar{\gamma}\,)+\frac{d\rho_g}{\partial P}(\bar{\gamma}\,)+\frac{d\bar{\gamma}}{\partial P}(\rho_g-\rho_f)\right]A_{CS}L_2\dot{P}$$

$$+\left(\left(\frac{d\rho_3}{dP}\Big|_{h_3}\right)+\frac{1}{2}\left(\frac{d\rho_3}{dh_3}\Big|_{P}\right)\frac{dh_f}{dP}\right)A_{CS}L_3\dot{P}+(\rho_1-\rho_g)A_{CS}\dot{L}_1$$

$$+A_{CS}(\rho_g-\rho_f)\dot{L}_1+A_{CS}(\rho_f-\rho_3)\dot{L}_1+A_{CS}(\rho_g-\rho_f)\bar{\gamma}\dot{L}_2$$

$$+A_{CS}(\rho_f-\rho_3)\dot{L}_2+\frac{1}{2}\left(\frac{d\rho_3}{dh_3}\Big|_{P}\right)A_{CS}L_3\dot{h}_{out}$$

$$=\dot{m}_{in}-\dot{m}_{out}-\frac{1}{2}\left(\frac{d\rho_1}{dh_1}\Big|_{P}\right)A_{CS}L_1\dot{h}_{in}$$

The conservation of refrigerant energy for superheated vapor region is calculated as,

$$\int_0^{L_1}\frac{\partial(\rho A_{CS}h)}{\partial t}dz \quad \textbf{A-47}$$

$$= A_{CS}(\rho_1 h_1 - \rho_g h_g)\dot{L}_1 + \left[\left[\left(\frac{\partial \rho_1}{\partial P}\Big|_{h_1}\right) + \frac{1}{2}\left(\frac{\partial \rho_1}{\partial h_1}\Big|_{P}\right)\frac{dh_g}{dP}\right] + \frac{1}{2}\frac{dh_g}{dP}\rho_1\right] A_{CS} L_1 \dot{P} + \frac{1}{2}\left[\left(\frac{\partial \rho_1}{\partial h_1}\Big|_{P}\right) + \rho_1\right] A_{CS} L_1 \dot{h}_{in}$$

$$\int_0^{L_1} \frac{\partial (A_{CS} P)}{\partial t} dz \qquad \textbf{A-48}$$

$$= A_{CS} \int_0^{L_1} \frac{\partial (P)}{\partial t} dz$$

$$= A_{CS}\left[\frac{d}{dt}(PL_1) - P\dot{L}_1\right]$$

$$= A_{CS}\dot{P}L_1$$

$$\int_0^{L_1} \frac{\partial (\dot{m}h)}{\partial z} dz \qquad \textbf{A-49}$$

$$= \dot{m}_{int_1} h_g - \dot{m}_{in} h_{in}$$

$$\int_0^{L_1} p_i \alpha_i (T_w - T_r) dz \qquad \textbf{A-50}$$

$$= p_i \alpha_i L_1 (T_{w_1} - T_{r_1})$$

$$= \alpha_{i_1} A_i \frac{L_1}{L_{total}} \left(T_{w_1} - T_{r_1}\right)$$

Combining Equation A-47, A-48, A-49 and A-50, conservation of refrigerant energy in the two-phase fluid region can be presented as,

$$A_{CS}(\rho_1 h_1 - \rho_g h_g)\dot{L}_1 + \left[\left[\left(\frac{\partial \rho_1}{\partial P}\Big|_{h_1}\right) + \frac{1}{2}\left(\frac{\partial \rho_1}{\partial h_1}\Big|_{P}\right)\frac{dh_g}{dP}\right] + \frac{1}{2}\frac{dh_g}{dP}\rho_1 - 1\right]A_{CS}L_1\dot{P}$$

$$+ \frac{1}{2}\left[\left(\frac{\partial \rho_1}{\partial h_1}\Big|_{P}\right) + \rho_1\right]A_{CS}L_1\dot{h}_{in} \qquad \textbf{A-51}$$

$$= \dot{m}_{in}h_{in} - \dot{m}_{int_1}h_g + \alpha_{i_1}A_i\frac{L_1}{L_{total}}(T_{w_1} - T_{r_1})$$

Substituting Equation A-41 into Equation A-51, conservation of refrigerant energy in the two-phase fluid region can be presented as,

$$\left[\left[\left(\frac{\partial \rho_1}{\partial P}\Big|_{h_1}\right) + \frac{1}{2}\left(\frac{\partial \rho_1}{\partial h_1}\Big|_{P}\right)\frac{dh_g}{dP}\right] + \frac{1}{2}\frac{dh_g}{dP}\rho_1 - 1\right]A_{CS}L_1\dot{P}$$

$$- h_g\left[\left(\frac{\partial \rho_1}{\partial P}\Big|_{h_1}\right) + \frac{1}{2}\left(\frac{\partial \rho_1}{\partial h_1}\Big|_{P}\right)\frac{dh_g}{dP}\right]A_{CS}L_1\dot{P} + A_{CS}(\rho_1 h_1 - \rho_g h_g)\dot{L}_1$$

$$- h_g(\rho_1 - \rho_g)A_{CS}\dot{L}_1 \qquad \textbf{A-52}$$

$$= \dot{m}_{in}h_{in} - \dot{m}_{in}h_g + \alpha_{i_1}A_i\frac{L_1}{L_{total}}(T_{w_1} - T_{r_1})$$

$$- \frac{1}{2}\left[\left(\frac{\partial \rho_1}{\partial h_1}\Big|_{P}\right)h_1 + \rho_1\right]A_{CS}L_1\dot{h}_{in} + \frac{1}{2}h_g\left(\frac{\partial \rho_1}{\partial h_1}\Big|_{P}\right)A_{CS}L_1\dot{h}_{in}$$

The conservation of refrigerant energy for two-phase fluid region is calculated as,

$$\int_{L_1}^{L_1+L_2}\frac{\partial(\rho A_{CS}h)}{\partial t}dz \qquad \textbf{A-53}$$

$$= \left(\frac{d(\rho_f h_f)}{dP}(1-\bar{\gamma}) + \frac{d(\rho_g h_g)}{dP}(\bar{\gamma})\right.$$

$$\left. + (\rho_g h_g - \rho_f h_f)\frac{d\bar{\gamma}}{dP}\right)A_{CS}L_2\dot{P}$$

$$+ (\rho_g h_g - \rho_f h_f)A_{CS}\dot{L}_1 + \bar{\gamma}(\rho_g h_g - \rho_f h_f)A_{CS}\dot{L}_2$$

$$\int_{L_1}^{L_1+L_2} \frac{\partial(A_{CS}P)}{\partial t} dz \tag{A-54}$$

$$= A_{CS} \int_0^{L_1} \frac{\partial(P)}{\partial t} dz$$

$$= A_{CS} \left[\frac{d}{dt}(PL_2) - P\dot{L}_2 \right]$$

$$= A_{CS} \dot{P} L_2$$

$$\int_{L_1}^{L_1+L_2} \frac{\partial(\dot{m}h)}{\partial z} dz \tag{A-55}$$

$$= \dot{m}_{int_2} h_f - \dot{m}_{int_1} h_g$$

$$\int_{L_1}^{L_1+L_2} p_i \alpha_i (T_w - T_r) dz \tag{A-56}$$

$$= p_i \alpha_{i_2} L_2 (T_{w_2} - T_{r_2})$$

$$= \alpha_{i_2} A_i \frac{L_2}{L_{total}} \left(T_{w_2} - T_{r_2}\right)$$

Combining Equation A-53, A-54, A-55 and A-56, conservation of refrigerant energy in the two-phase fluid region can be presented as,

$$\left(\frac{d\left(\rho_f h_f\right)}{dP} (1 - \bar{\gamma}) + \frac{d\left(\rho_g h_g\right)}{dP} (\bar{\gamma}) + \left(\rho_g h_g - \rho_f h_f\right) \frac{d\bar{\gamma}}{dP} - 1 \right) A_{CS} L_2 \dot{P}$$
$$+ \left(\rho_g h_g - \rho_f h_f\right) A_{CS} \dot{L}_1 + \bar{\gamma} \left(\rho_g h_g - \rho_f h_f\right) A_{CS} \dot{L}_2 \tag{A-57}$$
$$= \dot{m}_{int_1} h_g - \dot{m}_{int_2} h_f + \alpha_{i_2} A_i \frac{L_2}{L_{total}} \left(T_{w_2} - T_{r_2}\right)$$

Substituting Equation A-41 and A-42 into Equation A-57, conservation of refrigerant energy in the two-phase fluid region can be presented as,

$$\left(\frac{d(\rho_f h_f)}{dP}(1-\bar{\gamma}) + \frac{d(\rho_g h_g)}{dP}(\bar{\gamma}) + (\rho_g h_g - \rho_f h_f)\frac{d\bar{\gamma}}{dP} - 1\right) A_{CS} L_2 \dot{P} \quad \textbf{A-58}$$

$$+ h_g \left[\left(\frac{\partial \rho_1}{\partial P}\Big|_{h_1}\right) + \frac{1}{2}\left(\frac{\partial \rho_1}{\partial h_1}\Big|_{P}\right)\frac{dh_g}{dP}\right] A_{CS} L_1 \dot{P}$$

$$+ h_f \left[\left(\frac{d\rho_3}{dP}\Big|_{h_3}\right) + \frac{1}{2}\left(\frac{d\rho_3}{dh_3}\Big|_{P}\right)\frac{dh_f}{dP}\right] A_{CS} L_3 \dot{P} + (\rho_g h_g - \rho_f h_f) A_{CS} \dot{L}_1$$

$$+ h_g(\rho_1 - \rho_g) A_{CS} \dot{L}_1 + \bar{\gamma}(\rho_g h_g - \rho_f h_f) A_{CS} \dot{L}_2 + h_f(\rho_f - \rho_3) A_{CS} \dot{L}_2$$

$$+ \frac{1}{2} h_f \left(\frac{\partial \rho_3}{\partial h_3}\Big|_{P}\right) A_{CS} L_3 \dot{h}_{out}$$

$$= \dot{m}_{in} h_g - \dot{m}_{out} h_f + \alpha_{i_2} A_i \frac{L_2}{L_{total}} (T_{w_2} - T_{r_2})$$

$$- \frac{1}{2} h_g \left(\frac{\partial \rho_1}{\partial h_1}\Big|_{P}\right) A_{CS} L_1 \dot{h}_{in}$$

The conservation of refrigerant energy for subcooled liquid region is calculated as,

$$\int_{L_1+L_2}^{L_{total}} \frac{\partial(\rho A_{CS} h)}{\partial t} dz \quad \textbf{A-59}$$

$$= A_{CS}\left[(\rho_f h_f - \rho_3 h_3)\dot{L}_1 + (\rho_f h_f - \rho_3 h_3)\dot{L}_2\right]$$

$$+ A_{CS}\left[\left(\frac{\partial \rho_3}{\partial P}\Big|_{h_3}\right)\dot{P}\right.$$

$$\left. + \left(\frac{\partial \rho_3}{\partial h_3}\Big|_{P}\right)\dot{h}_3\right] h_3 L_3 A_{CS} L_3 \dot{h}_3$$

$$A_{CS}\left[\left(\rho_f h_f - \rho_3 h_3\right)\dot{L}_1 + \left(\rho_f h_f - \rho_3 h_3\right)\dot{L}_2\right]$$

$$+\left[\left[\left(\frac{\partial \rho_3}{\partial P}\Big|_{h_3}\right)\dot{P} + \frac{1}{2}\left(\frac{\partial \rho_3}{\partial h_3}\Big|_{P}\right)\left(\frac{dh_f}{dP}\right)\right]h_3\right.$$

$$\left.+\frac{1}{2}\frac{dh_f}{dP}\rho_3\right]A_{CS}L_3\dot{P}$$

$$+\frac{1}{2}\left[\left(\frac{\partial \rho_3}{\partial h_3}\Big|_{P}\right)h_3 + \rho_3\right]A_{CS}L_3\dot{h}_{out}$$

$$\int_{L_1+L_2}^{L_{total}} \frac{\partial (A_{CS}P)}{\partial t}\,dz \qquad \textbf{A-60}$$

$$= A_{CS}L_3\dot{P}$$

$$\int_{L_1+L_2}^{L_{total}} \frac{\partial (\dot{m}h)}{\partial z}\,dz \qquad \textbf{A-61}$$

$$= \dot{m}_{out}h_{out} - \dot{m}_{int_2}h_f$$

$$\int_{L_1+L_2}^{L_{total}} p_i\alpha_{i_2}(T_{w_2} - T_{r_2})dz \qquad \textbf{A-62}$$

$$= p_i\alpha_{i_3}L_{total}\frac{L_3}{L_{total}}(T_{w_3} - T_{r_3})$$

$$= \alpha_{i_3}A_i\frac{L_3}{L_{total}}\left(T_{w_3} - T_{r_3}\right)$$

Combining Equation A-56, A-57, A-58 and A-59, conservation of refrigerant energy in the superheated vapor region can be presented as,

$$A_{CS}\left[\left(\rho_f h_f - \rho_3 h_3\right)\dot{L}_1 + \left(\rho_f h_f - \rho_3 h_3\right)\dot{L}_2\right] \quad \textbf{A-63}$$

$$+\left[\left[\left(\frac{\partial \rho_3}{\partial P}\Big|_{h_3}\right)\dot{P} + \frac{1}{2}\left(\frac{\partial \rho_3}{\partial h_3}\Big|_{P}\right)\left(\frac{dh_f}{dP}\right)\right]h_3 + \frac{1}{2}\frac{dh_f}{dP}\rho_3 - 1\right]A_{CS}L_3\dot{P}$$

$$+\frac{1}{2}\left[\left(\frac{\partial \rho_3}{\partial h_3}\Big|_{P}\right)h_3 + \rho_3\right]A_{CS}L_3\dot{h}_{out}$$

$$= \dot{m}_{int_2}h_f - \dot{m}_{out}h_{out} + \alpha_{i_3}A_i\frac{L_3}{L_{total}}\left(T_{w_3} - T_{r_3}\right)$$

Substituting Equation A-45 into Equation A-63, conservation of refrigerant energy in the subcooled liquid region can be presented as,

$$A_{CS}\left[\left(\rho_f h_f - \rho_3 h_3\right)\dot{L}_1 + \left(\rho_f h_f - \rho_3 h_3\right)\dot{L}_2\right] \quad \textbf{A-64}$$

$$+\left[\left[\left(\frac{\partial \rho_3}{\partial P}\Big|_{h_3}\right)\dot{P} + \frac{1}{2}\left(\frac{\partial \rho_3}{\partial h_3}\Big|_{P}\right)\left(\frac{dh_f}{dP}\right)\right]h_3 + \frac{1}{2}\frac{dh_f}{dP}\rho_3 - 1\right]A_{CS}L_3\dot{P}$$

$$+\frac{1}{2}\left[\left(\frac{\partial \rho_3}{\partial h_3}\Big|_{P}\right)h_3 + \rho_3\right]A_{CS}L_3\dot{h}_{out}$$

$$-h_f\left(\left(\frac{d\rho_3}{dP}\Big|_{h_3}\right) + \frac{1}{2}\left(\frac{d\rho_3}{dh_3}\Big|_{P}\right)\frac{dh_f}{dP}\right)A_{CS}L_3\dot{P} - \frac{1}{2}h_f\left(\frac{d\rho_3}{dh_3}\Big|_{P}\right)A_{CS}L_3\dot{h}_{out}$$

$$-A_{CS}h_f\left(\rho_f - \rho_3\right)\left(\dot{L}_1 + \dot{L}_2\right)$$

$$= \dot{m}_{out}h_f - \dot{m}_{out}h_{out} + \alpha_{i_3}A_i\frac{L_3}{L_{total}}\left(T_{w_3} - T_{r_3}\right)$$

Integrated conservation of refrigerant wall energy along the tube length in the superheat vapor region, Equation A-3 can be presented as,

$$\left(C_P\rho A\right)_W\left(\dot{T}_{w_1} + \frac{T_{w_1} - T_{int_1}}{L_1}\dot{L}_1\right) = \alpha_{i_1}A_i\left(T_{w_1} - T_{r_1}\right) + \alpha_o A_o\left(T_a - T_{w_1}\right) \quad \textbf{A-65}$$

Integrated conservation of refrigerant wall energy along the tube length in the two-phase fluid region, Equation (3) can be presented as,

$$(C_P\rho A)_W\left(\dot{T}_{w_2}\right) = \alpha_{i_2}A_i\left(T_{w_2} - T_{r_2}\right) + \alpha_o A_o\left(T_a - T_{w_2}\right) \quad \textbf{A-66}$$

Integrated conservation of refrigerant wall energy along the tube length in the subcooled liquid region, Equation A-3 can be presented as,

$$(C_P\rho A)_W\left(\dot{T}_{w_3} - \frac{T_{w_3} - T_{int_2}}{L_3}\left(\dot{L}_1 + \dot{L}_2\right)\right) = \alpha_{i_3}A_i\left(T_{w_3} - T_{r_3}\right) + \alpha_o A_o\left(T_a - T_{w_3}\right) \quad \textbf{A-67}$$

Condenser with Two-phase Fluid and Subcooled Liquid

When there is two-phase fluid and subcooled liquid in the condenser, the interface mass flowrate between the superheated vapor region and the two-phase fluid region $\dot{m}_{int_1}$ is equal to the inlet refrigerant mass flow rate $\dot{m}_{in}$ as shown in Equation A-68. Conservation of refrigerant mass for two-phase fluid, and subcooled regions are presented as in Equation A-69 and A-70.

$$\dot{m}_{int_1} = \dot{m}_{in} \quad \textbf{A-68}$$

$$A_{CS}\left(\rho_g - \rho_f\right)\bar{\gamma}\dot{L}_2 + \left[\frac{d\rho_f}{\partial P}\left(1 - \bar{\gamma}\right) + \frac{d\rho_g}{\partial P}\left(\bar{\gamma}\right) + \frac{d\bar{\gamma}}{\partial P}\left(\rho_g - \rho_f\right)\right]A_{CS}L_2\dot{P} \quad \textbf{A-69}$$

$$= \dot{m}_{int_1} - \dot{m}_{int_2}$$

$$\left(\left(\frac{d\rho_3}{dP}\Big|_{h_3}\right) + \frac{1}{2}\left(\frac{d\rho_3}{dh_3}\Big|_P\right)\frac{dh_f}{dP}\right)A_{CS}L_3\dot{P} + \frac{1}{2}\left(\frac{d\rho_3}{dh_3}\Big|_P\right)A_{CS}L_3\dot{h}_{out} \quad \textbf{A-70}$$

$$+ A_{CS}\left(\rho_f - \rho_3\right)\left(\dot{L}_1 + \dot{L}_2\right) = \dot{m}_{int_2} - \dot{m}_{out}$$

Adding Equation A-68, A-69 and A-70 together, the resulting conservation of refrigerant mass for the heat exchanger is presented as,

$$\left[\frac{d\rho_f}{\partial P}(1-\bar{\gamma}) + \frac{d\rho_g}{\partial P}(\bar{\gamma}) + \frac{d\bar{\gamma}}{\partial P}(\rho_g - \rho_f)\right] A_{CS} L_2 \dot{P}$$

$$+ \left(\left(\frac{d\rho_3}{dP}\Big|_{h_3}\right) + \frac{1}{2}\left(\frac{d\rho_3}{dh_3}\Big|_P\right)\frac{dh_f}{dP}\right) A_{CS} L_3 \dot{P} + A_{CS}(\rho_g - \rho_f)\bar{\gamma}\dot{L}_2 \qquad \textbf{A-71}$$

$$+ A_{CS}(\rho_f - \rho_3)(\dot{L}_1 + \dot{L}_2) + \frac{1}{2}\left(\frac{d\rho_3}{dh_3}\Big|_P\right) A_{CS} L_3 \dot{h}_{out} = \dot{m}_{in} - \dot{m}_{out}$$

Conservation of refrigerant energy in the two-phase fluid region can be presented as,

$$\left(\frac{d(\rho_f h_f)}{dP}(1-\bar{\gamma}) + \frac{d(\rho_g h_g)}{dP}(\bar{\gamma}) + (\rho_g h_g - \rho_f h_f)\frac{d\bar{\gamma}}{dP} - 1\right) A_{CS} L_2 \dot{P}$$

$$+ \bar{\gamma}(\rho_g h_g - \rho_f h_f) A_{CS} \dot{L}_2 \qquad \textbf{A-72}$$

$$= \dot{m}_{in} h_{in} - \dot{m}_{int_2} h_f + \alpha_{i_2} A_i \frac{L_2}{L_{total}}(T_{w_2} - T_{r_2})$$

Substituting Equation A-70 into Equation A-72 and eliminating $\dot{m}_{int_2}$, the final presentation of conservation of refrigerant energy in the two-phase fluid region is shown as,

$$\left(\frac{d(\rho_f h_f)}{dP}(1-\bar{\gamma}) + \frac{d(\rho_g h_g)}{dP}(\bar{\gamma}) + (\rho_g h_g - \rho_f h_f)\frac{d\bar{\gamma}}{dP} - 1\right) A_{CS} L_2 \dot{P}$$

$$- h_f \left[\left(\frac{d\rho_3}{dP}\Big|_{h_3}\right) + \frac{1}{2}\left(\frac{d\rho_3}{dh_3}\Big|_P\right)\frac{dh_f}{dP}\right] A_{CS} L_3 \dot{P} + \bar{\gamma}(\rho_g h_g - \rho_f h_f) A_{CS} \dot{L}_2 \qquad \textbf{A-73}$$

$$- h_f(\rho_f - \rho_3) A_{CS} \dot{L}_2 - \frac{1}{2} h_f \left(\frac{\partial \rho_3}{\partial h_3}\Big|_P\right) A_{CS} L_3 \dot{h}_{out}$$

$$= \dot{m}_{in} h_{in} - \dot{m}_{out} h_f + \alpha_{i_2} A_i \frac{L_2}{L_{total}}(T_{w_2} - T_{r_2})$$

Conservation of refrigerant energy in the subcooled liquid region can be presented as,

$$A_{CS}(\rho_f h_f - \rho_3 h_3)\dot{L}_2$$

$$+\left[\left[\left(\frac{\partial \rho_3}{\partial P}\Big|_{h_3}\right)\dot{P} + \frac{1}{2}\left(\frac{\partial \rho_3}{\partial h_3}\Big|_{P}\right)\left(\frac{dh_f}{dP}\right)\right]h_3 + \frac{1}{2}\frac{dh_f}{dP}\rho_3 - 1\right]A_{CS}L_3\dot{P}$$

$$+\frac{1}{2}\left[\left(\frac{\partial \rho_3}{\partial h_3}\Big|_{P}\right)h_3 + \rho_3\right]A_{CS}L_3\dot{h}_{out} \qquad \textbf{A-74}$$

$$= \dot{m}_{int_2}h_f - \dot{m}_{out}h_{out} + \alpha_{i_3}A_i\frac{L_3}{L_{total}}(T_{w_3} - T_{r_3})$$

Substituting Equation A-70 into Equation A-74 and eliminating $\dot{m}_{int_2}$, the final presentation of conservation of refrigerant energy in subcooled liquid region is shown as,

$$\left[\left[\left(\frac{\partial \rho_3}{\partial P}\Big|_{h_3}\right)\dot{P} + \frac{1}{2}\left(\frac{\partial \rho_3}{\partial h_3}\Big|_{P}\right)\left(\frac{dh_f}{dP}\right)\right]h_3 + \frac{1}{2}\frac{dh_f}{dP}\rho_3 - 1\right]A_{CS}L_3\dot{P}$$

$$+ h_f\left(\left(\frac{d\rho_3}{dP}\Big|_{h_3}\right) + \frac{1}{2}\left(\frac{d\rho_3}{dh_3}\Big|_{P}\right)\frac{dh_f}{dP}\right)A_{CS}L_3\dot{P} + A_{CS}(\rho_f h_f - \rho_3 h_3)\dot{L}_2$$

$$+ A_{CS}h_f(\rho_f - \rho_3)\dot{L}_2 + \frac{1}{2}\left[\left(\frac{\partial \rho_3}{\partial h_3}\Big|_{P}\right)h_3 + \rho_3\right]A_{CS}L_3\dot{h}_{out} \qquad \textbf{A-75}$$

$$+\frac{1}{2}h_f\left(\frac{d\rho_3}{dh_3}\Big|_{P}\right)A_{CS}L_3\dot{h}_{out}$$

$$= \dot{m}_{out}h_f - \dot{m}_{out}h_{out} + \alpha_{i_3}A_i\frac{L_3}{L_{total}}(T_{w_3} - T_{r_3})$$

Integrated conservation of refrigerant wall energy along the tube length in the two-phase fluid region, Equation A-3 can be presented as,

$$(C_P\rho A)_W\left(\dot{T}_{w_2} + \frac{T_{w_2} - T_{int_2}}{L_2}\dot{L}_2\right) = \alpha_{i_2}A_i(T_{w_2} - T_{r_2}) + \alpha_o A_o(T_a - T_{w_2}) \qquad \textbf{A-76}$$

Integrated conservation of refrigerant wall energy along the tube length in the subcooled liquid region, Equation A-3 can be presented as,

$$(C_P \rho A)_W \left(\dot{T}_{w_3} - \frac{T_{w_3} - T_{int_2}}{L_3} \dot{L}_2 \right) = \alpha_{i_3} A_i \left(T_{w_3} - T_{r_3} \right) + \alpha_o A_o \left(T_a - T_{w_3} \right) \quad \textbf{A-77}$$

Combined Heat Exchanger Model Derivation

This section presents the detailed model derivation of the combined heat exchanger. Mass flow rates and refrigerant energy are conserved at the interface of evaporator and condenser. The total mass flow rates at the outlet of the evaporators equal to the condenser inlet mass flow rate as shown in Equation A-78.

$$\sum_{j=1}^{n} \dot{m}_{ero_j} = \dot{m}_{cri} \quad \textbf{A-78}$$

Refrigerant energy at the outlet of the evaporators equal to the condenser inlet refrigerant energy as shown in equation A-79.

$$\sum_{j=1}^{n} h_{ero_j} \dot{m}_{ero_j} = \dot{m}_{cri} h_{cri} \quad \textbf{A-79}$$

Combining Equation A-78 and A-79 and the above switch moving boundary evaporator and switch moving boundary condenser governing equations, the combined multi-evaporator heat exchanger has the general form of Equation A-80. Equation A-81 shows an example of two-evaporator combined heat exchanger model. Substituting the detailed x states and f vectors shown in Equation A-82 to A-87 to Equation A-81, detailed matrix elements of two evaporators in parallel combined model are shown in Equation A-88. The detailed elements in z matrix and f vector are listed in Table A and Table B.

$$\begin{bmatrix} Z_{e_1,1} & Z_{e_1,2} & 0 & 0 & 0 & 0 & 0 \\ Z_{e_2,1} & 0 & Z_{e_2,2} & 0 & 0 & 0 & 0 \\ Z_{e_3,1} & 0 & 0 & Z_{e_3,2} & 0 & 0 & 0 \\ Z_{e_4,1} & 0 & 0 & 0 & Z_{e_4,2} & 0 & 0 \\ \vdots & 0 & 0 & 0 & 0 & \ddots & 0 \\ Z_{e_n,1} & 0 & 0 & 0 & 0 & Z_{e_n,2} & 0 \\ Z_{c_1} & Z_{c_2,1} & Z_{c_2,2} & Z_{c_2,4} & \dots & Z_{c_2,n} & Z_{c_3} \end{bmatrix} \begin{bmatrix} \dot{P} \\ \dot{x}_{e_1} \\ \dot{x}_{e_2} \\ \dot{x}_{e_3} \\ \vdots \\ \dot{x}_{e_n} \\ \dot{x}_c \end{bmatrix} = \begin{bmatrix} f_{e_1} \\ f_{e_2} \\ f_{e_3} \\ f_{e_4} \\ \vdots \\ f_{e_n} \\ f_c \end{bmatrix} \quad \textbf{A-80}$$

$$\begin{bmatrix} Z_{e_1,1} & Z_{e_1,2} & 0 & 0 \\ Z_{e_2,1} & 0 & Z_{e_2,2} & 0 \\ Z_{c_1} & Z_{c_2,1} & Z_{c_2,2} & Z_{c_3} \end{bmatrix} \begin{bmatrix} \dot{P} \\ \dot{x}_{e_1} \\ \dot{x}_{e_2} \\ \dot{x}_c \end{bmatrix} = \begin{bmatrix} f_{e_1} \\ f_{e_2} \\ f_c \end{bmatrix} \quad \textbf{A-81}$$

$$f_{e_1} = [f_{1,evap_1} \quad f_{2,evap_1} \quad f_{3,evap_1} \quad f_{4,evap_1} \quad f_{5,evap_1}]^T \quad \textbf{A-82}$$

$$f_{e_1} = [f_{1,evap_1} \quad f_{2,evap_1} \quad f_{3,evap_1} \quad f_{4,evap_1} \quad f_{5,evap_1}]^T \quad \textbf{A-83}$$

$$f_c = [f_{1,cond} \quad f_{2,cond} \quad f_{3,cond} \quad f_{4,cond} \quad f_{5,cond} \quad f_{6,cond} \quad f_{7,cond}]^T \quad \textbf{A-84}$$

$$x_{e_1} = \left[\left[L_{1,e_1} \quad h_{1,e_1} \quad T_{w_1,e_1} \quad T_{w_2,e_1} \quad \overline{\gamma}_{e_1}\right]\right]^T \quad \textbf{A-85}$$

$$x_{e_2} = \left[\left[L_{1,e_2} \quad h_{1,e_2} \quad T_{w_1,e_2} \quad T_{w_2,e_2} \quad \overline{\gamma}_{e_2}\right]\right]^T \quad \textbf{A-86}$$

$$x_c = [L_{2,c} \quad L_{3,c} \quad h_{cr3} \quad T_{w_1,c} \quad T_{w_2,c} \quad T_{w_3,c} \quad \overline{\gamma}_c] \quad \textbf{A-87}$$

$$
\begin{bmatrix}
Z_{11} & Z_{12} & Z_{13} & & & Z_{16} & & & & & & & & & & & \\
Z_{21} & Z_{22} & Z_{23} & & & Z_{26} & & & & & & & & & & & \\
Z_{31} & Z_{32} & Z_{33} & & & Z_{36} & & & & & & & & & & & \\
 & Z_{42} & & Z_{44} & & & & & & & & & & & & & \\
 & Z_{52} & & & Z_{55} & & & & & & & & & & & & \\
Z_{61} & & & & & & Z_{67} & Z_{68} & & & Z_{6,11} & & & & & & \\
Z_{71} & & & & & & Z_{77} & Z_{78} & & & Z_{7,11} & & & & & & \\
Z_{81} & & & & & & Z_{87} & Z_{88} & & & Z_{8,11} & & & & & & \\
 & & & & & & Z_{97} & & Z_{99} & & & & & & & & \\
 & & & & & & Z_{10,7} & & & Z_{10,10} & & & & & & & \\
Z_{11,1} & & & & & Z_{11,6} & & & & & Z_{11,11} & Z_{11,12} & Z_{11,13} & Z_{11,14} & & & \\
Z_{12,1} & & & & & & & & & & & Z_{12,12} & Z_{12,13} & Z_{12,14} & & & \\
Z_{13,1} & & & & & & & & & & & Z_{13,12} & Z_{13,13} & Z_{13,14} & & & \\
Z_{14,1} & & & & & Z_{14,6} & & & & & Z_{14,11} & Z_{14,12} & Z_{14,13} & Z_{14,14} & & & \\
 & & & & & & & & & & & Z_{15,12} & Z_{15,13} & & Z_{15,15} & & \\
 & & & & & & & & & & & Z_{16,12} & & & & Z_{16,16} & \\
 & & & & & & & & & & & & Z_{17,13} & & & & Z_{17,17}
\end{bmatrix}
\begin{bmatrix}
\dot{P} \\ \dot{L}_{e_1,1} \\ \dot{h}_{ero_1} \\ \dot{T}_{e_1,w_1} \\ \dot{T}_{e_1,w_2} \\ \dot{m}_{ero_1} \\ \dot{L}_{e_1,2} \\ \dot{h}_{ero_2} \\ \dot{T}_{e_2,w_1} \\ \dot{T}_{e_2,w_2} \\ \dot{m}_{ero_2} \\ \dot{L}_{c_2} \\ \dot{L}_{c_3} \\ \dot{h}_{cro} \\ \dot{T}_{c,w_1} \\ \dot{T}_{c,w_2} \\ \dot{T}_{c,w_3}
\end{bmatrix}
=
\begin{bmatrix}
f_{1,evap_1} \\ f_{2,evap_1} \\ f_{3,evap_1} \\ f_{4,evap_1} \\ f_{5,evap_1} \\ f_{1,evap_2} \\ f_{2,evap_2} \\ f_{3,evap_2} \\ f_{4,evap_2} \\ f_{5,evap_2} \\ f_{1,cond} \\ f_{2,cond} \\ f_{3,cond} \\ f_{4,cond} \\ f_{5,cond} \\ f_{6,cond} \\ f_{7,cond}
\end{bmatrix}
\tag{A-88}
$$

Table A: *Z* Matrix Elements

	Condition 1	Condition 2
Z_{11}	$A_{CS,e_1} L_{total,e_1} \left(\frac{d(\rho_{1,e_1} h_{1,e_1})}{dt} - 1 \right)$	$\left(\frac{d(\rho_{f,e_1} h_{f,e_1})}{dP} \left(1 - \bar{\gamma}_{e_1}\right) + \frac{d(\rho_{g,e_1} h_{g,e_1})}{dP} \left(\bar{\gamma}_{e_1}\right) + \left(\rho_{g,e_1} h_{g,e_1} - \rho_{f,e_1} h_{f,e_1}\right) \frac{d\bar{\gamma}_{e_1}}{dP} - 1 \right) A_{CS,e_1} L_{e_1} \dot{P} + h_{g,e_1} \left[\left(\frac{\partial \rho_{2,e_1}}{\partial P}\Big|_{h_{2,e_1}} \right) + \frac{1}{2} \left(\frac{\partial \rho_{2,e_1}}{\partial h_{2,e_1}}\Big|_{P} \right) \frac{dh_{g,e_1}}{dP} \right] A_{CS,e_1} L_{2,e_1} \dot{P}$
Z_{21}	0	$\left[\left[\left(\frac{\partial \rho_{2,e_1}}{\partial P}\Big|_{h_{2,e_1}} \right) + \frac{1}{2} \left(\frac{\partial \rho_{2,e_1}}{\partial h_{2,e_1}}\Big|_{P} \right) \frac{dh_{g,e_1}}{dP} \right] h_{2,e_1} + \frac{1}{2} \frac{dh_{g,e_1}}{dP} \rho_{2,e_1} - 1 \right] A_{CS,e_1} L_{2,e_1} - h_g \left[\left(\frac{\partial \rho_{2,e_1}}{\partial P}\Big|_{h_{2,e_1}} \right) + \frac{1}{2} \left(\frac{\partial \rho_{2,e_1}}{\partial h_{2,e_1}}\Big|_{P} \right) \frac{dh_{g,e_1}}{dP} \right] A_{CS,e_1} L_{2,e_1}$
Z_{31}	$A_{CS,e_1} L_{total,e_1} \frac{\partial \rho_{1,e_1}}{\partial P}\Big\|_{h_{1,e_1}}$	$\left[\frac{d\rho_{f,e_1}}{\partial P} \left(1 - \bar{\gamma}_{e_1}\right) + \frac{d\rho_{g,e_1}}{\partial P} \left(\bar{\gamma}_{e_1}\right) + \frac{d\bar{\gamma}_{e_1}}{\partial P} \left(\rho_{g,e_1} - \rho_{f,e_1}\right) \right] A_{CS,e_1} L_{1,e_1} + \left[\left(\frac{\partial \rho_{2,e_1}}{\partial P}\Big|_{h_{2,e_1}} \right) + \frac{1}{2} \left(\frac{\partial \rho_{2,e_1}}{\partial h_{2,e_1}}\Big|_{P} \right) \frac{dh_{g,e_1}}{dP} \right] A_{CS,e_1} L_{2,e_1}$
Z_{12}	0	$A_{CS,e_1} \left(1 - \bar{\gamma}_{e_1}\right) \left(\rho_{f,e_1} h_{f,e_1} - \rho_{g,e_1} h_{g,e_1}\right) + A_{CS,e_1} h_{g,e_1} \left(\rho_{g,e_1} - \rho_{2,e_1}\right)$
Z_{13}	$\left(\rho_{g,e_1} h_{g,e_1} - \rho_{f,e_1} h_{f,e_1}\right) \frac{d\bar{\gamma}_{e_1}}{dt} L_{total,e_1}$	0
Z_{16}	h_{ero_1}	h_{g,e_1}
Z_{22}	1	$A_{CS,e_1} \left(\rho_{g,e_1} h_{g,e_1} - \rho_{2,e_1} h_{2,e_1}\right) - A_{CS,e_1} \left(\rho_{g,e_1} - \rho_{2,e_1}\right)$
Z_{23}	0	$\frac{1}{2} \left[\left(\frac{\partial \rho_{2,e_1}}{\partial h_{2,e_1}}\Big|_{P} \right) h_{2,e_1} + \rho_{2,e_1} \right] A_{CS,e_1} L_{2,e_1} - \frac{1}{2} h_{g,e_1} \left(\frac{\partial \rho_{2,e_1}}{\partial h_{2,e_1}}\Big|_{P} \right) A_{CS,e_1} L_{2,e_1}$
Z_{26}	0	$h_{ero_1} - h_{g,e_1}$

Table A: Continued

	Condition 1	Condition 2
Z_{32}	0	$A_{CS,e_1}\left(1-\bar{\gamma}_{e_1}\right)\left(\rho_{f,e_1}-\rho_{g,e_1}\right)+A_{CS,e_1}\left(\rho_{g,e_1}-\rho_{2,e_1}\right)$
Z_{33}	$A_{CS,e_1}L_{total,e_1}\left.\frac{\partial\rho_{1,e_1}}{\partial h_{1,e_1}}\right\|_P$	$\frac{1}{2}\left(\left.\frac{\partial\rho_{2,e_1}}{\partial h_{2,e_1}}\right\|_P\right)A_{CS,e_1}L_{2,e_1}$
Z_{36}	1	1
Z_{42}	0	$(C_P\rho A)_{W,e_1}\left(\frac{T_{e_1,w_1}-T_{e_1,int}}{L_{1,e_1}}\right)$
Z_{44}	$(C_P\rho A)_{W,e_1}$	$(C_P\rho A)_{W,e_1}$
Z_{52}	0	$-(C_P\rho A)_{W,e_1}\left(\frac{T_{e_1,w_2}-T_{e_1,int}}{L_{2,e_1}}\right)$
Z_{55}	1	$(C_P\rho A)_{W,e_1}$
Z_{61}	$A_{CS,e_2}L_{total,e_2}\left(\frac{d\left(\rho_{1,e_2}h_{1,e_2}\right)}{dt}-1\right)$	$\left(\frac{d(\rho_{f,e_2}h_{f,e_2})}{dP}\left(1-\bar{\gamma}_{e_2}\right)+\frac{d(\rho_{g,e_2}h_{g,e_2})}{dP}\left(\bar{\gamma}_{e_2}\right)+\left(\rho_{g,e_2}h_{g,e_2}-\rho_{f,e_2}h_{f,e_2}\right)\frac{d\bar{\gamma}_{e_2}}{dP}-1\right)A_{CS,e_2}L_{e_2}\dot{P}+h_{g,e_2}\left[\left(\left.\frac{\partial\rho_{2,e_2}}{\partial P}\right\|_{h_{2,e_2}}\right)+\frac{1}{2}\left(\left.\frac{\partial\rho_{2,e_2}}{\partial h_{2,e_2}}\right\|_P\right)\frac{dh_{g,e_2}}{dP}\right]A_{CS,e_2}L_{2,e_2}\dot{P}$
Z_{71}	0	$\left[\left[\left(\left.\frac{\partial\rho_{2,e_2}}{\partial P}\right\|_{h_{2,e_2}}\right)+\frac{1}{2}\left(\left.\frac{\partial\rho_{2,e_2}}{\partial h_{2,e_2}}\right\|_P\right)\frac{dh_{g,e_2}}{dP}\right]h_{2,e_2}+\frac{1}{2}\frac{dh_{g,e_2}}{dP}\rho_{2,e_2}-1\right]A_{CS,e_2}L_{2,e_2}-h_{g,e_2}\left[\left(\left.\frac{\partial\rho_{2,e_2}}{\partial P}\right\|_{h_{2,e_2}}\right)+\frac{1}{2}\left(\left.\frac{\partial\rho_{2,e_2}}{\partial h_{2,e_2}}\right\|_P\right)\frac{dh_{g,e_2}}{dP}\right]A_{CS,e_2}L_{2,e_2}$
Z_{81}	$A_{CS,e_2}L_{total,e_2}\left.\frac{\partial\rho_{1,e_2}}{\partial P}\right\|_{h_{1,e_2}}$	$\left[\frac{d\rho_{f,e_2}}{\partial P}\left(1-\bar{\gamma}_{e_2}\right)+\frac{d\rho_{g,e_2}}{\partial P}\left(\bar{\gamma}_{e_2}\right)+\frac{d\bar{\gamma}_{e_2}}{\partial P}\left(\rho_{g,e_2}-\rho_{f,e_2}\right)\right]A_{CS,e_2}L_{1,e_2}+\left[\left(\left.\frac{\partial\rho_{2,e_2}}{\partial P}\right\|_{h_{2,e_2}}\right)+\frac{1}{2}\left(\left.\frac{\partial\rho_{2,e_2}}{\partial h_{2,e_2}}\right\|_P\right)\frac{dh_{g,e_2}}{dP}\right]A_{CS,e_2}L_{2,e_2}$
Z_{67}	0	$A_{CS,e_2}\left(1-\bar{\gamma}_{e_2}\right)\left(\rho_{f,e_2}h_{f,e_2}-\rho_{g,e_2}h_{g,e_2}\right)+A_{CS,e_2}h_{g,e_2}\left(\rho_{g,e_2}-\rho_{2,e_2}\right)$
Z_{68}	$\left(\rho_{g,e_2}h_{g,e_2}-\rho_{f,e_2}h_{f,e_2}\right)\frac{d\bar{\gamma}_{e_2}}{dt}L_{total,e_2}$	0

Table A: Continued

	Condition 1	Condition 2
$Z_{6,11}$	h_{ero_2}	h_{g,e_2}
Z_{77}	1	$A_{CS,e_2}\left(\rho_{g,e_2}h_{g,e_2}-\rho_{2,e_2}h_{2,e_2}\right)-A_{CS,e_2}\left(\rho_{g,e_2}-\rho_{2,e_2}\right)$
Z_{78}	0	$\frac{1}{2}\left[\left(\left.\frac{\partial\rho_{2,e_2}}{\partial h_{2,e_2}}\right\|_P\right)h_{2,e_2}+\rho_{2,e_2}\right]A_{CS,e_2}L_{2,e_2}-\frac{1}{2}h_{g,e_2}\left(\left.\frac{\partial\rho_{2,e_2}}{\partial h_{2,e_2}}\right\|_P\right)A_{CS,e_2}L_{2,e_2}$
$Z_{7,11}$	0	$h_{ero_2}-h_{g,e_2}$
Z_{87}	0	$A_{CS,e_2}\left(1-\overline{\gamma}_{e_2}\right)\left(\rho_{f,e_2}-\rho_{g,e_2}\right)+A_{CS,e_2}\left(\rho_{g,e_2}-\rho_{2,e_2}\right)$
Z_{88}	$A_{CS,e_2}L_{total,e_2}\left.\frac{\partial\rho_{1,e_2}}{\partial h_{1,e_2}}\right\|_P$	$\frac{1}{2}\left(\left.\frac{\partial\rho_{2,e_2}}{\partial h_{2,e_2}}\right\|_P\right)A_{CS,e_2}L_{2,e_2}$
$Z_{8,11}$	1	1
Z_{97}	0	$(C_P\rho A)_{W,e_2}\left(\frac{T_{e_2,w_1}-T_{e_2,int}}{L_{1,e_2}}\right)$
Z_{99}	$(C_P\rho A)_{W,e_2}$	$(C_P\rho A)_{W,e_2}$
$Z_{10,7}$	0	$-(C_P\rho A)_{W,e_2}\left(\frac{T_{e_2,w_2}-T_{e_2,int}}{L_{2,e_2}}\right)$
$Z_{10,10}$	1	$(C_P\rho A)_{W,e_2}$
$Z_{11,1}$	$\left(\frac{d(\rho_{f,c}h_{f,c})}{dP}(1-\bar{\gamma}_c)+\frac{d(\rho_{g,c}h_{g,c})}{dP}(\bar{\gamma}_c)+\left(\rho_{g,c}h_{g,c}-\rho_{f,c}h_{f,c}\right)\frac{d\bar{\gamma}_c}{dP}-1\right)A_{CS,c}L_{2,c}-A_{CS,c}L_{2,c}+h_{f,c}\left[\left(\left.\frac{d\rho_{3,c}}{dP}\right\|_{h_{3,c}}\right)+\frac{1}{2}\left(\left.\frac{d\rho_{3,c}}{dh_{3,c}}\right\|_P\right)\frac{dh_{f,c}}{dP}\right]A_{CS,c}L_{3,c}$	$A_{CS,c}L_{1,c}\left[\left(\left.\frac{\partial\rho_{1,c}}{\partial P}\right\|_{h_{1,c}}\right)+\frac{1}{2}\left(\left.\frac{\partial\rho_{1,c}}{\partial h_{1,c}}\right\|_P\right)\frac{dh_{g,c}}{dP}\right]h_{1,c}+\frac{1}{2}A_{CS,c}L_{1,c}\frac{dh_{g,c}}{dP}\rho_{1,c}-A_{CS,c}L_{1,c}-h_{g,c}\left[\left(\left.\frac{\partial\rho_{1,c}}{\partial P}\right\|_{h_{1,c}}\right)+\frac{1}{2}\left(\left.\frac{\partial\rho_{1,c}}{\partial h_{1,c}}\right\|_P\right)\frac{dh_{g,c}}{dP}\right]A_{CS,c}L_{1,c}$
$Z_{12,1}$	0	$\left(\frac{d(\rho_{f,c}h_{f,c})}{dP}(1-\bar{\gamma}_c)+\frac{d(\rho_{g,c}h_{g,c})}{dP}(\bar{\gamma}_c)+\left(\rho_{g,c}h_{g,c}-\rho_{f,c}h_{f,c}\right)\frac{d\bar{\gamma}_c}{dP}-1\right)A_{CS,c}L_{2,c}+h_{g,c}\left[\left(\left.\frac{\partial\rho_{1,c}}{\partial P}\right\|_{h_{1,c}}\right)+\frac{1}{2}\left(\left.\frac{\partial\rho_{1,c}}{\partial h_{1,c}}\right\|_P\right)\frac{dh_{g,c}}{dP}\right]A_{CS,c}L_{1,c}+h_{f,c}\left[\left(\left.\frac{\partial\rho_{3,c}}{\partial P}\right\|_{h_{3,c}}\right)+\frac{1}{2}\left(\left.\frac{\partial\rho_{3,c}}{\partial h_{3,c}}\right\|_P\right)\frac{dh_{f,c}}{dP}\right]A_{CS,c}L_{3,c}$

Table A: Continued

	Condition 1	Condition 2
$Z_{13,1}$	$A_{CS,c}L_{3,c}\left[\left(\frac{\partial\rho_{3,c}}{\partial P}\Big\vert_{h_{3,c}}\right)+\frac{1}{2}\left(\frac{\partial\rho_{3,c}}{\partial h_{3,c}}\Big\vert_{P}\right)\frac{dh_{f,c}}{dP}\right]h_{f,c}+\frac{1}{2}A_{CS,c}L_{3,c}\rho_{3,c}\frac{dh_{f,c}}{dP}-A_{CS,c}L_{3,c}-\left[\left(\frac{\partial\rho_{3,c}}{\partial P}\Big\vert_{h_{3,c}}\right)+\frac{1}{2}\left(\frac{\partial\rho_{3,c}}{\partial h_{3,c}}\Big\vert_{P}\right)\frac{dh_{f,c}}{dP}\right]A_{CS,c}L_{3,c}h_{cri}$	$\left\{\left[\left(\frac{\partial\rho_{3,c}}{\partial P}\Big\vert_{h_{3,c}}\right)+\frac{1}{2}\left(\frac{\partial\rho_{3,c}}{\partial h_{3,c}}\Big\vert_{P}\right)\frac{dh_{f,c}}{dP}\right]h_{3,c}+\frac{1}{2}\frac{dh_{f,c}}{dP}\rho_{3,c}-1\right\}A_{CS,c}L_{3,c}-h_{f,c}\left[\left(\frac{\partial\rho_{3,c}}{\partial P}\Big\vert_{h_{3,c}}\right)+\frac{1}{2}\left(\frac{\partial\rho_{3,c}}{\partial h_{3,c}}\Big\vert_{P}\right)\frac{dh_{f,c}}{dP}\right]A_{CS,c}L_{3,c}$
$Z_{14,1}$	$\left[\frac{d\rho_{f,c}}{dP}(1-\bar{\gamma}_c)+\frac{d\rho_{g,c}}{dP}(\bar{\gamma}_c)+(\rho_{g,c}-\rho_{f,c})\frac{d\bar{\gamma}_c}{dP}\right]A_{CS,c}L_{2,c}+\left[\left(\frac{\partial\rho_{3,c}}{\partial P}\Big\vert_{h_{3,c}}\right)+\frac{1}{2}\left(\frac{\partial\rho_{3,c}}{\partial h_{3,c}}\Big\vert_{P}\right)\frac{dh_{f,c}}{dP}\right]A_{CS,c}L_{3,c}$	$\left[\left(\frac{\partial\rho_{1,c}}{\partial P}\Big\vert_{h_{1,c}}\right)+\frac{1}{2}\left(\frac{\partial\rho_{1,c}}{\partial h_{1,c}}\Big\vert_{P}\right)\frac{dh_{g,c}}{dP}\right]A_{CS,c}L_{1,c}+\left[\frac{d\rho_{f,c}}{dP}(1-\bar{\gamma}_c)+\frac{d\rho_{g,c}}{dP}(\bar{\gamma}_c)+(\rho_{g,c}-\rho_{f,c})\frac{d\bar{\gamma}_c}{dP}\right]A_{CS,c}L_{2,c}+\left[\left(\frac{\partial\rho_{3,c}}{\partial P}\Big\vert_{h_{3,c}}\right)+\frac{1}{2}\left(\frac{\partial\rho_{3,c}}{\partial h_{3,c}}\Big\vert_{P}\right)\frac{dh_{f,c}}{dP}\right]A_{CS,c}L_{3,c}$
$Z_{11,6}$	$-h_{ero_1}$	$h_{g,c}-h_{ero_1}$
$Z_{11,11}$	-1	-1
$Z_{14,6}$	$-h_{ero_2}$	$h_{g,c}-h_{ero_2}$
$Z_{14,11}$	-1	-1
$Z_{11,12}$	$A_{CS,c}(\rho_{g,c}h_{g,c}-\rho_{f,c}h_{f,c})\bar{\gamma}_c+A_{CS,c}(\rho_{f,c}-\rho_{3,c})h_{f,c}$	$(-h_{1,c}+h_{g,c})\rho_{1,c}A_{CS,c}$
$Z_{11,13}$	0	$(-h_{1,c}+h_{g,c})\rho_{1,c}A_{CS,c}$
$Z_{11,14}$	$\frac{1}{2}\left(\frac{\partial\rho_{3,c}}{\partial h_{3,c}}\Big\vert_{P}\right)A_{CS,c}L_{3,c}h_{f,c}$	0
$Z_{12,12}$	1	$A_{CS,c}(1-\bar{\gamma}_c)\rho_{f,c}h_{f,c}+A_{CS,c}h_{g,c}(\bar{\gamma}_c\rho_{g,c}-\rho_{1,c})$
$Z_{12,13}$	1	$A_{CS,c}(\rho_{3,c}h_{f,c}-\rho_{1,c}h_{g,c})$
$Z_{12,14}$	0	$\frac{1}{2}h_{f,c}\left(\frac{\partial\rho_{3,c}}{\partial h_{3,c}}\Big\vert_{P}\right)A_{CS,c}L_{3,c}$
$Z_{13,12}$	$A_{CS,c}\rho_{3,c}(h_{f,c}-h_{3,c})$	0
$Z_{13,13}$	0	$A_{CS,c}(1-\bar{\gamma}_c)(h_{3,c}-h_{f,c})$
$Z_{13,14}$	$A_{CS,c}L_{3,c}\left[\frac{1}{2}\left(\frac{\partial\rho_{3,c}}{\partial h_{3,c}}\Big\vert_{P}\right)(h_{3,c}-h_{cri})+\frac{1}{2}\rho_{3,c}\right]$	$\frac{1}{2}\left[\left(\frac{\partial\rho_{3,c}}{\partial h_{3,c}}\Big\vert_{P}\right)h_{3,c}+\rho_{3,c}\right]A_{CS,c}L_{3,c}-\frac{1}{2}h_{f,c}\left(\frac{\partial\rho_{3,c}}{\partial h_{3,c}}\Big\vert_{P}\right)A_{CS,c}L_{3,c}$

Table A: Continued

	Condition 1	Condition 2
$Z_{14,12}$	$A_{CS,c}(\rho_{g,c}-\rho_{f,c})\bar{\gamma}_c + A_{CS,c}(\rho_{f,c}-\rho_{3,c})$	$A_{CS,c}\bar{\gamma}_c(\rho_{g,c}-\rho_{f,c})$
$Z_{14,13}$	0	$A_{CS,c}(\rho_{3,c}-\rho_{f,c})$
$Z_{14,14}$	$\frac{1}{2}\left(\frac{\partial\rho_{3,c}}{\partial h_{3,c}}\Big\vert_P\right)A_{CS,c}L_{3,c}$	$\frac{1}{2}\left(\frac{\partial\rho_{3,c}}{\partial h_{3,c}}\Big\vert_P\right)A_{CS,c}L_{3,c}$
$Z_{15,12}$	0	$-(C_P\rho A)_{W,c}\left(\frac{T_{c,w_1}-T_{c,int_1}}{L_{1,c}}\right)$
$Z_{15,13}$	0	$-(C_P\rho A)_{W,c}\left(\frac{T_{c,w_1}-T_{c,int_1}}{L_{1,c}}\right)$
$Z_{15,15}$	1	$(C_P\rho A)_{W,c}$
$Z_{16,12}$	$(C_P\rho A)_{W,c}\left(\frac{T_{c,w_2}-T_{c,int_2}}{L_{2,c}}\right)$	0
$Z_{16,16}$	$(C_P\rho A)_{W,c}$	$(C_P\rho A)_{W,c}$
$Z_{17,13}$	$(C_P\rho A)_{W,c}\left(\frac{T_{c,w_3}-T_{c,int_2}}{L_{3,c}}\right)$	$(C_P\rho A)_{W,c}\left(\frac{T_{c,w_3}-T_{c,int_2}}{L_{3,c}}\right)$
$Z_{17,17}$	$(C_P\rho A)_{W,c}$	$(C_P\rho A)_{W,c}$

Table B: f Vector Elements

$f_{1,evap_1}$	$\dot{m}_{eri_1}h_{eri_1}-\dot{m}_{ero_1}h_{ero_1}+\alpha_{i_1,e_1}A_{i,e_1}(T_{w_1,e_1}-T_{r_1,e_1})$	$\dot{m}_{eri_1}h_{eri_1}+\alpha_{i_1,e_1}A_{i,e_1}\frac{L_{1,e_1}}{L_{total,e_1}}(T_{w_1,e_1}-T_{r_1,e_1})$
$f_{2,evap_1}$	0	$\alpha_{i_2,e_1}A_{i,e_1}\frac{L_{2,e_1}}{L_{total,e_1}}(T_{w_2,e_1}-T_{r_2,e_1})$
$f_{3,evap_1}$	$\dot{m}_{eri_1}$	$\dot{m}_{eri_1}$
$f_{4,evap_1}$	$\alpha_{i_1,e_1}A_{i,e_1}(T_{w_1,e_1}-T_{r_1,e_1})+\alpha_{o,e_1}A_{o,e_1}(T_{a,e_1}-T_{w_1,e_1})$	$\alpha_{i_1,e_1}A_{i,e_1}(T_{w_1,e_1}-T_{r_1,e_1})+\alpha_{o,e_1}A_{o,e_1}(T_{a,e_1}-T_{w_1,e_1})$
$f_{5,evap_1}$	$k_e(T_{w_1,e_1}-T_{w_2,e_1})$	$\alpha_{i_2,e_1}A_{i,e_1}(T_{w_2,e_1}-T_{r_2,e_1})+\alpha_{o,e_1}A_{o,e_1}(T_{a,e_1}-T_{w_1,e_1})$
$f_{1,evap_2}$	$\dot{m}_{eri_2}h_{eri_2}-\dot{m}_{ero_2}h_{ero_2}+\alpha_{i_1,e_2}A_{i,e_2}(T_{w_1,e_2}-T_{r_1,e_2})$	$\dot{m}_{eri_2}h_{eri_2}+\alpha_{i_1,e_2}A_{i,e_2}\frac{L_{1,e_2}}{L_{total,e_2}}(T_{w_1,e_2}-T_{r_1,e_2})$
$f_{2,evap_2}$	0	$\alpha_{i_2,e_2}A_{i,e_2}\frac{L_{2,e_2}}{L_{total,e_2}}(T_{w_2,e_2}-T_{r_2,e_2})$
$f_{3,evap_2}$	$\dot{m}_{eri_2}$	$\dot{m}_{eri_2}$
$f_{4,evap_2}$	$\alpha_{i_1,e_2}A_{i,e_2}(T_{w_1,e_2}-T_{r_1,e_2})+\alpha_{o,e_2}A_{o,e_2}(T_{a,e_2}-T_{w_1,e_2})$	$\alpha_{i_1,e_2}A_{i,e_2}(T_{w_1,e_2}-T_{r_1,e_2})+\alpha_{o,e_2}A_{o,e_2}(T_{a,e_2}-T_{w_1,e_2})$
$f_{5,evap_2}$	$k_e(T_{w_1,e_2}-T_{w_2,e_2})$	$\alpha_{i_2,e_2}A_{i,e_2}(T_{w_2,e_2}-T_{r_2,e_2})+\alpha_{o,e_2}A_{o,e_2}(T_{a,e_2}-T_{w_1,e_2})$

Table B: Continued

$f_{1,cond}$	$-\dot{m}_{cro}h_{f,c} + \alpha_{i_1,c}A_{i,c}\frac{L_{2,c}}{L_{total,c}}\left(T_{w_2,c} - T_{r_2,c}\right)$	$\alpha_{i_1,c}A_{i,c}\frac{L_{1,c}}{L_{total,c}}\left(T_{w_1,c} - T_{r_1,c}\right) - \frac{1}{2}\left[\left(\frac{\partial\rho_{1,c}}{\partial h_{1,c}}\Big\vert_P\right)h_{1,c} + \rho_{1,c}\right]A_{CS,c}L_{1,c}\dot{h}_{cri} + \frac{1}{2}h_{g,c}\left(\frac{\partial\rho_{1,c}}{\partial h_{1,c}}\Big\vert_P\right)A_{CS,c}L_{1,c}\dot{h}_{cri}$
$f_{2,cond}$	0	$\dot{m}_{cri}h_{g,c} - \dot{m}_{cro}h_{f,c} + \alpha_{i_1,c}A_{i,c}\frac{L_{2,c}}{L_{total,c}}\left(T_{w_2,c} - T_{r_2,c}\right) - \frac{1}{2}h_{g,c}\left(\frac{\partial\rho_{1,c}}{\partial h_{1,c}}\Big\vert_P\right)A_{CS,c}L_{1,c}\dot{h}_{cri}$
$f_{3,cond}$	$\dot{m}_{cro}h_{cri} - \dot{m}_{cro}h_{cro} + \alpha_{i_3,c}A_{i,c}\frac{L_{3,c}}{L_{total,c}}\left(T_{w_3,c} - T_{r_3,c}\right)$	$\dot{m}_{cro}h_{cri} - \dot{m}_{cro}h_{cro} + \alpha_{i_3,c}A_{i,c}\frac{L_{3,c}}{L_{total,c}}\left(T_{w_3,c} - T_{r_3,c}\right)$
$f_{4,cond}$	$-\dot{m}_{cro}$	$-\dot{m}_{cro} - \frac{1}{2}\left(\frac{\partial\rho_{1,c}}{\partial h_{1,c}}\Big\vert_P\right)A_{CS,c}L_{1,c}\dot{h}_{cri}$
$f_{5,cond}$	$k_c\left(T_{w_1,c} - T_{w_2,c}\right)$	$\alpha_{i_1,c}A_{i,c}\left(T_{r_1,c} - T_{w_1,c}\right) + \alpha_{o,c}A_{o,c}\left(T_{a,c} - T_{w_1,c}\right)$
$f_{6,cond}$	$\alpha_{i_2,c}A_{i,c}\left(T_{r_2,c} - T_{w_2,c}\right) + \alpha_{o,c}A_{o,c}\left(T_{a,c} - T_{w_2,c}\right)$	$\alpha_{i_2,c}A_{i,c}\left(T_{r_2,c} - T_{w_2,c}\right) + \alpha_{o,c}A_{o,c}\left(T_{a,c} - T_{w_2,c}\right)$
$f_{7,cond}$	$\alpha_{i_3,c}A_{i,c}\left(T_{r_3,c} - T_{w_3,c}\right) + \alpha_{o,c}A_{o,c}\left(T_{a,c} - T_{w_3,c}\right)$	$\alpha_{i_3,c}A_{i,c}\left(T_{r_3,c} - T_{w_3,c}\right) + \alpha_{o,c}A_{o,c}\left(T_{a,c} - T_{w_3,c}\right)$